Universidade do Minho
Escola de Engenharia

Ana Sofia Freitas Ferreira Araújo

Modelling of the Seismic Performance of Connections and Walls in Ancient Masonry Buildings

dezembro de 2014

Universidade do Minho
Escola de Engenharia

Ana Sofia Freitas Ferreira Araújo

Modelling of the Seismic Performance of Connections and Walls in Ancient Masonry Buildings

Tese de Doutoramento em Engenharia Civil

Trabalho efetuado sob a orientação do
Professor Doutor Paulo José Brandão Barbosa Lourenço
do
Professor Doutor Daniel Vitorino de Castro Oliveira
e do
Professor Doutor Guido Magenes

dezembro de 2014

STATEMENT OF INTEGRITY

I hereby declare having conducted my thesis with integrity. I confirm that I have not used plagiarism or any form of falsification of results in the process of the thesis elaboration.

I further declare that I have fully acknowledged the Code of Ethical Conduct of the University of Minho.

University of Minho, ______________________________

Full name: Ana Sofia Freitas Ferreira Araújo

Signature: ____

ACKNOWLEGDMENTS

This research work has been developed at the Civil Engineering Department of University of Minho, Portugal. This work was financially supported by the Portuguese Science and Technology Foundation (FCT) by grant No. SFRH/BD/71599/2010, which is gratefully acknowledged.

Above all, I would express my sincere gratitude to my supervisors in the University of Minho, Prof. Paulo Lourenço and Prof. Daniel Oliveira for their guidance and full support during these years. This work would not have been possible without their encouragement, interesting discussions and careful reading.

I would also like to thank to my co-supervisor, Prof. Guido Magenes, for the important support and interesting discussions provided during this work.

My sincere thanks to my colleagues, Nuno Mendes and Rui Silva who were critical in providing me technical help, useful advices and support during these years.

I express my profound gratitude to my friend and colleague Afonso Parente for his unconditional availability, patience, full support, encouragement and most of all his friendship. My sincere gratitude to my friend and colleague Sandra Cunha for the patience, relaxing moments and great encouragement. You two were always available to help me and to share your insightful advices.

I am very grateful to my parents, Alvaro and Gabriela and to my sisters Cristina, Maria João and Claudia who have been with me throughout my life and whose love and sacrifices brought me where I am today.

I am greatly indebted in to my husband Pedro for all the support and help he provided. The constant encouragement, support, love and patience, particularly during the long hours of writing, allowing me to complete my thesis. I also thank the tremendous help in the aesthetic components of this work.

I dedicate this work to my parents, my sisters, and my husband who supported me through all steps of the way. I couldn't have made this without you.

And last but not least, I would like to thank to my family and my friends for the patience, encouragement and support during all these years.

ABSTRACT

Unreinforced masonry construction is predominant in many urban areas world-wide. Many of these constructions are vulnerable to earthquakes, which are the main cause of damage and loss of cultural heritage. Lessons learned from earthquake surveys proved that a satisfactory seismic performance is attained when the structure behaves as a monolithic box.

This thesis tackles the problem of earthquake-impact on heritage masonry construction, starting from the basic consideration that efficient protection and strengthening can only be achieved with the proper knowledge of the behaviour of the structural elements and its connections. A numerical approach is proposed aiming at studying and further characterize the behaviour of stone masonry walls and anchors injected in masonry walls (used to strengthen connections between structural components). The knowledge provided by these studies is then applied in the seismic assessment of a typical masonry building.

The numerical study of the in-plane behaviour of masonry walls was carried out based on an experimental programme carried out at EUCENTRE. The finite element models, considering walls with distinct slenderness ratios and pre-compression levels, were calibrated against the experimental results. Good agreement between experimental and numerical results was achieved both considering the global force-displacement behaviour and failure mechanism. Moreover, the validated models were used to carry out parametric analyses varying the geometric wall configuration and pre-compression level and the influence of these parameters in the wall response was evaluated. The drift capacity of the walls numerically analysed was compared with the drift limits imposed by codes showing that drift limit recommended in codes for shear is not accomplished for all the walls. For this reason, some walls were analysed considering more realistic boundary conditions. In this cases, the drift limit was fulfilled for most of the walls. Finally, the usage of a simplified formulations to predict the strength capacity of walls is also addressed. The comparison between the numerical results with the lateral shear strength estimated by simplified models, demonstrated that these expressions can predict with very good approximation both the failure mode and the lateral resistance of a wall.

The numerical study of injected anchors in masonry was supported by an experimental campaign carried out at University of Minho. This work resorted to a detailed finite element model, which reproduces the experimental test setup, validated against the experimental results. The modelling approach adopted allowed for an accurate characterization of the behaviour of all structural elements, both in terms of stress field and displacement distribution. Then, the numerical model was used as a “numerical laboratory”, where the sensitivity of the results to the input of material parameters, geometrical features and actions was analysed. Among all the conditions studied through the parametrical analyses, the anchor embedment depth was the parameter that most influences the structural behaviour of the system, increasing significantly the ultimate capacity. Finally, simplified analytical methods to estimate the strength capacity of injected anchors on masonry were reviewed and the achieved values and failure modes agreed reasonably well with the numerical analysis.

Finally, the seismic assessment of a typical masonry building located in Lisbon was carried out. The seismic performance of this building was evaluated based on different assumptions related to the connections between structural components: lack of effective connections between elements, improved wall-to-wall connections and effective connections among all elements. Pushover analysis adopting the model that simulates the building response considering ineffective connections between structural elements showed rather low capacity when compared with the other models that include the strengthening of connections (either wall-to-wall or both wall-to-wall and wall-to-floor connections). These results demonstrated that the building seismic performance is significantly enhanced by the improvement of the connections behaviour, i.e. by accomplishing a monolithic box-like behaviour. Strengthening interventions for the improvement of the connections by installing injected anchors in masonry walls were also designed.

RESUMO

A conservação de edifícios antigos é um tema que tem suscitado um interesse crescente na comunidade em geral, pela necessidade de preservação do património edificado. As construções antigas de alvenaria não reforçada são predominantes em muitas cidades mundiais, e devido à sua vulnerabilidade às ações sísmicas, a avaliação da sua segurança torna-se essencial. Do estudo e análise do comportamento dos efeitos da ação sísmica neste tipo de edifícios, conclui-se que uma adequada resposta sísmica é alcançada quando a estrutura apresenta um comportamento monolítico.

Este trabalho aborda o impacto sísmico em edifícios antigos de alvenaria, com o pressuposto base de que um reforço eficiente apenas se consegue com o conhecimento do comportamento dos vários elementos estruturais e sua interligação. Através da abordagem numérica proposta neste trabalho, pretende-se estudar e caracterizar o comportamento de paredes de alvenaria e soluções de reforço com ancoragens injetadas nestes elementos, uma vez que os estudos existentes são maioritariamente experimentais. O conhecimento obtido a partir destes estudos numéricos é depois aplicado na avaliação sísmica de um edifício típico de alvenaria.

O estudo numérico do comportamento de paredes de alvenaria sujeitas a cargas no seu plano, baseou-se num programa experimental desenvolvido no EUCENTRE. Os modelos de elementos finitos utilizados foram calibrados com os resultados experimentais relativos a paredes com diferentes configurações geométricas e níveis de carga. Os modelos numéricos validados foram posteriormente utilizados em análises paramétricas, variando a configuração geométrica e o nível de compressão na parede, o que permitiu avaliar a influência destes parâmetros na resposta da mesma. Foram também analisados os deslocamentos laterais das paredes e comparados com os limites regulamentares, constatando-se que estes limites nem sempre são cumpridos. Por este motivo, algumas paredes das foram reanalisadas numericamente considerando diferentes condições de fronteira na tentativa de aproximar o seu comportamento a uma situação mais real. Estes novos resultados demonstraram que os limites regulamentares são cumpridos para a grande maioria das paredes estudadas. Posteriormente os resultados numéricos foram comparados com obtidos através da aplicação de expressões analíticas.

O estudo numérico de ancoragens injetadas em paredes de alvenaria teve como suporte a campanha experimental realizada na Universidade do Minho, tendo sido construído um modelo de elementos finitos detalhado, posteriormente calibrado com estes resultados experimentais. Dada a confiança no modelo numérico, este foi utilizado como laboratório numérico, onde foi avaliada a sensibilidade dos resultados aos parâmetros materiais, geométricos e ações, fornecendo informação importante na compreensão do comportamento deste sistema em diversas condições. De todas as condições estudadas, o comprimento de ancoragem foi o parâmetro que mais influenciou o comportamento global da parede. A capacidade das ancoragens foi estimada por métodos analíticos simplificados, que demonstraram razoável aproximação aos resultados numéricos.

A avaliação sísmica de um edifício típico em alvenaria localizado em Lisboa foi realizada recorrendo a três modelos numéricos que incluem a adoção de diferentes considerações relativas às ligações entre elementos estruturais. A análise “pushover” adotando um modelo que simula a resposta do edifício considerando ineficientes as ligações entre elementos estruturais, revelou uma baixa capacidade sísmica quando comparada com os resultados dos modelos que incluem reforço de ligações. Deste modo, demonstra-se que a resposta sísmica do edifício é significativamente melhorada com o reforço das ligações, que conferem um comportamento monolítico à estrutura. Apresenta-se ainda o dimensionamento das soluções de reforço para as diversas ligações dos elementos estruturais do edifício, considerando a utilização de sistemas de ancoragem.

CONTENTS

Acknowlegdments i

Abstract iii

Resumo v

Contents vii

List of Figures xiii

List of Tables xxv

List of Symbols xxvii

Chapter 1 1

Introduction 1

1.1. Motivation 2

1.2. Aims and methods of the research 5

1.3. Outline of the Thesis 6

Chapter 2 7

Overview on the Seismic behaviour of masonry buildings 7

2.1. Introduction 8

2.2. General Aspects on Masonry buildings 10

2.3. Seismic Behaviour 11

2.3.1. Diaphragms 14

2.3.2. Out-of-plane behaviour 15

2.3.3. In-plane behaviour ... 17
2.3.4. Connections ... 20
2.4. Strengthening techniques ... 20
2.4.1. Walls and floors ... 21
2.4.2. Connections ... 22
2.5. Analysis Methods and Modelling Issues ... 23
Chapter 3 ... 27
In-plane behaviour of Masonry Walls ... 27
3.1. Introduction ... 28
3.2. Outline of the Experimental Research Programme ... 29
3.3. Numerical Models ... 32
3.3.1. Models Definition ... 32
3.3.2. Models Calibration ... 34
3.4. Non-linear Analyses ... 36
3.4.1. Definition of the Material Behaviour ... 36
3.4.2. Non-linear Analyses Results ... 38
3.5. Parametric Analyses ... 44
3.6. Drift Capacity ... 50
3.7. Analytical Evaluation ... 55
3.7.1. European Equations ... 56
3.7.2. FEMA Predictions ... 59
3.7.3. NZSEE Predictions ... 59
3.7.4. In-plane Strength of the Walls ... 60
3.8. Final Considerations ... 62

Chapter 4 65

Behaviour of injected anchors on Masonry walls 65

4.1. Introduction 66

4.2. Experimental Contextualization 69

4.3. Numerical Study 73

4.3.1. Introduction 73
4.3.2. Modelling Strategy 74
4.3.3. Initial Linear Analysis 77
4.3.4. Initial Validation 79
4.3.5. Nonlinear Analyses 80
Nonlinear Formulation 80
Nonlinear Analyses Results 82

4.4. Parametrical Study 87

4.4.1. Masonry Parameters 87
Elastic Modulus 87
Compressive Strength 89
Compressive Fracture Energy 91
Tensile Strength 92
Tensile Fracture Energy 94
4.4.2. Pre-compression Level 95
4.4.1. Geometric Parameters 96
Anchor Dimension 96
Embedment Depth 97
Anchors Spacing 98
4.4.2. Conclusions 99

4.5. Analytical Evaluation 100

4.5.1. MSJC Formulation 100
4.5.2. Gigla and Wenzel Formulation 101

4.5.3. ACI 318 Formulation ... 102
4.5.4. CEB Formulation ... 103
4.5.5. Fib Formulation ... 104
4.5.6. Arifpovic and Nielsen Formulation ... 105
4.5.7. Results and Discussion ... 105

4.6. Final Considerations ... 110

Chapter 5 ... 113

Masonry Building: Case of Study ... 113

5.1. Introduction ... 114

5.2. Description of the Case of Study ... 115

5.3. Strengthening Solution/Intervention ... 117

5.3.1. Safety Requirements ... 118
5.3.2. Evaluation of the Wall Safety ... 120
5.3.3. Wall-to-wall Connections ... 120
5.3.4. Wall-to-floor Connections ... 124

5.4. Numerical Study ... 126

5.4.1. Model 1 ... 128
5.4.2. Model 2 ... 131
5.4.3. Model 3 ... 133
5.4.4. Comparison between the models ... 136

5.5. Validation of the building capacity by simplified methods ... 136

5.5.1. Bilinear Pushover Curves ... 136
5.5.2. Macro-block approach ... 137

5.6. FEMA ... 138

5.7. Final Remarks ... 141

Chapter 6 143

Conclusions and Future Work 143

6.1. Conclusions 144

6.1.1. Masonry Walls Study 144
6.1.2. Injected Anchors Study 145
6.1.3. Typical Masonry Building 145

6.2. Future Works 146

Bibliography 147

Annex A 159

Annex B 175

List of Figures

Figure 1.1 Earthquake damage: (a) Maharashtra 1993 (India); (b) Azores 1998 (Portugal); (c) Bhuj Gujarat 2001 (India); (d) Bhutan 2009; (e) L’Aquila 2009 (Italy); (f) Christchurch 2011 (New Zealand). 3

Figure 2.1 Examples of Masonry Buildings: (a) Colosseum, Rome and (b) City centre, Porto. 8

Figure 2.2 Typical behaviour of quasi-brittle materials under uniaxial loading (a) Tensile; (b) Compressive; (c) Shear – compression (Lourenço 1996a). ... 11

Figure 2.3 Scheme of a typical masonry building under earthquake excitation (adapted from Moon 2004). 11

Figure 2.4 Typical deformation and damage of unreinforced masonry buildings under seismic loads (adapted from Tomaževič 1999). 12

Figure 2.5 Examples of collapse mechanisms in buildings (a) Local out-of-plane, (b) Global in-plane (Magenes 2006). 13

Figure 2.6 Abacus of damage mechanisms (a) Civil constructions; (b) Religious constructions... 14

Figure 2.7 Examples of out-of-plane failures during earthquakes: (a) Overturning of façade; (b) Overturning of portions of the façade; (c) Partial overturning of façade (effect of openings); (d) Overturning of corner wedge................. 16

Figure 2.8 Examples of in-plane failures.. 17

Figure 2.9 Typical in-plane masonry wall and main structural elements (adapted from Calderini et al. 2008). 18

Figure 2.10 Typical failure mechanisms of masonry piers: (a) Toe crushing; (b) Rocking; (c) Sliding; and (d) Diagonal Cracking. 19

Figure 2.11 Typical seismic behaviour: (a) Flexible floor and weak connection between orthogonal walls; (b) Flexible floor and good connection between orthogonal walls; (c) Rigid floor and good connection between orthogonal walls (Tomaževič 1999). 20

Figure 2.12 Transversal ties in masonry walls. 21

Figure 2.13 Strengthening techniques using injected anchors for the connection between structural elements: (a) Wall to floor connection; (b) Wall to half-timber-wall connection (Moreira et al. 2012). 23

Figure 2.14 Analysis methods. 24

Figure 3.1 Wall specimens for in-plane cyclic tests: (a) CS01 wall; (b) CS02 wall; (c) CT01 wall; (d) CT02 wall. 30

Figure 3.2 Scheme of the experimental test setup. 30

Figure 3.3 Experimental test results. 31

Figure 3.4 Representative scheme of the numerical models (dimensions in meters). 32

Figure 3.5 Numerical models (mesh discretization): (a) CT walls and (b) CS walls. 33

Figure 3.6 Linear elastic analyses: (a) CS01 Wall; (b) CS02 Wall; (c) CT01 Wall; (d) CT02 Wall. 34

Figure 3.7 Constitutive models for masonry (tension and compression). 37

Figure 3.8 Force-displacement curve for CS01 wall. 38

Figure 3.9 Strains distribution for CS01 wall: (a) Tensile damage at peak load; (b) Tensile damage at final stage; (c) Compressive strain distribution at final stage. 39

Figure 3.10 Force-displacement curves for CS02 wall: (a) Results with E=2000 MPa; (b) Results with E=1100 MPa. 40

Figure 3.11 Strains distribution for CS02 wall with E=2000 MPa: (a) Tensile damage at peak load; (b) Tensile damage at final stage; (c) Compressive strain distribution at final stage. 41

Figure 3.12 Strains distribution for CS02 wall with E=1100 MPa: (a) Tensile damage at peak load; (b) Tensile damage at final stage; (c) Compressive strain distribution at final stage. 41

Figure 3.13 Force-displacement curve for CT01 wall. 42

Figure 3.14 Strains distribution for CT01 wall: (a) Tensile damage at peak load; (b) Tensile damage at final stage; (c) Compressive strain distribution at final stage. 42

Figure 3.15 Force-displacement curve for CT02 wall. 43

Figure 3.16 Strains distribution for CT02 wall: (a) Tensile damage at peak load; (b) Tensile damage at final stage; (c) Compressive strain distribution at final stage. 44

Figure 3.17 Numerical model for CM walls. 46

Figure 3.18 Force-displacement curves of the parametric analyses - Comparison according the compression level: (a) 0.5 MPa; (b) 0.35 MPa; (c) 0.2 MPa….. 47

Figure 3.19 Force-displacement curves of the parametric analyses - Comparison according the geometric configuration: (a) *h/l* =1; (b) *h/l* =1.33; (c) *h/l* =2… 48

Figure 3.20 Maximum principal strain distribution for the parametrical analyses in at final stage (a possible border between flexure and shear modes is provided)… 49

Figure 3.21 Drift capacity. 52

Figure 3.22 Drift variation in function of the relation between the vertical stress and masonry compressive strength: (a) Scatter graph; (b) Box diagram. 53

Figure 3.23 Drift variation in function of the slenderness ratio: (a) Scatter graph; (b) Box diagram. 54

Figure 3.24 Estimation of the drift capacity considering at the top wall the stiffness provided by 0.5 m of spandrels. 55

Figure 3.25 Equilibrium of the wall subjected to vertical and horizontal loads with crushing at the base corner. 57

Figure 3.26 Overturning around O. 57

Figure 3.27 Calculation of the length of the compression zone. 58

Figure 3.28 Diagonal Cracking. 58

Figure 3.29 Comparison between numerical shear strength and predictions by analytical models. 62

Figure 4.1 Strengthening solution with parallel anchors: (a) 3D view of the timber frame wall and the connecting anchoring system; (b) Connecting system; (c) Top view strengthening system (adapted from (Cóias 2007). 67

Figure 4.2 Possible failure mechanisms in anchoring systems: (a) Steel failure; (b) Masonry cone failure; (c) Sliding failure along the outer interface; (d) Sliding failure along the inner interface. 68

Figure 4.3 Specimen configuration and test setup (in millimetres): (a) Front view with the location of anchors; (b) Plan view of the anchors; (c) Cross section of wall and test set-up. 71

Figure 4.4 Specimen and test setup configuration in the laboratory. 71

Figure 4.5 Example of one pair of injected anchors after testing: (a) Crack pattern; (b) Sliding on the grout/masonry interface. 72

Figure 4.6 Envelope of the force-displacement curves resultant from the experimental tests. 73

Figure 4.7 Modelling strategy used to model the anchoring system (representative thickness in the interfaces). 74

Figure 4.8 Finite elements used in the model: a) CHX60; b) CTP45 e c) CQ48I (TNO DIANA 2009). 75

Figure 4.9 Numerical model mesh. 75

Figure 4.10 Compressive stress distribution on the wall after the application of the vertical load (in kPa). 77

Figure 4.11 Sliding failure along the inner interface. 78

Figure 4.12 Sliding failure along the outer interface. 78

Figure 4.13 Masonry cone failure. 79

Figure 4.14 Comparison between the experimental envelope and numerical behaviour in the linear range. 79

Figure 4.15 Mechanical behaviour of masonry: (a) Tension; (b) Compression; (c) Shear (applicable for FCM). 81

Figure 4.16 Integration schemes for the numerical elements: (a) CHX60; (b) CTP45; (c) CQ48I (TNO DIANA 2009). 82

Figure 4.17 Force-displacement curves for the RCM and FCM formulations and experimental envelope. 83

Figure 4.18 Division in sections of the model for the analysis of the results. 83

Figure 4.19 Maximum principal strains at peak load for FCM: (a) Lateral view (undeformed and deformed shape); (b) Top view (undeformed and deformed shape). 84

Figure 4.20 Maximum principal strains at peak load for RCM: (a) Lateral view (undeformed and deformed shape); (b) Top view (undeformed and deformed shape). 84

Figure 4.21 Maximum principal strains at final stagefor FCM: (a) Lateral view (undeformed and deformed shape); (b) Top view (undeformed and deformed shape). 85

Figure 4.22 Maximum principal strains at final stage for RCM: (a) Lateral view (undeformed and deformed shape); (b) Top view (undeformed and deformed shape). 85

Figure 4.23 Contour map of the out-of-plane displacements: (a) FCM; (b) RCM....... 86

Figure 4.24 Force-displacement curves for the parametric analysis of the masonry elastic modulus. 88

Figure 4.25 Maximum principal strains at final stage for the $0.5 \times Eref$ analysis: (a) Lateral view; (b) Top view. 88

Figure 4.26 Maximum principal strains at final stage for the $2.0 \times Eref$ analysis: (a) Lateral view; (b) Top view. 89

Figure 4.27 Stress-strain compressive behaviour varying the compressive strength. .. 89

Figure 4.28 Force-displacement curves for the parametric analysis of the masonry compressive strength. 90

Figure 4.29 Strains distribution at final stage for the $0.5 \times fc,ref$ analysis: (a) Tensile -lateral view; (b) Tensile - top view; (c) Compressive -lateral view; (d) Compressive - top view. 90

Figure 4.30 Strains distribution at final stage for the $2.0 \times fc,ref$ analysis: (a) Tensile -lateral view; (b) Tensile - top view; (c) Compressive -lateral view; (d) Compressive - top view. 91

Figure 4.31 Stress-strain compressive behaviour varying the compressive fracture energy. 91

Figure 4.32 Force-displacement curves for the parametric analysis of the masonry compressive fracture energy. 92

Figure 4.33 Stress-strain tensile behaviour varying the tensile strength. 92

Figure 4.34 Force-displacement curves for the parametric analysis of the masonry tensile strength. 93

Figure 4.35 Maximum principal strains at final stage for the $0.5 \times ft,ref$ analysis: (a) Lateral view; (b) Top view. 93

Figure 4.36 Maximum principal strains at final stage for the $2.0 \times ft,ref$ analysis: (a) Lateral view; (b) Top view. 94

Figure 4.37 Stress-strain tensile behaviour varying the tensile fracture energy. 94

Figure 4.38 Force-displacement curves for the parametric analysis of the masonry tensile fracture energy. 95

Figure 4.39 Force-displacement curves for the parametric study of the pre-compression level. 95

Figure 4.40 Modification of the anchoring system dimension. 96

Figure 4.41 Force-displacement curves for the parametric study of the anchor dimensions. 96

Figure 4.42 Modification of the wall thickness and anchor embedment depth. 97

Figure 4.43 Force-displacement curves for the parametric study of the embedment depth. 97

Figure 4.44 Maximum principal strains at final stage for the embedment depth parametric analysis: (a) Lateral view; (b) Top view. 98

Figure 4.45 Modification of the spacing between anchors. 98

Figure 4.46 Parametrical study of the anchors spacing: (a) Modifications on the model settings; (b) Force-displacement curve. 99

Figure 4.47 Maximum principal strains at final stage for the anchor spacing parametric analysis: (a) Lateral view; (b) Top view. 99

Figure 4.48 Geometrical parameters for equation (4.5) (Gigla 2004). 102

Figure 4.49 Calculation of ANc and ANa (ACI 318 2011). 103

Figure 4.50 Comparison between the experimental mean value and analytical predictions of the anchoring system capacity. 107

Figure 4.51 Comparison between the analytical expressions and the parametric analysis of the anchor dimension. 108

Figure 4.52 Comparison between the analytical expressions and the parametric analysis of the embedment depth. 109

Figure 4.53 Comparison between the analytical expressions and the parametric analysis of the anchors spacing. 109

Figure 5.1 Typical masonry buildings in Alvalade neighbourhood, Lisbon. 115

Figure 5.2 Elevation of the building: (a) Front elevation; (b) Rear elevation. 116

Figure 5.3 Plan of the ground floor. 116

Figure 5.4 Plan of the first and second floors. 117

Figure 5.5 Kinematic mechanism concerning the out-of-plane overturn of the façade wall. 118

Figure 5.6 Wall-to-wall strengthening solution (plan view). 121

Figure 5.7 Kinematic mechanism concerning the out-of-plane overturn of the façade wall with the consideration of the wall-to-wall strengthening system.... 121

Figure 5.8 Equilibrium of the upper part of the wall used for the calculation of T_3……… .... ……122

Figure 5.9 Equilibrium of the upper part of the wall used for the calculation of T_2……… 123

Figure 5.10 Schematic representation of the wall-to-wall strengthening solution in each floor level. 123

Figure 5.11 Wall-to-floor strengthening solution: (a) Plan view; (b) Perspective. ... 124

Figure 5.12 Kinematic mechanism concerning the out-of-plane overturn of the façade wall with the consideration of the wall-to-floor strengthening system... 125

Figure 5.13 Equilibrium mechanisms: (a) Upper part of the wall for the calculation of T_3; (b) Two upper floors of the wall for the calculation of T_2. 126

Figure 5.14 Schematic representation of the wall-to-floor strengthening solution. .. 126

Figure 5.15 Curved shell element (CQ40S) (adapted from TNO DIANA (2009)).... 127

Figure 5.16 Global view of the building with the representation of the loading direction….. 128

Figure 5.17 Mesh of the numerical Model 1. 128

Figure 5.18 Capacity curves for Model 1. 129

Figure 5.19 Maximum principal strains distribution showing the damage evolution in +Y direction: (a) Second peak load; (b) Drop after the peak (80 mm); (c) Final stage. 130

Figure 5.20 Maximum principal strains distribution showing the damage evolution in –Y direction: (a) Inflection point; (b) Peak load; (c) Final stage. 131

Figure 5.21 Mesh of the numerical Model 2. 131

Figure 5.22 Capacity curves for Model 2. 132

Figure 5.23 Maximum principal strains distribution showing the damage evolution in +Y direction: (a) Peak load; (b) Final stage. 132

Figure 5.24 Maximum principal strains distribution showing the damage evolution in –Y direction: (a) First inflection point; (b) Peak load; (c) Final stage. 133

Figure 5.25 Truss element (L6TRU) (adapted from TNO DIANA (2009)) 133

Figure 5.26 Schematic representation of one floor of the building, including the description of the materials. 134

Figure 5.27 Mesh of the numerical Model 3. 134

Figure 5.28 Capacity curves for Model 3. 135

Figure 5.29 Maximum principal strains distribution showing the damage evolution in +Y direction: (a) First inflection point; (b) Peak load; (c) Final stage. 135

Figure 5.30 Maximum principal strains distribution showing the damage evolution in –Y direction: (a) First inflection point; (b) Peak load; (c) Final stage. 135

Figure 5.31 Comparison between the model responses: (a) +Y direction; (b) –Y direction. 136

Figure 5.32 Bilinear approximation. 137

Figure 5.33 Bilinear approximation of FEM results: (a) +Y direction; (b) -Y direction… 137

Figure 5.34 Model using macro-elements (taken from (Lamego 2014)). 138

Figure 5.35 Comparison between the FEM results with the results obtained by using the macro-modelling approach: (a) +Y direction; (b) -Y direction 138

Figure 5.36 Schematic illustrating the definition of structural components in lateral walls. 139

List of Tables

Table 2.1 In-plane failure modes. 19

Table 3.1 Mechanical properties of masonry (tests on 6 specimens). 29

Table 3.2 Material properties for the preliminary linear analysis phase. 33

Table 3.3 Calibrated elastic modulus for each wall. 35

Table 3.4 Mechanical properties for masonry. 38

Table 3.5 Parametric analyses (in grey the walls experimentally tested and numerically validated). 45

Table 3.6 Elastic modulus for the parametric analysis. 46

Table 3.7 Comparison between the experimental and numerical conventional drift capacity. 51

Table 3.8 Drift capacity of the parametric analysis walls. 52

Table 3.9 Analytical expressions according to the failure mode. 56

Table 3.10 Strength prediction. 61

Table 4.1 Mechanical properties of masonry. 72

Table 4.2 Material properties adopted. 76

Table 4.3 Interface Stiffness. 79

Table 4.4 Non-linear updated parameters for the masonry constitutive laws definition.. 81

Table 4.5 Prediction of the anchor strength according to the distinct formulations…… 106

Table 5.1 Material properties. 117

Table 5.2 Loads of the kinematic mechanism in [KN/per 1 meter wall]. 118

Table 5.3 Calculation of the participant mass M*.. 119

Table 5.4 Non-linear properties.. 127

Table 5.5 Parameters used to compute the strength capacity of each pier. 140

Table 5.6 Strength of the piers. 140

List of Symbols

α	Load coefficient
α_1	Coefficient to take into consideration the boundary conditions [$\alpha_1 = 0.5$ for the case of fixed-fixed conditions and $\alpha_1 = 1$ for a cantilever wall]
α_2	Coefficient to take into consideration the boundary conditions [$\alpha_2 = 1.0$ for fixed-fixed pier or equal to $\alpha_2 = 0.5$ for cantilever wall]
α_V	Effective aspect ratio [$\alpha_V = \frac{h_0}{l}$]
ν	Coefficient of Poisson
γ	Density
σ	Compressive stress
τ_u	Bond strength
Ψ_c	Modification factor for anchors located in a region where the base material indicates no cracking at service loads
Ψ_{cp}	Modification factor for splitting
Ψ_{ec}	Modification factor for anchor groups loaded eccentrically
Ψ_{ed}	Modification factor for edge distances less than 1.5 l_{ef}
Ψ_g	Factor that takes into consideration the effect of the failure surface of anchor groups
Ψ_s	Factor that takes into account the distribution of stresses due to the edges of the substrate member
$X_{B,W}$	Term to describe the increase of bond strength inside water absorptive stone material.
A	Area of the horizontal cross section
A_s	Steel bar area.
A_0	Overlapping area of the anchors
A_B	Contact area between grout and units
$A_{A,d}$	Surface of injected grout surrounding the steel bar
$A_{G,d}$	Surface of injected grout
A_{Nc}	Projected failure area of a single anchor or group of anchors limited by the edge distance or spacing
A_{pt}	Projected area on the masonry surface of a right circular cone
A_{Nco}	Projected concrete failure area of a single anchor, for calculation of strength in tension if not limited by edge distance or spacing

A_{Nc}	Projected concrete failure area of a single anchor or group of anchors, for calculation of strength in tension
c	Cohesion
c_a	Distance from the centre the anchor to the edge of masonry
d_s	Steel bar diameter
d_B	Borehole diameter
E	Elastic modulus
G_c	Compressive fracture energy
G_t	Tensile fracture energy
h_0	Effective height - determined according to the boundary conditions of the wall (distance from zero moment)
h	Wall height
f_c	Compressive strength of masonry
f_{cb}	Compressive strength of the unit
f_{cj}	Compressive strength of the mortar
f_{ci}	Compressive strength of the interface between mortar and units
$f_{G,c}$	Compressive strength of grout
f_t	Tensile strength of masonry
f_{ut}	Direct tensile strength of units
f_{uta}	Specified tensile strength of anchor steel
f_y	Anchor yield strength
l	Wall length
l_c	Length of the effective compression zone
l_{ef}	Effective embedment depth
l_u	Unit length
M	Bottom moment
n	Number of anchors in the group
N	Axial compressive force
t	Wall thickness
T	Anchor tensile force
T_b	Material breakout strength of a single anchor in tension
V	Shear force
V_c	Toe crushing strength

V_f	Flexural strength
V_r	Rocking strength
V_s	Sliding strength
V_t	Diagonal tension strength
W	Weight
μ	Coefficient of friction

CHAPTER 1

INTRODUCTION

1.1. MOTIVATION

Stone masonry is a traditional form of construction that has been practiced for centuries worldwide, ranging from typical buildings to cultural and historical landmarks. The earliest records of history show masonry to be one of the basic and most common construction material, being used for the construction of some of the most important monuments and structures around the world. Masonry constructions also represent the vast majority of the traditional buildings nowadays.

The increasing awareness regarding the preservation of heritage and traditional masonry buildings is a result of a collective social responsibility to protect the heritage, aiming at guaranteeing that the cultural identity is perpetuated for future generations. Moreover, the functions that these structures still maintain in our days justify the concern about its safety. Many of these constructions are vulnerable to earthquakes which are the main cause of damage and loss of cultural heritage. Moreover the damage and collapse of these structures during a seismic event is a permanent threat for human lives.

As proven by historical data, many ancient towns and cities all over the world have already been seriously affected by seismic actions, leading to severe human, cultural and economic losses. Examples of devastation caused by heavy damage or the collapse of stone masonry buildings in past earthquakes are shown in Figure 1.1. In India, most of the 13,800 deaths during the 2001 Bhuj earthquake (Figure 1.1c), and more than 8,000 deaths in the 1993 Maharashtra earthquake (Figure 1.1a), were attributed to collapses of traditional stone masonry buildings. Azores earthquake in 1998 caused nine casualties and severe destruction in many masonry buildings affecting more than 5,000 people in Portugal (Figure 1.1b). Also in the 2009 Bhutan earthquake, many of the causalities were associated to the total or local collapse of masonry structures (Figure 1.1d). From observation of damage caused by more recent earthquakes, L’Aquila 2009 in Italy (Figure 1.1e) and Christchurch 2011 in New Zealand (Figure 1.1f), it could be concluded that the level of damage found in masonry structures is not so devastating as verified in past earthquakes. Post-earthquake surveys were performed in L’Aquila (D’Ayala and Paganoni 2010) and Christchurch (Senaldi et al. 2012) in order to assess the seismic performance of unreinforced stone masonry buildings and retrofitted constructions. These investigations showed that, although the damage is limited by local collapses (total collapses observed was minor) and some examples of successful retrofitted structures were verified, unreinforced stone masonry buildings reveal a poor seismic performance.

(a)

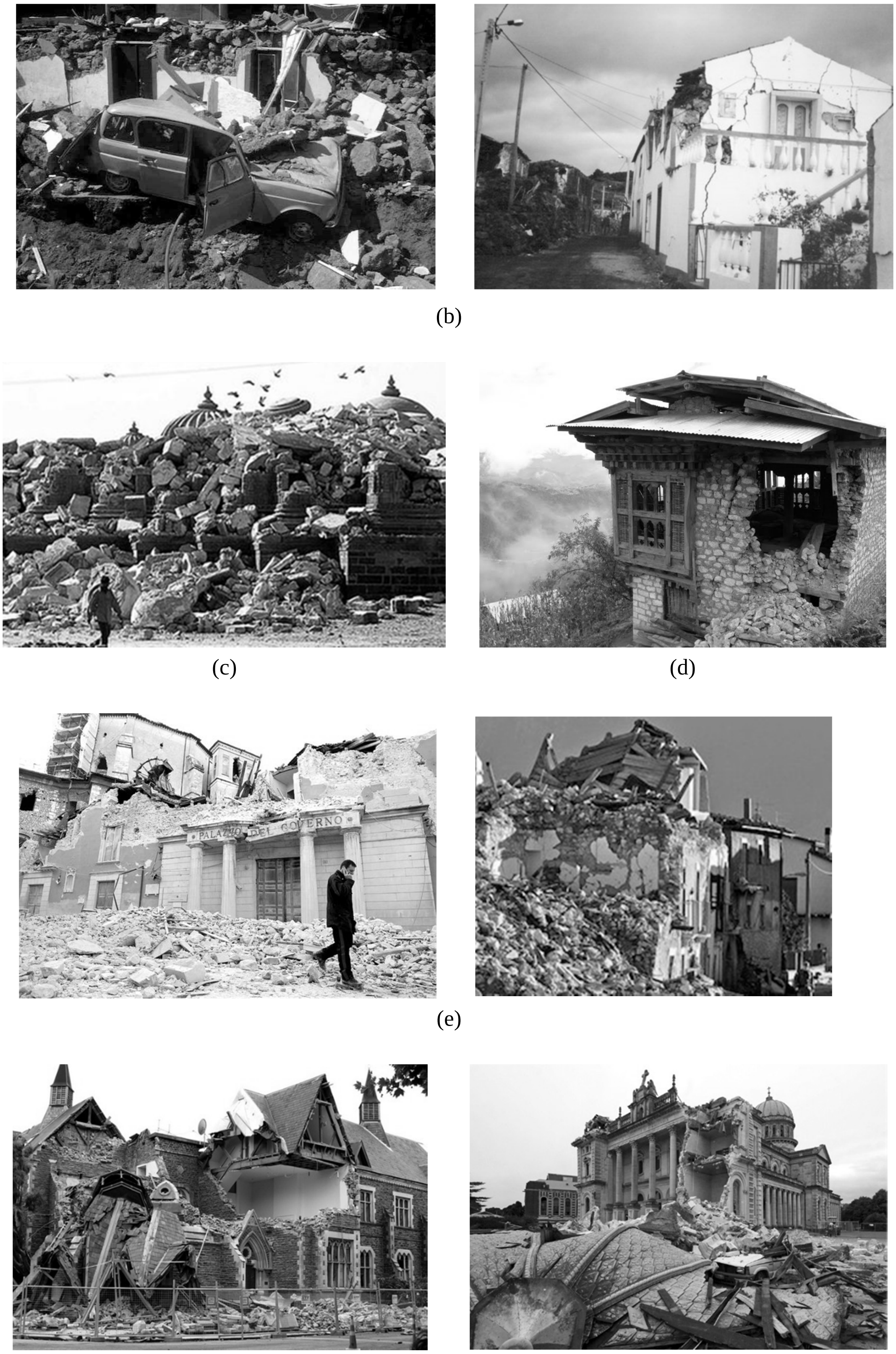

(b)

(c) (d)

(e)

(f)

Figure 1.1 Earthquake damage: (a) Maharashtra 1993 (India); (b) Azores 1998 (Portugal); (c) Bhuj Gujarat 2001 (India); (d) Bhutan 2009; (e) L'Aquila 2009 (Italy); (f) Christchurch 2011 (New Zealand).

Damage surveys of past earthquakes have shown that damage and the collapse of masonry buildings cause major human and economic losses in areas where this construction is widespread. The lack of proper strengthening interventions in masonry buildings to prevent damage and casualties while preserving cultural value, clearly stands out. The development of suitable and appropriate retrofitting measures to improve the seismic performance of traditional masonry buildings can only be accomplished by gaining knowledge on the behaviour the structural elements and its connections.

The key components of a typical stone masonry building include floor/roof systems, structural walls, and connections between elements. The analysis of damage patterns can identify the main causes of the poor seismic performance of these buildings:

- Foundation problems;
- Ungluing of wall wythes;
- Floor and/or roof collapse from inadequate wall-to floor (or wall-to-roof) anchorage;
- Damage and/or separation of walls at intersections;
- Out-of-plane wall collapse due to the lack of orthogonal connection;
- Poor quality of construction;
- Lack of structural integrity;

Lessons learned from earthquake surveys regarding the influence of the structural components and connections behaviour on the seismic performance of masonry buildings proved that, a satisfactory seismic performance is attained when the structure behaves as a monolithic box. When the walls are not properly connected at their intersections, it is expected that they vibrate on its own when subjected to earthquake ground shaking. Buildings with regular structural organization, with the walls connected together at the floor levels, have often performed well (Tomaževič 1999).

The key strategies to improve the seismic safety of masonry buildings involves the enhancement of the structural integrity of the entire building by ensuring a box-like response. The global behaviour of the building is obviously dependent on the efficiency of the connections between structural elements (the walls have to be tied together and anchored to the floor and to the roof). In this manner, seismic loads can be transferred through the floor and roof diaphragms to the in-plane walls, behaving in a more stable way. The knowledge of the in-plane performance of the structural walls, which are the basic resisting elements to seismic loads, is also essential for the proper understanding of masonry buildings global behaviour.

The structural in-plane behaviour of masonry walls have been experimentally studied by several researchers (e.g. Abrams and Shah 1992; Anthoine et al. 1995; Angelini et al. 2007; Alcaino and Santa-Maria 2008; Magenes et al. 2008a; Churilov and Dumova-Jovanoska 2010; Freeda et al. 2012; Andreini et al. 2013; Churilov and Dumova-Jovanoska 2013). Nevertheless, the huge number of possible combinations generated by the geometry, the characteristics of mortar, the nature and arrangement of units, as well as the construction techniques makes the proper characterization of different masonry walls almost impossible.

1.2. AIMS AND METHODS OF THE RESEARCH

Since the seismic performance of masonry walls and the behaviour of strengthened connections are two major issues within the global seismic behaviour of typical masonry buildings, contributions on these topics are intended to be given.

The present study tackles the problem of earthquake-impact on heritage masonry constructions, starting from the basic consideration that efficient protection and strengthening can only be achieved with the proper knowledge of the behaviour of the structural elements and its connections. This research includes the numerical study of:

- The in-plane behaviour of masonry walls which are considered the most relevant structural element;
- The strengthened connections between structural elements in masonry buildings, by means of injected anchors installed in masonry walls;
- The global behaviour of a typical masonry building.

Thus, the present work aims to provide a better insight on the impact that individual components behavior and their interaction have in the global response of the building. This will be accomplished by: the characterization of the in-plane performance of stone masonry walls; by investigating the behaviour of injected anchors installed in masonry walls to strengthen the connection between structural elements; and by evaluation the influence of these parameters in the global behaviour of a typical masonry building.

The methodology followed for the characterization of the behaviour of masonry walls and injected anchors installed in masonry is similar. The main steps carried out within these studies are the following:

- Selection of the experimental campaign to sustain the numerical study;
- Construction of finite element model trying to accurately simulate the behaviour observed during experimental testing;
- Calibration and validation of the numerical results against the experimental data;
- Conduct nonlinear analysis to characterize the behaviour;
- Perform parametrical analysis to further evaluate the behaviour of the component under study in different conditions;
- Assess the available analytical formulations by comparing with the experimental and numerical results.

The knowledge provided by these studies is used in the seismic assessment of a typical masonry building well as in the evaluation of how the retrofit techniques contribute to overall building response.

1.3. OUTLINE OF THE THESIS

The thesis outline is divided into six Chapters that follow the path presented in the previous section. Chapter 1 describes the motivation, the aim and scope of the work, as well as the content of the thesis. Chapter 2 provides an overview on the seismic performance of traditional masonry structures. The gathered information regarding structural components features and seismic behaviour was presented, focusing in the in-plane failure mechanism of walls. The role of the connections between structural elements is also addressed and discussed. This is followed by a brief description of known strengthening interventions available for stone masonry buildings, giving special attention to solutions that included injected anchors. The literature review also included the discussing, addressing advantages and limitations, regarding the different available modelling techniques and analysis methods for the simulation of stone masonry. The literature review provided the basis for the definition of the working strategy, taking into account both the inherent recommendations and limitations.

Chapter 3 presents the study of stone masonry walls under in-plane loading. An experimental campaign carried out in EUCENTRE was used to calibrate and validate the finite element model. The results of the nonlinear analysis are presented and compared with the experimental results in terms of force-displacement curves and damage pattern. Parametric analysis results, aiming at characterize the behavior of masonry walls with different geometries and levels of per compression, are also presented and discussed. Furthermore, the drift capacity of these walls is also addressed. Finally, analytical formulations available in literature to predict the in-plane strength of masonry walls were discussed and compared against the numerical and experimental results.

Chapter 4 deals with the study of injected anchors installed in masonry walls as a way to strengthen the connections between structural elements. This investigation involves the construction of a finite element model that simulates the experimental results taken from the campaign carried out at the University of Minho. The numerical modelling validation process is also presented as well as the numerical results obtained from it. A discussion involving the evaluation of which model (total strain fixed crack model or total strain rotating crack) better simulates the behaviour of the system is provided. The influence of several key parameters in the behaviour of the anchoring system is also presented in this Chapter. Finally, analytical expressions to predict the strength of the anchoring system injected in masonry are discussed and compared with the values estimated numerically.

In Chapter 5 the seismic assessment of a traditional masonry building of Lisbon is presented. The purpose of this chapter is to apply the knowledge obtained through the studies presented in Chapter 3 and Chapter 4 in the study of the global seismic behaviour of a typical masonry building. The seismic response is evaluated, firstly considering ineffective connections among structural elements, then assuming efficient connections among walls and finally assuming a global structural response of the structure with the additional contribution of the floors. The results from pushover analysis proportional to the mass are presented and discussed. The design of strengthening solutions for the improvement of the wall-to-wall and wall-to floor connections behaviour is also presented. Chapter 6 contains a summary of the conclusions drawn from this investigation and the most promising future works are suggested.

Chapter 2

OVERVIEW ON THE SEISMIC BEHAVIOUR OF MASONRY BUILDINGS

2.1. INTRODUCTION

Unreinforced masonry construction is predominant in many urban areas world-wide, particularly in the form of impressive historical buildings as landmarks of ancient cultures and typical residential buildings in cities hearts (Figure 2.1).

Considering past and more recent earthquakes, it has been recognized that masonry buildings, particularly if inadequately tied, are very vulnerable to earthquakes (Abrams 2001; Lagomarsino 2006; Furukawa and Kiyono 2009). Most of masonry buildings that undergo seismic action lead to deaths due to an inadequate resilience of the structure. In the past, masonry buildings were constructed by learning from the experience on similar structures, refining the proportions of structural elements by a deep perception of their structural behaviour (Lagomarsino 2006). The conception of these buildings was a result of a trial and error process that took into account only static actions. In this way, masonry buildings are generally able to carry the vertical loads in a safe and stable way (Betti and Vignoli 2008a), but from a structural point of view, they tend to fail to respond well to seismic loads. As such, the architectonic and cultural world heritage is at permanent risk due to the threat that earthquakes represent. Unfortunately, many areas in Europe are characterized by a high level of seismic hazard and the vulnerability of ancient masonry structures is often relevant (Lagomarsino 2006). In recent years, many archival sources and in situ surveys carried out after seismic events proved that many heritage buildings are damaged by earthquakes, stressing the need for safety evaluation of ancient buildings in seismic zones. Several examples of studies regarding masonry constructions affected by past earthquakes can be found in literature, e.g. (Corradi et al. 2002; Dogangun et al. 2009; Furukawa and Kiyono 2009; Sturm et al. 2009).

(a) (b)

Figure 2.1 Examples of Masonry Buildings: (a) Colosseum, Rome and (b) City centre, Porto.

The increasing awareness regarding the preservation of heritage buildings as a way to protect them for future generations leads to the need for the study and assessment of masonry buildings in historical centres around the world, like in Portugal, Italy, Greece, Turkey, Peru, Mexico, etc. (Sturm et al. 2009). The concerns regarding the structural safety of these buildings are justified by the functions that these constructions still maintain nowadays. Considering that seismic events are also a threat to human live, it is imperative to gain knowledge on how masonry buildings may behave and potentially collapse, so as to minimize casualties and injuries to people (Furukawa and Kiyono 2009). Due to the high seismic vulnerability of masonry constructions, research on the seismic behaviour of masonry structures is nowadays very much dedicated to existing buildings with the aim of evaluating and reducing their seismic vulnerability (Magenes 2006).

Performing a structural analysis of a heritage masonry construction is a complex and difficult task (Lourenço 2002) and (Lourenço et al. 2011), given the unknowns about the condition of the building, its history and building phases, the morphology of structural elements, the connection between structural elements, among other aspects. A suitable analysis of a masonry building should include the numerical modelling of its structure, with constitutive laws accurately describing the mechanical behaviour of the material. Then, the model must be calibrated against experimental results to assure the necessary reliability of the results. Nonetheless, to be properly implemented and effectively used, most of the current available tools require a large amount of resources: in terms of money, time, computational effort and knowledge (Vélez 2003).

In the last years, due to increasing awareness in society about heritage buildings, there has been a major advance in modelling and analysis techniques of masonry structures. Several methods of analysis and computational tools are currently available for the assessment of the mechanical behaviour of masonry structures (Freeman 1998; Fajfar and Eeri 2000; FEMA 356 2000; Magenes 2000; Priestley 2000; Chopra and Goel 2001; Vamvatsikos and Cornell 2002; EC8 2003; Penna et al. 2004; Schnept et al. 2007; Lourenço et al. 2007a; Betti and Vignoli 2008a; Binda et al. 2009; Dyavanal and Annigeri 2009; Antoniou and Pinho 2010; Mendes and Lourenço 2010; Penna et al. 2013).

Although the application of modern concepts of mechanics and the constant development of advanced tools for the structural analysis of masonry constructions, there is the need for improved knowledge about important issues such as: constitutive laws that define masonry behaviour; masonry components behaviour; efficiency of connections, among others. These issues can be further studied through experimental testing allied to numerical modelling approaches. Since masonry is a complex material to model due to the inherent anisotropy and variability of properties, only a few authors implemented constitutive non-linear models able to consider different strength and deformation capacity along the material axes, e.g. (Lourenço 2000) for finite elements and (Milani et al. 2007) for limit analysis. These models are not widely disseminated and can be hard to apply in traditional buildings given the difficulties to characterize the existing fabric with a high level of detail. An alternative, lowest-complexity level, solution is to adopt simple geometrical indices, e.g. (Lourenço and Roque 2006), to make a first, non-binding, screening of seismic assessment.

The knowledge obtained by an appropriate seismic evaluation of a structure can be used for the design of an appropriate repair/strengthening intervention (if needed) and enables the study of effects of these strengthening on the considered structure. Actually, recent earthquakes have revealed cases of inadequate implementation of repair/strengthening techniques, mostly due to incompatibility between the existing structure and the intervention technique or materials. The lack of knowledge on the existing materials, on their structural behaviour and interaction with the strengthening are the main causes of the inappropriate choice of the intervention techniques.

The purpose of the present section is to outline some general aspects concerning masonry buildings including the performance of materials and structural behaviour of components. Strengthening techniques currently applied to these buildings are also briefly outlined. The modelling strategies and analysis methods available to assess the seismic behaviour of masonry buildings and applied during the thesis work, are also addressed.

2.2. GENERAL ASPECTS ON MASONRY BUILDINGS

As mentioned above, masonry is the oldest building material used around the world. Therefore, the understanding of the masonry characteristics (composition, mechanical properties, units' arrangement, ratio between units and mortar, etc.) is essential for the seismic assessment of masonry structures.

Masonry is a heterogeneous material because of its constitution: a combination of units connected, or not, by mortar in order to obtain structural elements like walls, pillars, arches and vaulted systems (Casarin 2006). The masonry constituents, units and mortar, present different mechanical characteristics. Units are the resistant elements, while the role of mortar is connecting the single blocks to obtain a solid composite and to distribute and to transmit stresses. The diversity generated by the combination between the arrangement, the characteristics and geometry of units and mortar hinders the characterization of the masonry behaviour. The mechanical behaviour of the different types of masonry generally exhibits a common feature: a very low tensile strength. This property is so important that it has determined the structural shape of historical constructions.

There are significant difficulties in performing advanced tests of existent structures because, besides masonry having numerous variations, it is impossible to characterize the behaviour of the whole structure based on a single specimen. Achieving good characterization of existing structures and materials, detailed enough in order to be used by advanced numerical models, is, most of the time, a very demanding task (Oliveira 2003). Non-destructive and minor destructive tests give valuable data without damaging the building. Unfortunately it does not provide enough information about the characterization of the structural material required by advanced modelling. Though, the feasibility of performing destructive tests on old buildings, either in situ or by removing samples large enough to be representative, is not possible due to conservation issues in most cases. The most conscientious option and the one usually chosen is to perform laboratory tests on masonry specimens representative of real constructions.

The structural performance of masonry depends on several factors and it can only be characterized if the following factors are known: the geometry; the characteristics of its morphology, for instance if they are single- or multiple-leaf walls, and how the connection between the leaves is; the physical, chemical and mechanical components (brick, stone, mortar) and finally, the characteristics of masonry as a composite material (Binda and Saisi 2005). Compressive tests are generally easy to perform and give a good indication of the general characteristics of the materials (Lourenço 2002). Masonry has a non-linear behaviour and manifests a non-ductile post peak softening behaviour, which consists in a gradual strength decrement in a masonry specimen under a continuous increase of deformation. This characteristic is typical of quasi-brittle materials. Figure 2.2 shows the characteristic stress-displacement diagrams for quasi-brittle materials in uniaxial tensile and compression, as well as shear-compression loading (Lourenço 1996a).

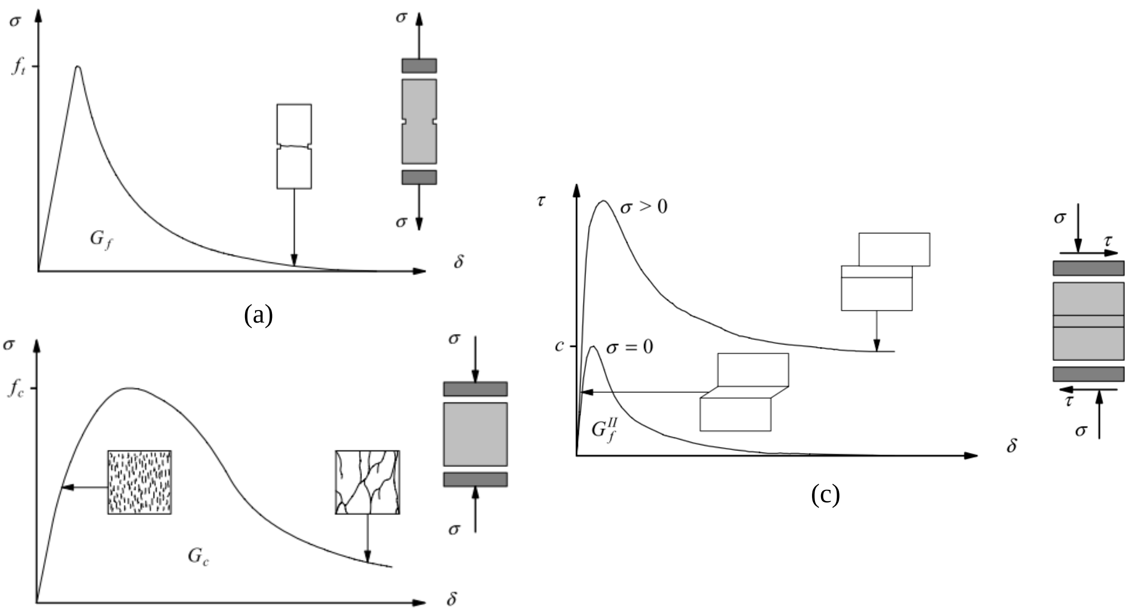

(a)

(b)

(c)

Figure 2.2 Typical behaviour of quasi-brittle materials under uniaxial loading (a) Tensile; (b) Compressive; (c) Shear – compression (Lourenço 1996a).

2.3. SEISMIC BEHAVIOUR

Typical unreinforced masonry buildings are, in general, composed of multiple load-bearing masonry walls arranged in orthogonal planes, with relatively flexible floor diaphragms. In the presence of a seismic event, it is generally assumed, for simplicity purposes, that the direction of the ground motion is parallel to one of the main directions of the building, distinguishing in-plane walls (parallel to the direction of ground motion) and out-of-plane walls (perpendicular to the direction of ground motion). The vertical (walls) and horizontal structural elements (diaphragms) of typical masonry buildings under earthquake excitation are schematically illustrated in Figure 2.3.

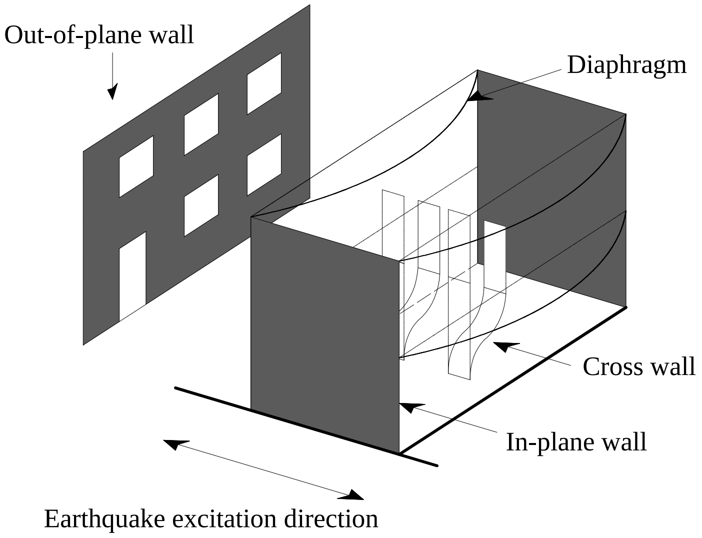

Figure 2.3 Scheme of a typical masonry building under earthquake excitation (adapted from Moon 2004).

The seismic response of a masonry building is defined by the interactions between the in-plane walls, the out-of-plane walls, and the floor diaphragms through their connections. Post-earthquake damage surveys carried out worldwide enabled the characterization of the typical behaviour of masonry buildings under seismic loads. The deformation and typical type of damage in structural walls of a simple masonry building subjected to seismic loads is presented in Figure 2.4. The characteristic damage pattern includes: cracks at the corners and wall intersections, which occurs as a result of insufficient connections; out-of-plane bending due to lack of connection between walls and floors; diagonal cracking in the in-plane walls, among others. Thus, damage in masonry buildings can be essentially interpreted on the basis of two fundamental collapse mechanisms: out-of-plane and in-plane. During an earthquake both out-of-plane and in-plane response are simultaneously mobilized.

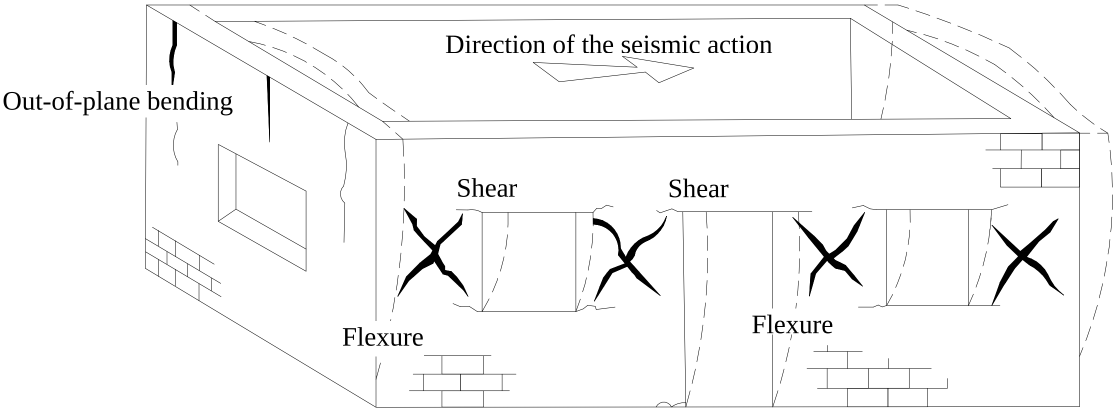

Figure 2.4 Typical deformation and damage of unreinforced masonry buildings under seismic loads (adapted from Tomaževič 1999).

Masonry buildings represent a box-type structural system with vertical structural elements, walls, connected to horizontal diaphragms, floors and roof. Considering the typical structural organization of these elements, the capability of the structures to redistribute horizontal loads depends on the connection between orthogonal walls, the flexibility of the diaphragms and their connection to the masonry walls (Lourenço et al. 2011). The combination of the referred aspects provides the so called “box behaviour” to the building, which usually leads to a good performance of the structure when subjected to horizontal actions (Lourenço et al. 2009; D’Ayala 2011). However, the hypothesis of the box behaviour is very often far from the reality of the building response since it depends on the connections between elements and on the diaphragm stiffness. In the majority of the cases the structural elements behave separately.

Evidence from the recent 2011 New Zealand earthquakes, among many others, confirmed that out-of-plane wall collapse was one of the main collapse mechanisms observed in masonry buildings, which is strongly dependent on the connection quality (Senaldi et al. 2012). When not properly connected to the roof, floors and perpendicular walls, a masonry wall can easily become unstable and collapse out-of-plane, compromising in this manner the global capacity of the structure. When walls are seismically excited in their own plane, the excitation has generally a small amplification because of the large stiffness and low natural period. On the contrary, walls subjected out-of-plane present a quite large seismic amplification, due to their low stiffness and high natural period.

Hence, the structural performance of traditional masonry buildings to seismic actions depends on their capability to redistribute the horizontal loads through vertical elements, which allows exploring in-plane strength of the walls at its maximum and preventing local out-of-plane mechanisms. Assuming that the quality and state of conservation of vertical elements is good and that the horizontal elements have enough stiffness to redistribute horizontal actions, the building global performance is greatly influenced by the effectiveness of the connections between vertical elements and between vertical and horizontal elements. If these connections are ineffective, a global behaviour cannot be achieved and the building may collapse under the effect of low seismic excitations by developing local mechanisms (see Figure 2.5 for local and global mechanisms).

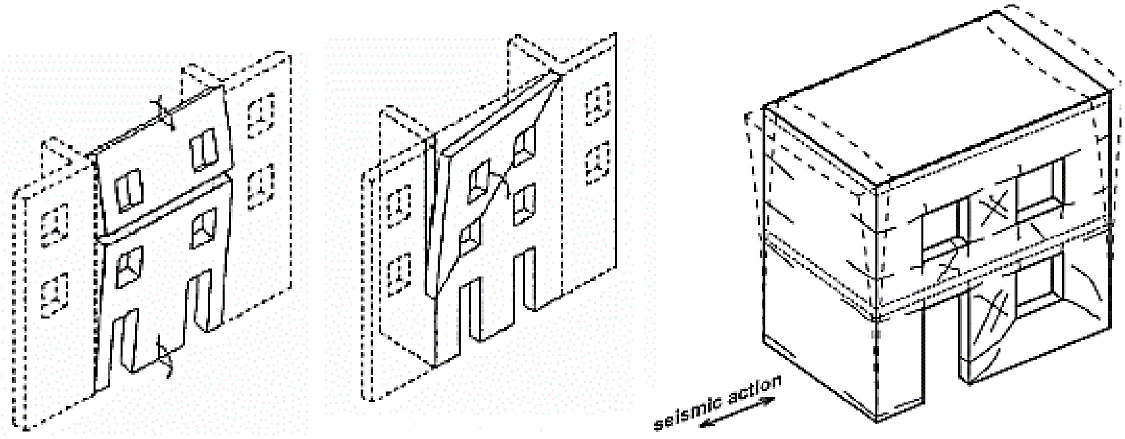

(a) (b)

Figure 2.5 Examples of collapse mechanisms in buildings (a) Local out-of-plane, (b) Global in-plane (Magenes 2006).

In existing masonry buildings, local collapses often occur in case of an earthquake, generally due to loss of equilibrium of masonry parts, rather than a global failure mode associated with lack of integrity of the structure. Post-earthquake surveys and experimental research, conducted in the last years regarding the effects of earthquakes on ancient buildings, allowed the compilation of the typical seismic failure/collapse mechanisms associated to different masonry building types in an abacus in the form of graphical interpretation schemes (Lagomarsino 1998a; D’Ayala and Speranza 2002; Di et al. 2002; Binda et al. 2006; Cóias 2007; Franchetti 2009). This abacus represents local failures (loss of equilibrium) in different parts of the structure and was developed for religious and civilian constructions (isolated or aggregate constructions). Some examples are presented in Figure 2.6. The position of the openings (doors and windows) strongly affects the behaviour of the collapse mechanism, both for in-plane and out-of-plane failures.

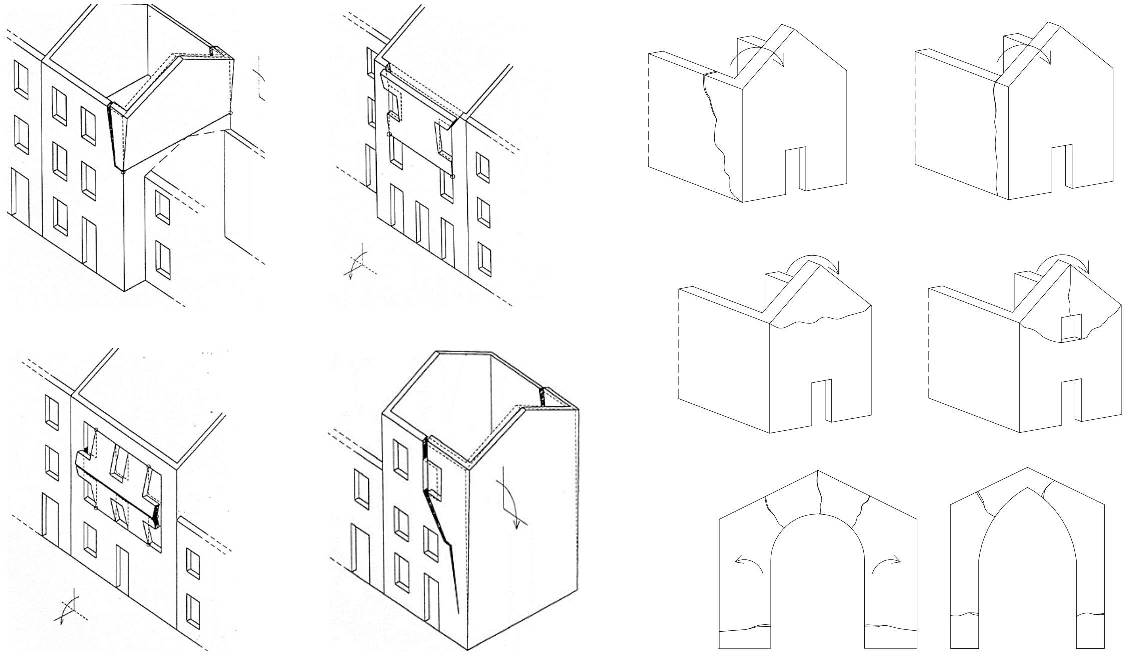

(a) (b)

Figure 2.6 Abacus of damage mechanisms (a) Civil constructions; (b) Religious constructions (Lagomarsino 1998b; Beolchini et al. 2002; Binda et al. 2006; Franchetti 2009).

2.3.1. Diaphragms

It is not commonly observed in previous earthquakes that the failure occurs in the wood diaphragm itself (Yi 2004). Instead, observed seismic damage in unreinforced masonry structures often includes out-of-plane failures of walls as a result of excessive deflections of diaphragms and insufficient connections between them. As stated above, the interaction between diaphragms (floors and roof) and out-of-plane walls can compromise the seismic response of the entire building. This interaction is governed not only by the diaphragm stiffness but also by the strength and stiffness of the connections between these two elements.

The walls' response to a given seismic action excites the floor diaphragms in their borders (Paulay and Priestley 1992). The structural system has to be capable of transferring forces from the out-of-plane walls through the diaphragms to the in-plane walls (Moon 2004). If the floor diaphragm is rigid, it acts as a hinge support to the out-of-plane wall and the displacements and accelerations in the floor will be equal to the wall in the connection (Paulay and Priestley 1992; Yi 2004). Contrarily, if the floor is flexible the displacements and accelerations of the floor borders and walls are not the same, and the support of the floor to the out-of- plane masonry walls can be consider like a spring support (Paulay and Priestley 1992; Yi 2004). A floor with greater rigidity is able to transmit forces to the masonry more effectively with respect to a floor with greater flexibility. Flexible diaphragms typically exhibits significant bending and shear deformations under lateral forces. Most of masonry buildings are constructed with wooden floor and roof diaphragms that are rather flexible and are often poorly tied into the walls (Park et al. 2008).

Most of the Portuguese traditional buildings are made of unreinforced stone masonry walls and flexible timber diaphragms, with the exception of a few cases in which the timber floors and roofs provide efficient in-plane stiffness (Vasconcelos 2005). So, most of the diaphragms in existing masonry structures are rather flexible leading to large acceleration amplifications when subjected to horizontal loads (Moon 2004).

However, inappropriate use of techniques to increase the floor in-plane stiffness, for instance the introduction of concrete floors, leads to an increase in mass with the increase of seismic loads thus compromising the seismic response of the structure. A proper retrofit strategy for existing masonry buildings should account for the influence of the diaphragm flexibility and mass distribution on the response of the entire structure. Some experimental research has been conducted on the seismic behaviour of masonry buildings with relatively flexible diaphragms (Moon 2004; Yi 2004; Magenes et al. 2010a). Recently, Senaldi et al. (2013) carried out an extensive experimental work through full scale shaking table tests to study the influence of stiffened floor and roof diaphragms on the seismic response of a stone masonry building. For that purpose, a representative of existing stone masonry structures building with flexible wooden diaphragms was tested. Two other buildings, identical to the first one, were strengthened with the aim at improving the wall-to-floor and wall-to-roof connections and increasing diaphragm stiffness. Successful results were obtained for the strengthened buildings, which ensured a global response, preventing the occurrence of local failure mechanisms, through the enhancement of connections between walls and floors and the stiffening of floor and roof diaphragms. A critical discussion regarding the influence of the in-plane stiffness of the diaphragms on the overall seismic performance of masonry buildings is also addressed by Brignola and Podestà (2009).

So, to guarantee the box behaviour, assuring that the horizontal forces are absorbed by the walls in their plane, three conditions have to be accomplished: sufficiently and suitable rigid diaphragm; adequate connection between walls and appropriate wall-floor and wall-roof link.

2.3.2. Out-of-plane behaviour

The out-of-plane failure of unreinforced masonry walls constitutes the most serious life-safety hazard for masonry buildings. For this reason, the out-of-plane failure is the most demanding and represents the response of masonry walls to horizontal actions perpendicular to their plane, which generally fail by overturning (Casarin 2006).

Surveys of seismic damage in masonry structures lead to conclude that the collapse often includes out-of-plane failures of walls, driven by excessive deformation of diaphragms and the insufficient connections among them (Magenes and Calvi 1997). However, this type of failure can be prevented if sufficient anchorage is provided between walls and floors and effective connection between in-plane and out-of-plane walls.

This type of failure is typically local, usually happening in structural elements causing the collapse of parts of the building. Figure 2.7a presents an out-of-plane rotation of the facade due to lacking of connection between orthogonal walls and diaphragms. An out-of-plane collapse, with the overturning of the façade walls of the top floor, is shown in Figure 2.7b for a building damaged by the 2011 Christchurch earthquake. This failure was a result of the lack of connection between internal and exterior walls not allowing the box behaviour to develop. An example of a failure mechanism caused by the inadequate consolidation of the walls with the rigid floor is presented in Figure 2.7c. Finally, Figure 2.7d presents an example of the overturning of a corner wedge due to ineffective connection between external walls, insufficient anchoring of the floors to the perimeter walls and the presence of openings near the edges (the crack line often follow the distribution of the façade openings).

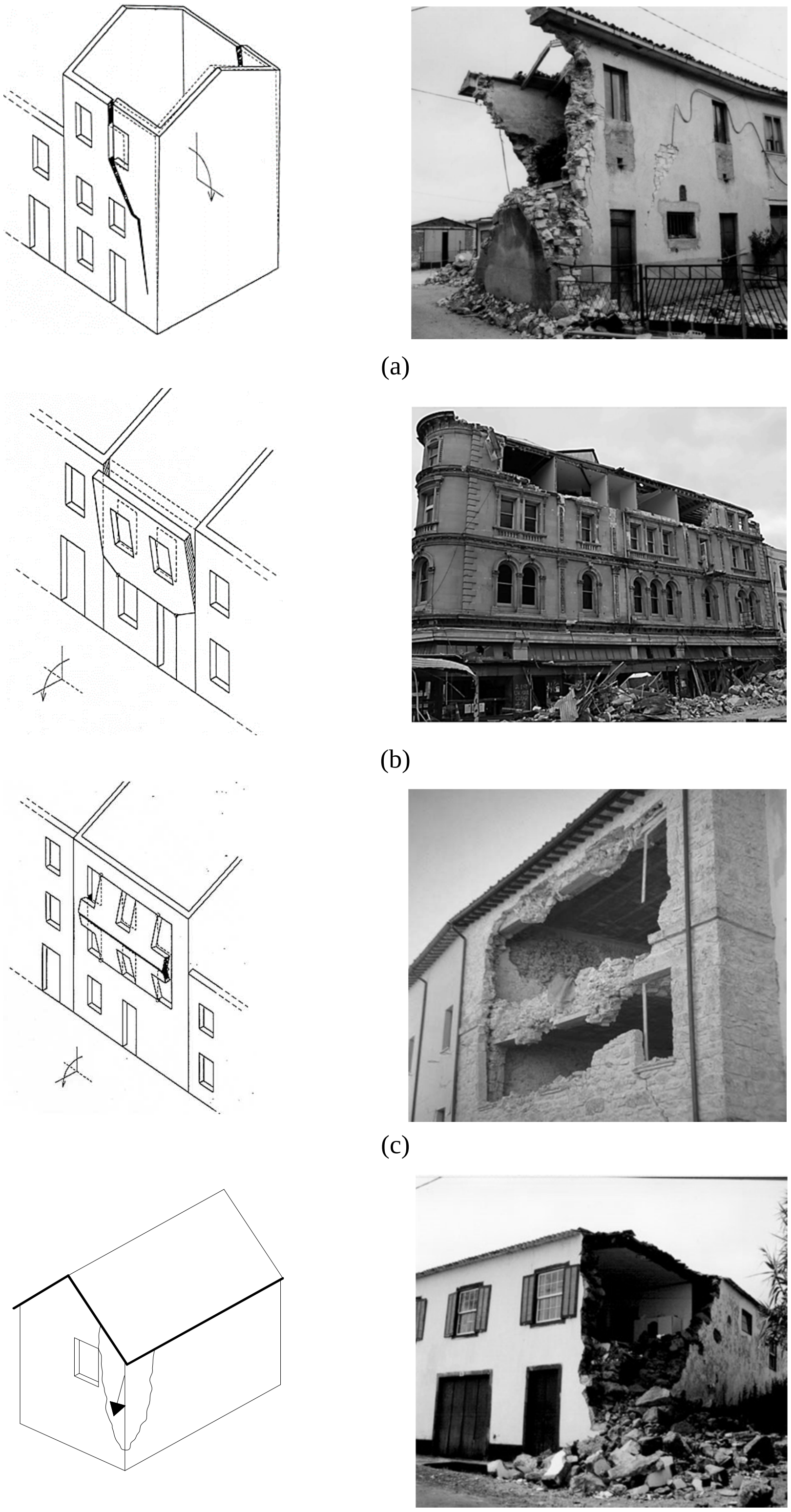

(a)

(b)

(c)

(d)

Figure 2.7 Examples of out-of-plane failures during earthquakes: (a) Overturning of façade; (b) Overturning of portions of the façade; (c) Partial overturning of façade (effect of openings) (Binda et al. 2006); (d) Overturning of corner wedge (Lagomarsino 1998b; Beolchini et al. 2002; Binda et al. 2006; Franchetti 2009).

2.3.3. In-plane behaviour

The in-plane behaviour of masonry walls can be activated when an effective overall building response is accomplished by preventing brittle out-of-plane failure with appropriate connections between elements. Therefore, if connections are improved by appropriate reinforcement systems (for instance: steel ties at the floor levels, reinforcement solutions for the connections) in order to prevent local mechanisms, a global behaviour governed by the wall in-plane response can then develop.

Examples of typical in-plane failures verified during past earthquakes are presented in Figure 2.8. The damage verified in the in-plane walls is remarkably different from the damage caused by an out-of-plane failure (Figure 2.7 and Figure 2.8). Out-of-plane failures often involve the collapse of part of the structure, which not verified for the in-plane failures.

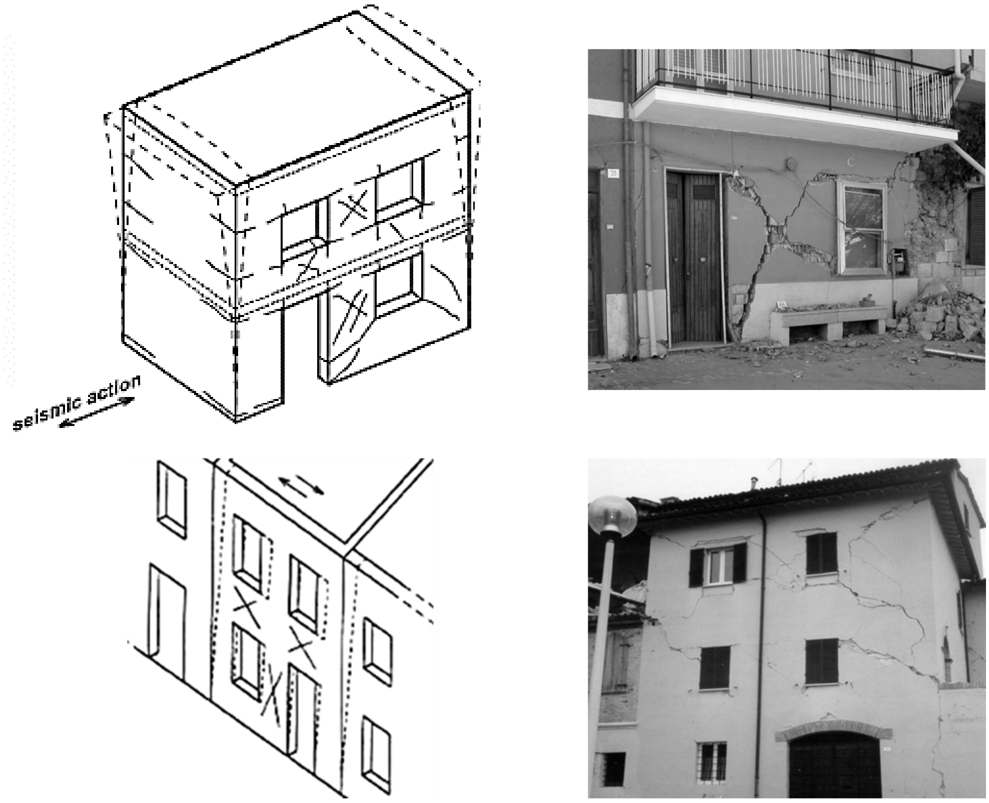

Figure 2.8 Examples of in-plane failures (Beolchini et al. 2002; Magenes and Griffith 2009a).

Methods to assess the seismic performance of existing masonry buildings based on the individualization of the in-plane response of structural walls are well known and have been extensively used. The POR method was developed in the 1980s and considers a storey failure mechanism in which the global response of each storey in terms of base shear-storey displacement is computed as the sum of the individual response of each wall (Tomaževič 1978). The structure is schematized taking into account only the resistance of the vertical masonry elements. This method assumes the following basic hypotheses: infinitely rigid floors in their plane; box behaviour; decomposition of the building in resistant walls; only translation in the panel ends and elastic-plastic material. Likewise, the simplified linear static analysis presented in FEMA 356 (2000) assumes the decomposition of the building in resistant walls which are relatively rigid elements. In case of linear analysis, the safety verification with reference to the ultimate limit state consists in the comparison between the resistance of each structural element and the action for each failure mechanism. This last method is further discussed in Chapter 5.

In a common masonry wall with openings (doors and windows) two main elements can be distinguish: piers, which are the shear walls between openings, and spandrels, which are the beams above and below openings (see Figure 2.9) Piers are the principal vertical resistant elements to seismic loads. Generally, in-plane failures occur in only one of these two elements, and the final collapse of masonry structures is usually a result of pier failure (Calvi et al. 1996).

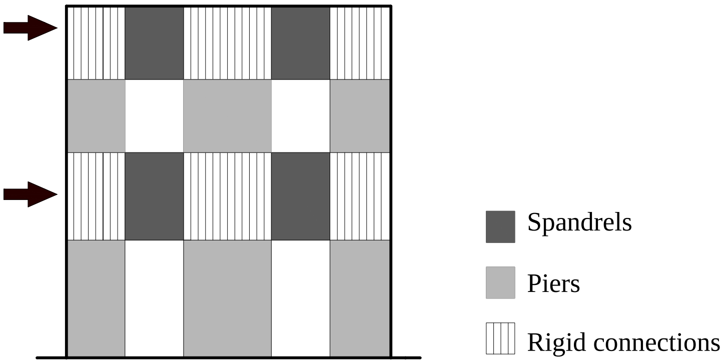

Figure 2.9 Typical in-plane masonry wall and main structural elements (adapted from Calderini et al. 2008).

According to post-earthquake surveys and experimental studies, four types of failure mechanisms define the behaviour of structural masonry walls under in-plane seismic actions: rocking and toe crushing (flexural); sliding and diagonal cracking (shear) (Moon 2004; Calderini et al. 2008). Various publications (Magenes and Calvi 1997; Tomaževič 1999; Mallardo et al. 2008) identify a total of three failure modes, in which rocking and toe crushing are not considered separately, being instead named flexural failure. Rocking occurs when the wall begins to behave as a nearly rigid body rotating about the toe, usually when the vertical load is low in relation to compressive strength of the pier and the horizontal load produces a flexural motion making the pier bend around the toe (Figure 2.10a). Toe crushing failure, typically observed after rocking deformations, is usually associated with the compressive failure of masonry occurring at the toe of the pier (Figure 2.10b). This failure mode typically happens when the vertical load applied is high and the horizontal load causes progressive sub-vertical cracks in the corner of the pier.

The sliding failure is characterized by the wall deformation by sliding along a horizontal bed joint plane, usually located at one of the extremities of the pier (Figure 2.10c). Within the diagonal cracking mode the failure occurs due to the formation of diagonal cracks that usually develop in the centre of the wall and propagate toward the corners (Figure 2.10d). This failure mode generally occurs in the bond between unit and mortar because this is often the weakest link in masonry assemblages (Lourenço 2002). The cracks propagate through the mortar joints, in a stair-stepped manner, or directly through the units depending on the relative strength of the bond and units. Walls will fail in the weakest of these failure modes and its occurrence depends mainly on the wall's geometry (relation between height and width), boundary conditions, compression stress state and masonry mechanical properties.

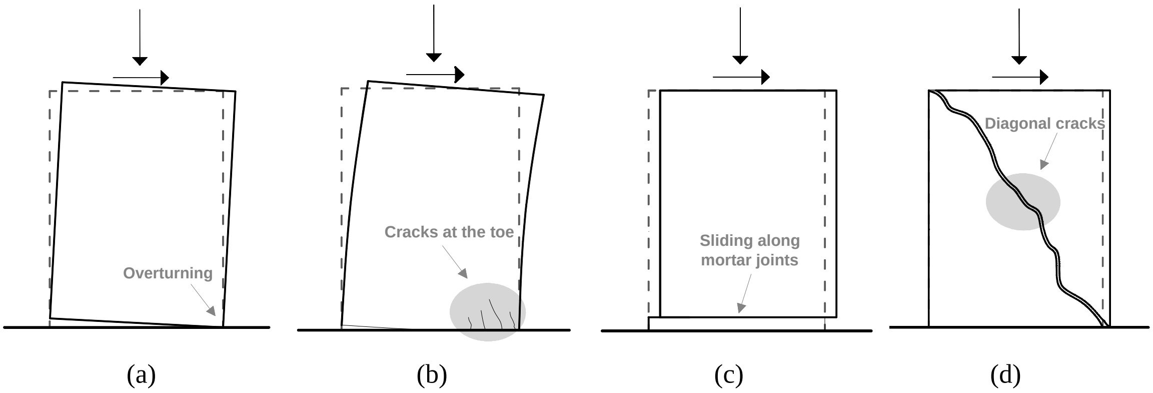

Figure 2.10 Typical failure mechanisms of masonry piers: (a) Toe crushing; (b) Rocking; (c) Sliding; and (d) Diagonal Cracking (adapted from Moon 2004 and Calderini et al. 2008).

These four failure modes can be classified according to the type of behaviour: deformation-controlled or force-controlled modes, see Table 2.1. Toe crushing and diagonal cracking failures are force controlled since is the applied horizontal force that governs the capacity of the pier, while rocking and sliding behaviour are controlled by the displacements of the pier since the instability is attained for a certain maximum displacement. Typically these last failure modes can exhibit large deformation capacities.

Table 2.1 In-plane failure modes.

Mode	Flexure	Shear
Force Controlled	Toe Crushing	Diagonal Cracking
Displacement Controlled	Rocking	Sliding

The characterization of the behaviour of historic masonry walls due to in-plane loading has been carried out by several authors thorough experimental campaigns (e.g. (Anthoine et al. 1995; Oliveira 2003; Vasconcelos 2005; Angelini et al. 2007; Seki et al. 2008; Magenes et al. 2008b; Elmenshawi et al. 2010; Magenes et al. 2010b; Capozucca 2011; Silva 2012; Churilov and Dumova-Jovanoska 2013)). Still, the huge number of possible combinations generated by geometry, mechanical properties of masonry, compressive stress state as well as boundary conditions are a permanent challenge for the characterization of masonry walls. Numerical analysis can be considered as auxiliary to experimental tests, allowing the assessment of masonry walls in-plane behaviour when varying some parameters without the need of extensive experimental work. For instance Anthoine et al. (1995), Annecchiarico et al. (2009) and Silva (2012) carried out numerical simulations as a complementary study of the experimental tests with this purpose.

Analytical formulations able to describe the behavior of each failure mode are available in literature (Turnsek and Cacovic 1971; Turnsek and Sheppard 1980; Mann and Muller 1982; Magenes and Calvi 1997; FEMA 356 2000; EC8 2003; NZSEE 2006; NTC 08 2009) and will be detailed discussed in Chapter 3.

2.3.4. Connections

Efficient connections between elements allow for the proper load transmission between out-of-plane walls to the more stable in-plane walls, thus avoiding local collapses, which, according to known earthquakes (Azores 1998, L'Aquila 2009 and Christchurch 2011) are the main cause of fatalities and cultural losses. Accordingly, the behaviour of single connections between structural elements can converge into an adequate global structural response of these buildings (D'Ayala 2011). Assuming that the quality and state of conservation of vertical elements is good and that the horizontal elements have enough stiffness to redistribute horizontal actions, the building global performance is greatly influenced by the effectiveness of the connections between vertical elements and between vertical and horizontal elements. If these connections are ineffective, a global behaviour cannot be achieved and the building may collapse under the effect of low seismic excitations by developing local mechanisms. Furthermore, the connections between the floor diaphragms and the masonry walls play an important role in the nonlinear behaviour of structure.

As can be seen in Figure 2.11, the response of a masonry building to an earthquake excitation strongly depends on how the walls are interconnected and anchored at the floor and roof levels. In the presence of a flexible floor to which walls are not tied, vertical cracks develop along the joints between walls at corners and intersections, leading to a possible out-of-plane local mechanism (Figure 2.11a). If the walls are well tied between them and connected with the floor, with a flexible or rigid diaphragm, the building vibrates as a monolithic structure (Figure 2.11b and Figure 2.11c). One of the basic condition to seismic resistance, the energy dissipation capacity of a building, can be significantly improved if a monolithic behaviour is ensured. Thus, the efficiency of the connections between structural elements determinates the behaviour of the building during an earthquake and can be a decisive factor in terms of whether or not collapse occurs under those conditions.

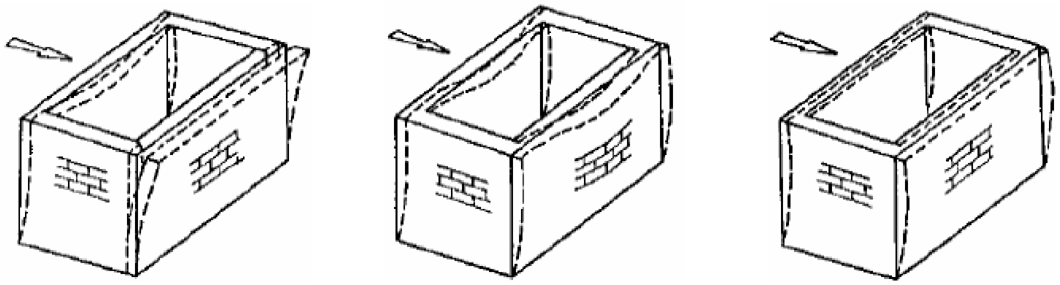

(a) (b) (c)

Figure 2.11 Typical seismic behaviour: (a) Flexible floor and weak connection between orthogonal walls; (b) Flexible floor and good connection between orthogonal walls; (c) Rigid floor and good connection between orthogonal walls (Tomaževič 1999).

2.4. STRENGTHENING TECHNIQUES

Different strengthening techniques have been developed to mitigate failure mechanisms that develop on masonry buildings during earthquakes. The intervention solutions for masonry buildings can be performed at an individual or global level, by improving the behaviour of specific structural parts of the buildings or by ensuring the monolithic behaviour of the structure (box behaviour). Some current solutions are referred hereafter, but not aiming to cover all possibilities of intervention. As this thesis includes the strengthening of connections using anchors, special attention to this technique is given here.

2.4.1. Walls and floors

Within the methods to improve the seismic capacity of masonry walls, the repointing of the masonry joints with an appropriate mortar is recurrent. (Corradi et al. 2008). Deep repointing of mortar joints consists in the removal of the deteriorated mortar and its substitution with new materials, which have better characteristics in terms of strength and durability. The typical construction of stone masonry walls, characterized by two outer leaves of stones with inner infill of smaller pieces of stones bonded with generally poor lime mortar, commonly creates many voids between the components. The filling of voids by injection of better quality cement mortar can considerable improve the resistance of a wall by restoring its continuity (Tomaževič 1999; Moon 2004).

The strengthening of walls by lateral confinement can also significantly improve the resistance and energy dissipation capacity of these elements (see Figure 2.12). Its purpose is to confine the cross section of the walls, especially walls composed by multiple leaves, promoting its structural integrity through a good bond between facings (Roque 2002). On the other hand, the application of FRP composite materials for strengthening masonry walls is an innovative and emerging retrofitting technique (Moon 2004). Bonding the walls with FRP is used to increase the strength and ductility of walls subjected to in-plane or out-of-plane loading (Valluzzi 2002; Marcari et al. 2007; Alcaino and Santa-Maria 2008; Zhuge 2008; Nardone et al. 2009).

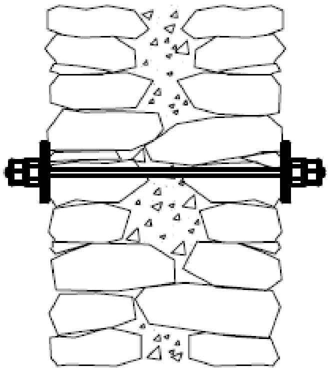

Figure 2.12 Transversal ties in masonry walls (Lamego 2014).

The main role of floors in the seismic behaviour of a masonry building is to transfer the horizontal actions through the vertical elements. There are different timber floor strengthening techniques to improve the in-plane stiffness. Few research works were carried out to characterize the original flexible timber floors and roofs and to study compatible techniques for their strengthening (Baldessari et al. 2009; Branco 2009; Gattesco 2009).

2.4.2. Connections

Besides the strengthening of individual structural walls, special care should be put in the strengthening of the connections in order to ensure structural integrity. The seismic response of masonry buildings to past earthquakes showed that the strengthening of connections between structural components (walls and floors) can enhance the global seismic performance in a significant way. Senaldi et al. (2012) presents some successful examples of retrofitted masonry buildings that survived to the recent 2011 NZ earthquake without suffering major damage. It was observed that the strengthening of connections using anchoring systems and the insertion of steel tie rods at floor and roof levels proved to be effective in preventing local out-of-plane collapse of walls under seismic events.

Improvement of the structural integrity of masonry buildings with steel ties, generally introduced at the floors level is an ancient and a recurrent practice, perhaps even the solution most often adopted in the past, in different times and cultures (Gavrilovic and Jekic 2009; Sendova et al. 2009). By connecting all the structural elements of the building, this technique can enhance in an effective way the seismic overall response of the structure.

The performance of connections in masonry buildings has been studied by a few authors, either evaluating the behaviour of a single connection or analysing the effect of connections on the global behaviour of a building. For example, the use of steel to strengthen ancient masonry buildings has been observed since the 1920s (Wenzel and Maus 1992). Some other examples of traditional and innovative strengthening solutions for connections can be found in (Magenes 2006; Mandara et al. 2009; Mazzolani et al. 2009; Modena et al. 2010). On the other hand, a dissipative device to improve the connection of perpendicular walls was recently proposed (D’Ayala and Paganoni 2014).

Injected anchors are particularly well suited to repair and strengthen ancient masonry buildings as they allow for an effective connection between elements, thus avoiding overturning of walls excited out-of-plane. Injected anchors are a common strengthening method for masonry buildings and a number works are available in literature (Wenzel and Maus 1992; Gigla and Wenzel 2000; Arifpovic and Nielsen 2004; Gigla 2004; Meyer and Eligehausen 2004; Weigel and Lyvers 2004; McGinley 2006; Algeri et al. 2010; Haman and Jaeger 2011). However, there is an evident lack of experimental and numerical studies to characterize the behaviour anchors applied to ancient masonry, which are necessary for a clear characterization of the structural behaviour of this strengthening solution.

Figure 2.13a illustrates a possible strengthening solution for the improvement of the behaviour of wall-to-floor connections using two parallels anchors injected in the masonry wall, linked to the floor with L-shape steel plates. Equally, a solution for the improvement of the connection between external and internal walls is shown in Figure 2.13b, consisting of two parallel anchors injected in the external masonry wall and connected to the internal wall by means of suitable steel plates. Due to its importance, injected anchors will be further addressed in Chapter 4.

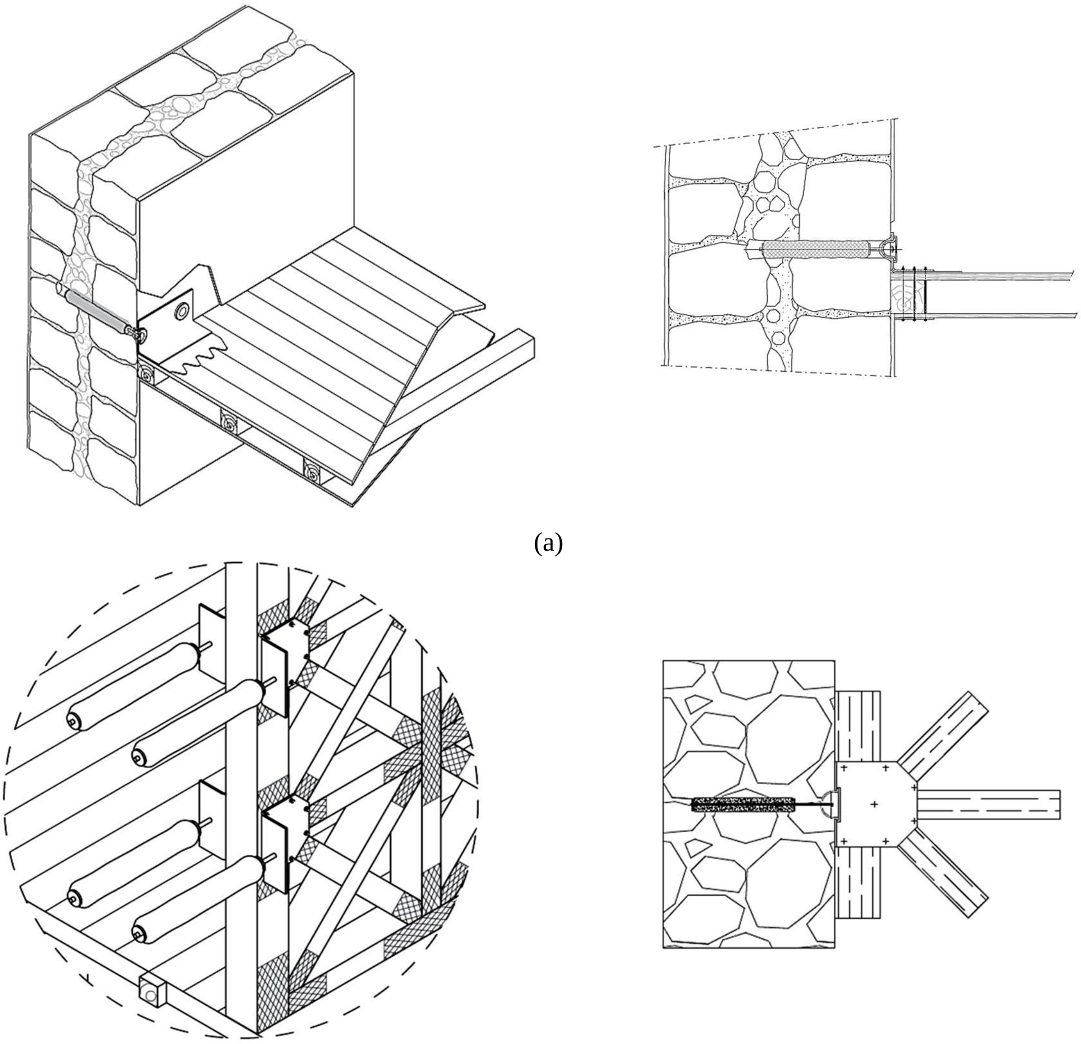

(a)

(b)

Figure 2.13 Strengthening techniques using injected anchors for the connection between structural elements: (a) Wall to floor connection; (b) Wall to half-timber-wall connection (Moreira et al. 2012).

Although experimental campaigns aiming at studying the behaviour of injected anchors in both brick and stone masonry walls have been carried out by a number of researchers (Meyer and Eligehausen 2004; Arifpovic and Nielsen 2004; Gigla 2004; Algeri et al. 2010; Haman and Jaeger 2011), the design of injection anchors for masonry is still a challenge due to the lack of codes and recommendations regarding the estimation of the strength capacity. A detailed discussion on the analytical formulations available in literature is carried out in Chapter 4.

2.5. ANALYSIS METHODS AND MODELLING ISSUES

The analysis methods to assess the seismic behaviour of masonry buildings have been progressively developed. The need for more suitable methods for the analysis of heritage masonry structures has stimulated the research on this subject and as a result numerical analysis methods have made significant progress in the last decades. Advanced analysis methods have been developed combining accurate material description and structural models, particularly in the field of finite element analyses (Orduña 2003).

The assessment of the seismic behaviour of masonry structures or substructures can be obtained by applying a static or dynamic analysis with linear or non-linear behaviour. In addition, masonry buildings can be studied by limit analysis, evaluating the main failure mechanisms likely to occur, in order to obtain the mechanism that triggers the collapse and the corresponding load at failure. Figure 2.14 presents a scheme that groups the main analysis methods used for the seismic analysis masonry structures.

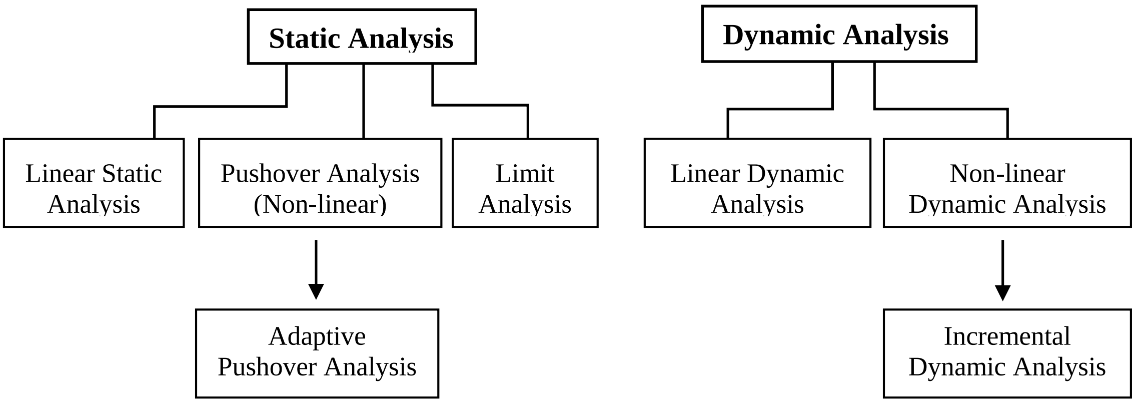
Static Analysis
Dynamic Analysis
Linear Static Analysis
Pushover Analysis (Non-linear)
Limit Analysis
Linear Dynamic Analysis
Non-linear Dynamic Analysis
Adaptive Pushover Analysis
Incremental Dynamic Analysis

Figure 2.14 Analysis methods.

In general, linear static analyses are not appropriate for ancient constructions, considering that masonry presents non-linear behaviour since very low load levels due to the low tensile strength of masonry (Orduña 2003). The non-linear nature of masonry behaviour and the intrinsic dynamic aspect of seismic actions suggest that the best option to evaluate the vulnerability of a building to an earthquake is considering both the non-linearity of the material and the dynamic nature of the excitation.

Non-linear dynamic analysis with time integration is the most powerful method, which, provided with accurate and appropriate constitutive models, can give very rigorous results. Here the action is characterized by sets of natural, synthetic or artificial accelerograms. Response time histories analyses are obtained from numerical integration of differential equations of motion, considering the inertia and damping effects. Another non-linear dynamic approach is the incremental dynamic analysis. This is a parametric method and consists on subjecting the structure to a series of nonlinear time-history analyses of increasing intensity to estimate the structural capacity under earthquake loading. Incremental dynamic analysis provides a continuous picture of the system response, from elasticity to yielding and final to collapse and the results of this method are plotted a curved of response parameterized versus the record intensity level (Marcari and Abrams 2009) (Vamvatsikos & Cornell, 2002). The main objective of this approach is attaining a more accurate indication of the nonlinear dynamic response of a structure under earthquake action. Examples of the application of incremental dynamics analysis to the seismic evaluation of structures can be found in literature (e.g. Mander et al. 2006; Lu et al. 2010). However, non-linear dynamic analysis requires very qualified analysts to perform and interpret the results; is a very time and cost consuming approach and requires for detail characterization of the mechanical behaviour of masonry. Hence, the intrinsic complexity and the additional computational effort makes the application of this method limited, typically used to evaluate the seismic resistance of valuable assets.

In linear dynamic methods, linear-elastic behaviour of the structure is considered and the seismic action simulated as dynamic. The usual approach is to use a modal analysis of a structure considering all the vibration modes and simulate the seismic action through a response spectrum. In this analysis method the non-linear material behaviour is studied by using global behaviour factors. As stressed by Lourenço (2001), the consideration of linear elastic behaviour for historical masonry structures is, generally, not recommend due to the strong non-linearity that masonry presents.

During the last few years, displacement-based methodologies, such as the pushover analysis, are being more and more recognized as practical and suitable tools for the evaluation of the seismic response of existing structures (Magenes 2000; Salonikios 2003). Pushover analysis can be an effective alternative to traditional methods of linear seismic analysis considering the difficulties related to non-linear time-history analysis (Augenti and Parisi 2009). The complexity and computational demand required by nonlinear dynamic analysis led to the development of new methods for the seismic assessment based on a simplified mechanical approach. These have been consolidated during the 1990s, as the capacity spectrum method (Freeman 1998) and N2 method (Fajfar and Eeri 2000) and were considered within modern regulations both for designing new structures and assessing existing ones (FEMA 356 2000; EC8 2003; OPCM 2003).

Pushover analysis includes material nonlinear behaviour and the seismic action is simulated by static horizontal forces. Pushover analysis has been gaining significance over recent years as a tool for the assessment of masonry structures (e.g. Casarin 2006; Galasco et al. 2006; Betti and Vignoli 2011; Lourenço et al. 2011; Araújo et al. 2012; Simões et al. 2012; Simões and Bento 2013). Many different approaches of pushover analysis are available depending on the load pattern chosen, being the most common: uniform distribution; proportional to the mass and proportional to the vibration modes. The uniform load pattern approach presupposes the linear distribution of the displacement along the height. In the proportional to the mass pushover approach, the seismic effect is defined by the base shear coefficient, which defines the percentage of the total weight of the building that must be considered as a horizontal force applied to the structure. The proportional to the mass analysis has been carried out for several researchers (Romano 2005; Casarin 2006; Mendes and Lourenço 2010; Betti and Vignoli 2011; Araújo et al. 2012; Simões et al. 2012). The modal proportional load pattern is obtained by applying a quasi-static horizontal load derived from the critical mode shapes of the structure or the fundamental vibration mode (Chopra and Goel 2001; Antoniou and Pinho 2004; Kalkan et al. 2006; Pan and Ohsaki 2006; Ferracuti et al. 2009).

The structural model of a masonry building should contemplate and simulate all the aspects that influence the structural response, including the geometry and morphology of the building, the material properties, the external actions, existing alterations and damage and the soil-structure interaction. However, the structural modelling approach must balance the realism with the model preparation efforts and time of the analysis, keeping the model as simple as possible. Fully three-dimensional models are usually very time-consuming: both in preparing the model, in performing the computation and mostly in analysing the results.

Advanced and complex numerical models are usually used for comprehensive analysis of single elements. After a calibration/validation process against experimental data, these models become valuable tools for carrying out parametrical analyses using different boundary conditions, type of loads and materials properties, connections, among others. A global model of the structure is generally used when the building resistance to seismic actions is provided by the combination of all the structural parts, such as floor diaphragms and in-plane response of structural walls.

The numerical representation of masonry can generally focus on the micro-modelling of the individual components, units and mortar, or the masonry as a composite. In the continuum finite element modelling approach, masonry is modelled as an equivalent material, rather than modelling units and mortar separately. The equivalent continuum models must represent the masonry intrinsic structure by means of appropriate constitutive relations, for example, derived from homogenization techniques (Lemos 2007; Lourenço 2009a).

Finite element analysis can be very time and computational consuming. For this reason, several methods based on macro-element discretization have been developed, requiring a low computational effort (Magenes 2006). The macro-model is an assembling of blocks attempting to represent the mechanical behaviour of the structure and already implemented in TreMuri and SAM II software. Normally the models are elaborated according to the damage observed in the structure and also taking into account the typical failure mechanisms reported in the literature (addressed in section 2.2.1).

The consideration of an analysis instead of another relies in several aspects. Firstly, an essential point is taking into consideration the compatibility of the analysis tool with the information sought, which also depends obviously of the geometry and structural characteristics of the building. Besides, the engineer must have depth knowledge regarding the analysis tool and method to be applied. At last, a good accordance between available financial resources, time requirements and accuracy of results is requested. The distinct methods of analysis have different computational and time efforts as well as different levels of accuracy. The idea of combining different analysis procedures for the assessment of masonry constructions is legitimately and widely diffuse (Brencich et al. 2001; Lourenço and Mourão 2001; Mele et al. 2003; Casarin 2006).

Chapter 3

IN-PLANE BEHAVIOUR OF MASONRY WALLS

3.1. INTRODUCTION

Bearing in mind the typical lay-out of a traditional masonry building, stone masonry walls are the most relevant structural element in the seismic response of the whole structure since they represent the basic resisting elements to horizontal actions. Masonry walls play an important role since besides withstanding vertical compressive forces, they are expected to resist to in-plane lateral loads usually induced by wind and earthquakes, which are transferred to them primarily by horizontal diaphragms. Post-earthquake investigations have shown that, once the out-of-plane mechanisms are prevented by proper measures, the seismic response of a building depends on the in-plane strength capacity of its walls. Consequently several investigations were done in the past to characterize the in-plane behaviour of masonry walls. A large majority of these studies consist of experimental campaigns, testing the shear resistance of piers. Nevertheless, very few of the latter focus on carrying out numerical studies, disregarding the potential of a computational lab.

This Chapter presents the study of the in-plane behaviour of masonry walls with different slenderness ratios and distinct levels of axial load, based on the experimental campaign performed at the EUCENTRE and University of Pavia on double leaf stone masonry piers (Galasco et al. 2010; Magenes et al. 2010b). The behaviour of the masonry walls subjected to compressive and shear loading was studied using advanced numerical simulations. Several numerical simulations were performed, starting with linear elastic analysis comprehending the global model response. First, numerical models were calibrated on the basis of results that emerged from the experimental campaign. Afterwards, validated models were used to carry parametric analysis varying the geometric wall configuration and pre-compression level, in order to evaluate the influence of these parameters on the in-plane behaviour.

As stressed in Chapter 2, masonry walls can suffer distinct failure modes depending on several parameters, including the pre-compression level and slenderness ratio. Numerical simulations using appropriate validated models can provide reliable results, particularly useful to carry out parametric studies, nearly impracticable from the experimental point of view due to time, and resources limitations. The confidence in these computational predictions rely on the validation of the numerical model against experimental results.

The drift capacity of the studied masonry walls is also outlined here, including the comparison and discussion with the drift limits imposed by codes. For this purpose, the mechanical properties of masonry were also varied, in order to obtain more extensive data. As the boundary conditions influence in the drift capacity, they are also addressed in this section.

Finally, the usage of the available simplified formulations to predict the strength capacity of walls is discussed. Analytical formulations have been developed and documented, trying to characterize the in-plane wall strength and taking into account the behaviour of different failure modes, by several researchers (Turnsek and Cacovic 1971; Turnsek and Sheppard 1980; Mann and Muller 1982; Magenes and Calvi 1997; Tomaževič 1999). Furthermore, guidelines have been proposed, e.g. in New Zealand (NZSEE 2006) and by the American Society of Civil Engineers (FEMA 356 2000), to determine which failure mode will govern the response, for a wall with particular material properties, axial load and boundary conditions. Thus, available formulations were used to estimate the lateral shear strength, and their predictions were compared among themselves and with the numerical and experimental masonry wall results.

3.2. OUTLINE OF THE EXPERIMENTAL RESEARCH PROGRAMME

A comprehensive experimental research work on masonry walls was carried out in EUCENTRE and University of Pavia laboratories, Italy (Galasco et al. 2009; Galasco et al. 2010; Magenes et al. 2010b). These walls were representative of existing buildings constructed with double-leaf stone walls. The masonry typology is constituted by two vertical leaves of stones placed side by side along the wall thickness. For this kind of masonry typology only few experimental results are available. The selected natural stones come from Bergamo and are sedimentary rocks made of calcareous sandstone. This stone was widely used in the past as a building material in Italy and is characterized by good mechanical properties, with a density of 2580 kg/m^3, a compressive strength of about 170 MPa and a flexural strength of about 19 MPa, as documented in (Magenes et al. 2010c). In order to satisfy the requirement of having a mortar consistent with historical buildings, a pre-mixed natural hydraulic lime mortar with a compressive strength non-exceeding 2 MPa was used.

Information about materials and construction characteristics of the undressed double leaf stone masonry and its mechanical characterization by uniaxial compression and diagonal compression tests are reported in (Magenes et al. 2010c). The testing program included 6 specimens with nominal dimensions of 1200x800x320 mm subjected to uniaxial compression and 6 specimens with nominal dimensions of 1000x1000x320 mm subjected to diagonal compression. Vertical compression tests consisted in applying a cyclic compression force on the masonry specimen, trying to distribute vertical stress as uniformly as possible and keeping the resultant force centred on the wall section. Detailed information about the loading and unloading cycles is provided in (Magenes et al. 2010c). The deformation was measured for increasing levels of compressive loads giving important information regarding the characteristics of masonry. Through the evaluation of the elastic behaviour range it is possible to characterize the elastic properties of masonry: Elastic modulus [E] and Poisson's coefficient [v]. Diagonal compression tests were used to determine the characteristics of shear stiffness [G] and strength of masonry [f_c, f_t]. The results from these tests allowed to collect some data concerning the mechanical properties of the masonry, which are summarized in Table 3.1.

As stated by Magenes et al. (2010c) the values of elastic modulus obtained from the experimental tests are significantly higher than those suggested by the Italian code (NTC 08 2008). These will be further discussed during the model calibration procedure.

Table 3.1 Mechanical properties of masonry (tests on 6 specimens) (Magenes et al. 2010b).

	f_c [MPa]	E [MPa]	f_t [MPa]	G [MPa]
Interval	3.07 – 3.48	2274 - 2826	0.112 – 0.161	740 - 940
Mean	3.28	2550	0.137	840

In-plane cyclic shear tests were carried out aiming at reproducing the behaviour of masonry piers subjected to in-plane reversed cyclic load, representative of the seismic action. Constant axial forces representative of gravity loads and a cyclic horizontal displacement history were applied at the top of the wall. Two geometric configurations were tested for different levels of pre-compression, 0.2 MPa and 0.5 MPa. All specimens have a nominal thickness of 320 mm and are 2.5 m high. Two of them are 2.5 m long with a slenderness ratio (*h/l*) equal to 1, which were named “squat” piers (CT01 and CT02), and another two are 1.25 m long with a slenderness ratio (*h/l*) equal to 2, named "slender" piers (CS01 and CS02). The dimensions of the specimens have been selected taking into consideration real walls (see Figure 3.1).

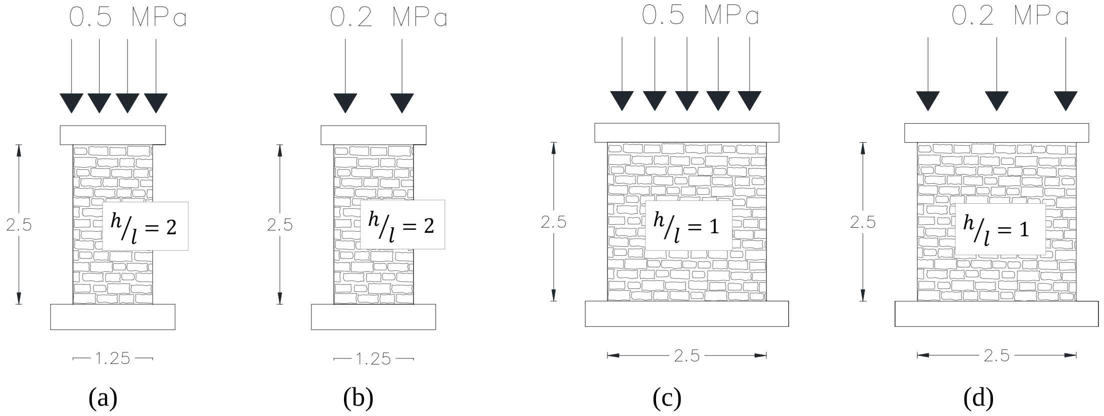

Figure 3.1 Wall specimens for in-plane cyclic tests: (a) CS01 wall; (b) CS02 wall; (c) CT01 wall; (d) CT02 wall (Magenes et al. 2010b).

Specimens were built on a 0.40 m thick reinforced concrete foundation fixed to the floor. The hydraulic actuators apply the axial load to the specimen through a steel loading beam connected to a reinforced concrete spreader beam directly cast on top of the specimen. A third actuator is used to impose horizontal displacements to the top of the piers. The test setup imposes fixed restrain conditions to the piers at the bottom and top, giving a double bending configuration to the tests (Figure 3.2).

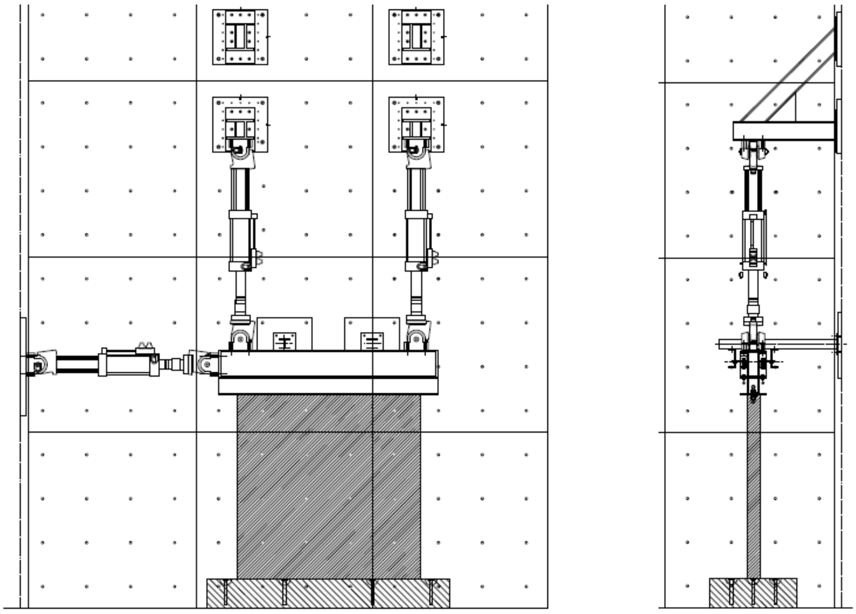

Figure 3.2 Scheme of the experimental test setup (Magenes et al. 2010b).

As a first step, specimens are subjected to axial load applied by vertical actuators which restrain the rotation of the steel top beam by means of a “hybrid” control (applying a constant total axial load and maintaining the same vertical displacement). In a following phase, the horizontal actuator applies a cyclic force in the top beam, force controlled at the beginning of the test and imposing increasing displacements afterwards. The test is stopped when the specimen presents potentially dangerous damage or a significant drop of lateral strength.

By subjecting the walls to shear in-plane loading, important information was gathered concerning the failure mechanisms, maximum displacement capacity and shear strength. The results provided by the tests, namely the force-displacement curves and failure modes, are presented in Figure 3.3 for each wall.

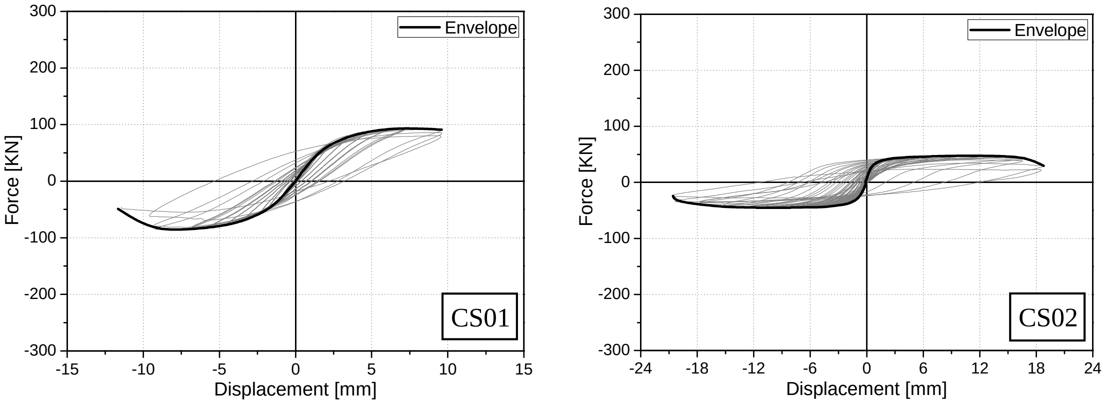

Failure: Shear

Failure: Flexure and Shear

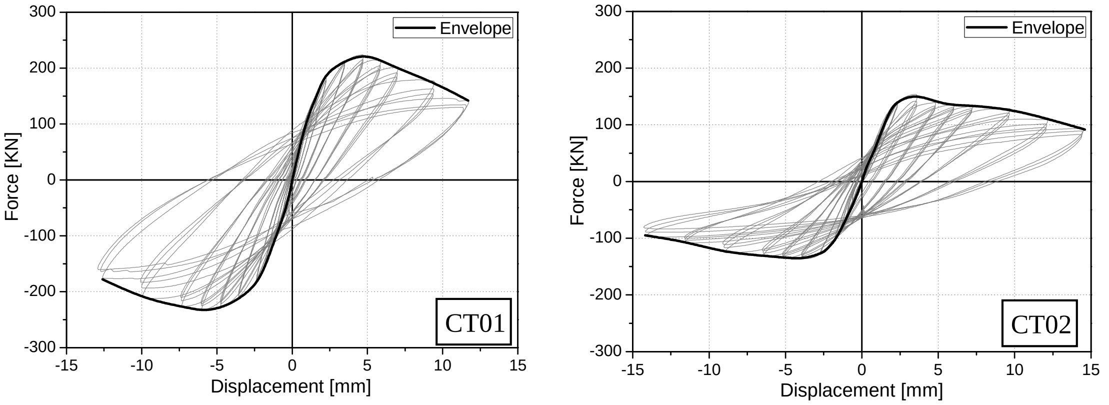

Failure: Shear

Failure: Shear

Figure 3.3 Experimental test results (Galasco et al. 2010).

Experiments revealed that piers CS01, CT01 and CT02 fail in shear by the development of diagonal cracking. The formation of diagonal cracks determined the maximum shear resistance, limiting as well the deformation capacity. The slender specimen CS02, characterized by low compression level, showed a combined flexural and shear failure. The deformation capacity of this wall was noticeably higher due to the flexural behaviour observed during the test.

The in-plane capacity of a masonry pier is strongly dependent on its slenderness (*h/l*) ratio. Slender piers achieve lower maximum horizontal force, less than half, in comparison to the squat piers with the same compression level. The maximum horizontal force reached by the specimens was: 94kN for CS01, 48kN for CS02, 234kN for CT01 and 154kN for CT02. The piers subjected to higher compressive loads proved to have more capacity in terms of horizontal load with a more brittle failure at the final branch, when compared with the ones with the same geometry. No evidences were found of the occurrence of significant sliding in any of the tests (possible sliding surfaces were monitored by displacement transducers).

3.3. NUMERICAL MODELS

3.3.1. Models Definition

Numerical models were used to represent the previously tested masonry walls aiming at further discussing and better understanding the experimental results. Since walls with two geometric configurations were tested, two different numerical models were constructed to represent squat (CT) and slender walls (CS) (Figure 3.4). The finite element method was adopted for carrying out all numerical calculations, using the software DIANA 9.4 (2009). The experimental setup was numerically simulated including, besides the masonry wall, the top concrete and steel beams and the reinforced concrete foundation. The steel loading beam was simulated with an equivalent rectangular section, without changing the inertia properties, fixing the height of the beam.

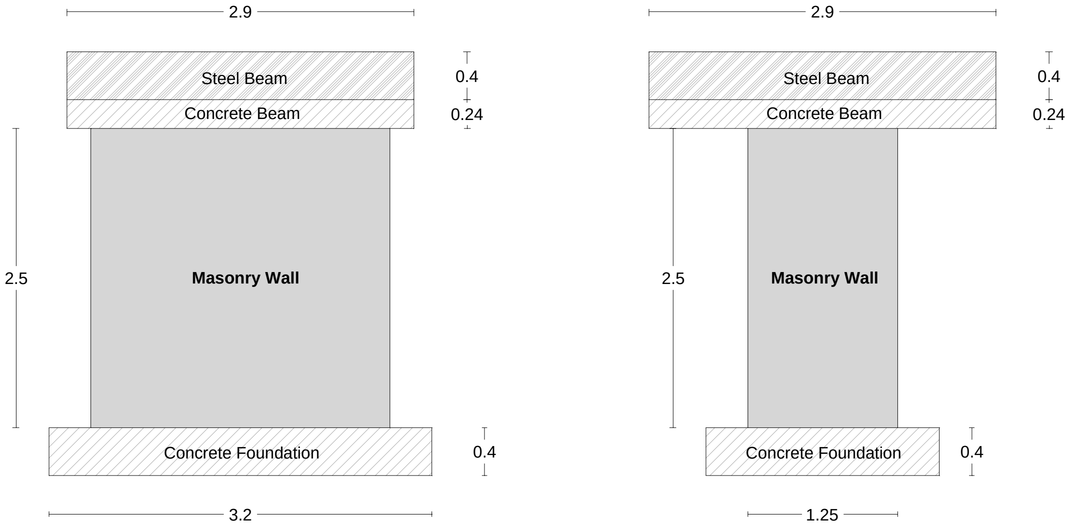

Figure 3.4 Representative scheme of the numerical models (dimensions in meters).

The masonry was modelled following a macro-modelling approach, assuming the masonry as a composite material, where joints are smeared out in continuum elements. This modelling strategy is a valuable alternative to the modelling of the masonry components (units, mortar and interfaces) and assumes the use of average mechanical properties for masonry (Lourenço 1996a; Lourenço 2009b). The macro modelling approach is well diffused and has been successfully used by several authors (Berto et al. 2004; Betti and Vignoli 2008b; Mallardo et al. 2008; Abruzzese et al. 2009; Annecchiarico et al. 2009), giving a reliable estimation of masonry response. By considering the masonry as a homogenous material, the computational time and memory requirements decreases substantially and the mesh generation is more straightforward, when compared with a model in which units and mortar joints are separately discretized (Lourenço 2002). Additionally, units and mortar distribution is not known in detail to allow the development of a reliable micro-model.

Finite element models were constructed using 2D plane stress elements since the stress components perpendicular to the face are negligible due to the small thickness of the walls, and the loading acts in the plane of the element. A regular mesh discretization was developed using eight-node quadrilateral isoparametric plane stress elements based on quadratic interpolation and Gauss integration for both models, CQ16M (TNO DIANA 2009). The model for the CT walls is presented in Figure 3.5(a) with a 1686 nodes and 534 elements mesh, and the model of CS walls is shown in Figure 3.5(b) and has 1472 nodes and 449 elements. The numerical simulation of the four walls experimentally tested was obtained by applying the corresponding pre-compression level in each wall.

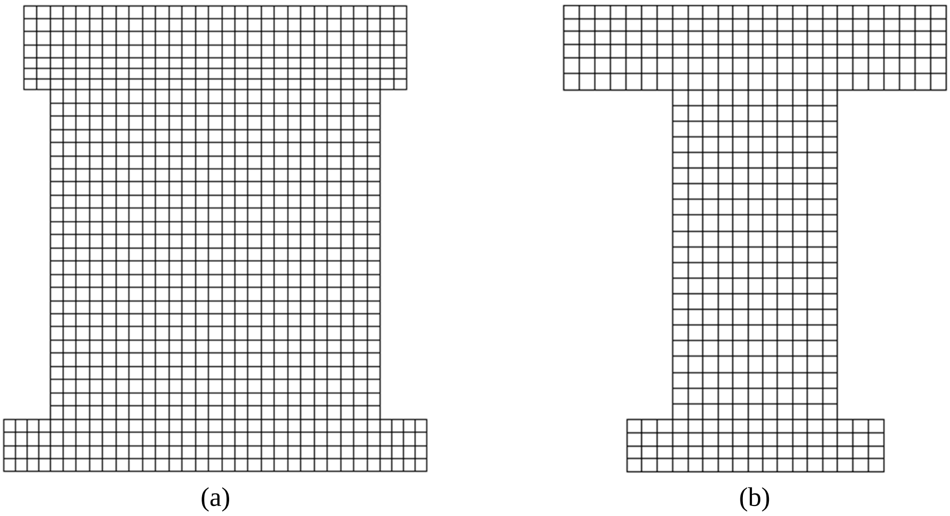
(a) (b)

Figure 3.5 Numerical models (mesh discretization): (a) CT walls and (b) CS walls.

Code values of elastic modulus, Poisson coefficient and density were used for concrete and steel. The masonry mechanical properties were assigned to the models as starting point in accordance with the experimental characterization. Table 3.2 summarizes the material properties used for the numerical models in this preliminary linear analysis stage. Note that no calibration process was carried out at this stage.

Table 3.2 Material properties for the preliminary linear analysis phase.

	Elastic modulus E [GPa]	Poisson coefficient ν [-]	Density γ [Kg/m3]
Masonry	2.55	0.2	1900
Steel	210	0.3	7850
Concrete	30	0.2	2500

The boundary conditions and the load application procedure are defined according to the experimental setup described in section 3.2. The model assumes that the different materials are fully connected, since no significant sliding between materials occurred during the experimental tests for any wall. Thus, fixed-fixed conditions are assured in the numerical models: pinned supports at the base reinforced concrete beam are imposed and the rotation at the top metallic beam is prevented using model constraints that impose dependencies between degrees of freedom. In this way, the possible rotation of the top metallic beam is not allowed, as imposed by the experimental apparatus.

Numerical models intent to be representative of the behaviour of this type of masonry walls given that these models will be used for an exhaustive parametric analyses.

3.3.2. Models Calibration

As previously referred, the numerical simulation of the masonry walls considered in a first instance linear elastic models, for comparison and calibration with the data emerged from the experimental shear tests. This is essential to obtain confidence in the numerical results. An attempt was made of calibrating the four different walls on the basis of linear analysis. Preliminary analyses were carried out using the available experimental parameters (see Table 3.2). Two types of loads representing the vertical compression and the envelope of the horizontal cyclic force were considered in each numerical analysis. The vertical compression was applied first uniformly to the top of the steel beam and the horizontal load was simulated by a displacement. It is noted that the self-weight of the wall, foundation and top beams is also considered in the analyses.

Figure 3.6 summarizes the linear force-displacement response of the four walls (CS01, CS02, CT01 and CT02). The numerical response is compared to the corresponding experimental envelope range, which is obtained by plotting the envelope in both directions, up to 10 millimeters of displacement. A quick analysis of the numerical model responses showed that the, in general, the model is much more stiff than the experimentally tested walls.

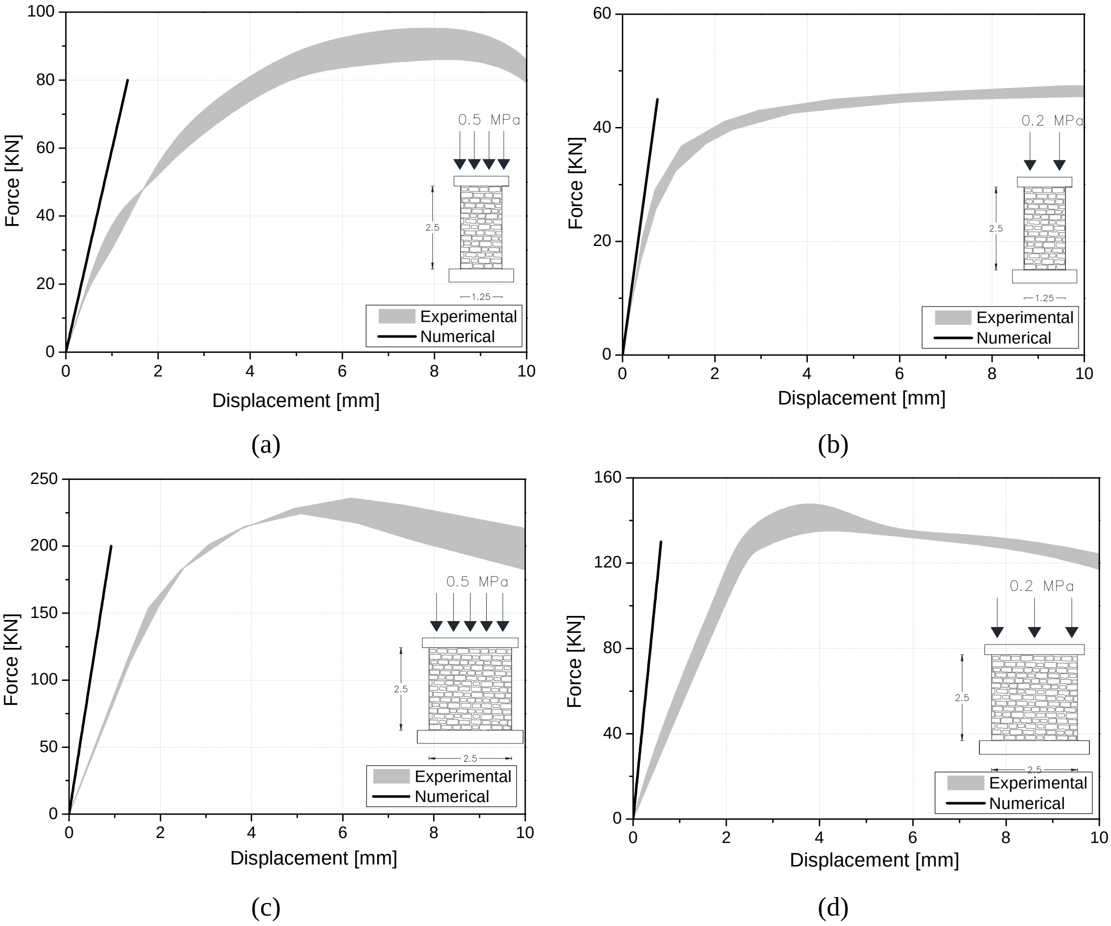

(a) (b)

(c) (d)

Figure 3.6 Linear elastic analyses: (a) CS01 Wall; (b) CS02 Wall; (c) CT01 Wall; (d) CT02 Wall.

The response of the slender walls (CS) indicates an initial stiffness higher than the verified experimentally, more significantly in CS01 wall (Figure 3.6a and Figure 3.6b). The results found for the squat walls also show significant differences between the numerical and experimental initial stiffness, even more noticeable in these walls (Figure 3.6c and Figure 3.6d). The stiffness variations found for numerical analysis and experimental response led to an analysis on the parameters with direct influence on the wall stiffness response.

In the numerical simulation the parameters that influence the wall stiffness in the linear range are the masonry elastic modulus, the geometric configuration and boundary conditions. There is no direct dependency on the compression stress level on the wall. Conversely, the analysis of the experimental results proved that the initial stiffness depends on the pre-compression stress level. Generally, walls with the same properties subjected to greater pre-compression level exhibit higher initial stiffness. Several experimental studies on the in-plane behaviour of masonry walls confirm the existence of a relation between the initial stiffness with the applied pre-compression (Magenes and Calvi 1992; Vasconcelos 2005; Angelini et al. 2007; Seki et al. 2008; Elmenshawi et al. 2010; Capozucca 2011; Silva 2012; Churilov and Dumova-Jovanoska 2013; Petry and Beyer 2014). This can be justified by joint closure as a consequence of a higher imposed compression on the wall, which results in a more stiff composite material. For this reason, the correct simulation of the experimentally tested walls requires the consideration of the pre-compression effect on the walls response since the boundary conditions are well defined. Information provided by University of Pavia concerning experimental data with the measured rotations on the top beam during testing confirmed that the rotations at the top are nearly inexistent and can be neglected for the four walls. This proves that the fixed-fixed boundary conditions numerically modelled simulate with very good approximation the testing conditions.

Numerically, the stiffness dependence from the level of compression is simple to consider but the lack of experimental data is evident. The definition of an equivalent elastic modulus, dependent on the level of pre-compression of the wall, seems therefore preferable. This also means that the elastic modulus defined experimentally may not be representative of all the walls since it was characterized considering using higher levels of compression on the specimens and the dependency is likely to be highly affected by the stone size and arrangement, and the quality of execution.

The adopted model calibration procedure, which consists on fitting the model behaviour with the experimental results, was carried by defining an equivalent elastic modulus for masonry. Table 3.3 presents the results obtained from the calibration process, in which the masonry elastic modulus is defined for each wall.

Table 3.3 Calibrated elastic modulus for each wall.

	CT01	**CT02**	**CS01**	**CS02**
***E* [MPa]**	1000	800	1500	2000

Analysing the elastic modulus resultant from the calibration process, it can be noticed that the slender walls (CS) do not follow the typical behaviour wherein for higher levels of compression on the wall the stiffness increases. Conversely, the experimental response of the wall with lower lever of compression (CS02) shows higher linear stiffness than CS01 wall. Similar experimental campaigns results on the in-plane behaviour of masonry walls subjected to distinct levels of compression, already referred previously, prove that in the majority of the cases walls in the same conditions tend to exhibit more stiff behaviours under higher levels of compression loads. This disparity can be related to differences in the quality of masonry for specimen CS02 or even aspects difficulties in the test set-up. For this reason this wall will be analysed considering the calibrated elastic modulus and also the elastic modulus readjusted in order to fit the relations found for similar in-plane tests on masonry walls.

The differences in the elastic modulus in what concerns the two different geometric configurations (CT and CS) can be explained by the in-situ wall construction conditions. As CS walls are smaller, the careful arrangement of the units during construction may have been higher. In conclusion, the considerable scatter found demonstrates the importance of the stress level and the execution (e.g. arrangement of units, mortar quantity, voids and shrinkage cracks) in the elastic stiffness of stone masonry walls.

3.4. NON-LINEAR ANALYSES

3.4.1. Definition of the Material Behaviour

Since masonry exhibits manifestly non-linear behaviour, an adequate material constitutive model needs to be selected in order to achieve reliable simulations. Total strain crack models, which describe the tensile and compressive behaviour of a material with one stress-strain relationship, are usually suitable for this purpose (TNO DIANA 2009). For modern, or regular, masonry, more sophisticated orthotropic models are available, e.g. (Lourenço and Rots 1997), but for stone ancient masonry, usually with irregular bond and multi-leaf, isotropic models are normally adopted. Within the total strain crack models, two distinct approaches can be distinguished: the Fixed Crack Model (FCM) and the Rotating Crack Model (RCM). In both formulations the crack is initiated when the maximum principal stress equals the tensile strength of the material, and its initial orientation is normal to the maximum principal strain. The main difference between these two formulations is related to the cracks orientation during the inelastic process. In the FCM the coordinate system is fixed upon cracking according to the principal strain directions and remain invariant during the total analysis process. Each integration point admit a maximum of two orthogonal cracks. The RCM allows a gradual correction of the initially crack direction as the crack plane can rotate during the analysis. The crack direction rotates with the principal strain axes ensuring that the crack remains normal to the direction of the maximum principal strain. In the fixed formulation, a shear retention parameter is required for the definition of the model shear behaviour, whilst in the rotating model the shear softening occurs implicitly as a result of the principal stress and strain conditions. An extensive research regarding these formulations was carried out by Rots (1988) which conclude that rotating cracks produce a more flexible response and correctly keep the maximum tensile stress under control, and can implicitly provide for shear softening across the plane of initial cracking. As stated by Rots (1988) several studies revealed realistic predictions for rotating cracks formulation, while fixed cracks models tended to behave too stiff in shear dominated applications. For these reasons, the RCM was used to carry out the nonlinear numerical analysis once the shear behaviour in this study is dominant. An additional discussion regarding the application of these two material models is provided in the next Chapter.

Parabolic and exponential stress-strain relations were used to describe the tensile and compressive behavior of masonry respectively, see Figure 3.7 where f_c and G_c stands for the compressive strength and fracture energy, f_t and G_t are the tensile strength and fracture energy and h is the crack bandwidth. In the continuum modelling approach masonry is described as a homogenous material and the required parameters were defined in accordance with experimental characterization results, previously calibrated elastic modulus and typical relations used for masonry (Lourenço 2009a; 2009b). The tensile and compressive fracture energy values, necessary for the constitutive models definition, were initially estimated based on these recommendations. The compressive fracture energy calculated according to the relation of the ductility index parameter (equation (3.1), available in the referred recommendations:

$$d = G_c / f_c \tag{3.1}$$

For $f_c < 12$ N/mm^2 a value of d = 1.6 mm is suggested, which is the case since experimental characterization tests defined f_c equal to 1.74 N/mm^2. Thus, the compressive fracture energy (G_c) takes a value of 2.8 N/mm. The indicative value for the tensile fracture energy (G_t) was calculated according to equation (3.2) considering that the recommended value for the ductility index (d) is 0.029 mm.

$$d = G_t / f_t \tag{3.2}$$

Table 3.4 presents the parameters to be used in the numerical analyses in which E is the elastic modulus and γ the density. The Poisson ratio was kept constant and equal to 0.2. Although the elastic modulus has been updated for each wall in order to accurately simulate the influence of the level of stress on the wall, the non-linear parameters are kept constant for all the analysis since no other data is available and the material used in the construction of the specimens had similar characteristics. In what concerns wall CS02, two nonlinear analyses will be carried out considering different elastic modulus, one in accordance with the calibration procedure and the other according to the expected elastic response.

Concrete and steel beams behaviour was defined as linear elastic due to the significantly higher strength of these materials compared to the masonry. The equilibrium solution of the equations in each step of the non-linear analysis is obtained through an iterative regular Newton-Raphson method and a convergence criterion based on the internal energy with tolerance of 10^{-3} was adopted.

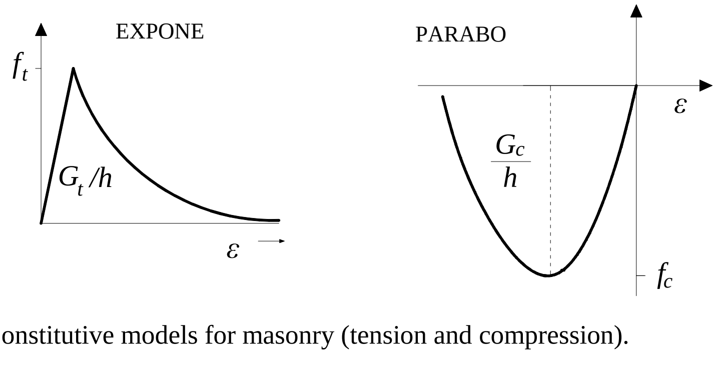

Figure 3.7 Constitutive models for masonry (tension and compression).

Table 3.4 Mechanical properties for masonry.

	E [MPa]	γ [Kg/m^3]	f_c [MPa]	G_c [N/mm]	f_t [MPa]	G_t [N/mm]
CS01	1500	1900	3,28	5,25	0,14	0,02
CS02	2000/1100	1900	3,28	5,25	0,14	0,02
CT01	1000	1900	3,28	5,25	0,14	0,02
CT02	800	1900	3,28	5,25	0,14	0,02

3.4.2. Non-linear Analyses Results

The loads considered in the non-linear analyses were the self-weight of the structure in a first step, the vertical compressive load in accordance with the wall under analysis, in a second step, and, at last, a horizontal displacement-controlled loading steadily increasing until failure.

The numerical response of the slender wall CS01 is obtained by imposing 0.5 MPa of pre-compression on the wall and applying horizontal displacements in small increments. In order to plot the capacity curve of the wall, a node in the top of the wall, consistent with the point measured during the experimental testing was selected. The numerical force-displacement curve is plotted and compared with the corresponding experimental envelope for wall CS01 in Figure 3.8. The numerical force-displacement response fits very well the experimental envelope considering the initial stiffness (previously validated), the maximum lateral resistance and also the nonlinear behaviour. The maximum in-plane capacity estimated numerically reaches 92 kN, which is very close to the 94 kN achieved in the experiments. The drift capacity of the walls will be further discussed in section 3.6.

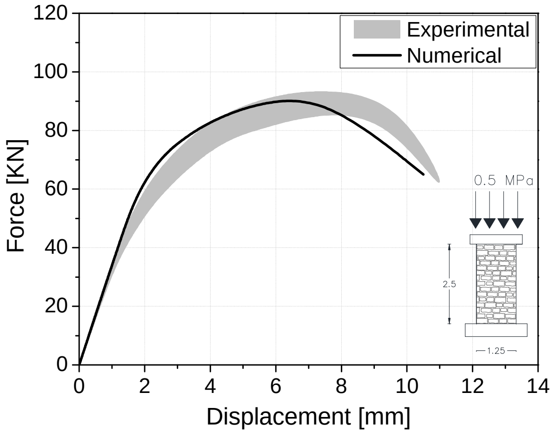

Figure 3.8 Force-displacement curve for CS01 wall.

The maximum principal strains distribution was also evaluated as an indicator of damage. At the peak load, the tensile strains are concentrated in opposite corners of the wall, resultant of the effect of the wall deformation, accompanied by the appearance of cracks in the diagonal of the pier (Figure 3.9a). The damage distribution in the nonlinear behaviour, which is representative of the state of damage near failure, is presented in Figure 3.9b and indicates a clear propagation of cracks through the wall diagonal. Here the damage pattern reveals a shear failure by the formation of diagonal cracks along the pier, which is in agreement with the failure mode found for the experimental test of this wall. The structural response in terms of compressive strains distribution is characterized by the formation of a large compressive strut in the wall diagonal around the area where the cracks develop as revealed by Figure 3.9c. These results are consistent with the expected damage considering the failure mode verified in experiments.

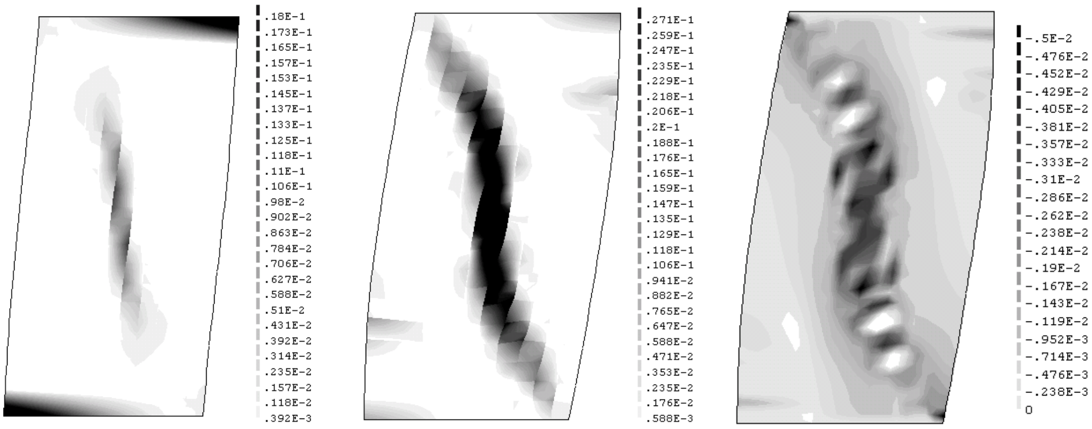
.18E-1
.173E-1
.165E-1
.157E-1
.153E-1
.145E-1
.137E-1
.133E-1
.125E-1
.118E-1
.11E-1
.106E-1
.98E-2
.902E-2
.863E-2
.784E-2
.706E-2
.627E-2
.588E-2
.51E-2
.431E-2
.392E-2
.314E-2
.235E-2
.157E-2
.118E-2
.392E-3
.271E-1
.259E-1
.247E-1
.235E-1
.229E-1
.218E-1
.206E-1
.2E-1
.188E-1
.176E-1
.165E-1
.159E-1
.147E-1
.135E-1
.129E-1
.118E-1
.106E-1
.941E-2
.882E-2
.765E-2
.647E-2
.588E-2
.471E-2
.353E-2
.235E-2
.176E-2
.588E-3
-.5E-2
-.476E-2
-.452E-2
-.429E-2
-.405E-2
-.381E-2
-.357E-2
-.333E-2
-.31E-2
-.286E-2
-.262E-2
-.238E-2
-.214E-2
-.19E-2
-.167E-2
-.143E-2
-.119E-2
-.952E-3
-.714E-3
-.476E-3
-.238E-3
0

(a) (b) (c)

Figure 3.9 Strains distribution for CS01 wall: (a) Tensile damage at peak load; (b) Tensile damage at final stage; (c) Compressive strain distribution at final stage.

As discussed before, the nonlinear analyses for CS02 wall were carried out considering two different elastic modulus for masonry, one considering the calibrated value against experimental stiffness (E=2000 MPa) and the other considering typical relations found in similar experimental research (E=1100 MPa). The nonlinear response considering the wall CS02 with the masonry elastic modulus calibrated according to the experimental stiffness (Figure 3.10a), shows good agreement with the experimental envelope, although the maximum in-plane capacity is slight overestimated. The final branch of the numerical curve is typical of the rocking behaviour presenting large displacement capacity.

The analysis considering a lower value for the masonry elastic modulus (E=1100 MPa) presents a force-displacement response similar to the previous (Figure 3.10b), with a clear difference in the initial stiffness as expected. It should be pointed out that the stiffness presented by this model lies at the lower limit of the experimental envelope, making it acceptable. The maximum horizontal load as well as the post-peak behaviour with high deformation capacity are very similar to the previous analysis. In terms of force-displacement curves both models can represent well the stiffness found by the experimental testing and the maximum wall capacity. The significant decrease of resistance verified in the experimental envelope in the final branch could not be fully simulated by the proposed numerical model. A possible explanation may raise on the non-consideration of the cyclic loading process. From the experimental point of view, the strength is dictated by flexural strength, but it is not far from the force needed to generate diagonal cracks. Since the experimental test is cyclic, a diagonal crack may have been possibly induced by the repetition of deformation cycles that do not reach the monotonic diagonal cracking condition but stayed close to it. As the numerical model used is not able to capture this phenomenon of damage accumulation due to cyclic loading, a strength degradation cannot be observed in the post peak branch of the load-displacement curve, even if a cyclic loading procedure has been adopted.

Still, the modelling approach presented here describe with good approximation the maximum capacity of the wall and the obtained behaviour predicts well the rocking failure mode. It is worth noting that even though the diagram does not exactly fit the envelope, the maximum force and failure behaviour are well estimated.

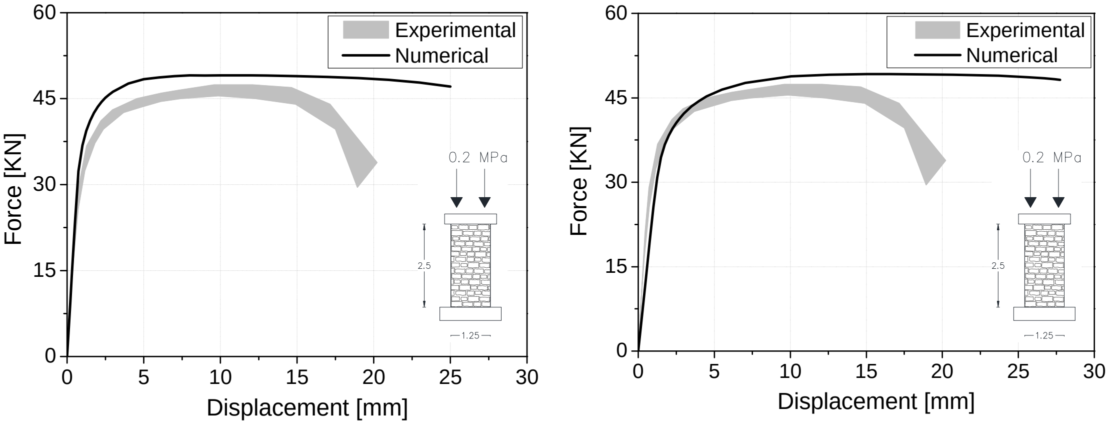

(a) (b)

Figure 3.10 Force-displacement curves for CS02 wall: (a) Results with E=2000 MPa; (b) Results with E=1100 MPa.

The damage pattern was also evaluated for both of the analysis by plotting the maximum and minimum principle strains distribution. Although some differences were found between the capacity curves of both the analyses, the strains distributions are nearly the same (see Figure 3.11 and Figure 3.12). Both in peak and post-peak behaviour the strains distribution indicate a concentration of damage in the left bottom and top right corner of the wall. This type of damage is characteristic of the flexural behaviour, with rocking. The analysis of the compressive strain distribution of the pier (Figure 3.11c and Figure 3.12c) shows a high concentration in the diagonal direction until the toe, also typical of flexure failures. Crushing at the toe is also perceptible by the strain concentration in this area.

Analysing not only the capacity curves but also the damage distribution obtained by these analyses, a clear flexural behaviour is observed, predicting the overturning of the wall over its toe. In the experimental tests a combined shear and flexure failure is described, initially characterized by flexural-rocking behaviour followed by the formation of shear cracks. The analyses results do not indicate the appearance of shear cracks, only the rocking behaviour is captured. The experimental tests show that the shear cracks appear due to sliding along units and mortar joints. Indeed, within the experimental framework another test was carried out on a wall with the same characteristics but constructed with better quality mortar and only rocking behaviour was verified. The comparison between the numerical and experimental results stresses the model limitations in the simulation of sliding between mortar joints behaviour. Only a micro-model could possibly simulate the behaviour found in the experimental test of this wall.

However, although the inherent and discussed limitations, this modelling approach is simple but uses sophisticated constitutive laws to describe the masonry behaviour giving relevant information regarding the maximum capacity and nonlinear behaviour of these walls.

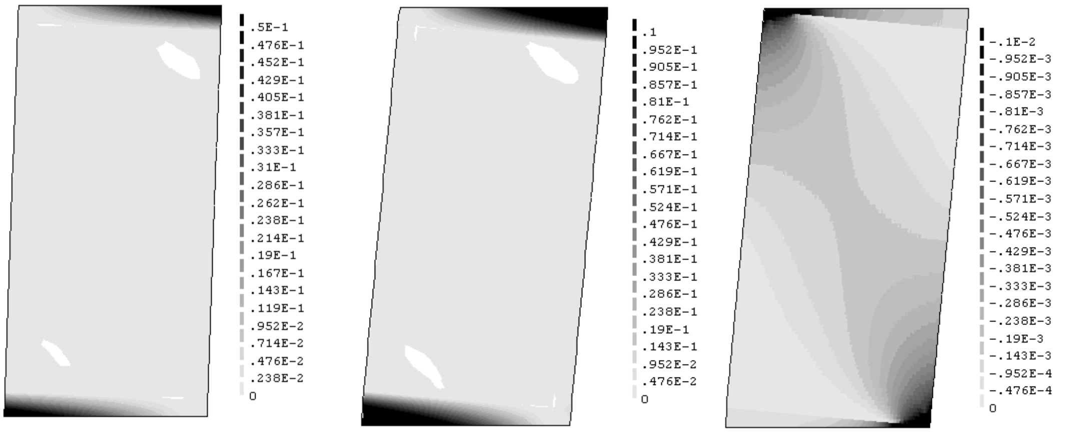

(a) (b) (c)

Figure 3.11 Strains distribution for CS02 wall with E=2000 MPa: (a) Tensile damage at peak load; (b) Tensile damage at final stage; (c) Compressive strain distribution at final stage.

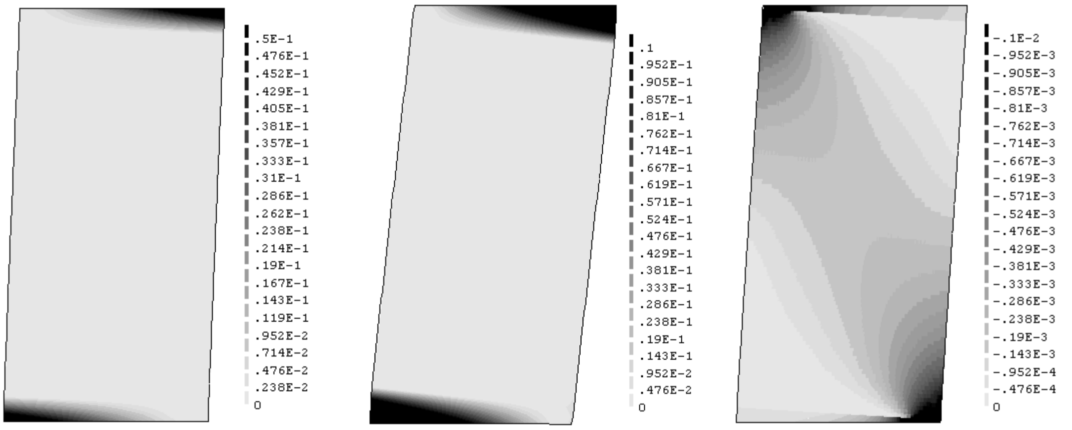

(a) (b) (c)

Figure 3.12 Strains distribution for CS02 wall with E=1100 MPa: (a) Tensile damage at peak load; (b) Tensile damage at final stage; (c) Compressive strain distribution at final stage.

The analysis results of the squat wall subjected to higher level of compression, CT01, showed that the in-plane behaviour of this wall is in agreement with the experimental monotonic envelope as the maximum capacity is well estimated and the non-linear behaviour fits with very good approximation the experimental curve (Figure 3.13). As calibrated, the linear numerical stiffness is in agreement with the experimental initial behaviour. The discontinuity visible in the capacity curve of this wall can be explained by the opening of the first crack in the model followed by the subsequent redistribution of stresses to adjacent elements. The maximum horizontal capacity measured during the experimental testing, 234 kN, is well estimated by the numerical analysis, predicting 224 kN of maximum horizontal load (only 4% of error). The softening after peak behaviour verified in the force-displacement curve with the loss of capacity of the wall follows the behaviour of the experimental envelope with very good approximation. As stressed previously the displacement capacity is discussed in section 3.6.

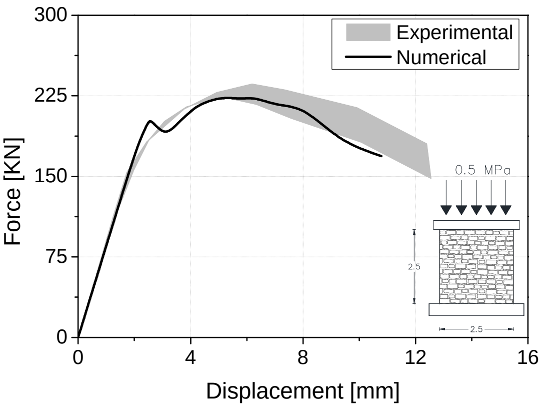

Figure 3.13 Force-displacement curve for CT01 wall.

Experimental results identified several diagonal cracks forming in the centre of this wall describing a pure shear failure. The analysis of the damage pattern by plotting the maximum principle strains at peak and post peak behaviour (Figure 3.14a and Figure 3.14b), demonstrates that the behaviour verified experimentally is well reproduced by the numerical model. The formation of diagonal cracks between the top corner and the wall toe evidences a clear shear failure with diagonal cracking developing at the pier centre. Due to the high level of pre-compression installed, the wall does not tend to rotate around the toe, instead it starts to develop diagonal cracks at the centre where the concentration of strains is higher at the peak load (see Figure 3.14a). In Figure 3.14c the concentration of compressive strains is presented showing a compressive strut in the wall diagonal, around the areas where the cracks are located.

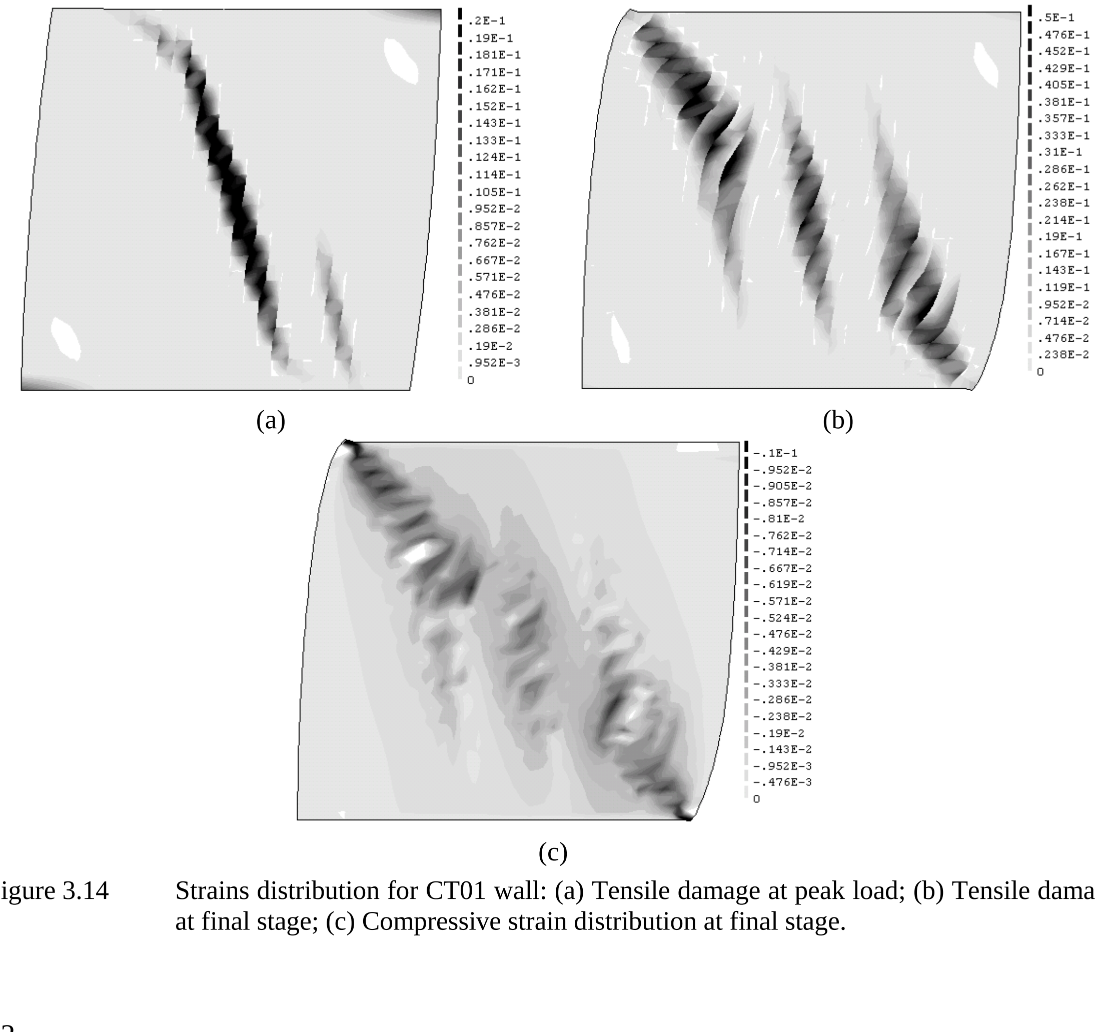
.2E-1
.19E-1
.181E-1
.171E-1
.162E-1
.152E-1
.143E-1
.133E-1
.124E-1
.114E-1
.105E-1
.952E-2
.857E-2
.762E-2
.667E-2
.571E-2
.476E-2
.381E-2
.286E-2
.19E-2
.952E-3
0
.5E-1
.476E-1
.452E-1
.429E-1
.405E-1
.381E-1
.357E-1
.333E-1
.31E-1
.286E-1
.262E-1
.238E-1
.214E-1
.19E-1
.167E-1
.143E-1
.119E-1
.952E-2
.714E-2
.476E-2
.238E-2
0
-.1E-1
-.952E-2
-.905E-2
-.857E-2
-.81E-2
-.762E-2
-.714E-2
-.667E-2
-.619E-2
-.571E-2
-.524E-2
-.476E-2
-.429E-2
-.381E-2
-.333E-2
-.286E-2
-.238E-2
-.19E-2
-.143E-2
-.952E-3
-.476E-3
0

(a) (b)

(c)

Figure 3.14 Strains distribution for CT01 wall: (a) Tensile damage at peak load; (b) Tensile damage at final stage; (c) Compressive strain distribution at final stage.

The numerical results obtained for the squat wall with lower compression level, CT02, demonstrate that the in-plane behaviour verified in experiments is numerically reasonably well reproduced. The comparison between the numerical force-displacement curve and the experimental envelope, presented in Figure 3.15, confirms that the maximum wall capacity is well predicted by the numerical analysis with a minor error around 5% (146 kN obtained numerically against the 154 kN measured experimentally). In what concerns the post-peak behaviour, slight differences can be found between numerical and experimental curves. After reaching the peak, the wall capacity decreases due to the formation of the first diagonal cracks. After this point, and as a result from the redistribution of stresses to non-damaged adjacent elements, the wall suffered a slight increase of its capacity before presenting a more pronounced decrease of the load capacity. The experimental envelope response also presents an evident drop after the peak but a gradual decrease on the wall capacity is verified until failure.

The damage evolution verified numerically is consistent with the experimental damage description characterized by shear behaviour (Figure 3.16). After the peak, where the tensile strains concentrate at the bottom and top corners due to the deformation of the wall (Figure 3.15a), the wall suffers a decrease in the capacity motivated by the formation of the first crack and fails in shear exhibiting a clear diagonal crack that crosses the wall from one corner to another (Figure 3.15b). The expectable diagonal compressive strut is also present when the minimum principle strains distribution are plotted (Figure 3.15c). The crack pattern resultant from the experimental testing of this wall presented cracking through the wall diagonals, consistent with the damage found in this analysis results. Even if the numerical curve in the nonlinear range does not fit exactly the experimental envelope, the maximum capacity is well estimated and the damage evolution is well described numerically, confirming the ability of the numerical model to simulate the wall behaviour.

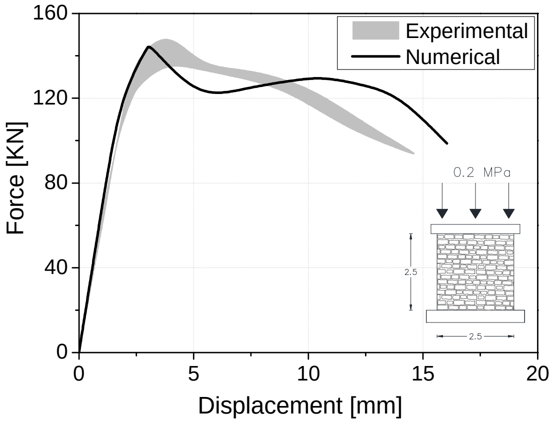

Figure 3.15 Force-displacement curve for CT02 wall.

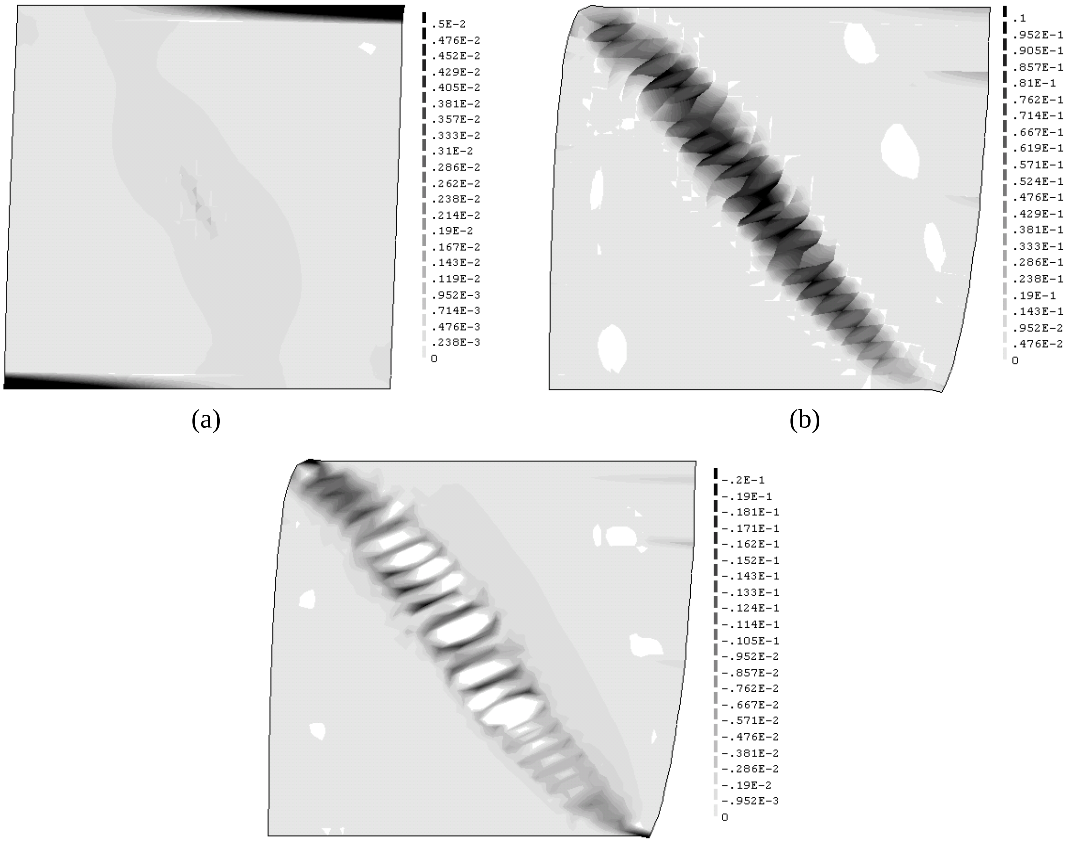
.5E-2
.476E-2
.452E-2
.429E-2
.405E-2
.381E-2
.357E-2
.333E-2
.31E-2
.286E-2
.262E-2
.238E-2
.214E-2
.19E-2
.167E-2
.143E-2
.119E-2
.952E-3
.714E-3
.476E-3
.238E-3
0
.1
.952E-1
.905E-1
.857E-1
.81E-1
.762E-1
.714E-1
.667E-1
.619E-1
.571E-1
.524E-1
.476E-1
.429E-1
.381E-1
.333E-1
.286E-1
.238E-1
.19E-1
.143E-1
.952E-2
.476E-2
0
-.2E-1
-.19E-1
-.181E-1
-.171E-1
-.162E-1
-.152E-1
-.143E-1
-.133E-1
-.124E-1
-.114E-1
-.105E-1
-.952E-2
-.857E-2
-.762E-2
-.667E-2
-.571E-2
-.476E-2
-.381E-2
-.286E-2
-.19E-2
-.952E-3
0

(a) (b)

(c)

Figure 3.16 Strains distribution for CT02 wall: (a) Tensile damage at peak load; (b) Tensile damage at final stage; (c) Compressive strain distribution at final stage.

Based on the comparison between numerical and experimental capacity curves and damage distribution, it can be concluded that the numerical models proposed are able to reproduce the experimental in-plane behaviour of masonry walls under combined vertical and shear loads, meaning that they can be used on the parametric analysis. The maximum horizontal load is well estimated (with minor errors for all the walls), the plastic strains evolution accurately describe the experimental behaviour and the failure modes were predicted well, with crack patterns consistent with those observed experimentally.

3.5. PARAMETRIC ANALYSES

Numerical modelling is commonly regarded as a complementary approach to further study different conditions and parameters, which is nearly impracticable from the experimental point of view. In this sense, parametric analyses considering an intermediate geometric configuration and compressive load, using the validated numerical models, are addressed and discussed in this section.

Parametric analysis aims to clarify the interaction between the pre-compression level and the wall slenderness ratio (*h/l*) in the in-plane response of the masonry walls under shear loading. Since four walls were experimentally tested and numerically studied by validated models, intermediate conditions of these walls are studied in accordance with Table 3.5. Walls with 2.5 m height and intermediate length of 1.875 m, comprising a slenderness (*h/l*) ratio of around 1.33 (named as CM walls), were included in the numerical analysis and a pre-compression level of 0.35 MPa was also evaluated. The in-plane response of more five masonry walls is numerically estimated, in a total of nine walls.

Since the validated reliable models are representative of the mechanical behaviour of the experimentally tested vertical elements, the numerical study is extended to other configurations and stress levels.

Table 3.5 Parametric analyses (in grey the walls experimentally tested and numerically validated).

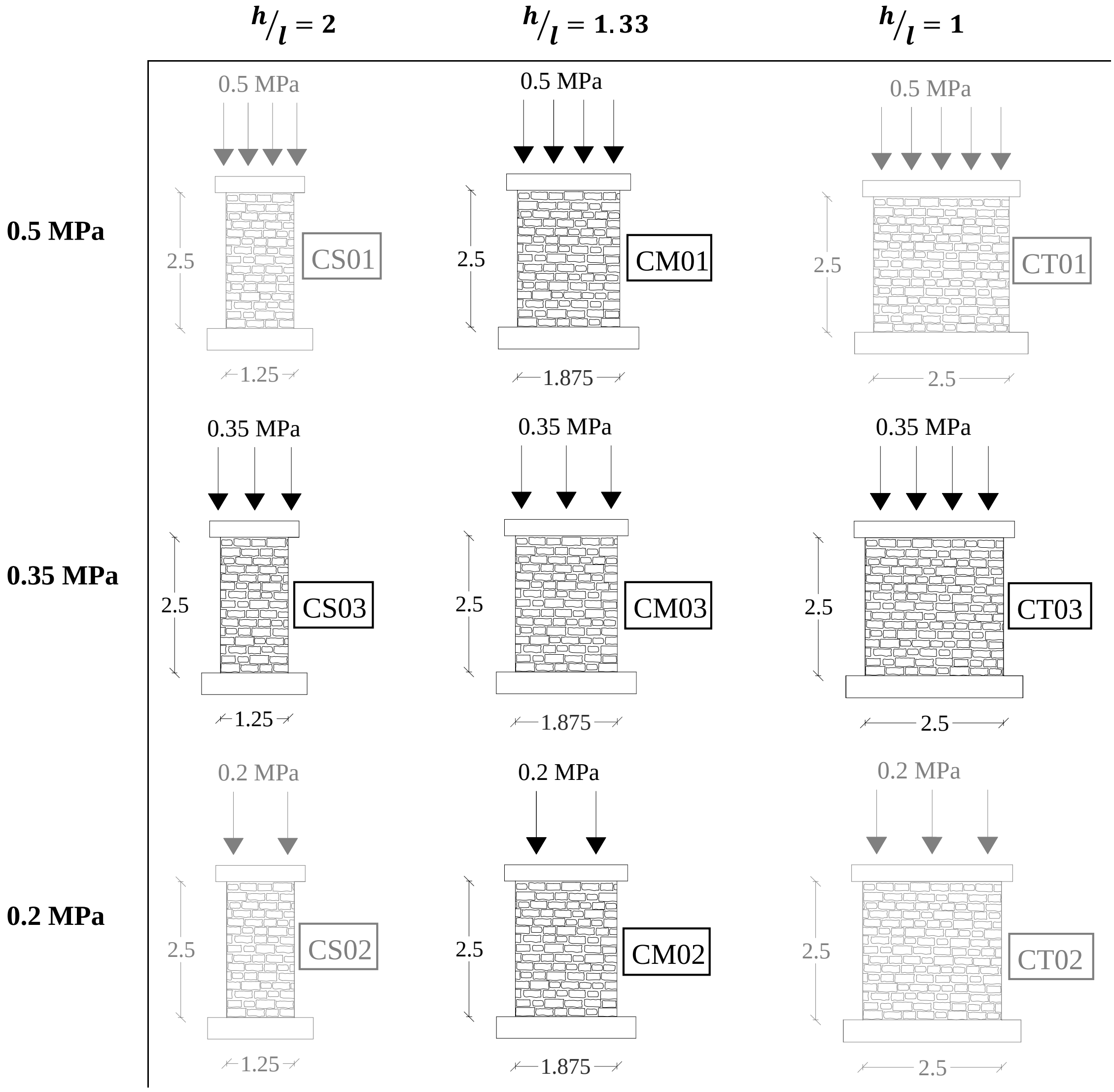
$h/l = 2$
$h/l = 1.33$
$h/l = 1$
0.5 MPa
0.5 MPa
0.5 MPa
0.5 MPa
2.5
CS01
2.5
CM01
2.5
CT01
1.25
1.875
2.5
0.35 MPa
0.35 MPa
0.35 MPa
0.35 MPa
2.5
CS03
2.5
CM03
2.5
CT03
1.25
1.875
2.5
0.2 MPa
0.2 MPa
0.2 MPa
0.2 MPa
2.5
CS02
2.5
CM02
2.5
CT02
1.25
1.875
2.5

Since the parametric analyses comprise a new geometric configuration (CM walls), a numerical model with the characteristics defined above was constructed and the mesh discretization includes 1692 nodes and 529 elements, as presented in Figure 3.17. The material constitutive laws, boundary conditions and analysis options used in this model follow the same considerations made in section 3.3 for CS and CT walls models.

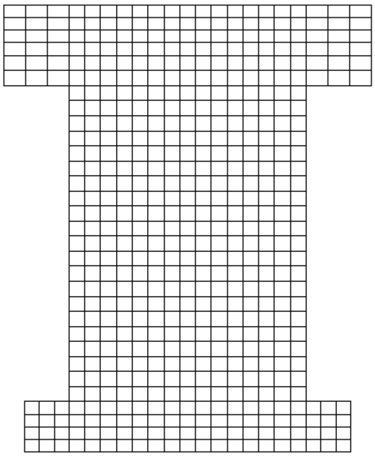

Figure 3.17 Numerical model for CM walls.

The analysis of the parametric models were performed with the same assumptions made for the validated models. As previously demonstrated, the masonry elastic modulus is dependent on the geometric configuration and pre-compression level. Aiming at simulating the correct stiffness of these walls, equivalent elastic modulus were defined for the parametric walls according to Table 3.6.

Table 3.6 Elastic modulus for the parametric analysis.

	Elastic modulus [MPa]		
σ = 0.5 MPa	**CT01** 1000	**CM01** 1300	**CS01** 1500
σ = 0.35 MPa	**CT03** 900	**CM03** 1100	**CS03** 1300
σ = 0.2 MPa	**CT02** 800	**CM02** 900	**CS02** 1100

The analyses results were grouped considering the pre-compression level and the geometric configuration in order to evaluate the influence of these parameters on the response of the wall. Figure 3.18 describes the influence of the geometrical configuration in the wall behaviour and it is observed that larger height/length ratios (for the same height) led to lower capacity of the wall, independently of the level of compressive stress. Analysing the results when the vertical compression was kept constant and the walls geometry varied, an increase in the lateral wall capacity around 90% on average was verified comparing walls of h/l ratio equal to 2 with *h/l* equal to 1.33. A moderate enhancement of the walls strength capacity near 30% was verified for walls of *h/l* ratio equal to 2 when compared to the 1.33 *h/l* ratio walls. This increase is not so pronounced for 0.35 MPa pre-compression level.

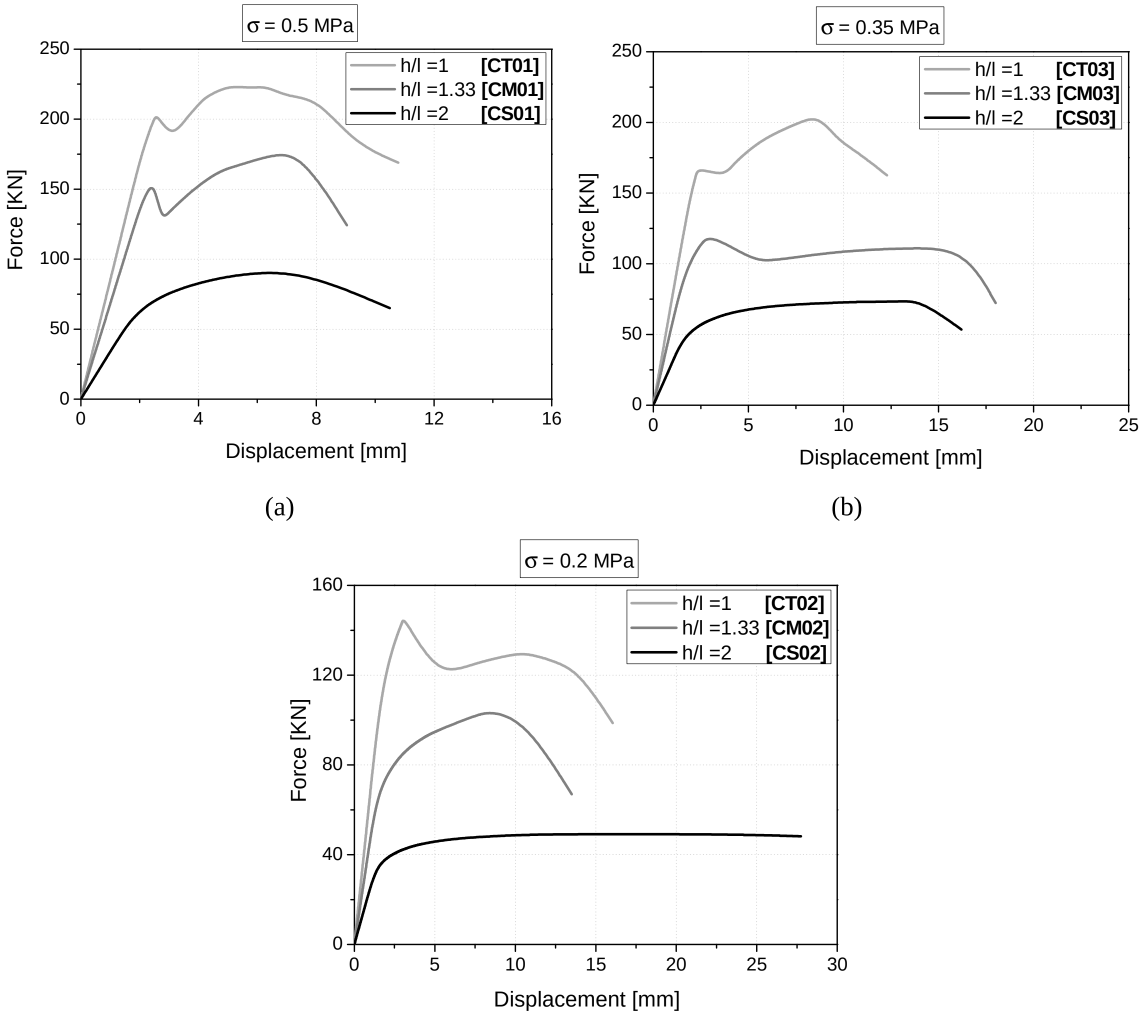

(a)

(b)

(c)

Figure 3.18 Force-displacement curves of the parametric analyses - Comparison according the compression level: (a) 0.5 MPa; (b) 0.35 MPa; (c) 0.2 MPa.

The contribution of the pre-compression level on the wall behaviour is assessed by the analysis of Figure 3.19 in which, for the same geometric configuration, the influence of the stress level is evaluated. It is clear that the lateral strength is enhanced by increasing the level of pre-compression on the wall, for all the geometric configurations. The maximum capacity increase is more or less consistent in all the geometric configurations. Besides the expected differences in the linear stiffness (obtained through the masonry elastic modulus), the non-linear behaviour response of the walls is also influenced by the level of pre-compression. Walls subjected to lower levels of pre-compression tend to exhibit a more ductile behaviour, with the exception of wall CM03 that present also a ductile response.

Walls with lower compression levels and greater height/length relations (slender configurations) tend to experiment a smooth evolution in the force-displacement curve, typical of flexural behaviours. The results of these analysis in which concerns the maximum capacity are very consistent and close to the expected, given other experimental tests results. It is observed also that the contribution of vertical stress level is dependent on the failure mode developed in the pier.

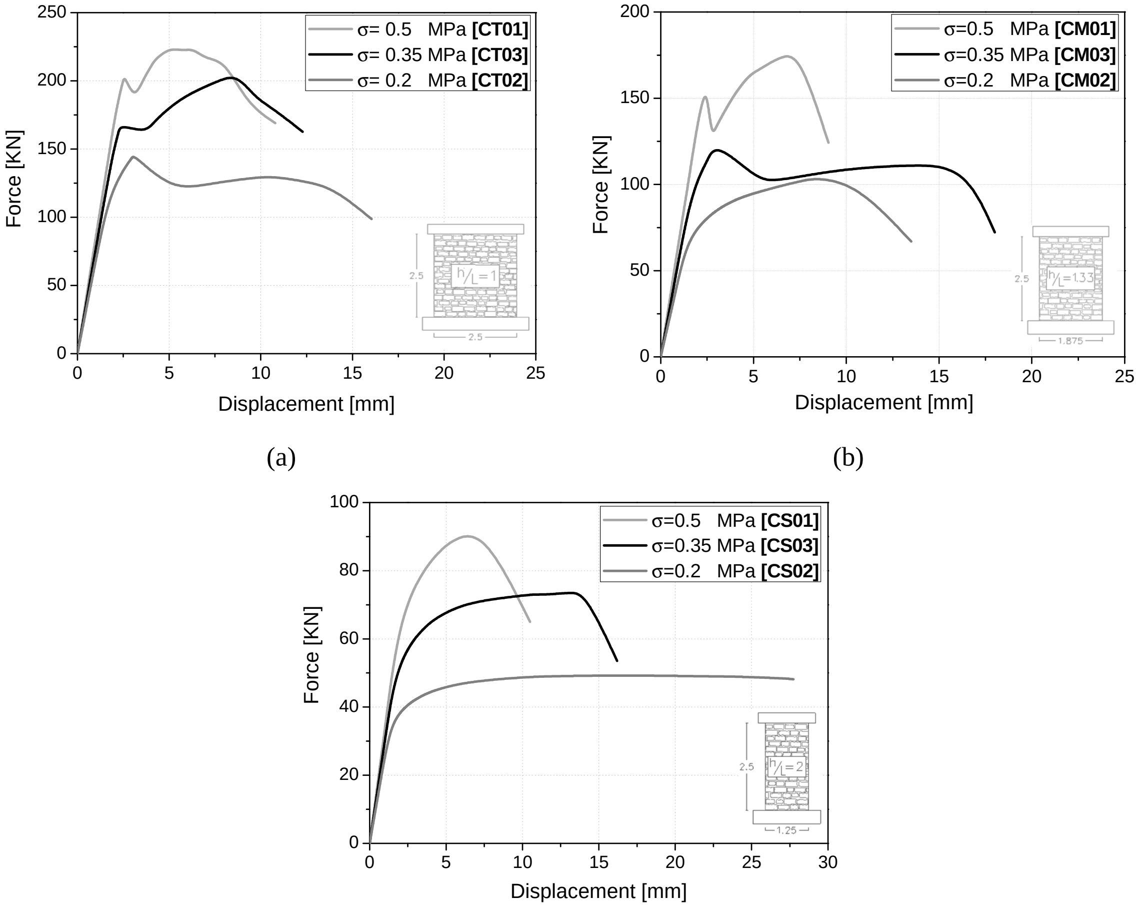

(a) (b)

(c)

Figure 3.19 Force-displacement curves of the parametric analyses - Comparison according the geometric configuration: (a) *h/l* =1; (b) *h/l* =1.33; (c) *h/l* =2.

In order to obtain a better insight on the influence of the vertical compression and geometric configuration in the failure mode, the maximum principal strains distribution were plotted as an indicator of damage for the post-peak behaviour. Figure 3.20 shows the damage distribution of the walls from the parametric analyses organized by level of compression and wall geometry. Analysing the damage patterns, the transition from the flexural behaviour to shear is notorious. Slender walls subjected to lower levels of pre-compression tend to experiment flexural behaviour with the overturning of the wall. The crack pattern of the walls is in accordance with the force-displacement curves presented above.

From the results it is possible to observe that the wall with slender configuration subjected to 0.35 MPa of compression (CS03 wall) suffers a combined shear flexure failure. The severe concentration of damage spreading from the top right corner and bottom left toe points out the flexural behaviour of this wall. Still, the concentration of strains in the diagonal of the pier, from the top corner to the bottom toe, indicates the beginning of the shear behaviour, which turns out to be the one governing the failure at the end with the development of diagonal cracking.

Similarly, the wall with mean slenderness ratio subjected to low compression (0.2 MPa), CM02 wall, presents a damage pattern typical of flexural behaviour including overturning of the wall (rocking) and also shear diagonal cracking in the centre of the wall. Although the evident flexure response experimented by this wall, failure occurs due to the diagonal cracking which spreads along the wall creating instability. The deformation capacity of this wall is more consistent with a shear failure (see Figure 3.18c or Figure 3.19b).

The walls with lower slenderness ratio configurations combined with high levels of pre-compression (CM03, CM01 and CT03), besides achieving more in-plane strength capacity, are clearly governed by shear behaviour. The crack patterned verified for the remaining walls was the development of diagonal cracks at the centre of the pier, as shown in Figure 3.20. The displacement capacity of these walls will be further discussed in the next section.

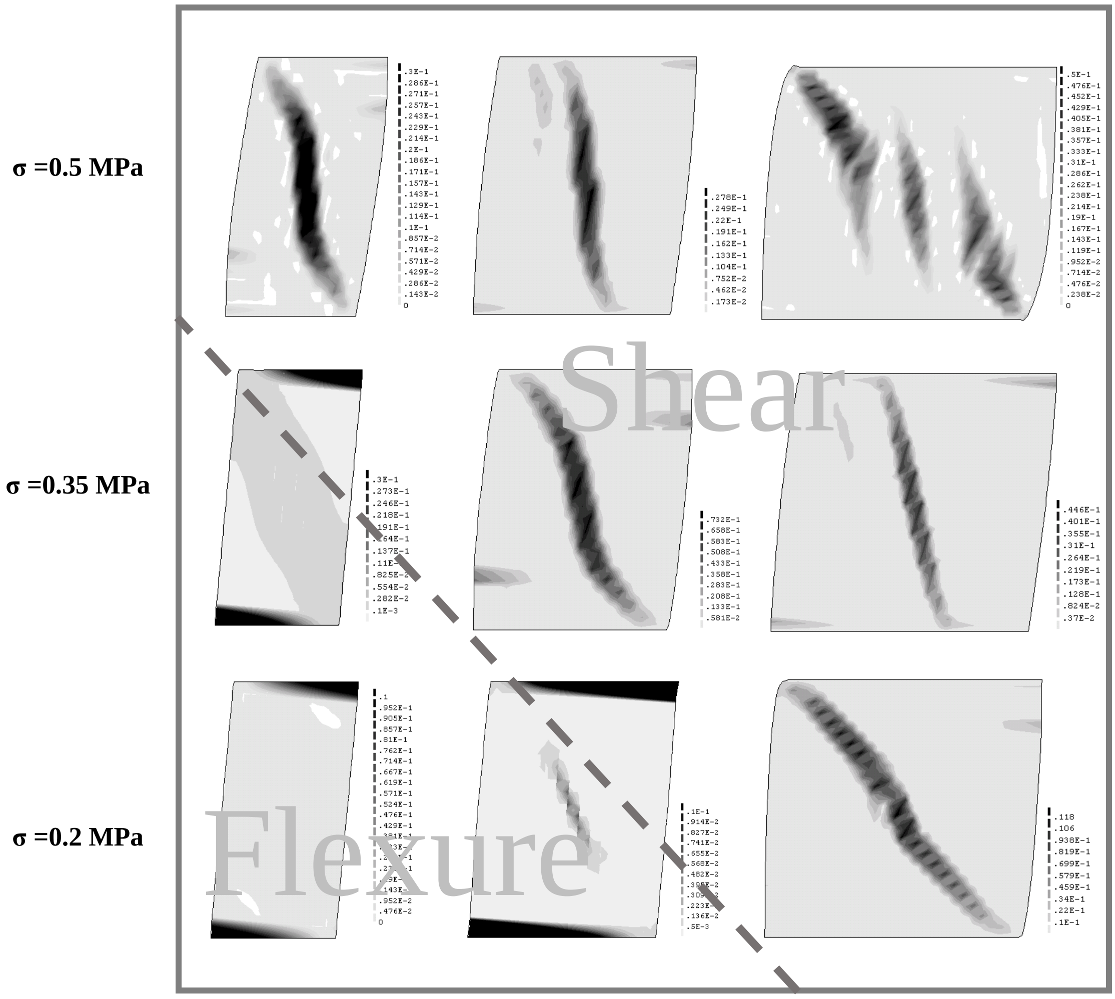

Figure 3.20 Maximum principal strain distribution for the parametrical analyses in at final stage (a possible border between flexure and shear modes is provided).

Numerical results revealed that both the slenderness ratio and the pre-compression level play a central role in the behaviour of masonry walls under in-plane loading, affecting not only the maximum lateral capacity but also the behaviour and failure mode. Parametric analysis carried out in this section enabled to verify in which manner the studied parameters are related, giving relevant information about the response of these walls. The obtained results are consistent, further validating the modelling approach.

3.6. DRIFT CAPACITY

The purpose of this section is firstly to compare the drift capacity obtained numerically with the experimental test results in order to validate the numerical approach and then to estimate the drift capacity for the walls in the parametric analysis. Additional numerical analysis varying the mechanical parameters of masonry were also carried out aiming at comparing the drift limits imposed for different codes with the ones obtained numerically. Here it is intended to give a contribution to the discussion on walls drift capacity.

In recent years, displacement-based methodologies have been progressively developed for the seismic assessment of existing masonry structures. It has been widely accepted that that structural damage is related to material strains and for this reason such methodologies provide a more reliable and realistic evaluation of the damage distribution (Russell 2010). Accordingly, the characterization of the drift capacity of masonry walls is required.

As mentioned before, several experimental campaigns on the in-plane strength characterization of masonry walls have been carried out in the last years, but only a few focus on the drift capacity topic. Experimental research on in-plane behaviour of masonry walls constructed with different materials has been summarized by Magenes and Penna (2011) regarding the ultimate drift capacities. There, a range of drift values is indicated for each type of masonry walls, categorized in shear and flexural failures. The drift capacity of each wall was determined in correspondence of a drop in the shear force-lateral displacement envelope curve equal or greater than 20% of the maximum shear force attained, except for walls governed by flexural failure in which no noticeable strength decay up to very high drift values was observed and the tests were stopped.

A compilation of the ultimate drift of masonry piers corresponding to different failure modes (or a combination of them) observed during the in-plane testing of several piers was also addressed by (Moon 2004). Finally, the drift capacity of masonry walls was also extensively investigated by Petry and Beyer (2014) through an experimental campaign which included the study of walls with distinct boundary conditions and axial load. In this document the authors provide a database compilation of available experimental tests results and the equivalent drift capacity.

In order to give contributions on the drift estimation for design and assessment of masonry structures, a set of numerical analyses using the validated models was performed. The ultimate displacement was defined as equal to a displacement corresponding to 80% of the maximum force, as recommended by EC8 (EC8-3 2004) and FEMA 356 (FEMA 356 2000). This is a conventional limit used by several authors (Costa 2007; Magenes and Penna 2011; Beyer 2012) and generally corresponds to a condition in which the wall is still capable of carrying the vertical load, but additional increases in the deformation demand could lead to the partial or total failure of the element. Accordingly, both the experimental and numerical force-displacement curves were used to assess the displacement capacity of the initial four walls (see Table 3.7). For wall CS02, which experiments a rocking/flexural behaviour according to the numerical analysis, the ultimate displacement could not be estimated since a dropped below 80% of the peak resistance was not verified in the analysis within a reasonable displacement. For this reason the experimental and numerical drift capacity of CS02 wall were not compared. In what concerns the other walls, comparing the drift capacity obtained in the numerical analysis with the experimental values, one can infer that the ultimate displacement is reasonably well estimated by the numerical models. The errors between the experimental and numerical drift capacity can be considered acceptable.

Table 3.7 Comparison between the experimental and numerical conventional drift capacity.

	Displacement Capacity [mm] / Drift [%]			
	CS01	**CS02**	**CT01**	**CT02**
Experimental	10.3 / 0.41	17.0 / 0.68	11.5 / 0.46	12.0 / 0.48
Numerical	9.7 / 0.39	> 25.0 / > 1.0	10.0 / 0.4	14.0 / 0.56
Error	6%	–	13%	16%

Several codes and guidelines proposed a maximum drift capacity for damage limitation depending on the failure mode of the element. The Eurocode (EC8-3 2004), Italian (OPCM 3274 2003; NTC 08 2008) and New Zealand (NZSEE 2006) codes, as well as FEMA guidelines, (FEMA 306 1998; FEMA 356 2000) recommendations are summarized and discussed in the following. EC8 – Part 3 estimates the drift capacity as a function of the type of behaviour (flexure or shear). The drift capacity of an unreinforced masonry wall controlled by flexure should be limited to 0.8% h_0/l, and to 0.4% drift when controlled by shear behavior. h_0 is the distance between the section where the flexural capacity is attained and the contraflexure point and l is the in-plane horizontal dimension of the wall (depth). In the Italian code (OPCM 3274 2003) the in-plane drift in flexure is set 0.8%, unlike Eurocode does not takes into account the h_0/l ratio, and 0.4% drift in shear. These values are defined based on solid brick or stone masonry walls tests since a larger experimental data base is available (Magenes 2006). The recommendations provided by NTC-08 (2008) limit the in-plane drift for flexural behaviour to 0.6% and for shear 0.3%, which are smaller than the values set up by the previous codes. The New Zealand code proposes drift capacities depending on the failure mode instead of the type of behaviour. Thus, rocking and shear sliding are limited to a 1% drift and toe crushing and diagonal cracking are limited to 0.5%. Finally, FEMA also distinguishes drift capacities for the different failure modes. In rocking failure, FEMA assumes 0.8% drift, similarly to EC8 and for the sliding along the joints failure mode a drift of 0.4%. For combined modes FEMA also establish drift limits, being for toe crushing, flexural cracking and bed joint sliding 1.2% of drift and for flexural cracking and toe crushing only a drift capacity of 0.3%.

These limits adopted by codes do not make distinction of masonry typologies and levels of axial load and only few take into account the boundary conditions. Several experimental campaigns have shown that the failure mode and consequently the displacement capacity of masonry walls is scattered and depends on the aforementioned conditions. A wide variation in drift capacity has been reported depending on the failure mode by Yi (2004) and Magenes and Penna (2011) in a compilation of available experimental tests. The drift capacity of unreinforced masonry walls is extensively discussed in the work of Petry and Beyer (2014), in which an empirical drift capacity equation that accounts for the boundary conditions, axial load and the size effect is proposed.

In order to evaluate the influence of the geometrical configuration and vertical stress level in the drift capacity, the force-displacement curves resultant from the parametric analyses were used to define the ultimate displacement according to the criteria defined above. The displacement capacity and equivalent drift is presented in Table 3.8 for the 9 walls. Excluding the wall CM03, numerical analyses showed that the lower the axial compression, the larger displacement capacity attained by the wall. Indeed, parametric analyses showed that walls subjected to higher levels of compression exhibit more stiff responses and higher strength in-plane capacities but the displacement capacity is limited. No evident relation was found in the drift capacity regarding the wall aspect ratio.

Table 3.8 Drift capacity of the parametric analysis walls.

	Drift Capacity		
σ = 0.5 MPa	**CS01** 9.7 mm / 0.39%	**CM01** 8.5 mm / 0.34%	**CT01** 10 mm / 0.40%
σ = 0.35 MPa	**CS03** 15.5 mm / 0.62%	**CM03** 17 mm / 0.68%	**CT03** 12.5 mm / 0.50%
σ = 0.2 MPa	**CS02** > 25 mm / > 1%	**CM02** 12.5 mm / 0.50%	**CT02** 14 mm / 0.56%

Aiming at extending the study of the drift capacity to provide more numerical data, a set of numerical analysis based on these 9 models was performed varying the mechanical parameters of masonry: (i) elastic modulus; (ii) compressive strength; (iii) compressive fracture energy; (iv) tensile strength; (v) tensile fracture energy. The purpose is to evaluate the drift capacity of these walls varying the elastic modulus -25% and +25% and the other parameters -50% and +50% of its initial value. These variations were performed modifying only one parameter at a time and in total 90 numerical analysis were carried out. The ultimate displacement for the sensitivity analysis of CS02 wall could not be evaluated due to the ductile flexural behaviour of this wall, as explained previously. Therefore, 80 values for the drift capacity were graphically plotted and compared with the 0.4% drift, as recommended by most of the codes for shear behaviour (see Figure 3.21). The results showed that the minimum drift of 0.4% proposed in the codes is not attained by all walls, as 26% of the values achieve drifts lower than 0.4% and 6% of them achieve a drift lower than 0.3%.

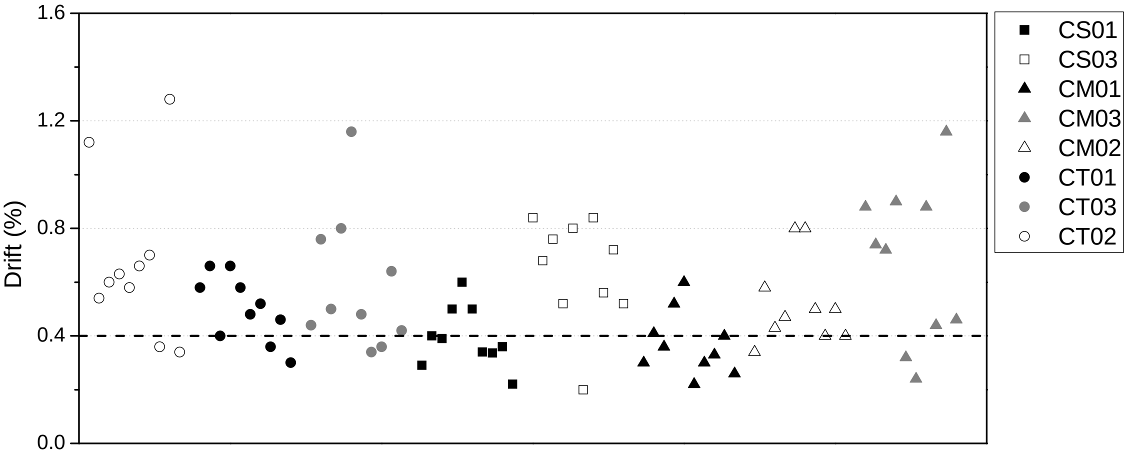

Figure 3.21 Drift capacity.

Aiming at assessing in what measure some parameters influence the walls drift capacity, diagrams which relate the drift capacity with the ratio between vertical stress and masonry compressive strength (Figure 3.22) and the slenderness ratio (Figure 3.23) were plotted. The vertical stress over masonry compressive strength ratio (σ/f_c) was selected in order to allow for a comparison of results provided by some authors (e.g. Petry and Beyer 2014). Besides the typical graph, a box diagram is also drawn, giving valuable information regarding the drift capacity distribution according to the studied parameters. The diagram indicates the spread of the numerical data: the maximum, the minimum, the median (the line in the middle of the box), the mean (represented by the white square) and the "box" which represents the data between 25% and 75%. The spacing between the different parts of the box indicate the degree of dispersion and skewness in the drift values. From Figure 3.22a, it is observed that the drift capacity seems to decrease for higher σ/f_c relations, which mean lower vertical stress levels. In the distribution presented in the box diagram (Figure 3.22b) this relation is not so apparent. The concentration of values for σ/f_c equal to 0.06, corresponding to the walls subject to 0.2 MPa of vertical stress, between 0.4% and 0.7%, is similar to the σ/f_c of 0.11 which is between 0.45% and 0.8%. Nevertheless, it should be noted that for the walls with 0.2 MPa stress, the graph include less values since wall CS02 suffers rocking behaviour and the drift could not be determined. Large values of drift capacity are expected (>0.8%) for this wall, so the box diagram for σ/f_c equal to 0.06 may not be representative (probably the concentration would be for higher values of drift capacity). In this manner, it can be affirmed that walls with lower level of pre-compression tend to exhibit a more ductile behaviour achieving higher drift capacities for lower levels of maximum in-plane strength. Clearly, less dispersion of the drift was verified for walls subjected to 0.5 MPa of pre-compression. These results corroborate the behaviour verified during the numerical study presented in the previous sections.

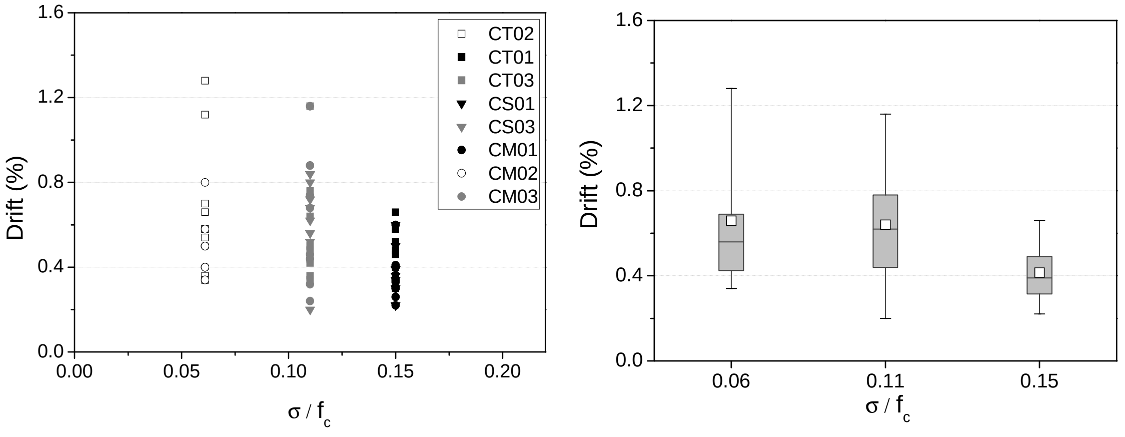

(a) (b)

Figure 3.22 Drift variation in function of the relation between the vertical stress and masonry compressive strength: (a) Scatter graph; (b) Box diagram.

In the assessment of the influence of the slenderness ratio on the lateral drift capacity of the walls, Figure 3.23 displays the drift distribution according to the walls configuration. It is expected that slender walls subjected to shear behaviour tend to exhibit limited horizontal displacement capacity, although this relation is not so evident when comparing with the other walls configuration drifts. Furthermore, walls governed by flexure behaviour or exhibiting combined shear and flexure behaviour reach larger displacement capacity. As observed in the parametric analyses results this type of responses is characteristic of slender walls subjected to lower levels of compression. For this reason, no direct relation can be addressed regarding the influence of the aspect ratio of the walls in the drift capacity.

The force displacement curves obtained in the sensitivity analyses varying the mechanical parameters of masonry are provided in Annex A. Analyzing the overall results from the sensitivity analysis, it should be stressed that parameters like the compressive and tensile fracture energy, and tensile strength influence in a significant way the walls horizontal drift. The results from the analyses varying the masonry elastic modulus show that the walls response only suffer a deviation in what concerns the linear stiffness, whilst similar path is verified in the nonlinear behaviour.

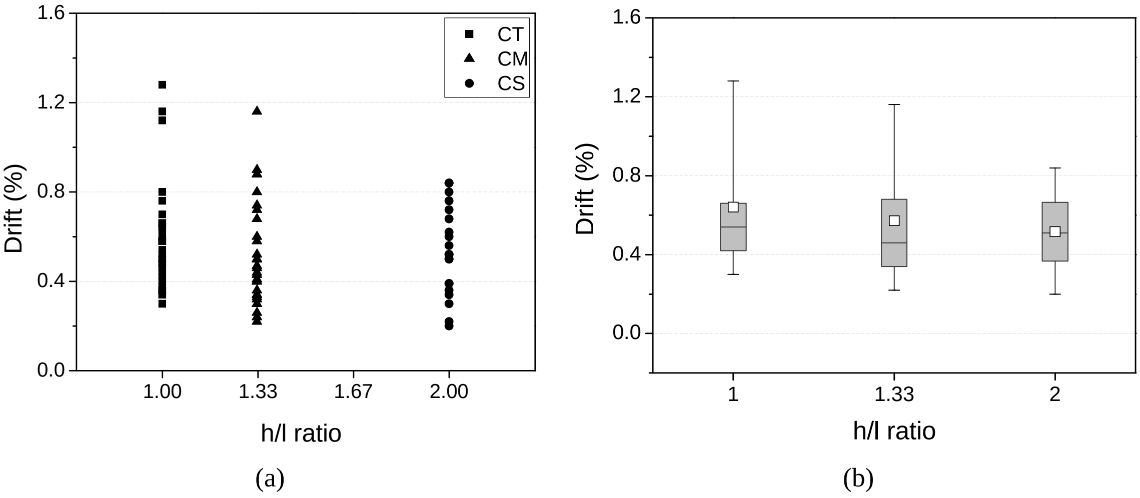

(a) (b)

Figure 3.23 Drift variation in function of the slenderness ratio: (a) Scatter graph; (b) Box diagram.

From the presented results it is possible to observe that the 0.4% drift recommended in codes for shear is not accomplished for all the walls, which raises doubts on the adoption on this limit for all walls. Nevertheless, the analysis of the seismic response of masonry buildings proved that in most cases a non-negligible contribution is provided by the coupling effect of masonry spandrel beams. For this reason, the fixed-fixed condition imposed by the numerical model may not reproduce with good approximation the real conditions in most of masonry buildings piers. In typical masonry buildings, walls are connected by horizontal diaphragms and spandrels which act as coupling elements to piers. The stiffness and strength of these connecting elements can vary but fixed conditions are hardly obtained. Since the drift capacity is highly dependent on the boundary conditions (Petry and Beyer 2014) and aiming at reproducing the boundary conditions of typical masonry buildings, interface elements were included in the previous numerical models on the top of the wall assuming a normal stiffness equivalent to the axial stiffness of a 0.5 m high spandrel placed on the top of the specimen. Only six specimens were considered, corresponding to the walls which attained lower drift capacities.

The results of these analysis showed a consistent increasing on the ultimate displacement, proving that the boundary conditions have an important influence in the horizontal drift capacity attained by the walls. An increase of 37% in average in the drift capacity was verified considering the stiffness provided by 0.5 m of spandrels on the top of the wall. In order to estimate the drift capacity in the remaining walls (not numerically analysed) a simple procedure was taken to give an idea of the drift distribution if different boundary conditions were considered. The drift values obtained previously were increased in 37% (since this is the mean increase) and plotted in Figure 3.24. With this simple procedure, an idea of the expected scattering of the analysed data is provided.

Analysing the drift distribution presented in Figure 3.24, the 0.4% of drift limit is accomplished for 94% of the walls demonstrating that the requirements proposed by codes for shear behaviour is fulfilled for most considering boundary conditions closer to the real ones. It is worth to emphasize that, according to NTC-08 recommendations, the drift limit in shear (0.3%) is accomplished for all walls.

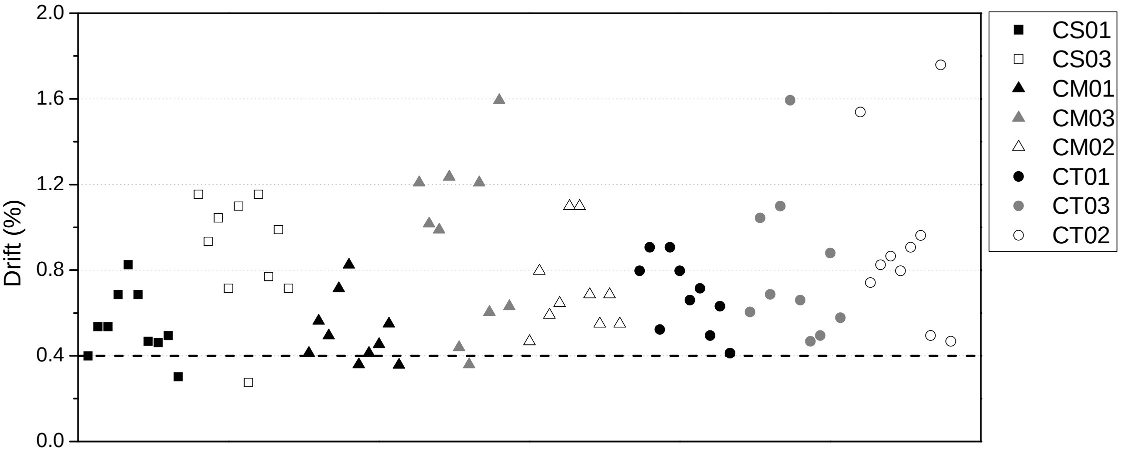

Figure 3.24 Estimation of the drift capacity considering at the top wall the stiffness provided by 0.5 m of spandrels.

3.7. ANALYTICAL EVALUATION

Analytical simplified formulations have been developed trying to characterize and estimate the masonry walls in-plane strength. As previously stated, post-earthquake surveys revealed that, when subjected to in-plane loading, masonry walls tend to fail by one of the four different failure modes (presented and discussed in Chapter 2). Several studies have been developed aiming at characterizing the shear resistance of walls through simplified analytic models. Experimental walls data is used to validate these models rather than on fundamental mechanistic theories and constitutive models (Yi 2004). Relevant European literature documents and codes include and discuss some of these analytical methods (e.g. Magenes and Calvi 1997; Tomaževič 1999; OPCM 3274 2003; EC6-3 2005).

In this section, the strength capacity of the numerically studied walls is estimated based on the simplified formulations proposed by some specific European literature hereinafter termed “European equations” (Turnsek and Cacovic 1971; Turnsek and Sheppard 1980; Mann and Muller 1982; Magenes and Calvi 1997; Tomaževič 1999; EC6-3 2005; NTC 08 2009; Magenes and Griffith 2009b), by U.S. Guidelines (FEMA 356 2000) and New Zealand code (NZSEE 2006). The analytical equations are discussed and the in-plane capacity is compared with the experimental and numerical results. All methods predict the shear behaviour of walls by equations to estimate the strength capacity of the walls according to the failure mode. Table 3.9 summarizes the equations applied and in the following a brief description of them is provided. Note that, given its large number, the description of the symbols used in the expressions is provided in the section: List of Symbols.

Table 3.9 Analytical expressions according to the failure mode.

<table>
<tr><th colspan="2"></th><th>European equations</th><th>FEMA 356</th><th colspan="2">NZSEE</th></tr>
<tr><td rowspan="2">Flexural Strength</td><td>Toe Crushing</td><td>$V_c = \frac{M}{\alpha_1 \cdot h}$
$= \frac{N \times \frac{1}{2}(l - \frac{N}{0.85 f_c . t})}{\alpha_1 \cdot h}$
(3.3)</td><td>$V_c = \alpha_2 \cdot N\left(\frac{l}{h}\right)\left(1 - \frac{N}{0.7 f_c . lt}\right)$
$\frac{l}{h} \geq 0.67$
(3.4)</td><td colspan="2" rowspan="2">$V_f = \frac{M}{h_0} = \frac{N\left(\frac{l}{2} - \frac{1}{2} \cdot \frac{N}{0.85 f_c \cdot t}\right)}{h_0}$
(3.5)</td></tr>
<tr><td>Rocking</td><td>$V_r = \frac{N . l}{2h \times \alpha_1}$
(3.6)</td><td>$V_r = 0.9\alpha_2 \times N\left(\frac{l}{h}\right)$
(3.7)</td></tr>
<tr><td rowspan="2">Shear Strength</td><td>Sliding</td><td>$V_s = l_c t \cdot c + \mu N$
$= \frac{1.5 lt \cdot c + \mu N}{1 + 3\frac{lt \cdot c \cdot \alpha_V}{N}}$
(3.8)</td><td>$V_s = v_{me} \times A$
$= 0.75\left(c + \frac{N}{A}\right) \times A$
$= 0.75 lt \cdot c + 0.75N$
$= 0.75 lt \cdot c + \mu N$
(3.9)</td><td colspan="2">$V_s = \frac{1.5c \cdot lt + \mu N}{1 + \frac{3\alpha_V \cdot c \cdot lt}{N}}$
(3.10)</td></tr>
<tr><td>Diagonal Tension</td><td>$V_t = \frac{f_t \times lt}{b}\sqrt{1 + \frac{N}{f_t \cdot lt}}$
$b = \begin{cases} 1.5 & h/l > 1.5 \\ h/l & 1 \leq h/l \leq 1.5 \\ 1 & h/l < 1 \end{cases}$
(3.11)</td><td>$V_t = f_t \times A \cdot \left(\frac{l}{h}\right)\sqrt{1 + \frac{N}{f_t \cdot lt}}$
(3.12)</td><td>${V_t}^j =$
$\frac{c \cdot lt + \mu N}{1 + \alpha_V}$
(3.13)</td><td>${V_t}^u =$
$\frac{f_{ut} \times lt\sqrt{1 + \frac{N}{f_{ut} \cdot lt}}}{2.3(1 + \alpha_V)}$
$(1 + \alpha_V) \leq 2.5$
(3.14)</td></tr>
</table>

3.7.1. European Equations

The lateral resistance of a wall subjected to in-plane load according to European literature (Turnsek and Cacovic 1971; Turnsek and Sheppard 1980; Mann and Muller 1982; Magenes and Calvi 1997; Tomaževič 1999; EC6-3 2005; NTC 08 2009; Magenes and Griffith 2009b) can be assessed by considering an analytic equation for each failure mode. Note that in flexural responses some authors do not distinguish the toe crushing and rocking failures once the analytical equations that describe their behaviour follow the same principles.

The shear resistance of a wall failing in toe crushing is conditioned by the crushing of the compressive zone which can be approximated to a proper stress distribution as illustrated in

Figure 3.25, neglecting the masonry tensile strength. The vertical stress distribution at the compressed toe is commonly assumed as an equivalent rectangular stress block with κ coefficient equal to 0.85. Thus, the equilibrium of forces in Figure 3.25 leads to the expression to estimate the wall strength for toe crushing (see Table 3.9, equation (3.3)). A factor α_1 to take into account the boundary conditions is also suggested by many authors (equal to 0.5 for fixed-fixed conditions and to 1 to cantilever walls), which is valid hereinafter.

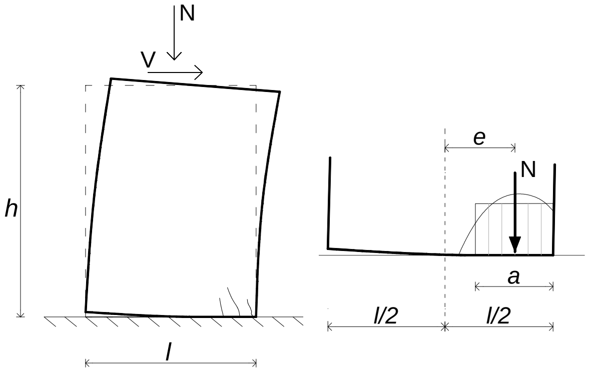

$$M = N.e \qquad N = \kappa f_c.a.t \Leftrightarrow a = \frac{N}{\kappa f_c.t}$$

$$e = \frac{l}{2} - \frac{a}{2} = \frac{1}{2}(l - a) \Leftrightarrow e = \frac{1}{2}\left(l - \frac{N}{\kappa f_c.t}\right)$$

$$M = N.e = N \times \frac{1}{2}\left(l - \frac{N}{\kappa f_c.t}\right)$$

Figure 3.25 Equilibrium of the wall subjected to vertical and horizontal loads with crushing at the base corner.

The rocking failure mode represents the overturning of the masonry pier, as the horizontal displacement increases the wall rotates around the toe. Thus, the shear strength of a wall failing in rocking is easily computed by the equilibrium of the rigid block around O (see Figure 3.26). Equation (3.6) describes the in-plane capacity of the wall for rocking, taking into account the boundary conditions through the parameter α_1.

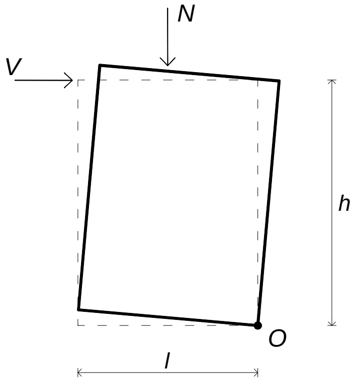

Figure 3.26 Overturning around O.

Bed-joint sliding failure occurs when the shear stress acting on the effective section exceeds the maximum bed-joint shear strength. It has been generally accepted that the shear resistance can be evaluated based on the Mohr-Coulomb formulation (Magenes and Calvi 1997) assuming the effective uncracked section length (as adopted by the EC6 on masonry structures). The length of the effective compression zone is calculated neglecting the masonry tensile strength and assumes a simplified distribution of compression stresses, as described by Figure 3.27. The obtained expression is easily deduced by these relations and is presented in Table 3.9, equation (3.8).

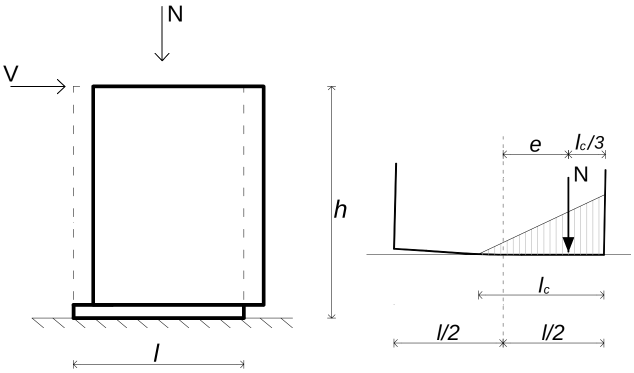

$$\frac{l_c}{3} = \frac{l}{2} - e \iff l_c = 3\left(\frac{l}{2} - e\right) \quad M = V.h_0$$

$$M = N.e \iff e = \frac{M}{N} \quad \alpha_V = \frac{h_0}{l}$$

$$l_c = 3\left(\frac{l}{2} - \frac{M}{N}\right) \iff l_c = 3l\left(\frac{1}{2} - \frac{V.h_0}{N.l}\right)$$

Figure 3.27 Calculation of the length of the compression zone.

Finally, the expression to estimate the lateral strength in diagonal cracking was formulated by (Mann and Muller 1982), based on the tests performed in Slovenia (Turnsek and Cacovic 1971; Turnsek and Sheppard 1980). As reported by (Tomaževič 1999), this formulation assumes that the diagonal cracks are caused by the principal tensile stresses developing in the wall (with a critical value according to the tensile strength of masonry) and accounts for the influence of the geometric configuration in the load distribution. Assuming that the masonry wall is an elastic, homogeneous and isotropic element, the lateral resistance of a masonry wall falling in shear by diagonal cracking (Figure 3.28) is evaluated through the expression (3.11). This formulation includes the consideration of a parameter b which is dependent on the pier aspect ratio $h/_l$, and accounts for the distribution of shear stress at the center of the wall. A value of b equal to 1.5 has been proposed for walls with slenderness ratio greater than 1.5, between 1 and 1.5 aspect ratios b is assumed equal to the relation $h/_l$ and a value of 1 has been proposed for walls with aspect ratio less than 1, giving good agreement with experimental results (Magenes and Calvi 1997).

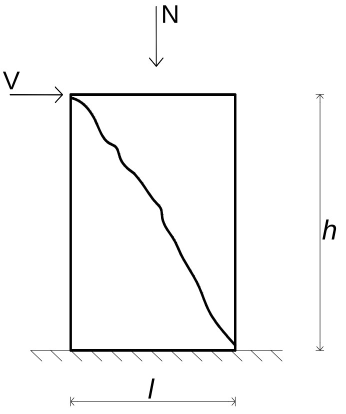

Figure 3.28 Diagonal Cracking.

The analytical predictions proposed by FEMA and NZSEE guidelines follow similar principals of the formulations presented above in some expressions and for this reason only a brief explanation will be addressed for these formulations.

3.7.2. FEMA Predictions

In FEMA recommendations (FEMA 356 2000), the in-plane capacity of walls components is evaluated as the lower value of the lateral strength, based on each of the four typical failure modes. Four analytical expressions, corresponding to the failure modes described in Chapter 2 by Figure 2.10, are proposed for the calculation of the strength capacity. Table 3.9 presents the equations provided by FEMA. The wall strength capacity is evaluated through equation (3.15), which considers the minimum value obtained for all failure modes. The factor α_2 reflects the boundary conditions: for a fixed-free cantilever wall, α_2 is taken as 0.5 and for a fixed-fixed pier equal to 1.0.

$$V_n = MIN(V_c;\ V_r;\ V_s; V_t) \tag{3.15}$$

For toe crushing (equation (3.4)), rocking (equation (3.7)) and diagonal (equation (3.12)) strength predictions the equations are very similar to the ones proposed by the European literature although some differences can be found. Here, in toe crushing strength prediction the vertical stress distribution at the compressed toe is considered 0.7fc (instead 0.85fc). In the equation for rocking failure a factor of 0.9 is introduced and the expression for diagonal cracking is equivalent of the one defined above in the case of walls with slenderness ratio (*h/l)* between 1 and 1.5. The modification introduced by the parameter b described above in the formulation to describe diagonal cracking has been discussed by some authors (Yi 2004; Russell 2010) which considered that it agrees better with the experimental results.

Similarly to the European expression, the strength prediction of sliding follows the Mohr-Coulomb criterion although here the effect of moment is not considered so the reduction in the effective length of the pier due to the presence of horizontal flexural cracks is not considered in FEMA (equation (3.9)). These recommendations are applied and discussed in detail by several researchers (Moon 2004; Yi 2004; Russell 2010; Ingham 2011).

3.7.3. NZSEE Predictions

Similarly, the New Zealand Society for Earthquake Engineering (NZSEE, 2006) provides guidelines for predicting the nominal in-plane lateral strength of masonry walls also summarized in Table 3.9 .Despite considering separate failure modes for several authors, rocking and toe crushing failure modes are often linked since the overturning of the wall includes the simultaneous crushing of the compressed toe. Considering this, in these recommendations only one equation to determine the flexural strength limit is provided (equation (3.5), similar to the “European” formula for toe crushing). Likewise, the equation recommended by for sliding shear is also defined through the same principles explained in section 3.7.1 (V_s equation (3.10)). The main difference of these guidelines is the consideration of two equations to estimate diagonal tension failure mode: one is intended to reflect crushing in mortar joints and is based on a Mohr-Coulomb failure criterion applied over the full length of the member (${V_t}^j$ in equation (3.13)) and the other intends to reflect shear associated with diagonal tension failure involving cracking through units (${V_t}^u$ in equation (3.14)).

3.7.4. In-plane Strength of the Walls

As given by the above expressions, the computation of the in-plane strength of a masonry wall is largely dependent on the axial load, the geometrical wall configuration and boundary conditions (fixed-fixed or cantilever walls). The limiting strength capacity was calculated for the studied walls according to these expressions, using the strength values from the analyses.

The results obtained by the application of the simplified expressions are summarized in Table 3.10 and Figure 3.29. The prediction by the formulations are compared with the lateral capacity achieved numerically for the nine walls. Table 3.10 presents the in-plane shear capacity achieved numerically for the nine walls under study and also the results from the application of the formulas defined above for each failure mode. In the analytical predictions, the lower value obtained considering all the failure modes is presented in bold. A comparison between the numerical and the estimated in-plane capacity of the walls is also provided in this table, dividing the predicted value by the numerical value. Finally, in the last column of Table 3.10 the obtained failure modes are compared. Since sliding could not be simulated by the proposed modelling strategy, the type of failure mode was compared considering shear and flexural failure.

The results show that only 10% of the failure modes is not well predict regarding shear and flexural behaviour. Besides, the failure modes inaccurately evaluated are related to FEMA formulations, which can raise doubts regarding some considerations taken by these guidelines. Analysing with more detail the obtained strength values for FEMA, it can be realized that the sliding shear expression seem not to describe accurately the behaviour since the effect of moment is not considered and the effective length is not used, as also discussed by (Yi 2004). Moreover, the expression provided in FEMA for diagonal cracking seem to be very conservative for *h/l* relations lower than 1 (slender walls), whilst the European expressions include the correction through *b* factor. The results also proved that the NZSEE expressions for the prediction of the walls strength for diagonal cracking failures, can estimate accurately the values obtained numerically.

The relation between the analytically predicted strength and the numerical values is near 1 in most cases, which reveals a good agreement between simplified formulations and experimental/numerical results (since the numerical models were also validated against the experimental). Globally the European and NZSEE formulations can predict well the failure mode and the lateral resistance of masonry walls.

Table 3.10 Strength prediction.

			Prediction [kN]					$\frac{V_{\text{min,predict}}}{V_{\text{numeric}}}$	Same failure mode?
	Numeric [kN]	Failure Modes / Formulations	Flexure		Shear				
			Toe Crushing	Rocking	Sliding	Diagonal Cracking			
CT02	146	European	180	198	**144**	186		0.99	Yes
		FEMA	**177**	178	269	186		1.21	No
		NZSEE	180		**144**	160	375	0.99	Yes
CT03	205	European	273	318	**209**	220		1.02	Yes
		FEMA	263	286	359	**220**		1.07	Yes
		NZSEE	273		209	**192**	391	0.94	Yes
CT01	225	European	352	438	268	**248**		1.10	Yes
		FEMA	334	394	449	**248**		1.10	Yes
		NZSEE	352		268	**223**	406	0.99	Yes
CM02	104	European	102	111	**92**	105		0.89	Yes
		FEMA	**99**	100	201	105		0.95	No
		NZSEE	102		**92**	108	253	0.89	Yes
CM03	121	European	153	179	137	**123**		1.02	Yes
		FEMA	148	161	269	**123**		1.02	Yes
		NZSEE	153		137	**129**	264	1.07	Yes
CM01	176	European	198	246	180	**140**		0.80	Yes
		FEMA	188	222	336	**140**		0.80	Yes
		NZSEE	198		180	**151**	274	0.86	Yes
CS02	49	European	**45**	50	47	62		0.92	Yes
		FEMA	59	**45**	134	47		0.92	Yes
		NZSEE	**45**		47	60	141	0.92	Yes
CS03	74	European	**68**	80	73	73		0.92	Yes
		FEMA	88	72	179	**55**		0.74	No
		NZSEE	**68**		73	72	147	0.92	Yes
CS01	92	European	88	110	99	**83**		0.90	Yes
		FEMA	112	99	224	**62**		0.67	Yes
		NZSEE	88		99	**84**	152	0.91	Yes

Figure 3.29 displays the results in a bar diagram. For each wall the in-plane strength according to the numerical results and analytical predictions are plotted. The in-plane strength capacity presented in the form of diagram allows for an easier interpretation of the results and promotes the comparison between walls. Here, the influence of the geometric configuration and compression load in the horizontal capacity of the wall is easily perceptible. In what concerns the analytical predictions, globally good agreement with the numerical was verified for all the formulations. For slender walls (CS) minor differences were found for European and NZSEE

predictions comparing with the achieved numerical lateral strength, and less reasonable errors for FEMA predictions when diagonal cracking is governing the failure. The strength capacity CM01 wall was slightly underestimated by the analytical formulations, being the expressions provided by NZSEE the ones giving closer values to the numerical values, with an error of around 14%. For the remaining CM walls (CM02 and CM03), the strength capacity is very well estimated by all the formulations as can be graphically confirmed in Figure 3.29. The in-plane capacity of CT01 wall was predicted with very good precision by NZSEE expressions and with good approximation by the others. Good agreement was also found in the estimation of the in-plane capacity of wall CT03 by the simplified formulations. European and NZSEE analytical predictions achieved very close strength values when compared to the numerical for wall CT02. FEMA mispredicted the failure mode for this wall and for this reason the strength capacity attained is overestimated.

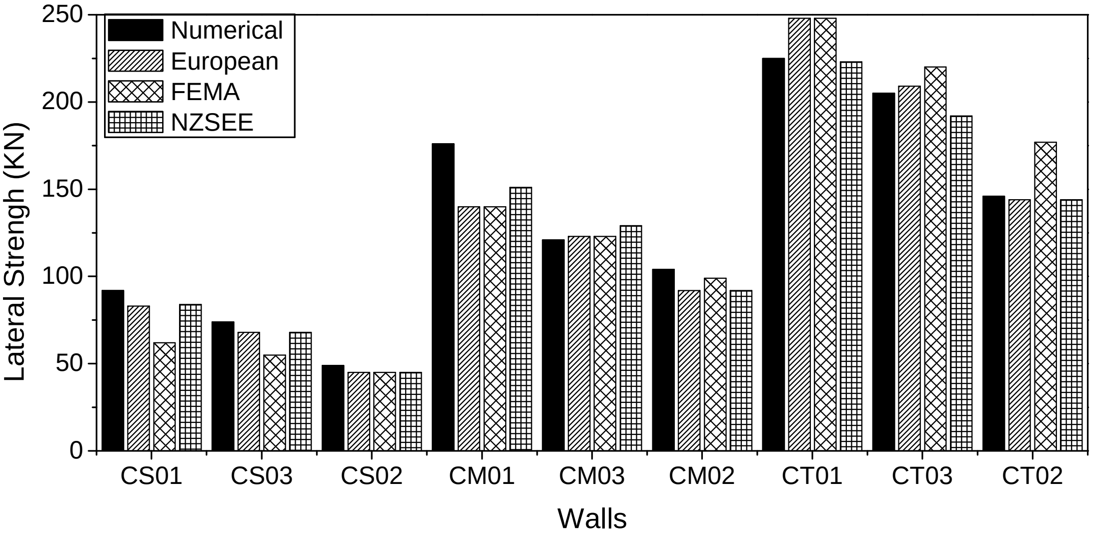

Figure 3.29 Comparison between numerical shear strength and predictions by analytical models.

Based on the investigated analytical models and comparison with the test results, it can be concluded that all the analytical models for unreinforced masonry walls can predict successfully and with good approximation the maximum shear capacity of the walls and failure modes regarding shear and flexural behaviour.

3.8. FINAL CONSIDERATIONS

In this Chapter a discussion on the in-plane behaviour of masonry walls with different slenderness ratios and distinct levels of axial load subjected to shear loading is addressed, using advanced numerical simulations. The numerical study was based on the experimental campaign performed at the EUCENTRE and University of Pavia on stone masonry piers. Aiming at simulating the in-plane behaviour of masonry walls experimentally tested, finite element models were prepared.

Linear analyses results showed large difference on the initial walls stiffness when compared with the measured experimental behaviour. The calibration procedure, as well as the analysis and comparison with similar available experimental results, allowed the conclusion that the elastic modulus should be updated according to the pre-compression level. In order to calibrate the numerical models, the elastic modulus of masonry was updated to adjust the walls stiffness to the experimental behaviour since it is highly influenced by the by axial pre-compression.

Good agreement was found between the experimental force-displacement envelope and the numerical capacity curve. The efficiency of finite element continuum modelling to forecast a representative failure mode of the masonry was investigated. Comparing with the failure in experiments, the failure modes were also well estimated by the numerical models, proving the potential of the presented numerical strategy to simulate the in-plane behaviour of masonry walls with accuracy. The limitation of the numerical approach to simulate sliding was discussed during the Chapter and it was considered that this would not provide significant changes in the prediction of the wall behaviour or strength capacity.

This work demonstrates that the understanding of the behaviour of masonry walls under in-plane loading can be significantly improved by numerical approaches. The validation of the numerical models is an imperative step to gain confidence in the subsequent results. The presented numerical strategy can be seen as a complementary way to study masonry piers, particularly useful for parametric studies after model validation.

With the purpose of extending the study of masonry walls to other configurations and stress levels, and taking advantage of the validated models, parametric analysis were carried out. The results allowed for the in-plane behaviour characterization of 5 additional walls, defining the lateral strength capacity and estimating the damage distribution. It was possible to confirm that flexure failure modes were predominant in slender walls with low levels of pre-compression. Walls with lower slenderness ratios subjected to higher compressive loads tend to exhibit typical shear behaviour with diagonal cracking developing at the centre of the pier. It was also demonstrated that the higher level of pre-compression the greater in-plane capacity of the walls and the larger slenderness relation the lower lateral capacity achieved by the walls.

The walls deformation capacity was also assessed and discussed according to the drift limits imposed by codes. Besides the 9 walls studied, the mechanical parameters of masonry were also varied in order to obtain a more extensive data in a total of 90 analyses. The study was intended to provide additional insight into how the parameters used in the analysis influenced on the capacity. The drift data attained in these numerical analysis were compiled and compared to drift codes limits. A number of walls did not fulfilled the limit imposed and for that reason different boundary conditions at the top of the wall were studied. With the purpose of simulating the coupling provided by spandrels, a stiffness equivalent to 0.5 m of masonry spandrels was considered to carry some additional analyses. Numerical models including interface elements at the top to simulate the stiffness provided by 0.5 m of spandrels were studied estimating an increase of 37% in average in the deformation capacity. Thus, considering this more realistic boundary conditions the typical drift limit in the codes is fulfilled for 94% of the walls.

Finally, the usage of a simplified formulations to predict the strength capacity of walls is also addressed, which are associated to distinct failure modes occurring in masonry walls under in-plane loading. The comparison between the numerical results with the lateral shear strength estimated by simplified models, revealed that these expressions can predict with very good approximation both the failure mode and the lateral resistance of a wall. FEMA expressions can mispredict the failure modes. European and NZSEE seem to better estimate the failure modes and predict with precision the walls in-plane capacity.

Chapter 4

BEHAVIOUR OF INJECTED ANCHORS ON MASONRY WALLS

4.1. INTRODUCTION

The widespread presence of masonry buildings worldwide emphasized the great vulnerability of the majority of these buildings to seismic events, mostly due to the lack of effective connections between elements (Mandara et al. 2009). It has been well documented by post-earthquakes surveys that the global seismic behaviour of masonry structures highly depends on the efficiency of the connections among vertical and horizontal structural elements.

As mentioned in Chapter 2, typical unreinforced masonry buildings are in general composed of multiple load-bearing masonry walls arranged in orthogonal planes, with relatively flexible floor diaphragms. The capability of the structures to redistribute horizontal loads depends on the connection between orthogonal walls, the flexibility of the diaphragms and their connection to the masonry walls (Lourenço et al. 2011). The combination of effective connections and floor diaphragms, stiff enough to redistribute the horizontal actions through in-plane walls, provides the so called “box behaviour” to the building, which usually leads to a good performance of the whole structure when subjected to horizontal actions (Lourenço et al. 2009; D’Ayala 2011). For this reason the strengthening of the connections between structural elements became an eminent issue in the past few years since it can improve the global performance of a masonry building in a significant way.

It is often stated that the culture and history of a country can be reported by its heritage buildings. Bearing this in mind, special attention should be given to the choice of potential reinforcement solutions. Accordingly, injected anchors are particularly well suited to repair and strengthen ancient masonry buildings considering aspects of minimum intervention and quality requirements, mainly because the function and appearance of the masonry will be not affected and the new elements will not be discernible (Gigla 2004). Furthermore, its design features allow for adaptations that meet safety requirements while still remaining sensitive to the original architecture. Indeed, the improvement of the connections behaviour by application of injected anchors is a recurrent technique in ancient and historic masonry. Potential strengthening solutions for connections between structural elements using injection anchors have been presented in section 2.4 (see Figure 2.13). In this work, the study of injected anchors in stone masonry walls as a possible solution to strengthen walls to half-timber-walls connections is addressed.

An experimental campaign recently carried out at University of Minho on connections aimed at assessing the performance of masonry-to-timber connections strengthened with injected anchors. These connections are representative of wall-to-wall connections found in ancient buildings built after the 1755 Lisbon earthquake. Figure 4.1 illustrates the strengthening solution adopted for the improvement of the connection between external and internal walls, consisting of two parallel Cintec® anchors injected in the external masonry wall and connected to the internal wall by means of suitable steel plates, as proposed in Cóias (2007). This technique basically consists on a tensile-resistant element, usually steel, inserted into a borehole filled with grout, which carries the tensile forces. Since an effective connection between perpendicular walls is granted by the injected anchors in masonry walls, the overturning of the external walls (out-of-plane collapse) is avoided and the horizontal forces can be transferred to the adjacent walls, which will present a more stable in-plane behaviour, activating global failure mechanisms.

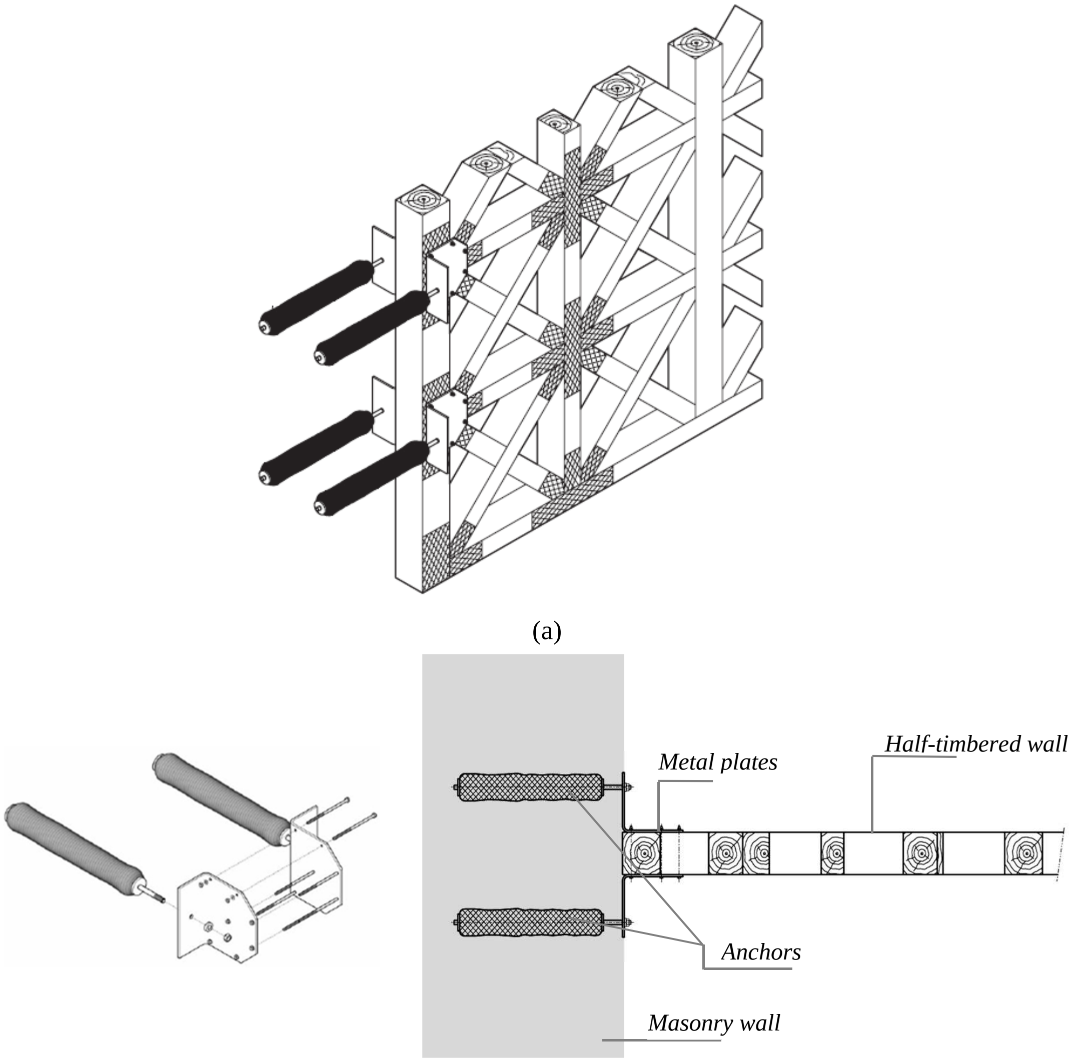
(a)

(b) (c)

Figure 4.1 Strengthening solution with parallel anchors: (a) 3D view of the timber frame wall and the connecting anchoring system; (b) Connecting system; (c) Top view strengthening system (adapted from (Cóias 2007).

Notwithstanding the importance of connections, the knowledge on the behaviour of injected anchors in masonry is very limited and only few experimental campaigns on injected anchors in masonry are available (Gigla and Wenzel 2000; Arifpovic and Nielsen 2004; Gigla 2004; Ashour and Alqedra 2005; Algeri et al. 2010). Experimental results indicate that the main factor limiting the capacity of the anchoring system is usually not the failure of steel or the steel/grout interface, but rather the somehow reduced shear and tensile strength of the masonry substrate to which the anchor is injected.

The failure modes experimentally identified for injected anchors in masonry seem to be similar to the ones found for anchors in concrete (Gigla and Wenzel 2000; Arifpovic and Nielsen 2004; Gigla 2004; Ashour and Alqedra 2005; Algeri et al. 2010). The load transfer between the steel element and the surrounding masonry comprises two interfaces: the outer intersection between masonry and grout, and the inner intersection between grout and the steel element. When subjected to tensile loading, injected anchors in masonry may exhibit the following failure mechanisms (see also Figure 4.2):

- Steel tensile failure: the anchor is loaded until the yielding of steel (Figure 4.2a);
- Masonry cone failure: shear cone-like surface failure that occurs in the masonry with detachment of a small part of the wall around the anchoring system (see Figure 4.2b);
- Sliding failure along the outer interface: sliding of the anchoring system by failure at the masonry-grout interface (outer interface) with the disconnection of the anchoring system from the wall (see Figure 4.2c);
- Sliding failure along the inner interface: sliding of the steel anchor along the steel-grout interface (inner interface), involving local failure (see Figure 4.2d).

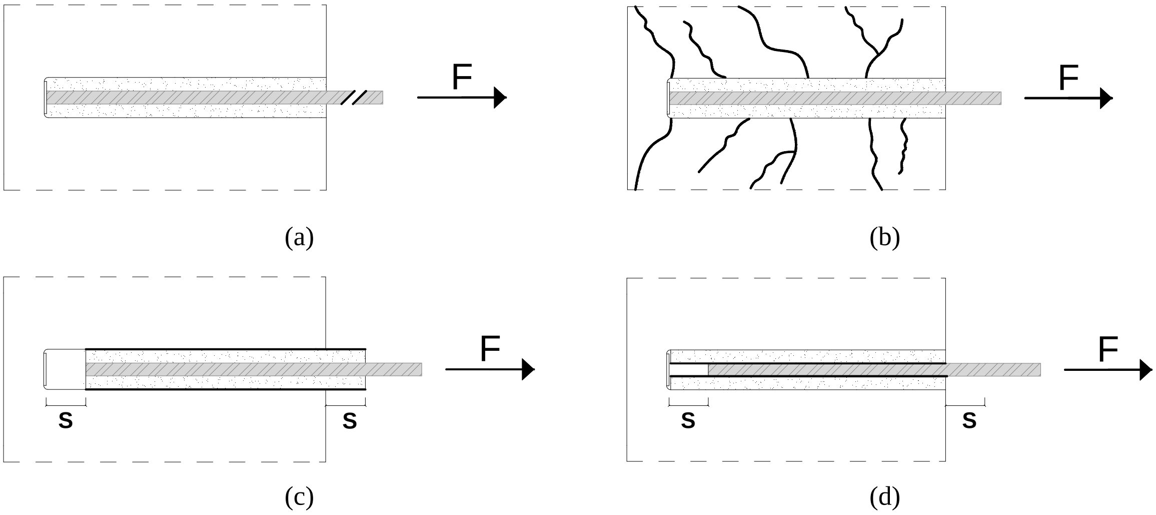

Figure 4.2 Possible failure mechanisms in anchoring systems: (a) Steel failure; (b) Masonry cone failure; (c) Sliding failure along the outer interface; (d) Sliding failure along the inner interface (adapted from Algeri et al. 2010).

Although the four individual failure mechanisms are possible, steel failure is rarely observed and takes place only in cases when the embedment depth and strength of the masonry are very high. A combination of two different failures was also observed experimentally (Arifpovic and Nielsen 2004; Gigla 2004). Usually, the masonry cone failure occurs with the presence of the cone formation simultaneously with sliding (also called bond failure) along the outer interface.

Masonry is a heterogeneous material with many variations with regards to the units' configuration, its strength and the mortar characteristics. The behaviour of the masonry components, as well as the organization and ratio of units and joints, has a significant influence in the ultimate capacity of the anchoring system, since the masonry global behaviour and bond strength of the injected anchor affects the load transfer mechanism (Meyer and Eligehausen 2004). For this reason the tensile force in anchors needs to be limited in accordance with the properties of the surrounding material.

As proved by previous experimental tests, the performance of injected anchors in masonry depends of several factors that combined can generate a diversity of different anchors conditions. Masonry properties, anchor embedment depth, spacing between anchors, anchor diameter among other factors influence the masonry behaviour and consequently affect the load transfer mechanism of injected anchors (Meyer and Eligehausen 2004). The study of the influence of these parameters on the behaviour of injected anchors in masonry is almost impractical from an experimental point of view and the numerical studies in this field are also scarce. For this reason, reliable numerical models, which simulate accurately the behaviour of the anchor injected in masonry, can be used as a numerical laboratory, where the sensitivity of the results to material parameters, geometrical features and actions can be studied.

In this Chapter an extensive numerical study based on the results from experimental tests carried out at the University of Minho is presented. The Chapter is organized into four sections, covering from the brief description of the experimental programme results, the development of the numerical model and its validation, going through parametric analyses to the application of simplified analytical expressions. Firstly, the outline of the experimental programme, which includes the most relevant results obtained in the tests and used in the numerical study, is addressed. Then, the numerical study resorts to a detailed 3D finite element model, which is intended to reproduce the experimental test setup and procedure. The numerical model calibration process was performed through the comparison with the experimental outcomes. Nonlinear analyses to numerically characterize the nonlinear behaviour of the anchoring system are also presented and discussed in this section. Additionally, the model validated against the experimental results was used to perform parametric analyses in order to evaluate the influence of key parameters discussed here and over section 2.4. Nonlinear analyses to evaluate the influence of the masonry quality, wall pre-compression level, embedment depth, anchors diameter and anchors spacing in the ultimate deformation capacity, ductility and failure mechanism are presented and discussed. The goal is to define critical parameters by studying the effect of selected variables on the behaviour of the anchors installed in the masonry wall. Finally, simplified analytical approaches to estimate the strength capacity of injected anchors on masonry are briefly reviewed and the results compared both with the experimental and numerical outcomes.

4.2. EXPERIMENTAL CONTEXTUALIZATION

In this section a brief contextualization of the experimental campaign carried out at University of Minho on injected anchors in masonry walls is presented. Detailed information regarding the experimental campaign can be found elsewhere (Moreira et al. 2012).

The strengthening solution proposed in the previous section consists of two injected anchors placed parallel to each other in an irregular stone masonry wall, connected to the half-timbered wall by means of steel angles. The specimens were designed without the half-timbered wall, focusing exclusively on the strengthening solution. The experimental campaign included the construction and testing of several real scale masonry walls in which parallel Cintec® anchors were applied. The applied Cintec® anchoring system is straightforward consisting on the injection of a cementitious grout into a fabric sock, which has already been placed in an oversized drilled hole (Cintec 2012).

Specimens intend to recreate as much as possible representative conditions of existing buildings from Lisbon constructed after the 1755 earthquake. Stone masonry walls were constructed with rubble limestone units from the surroundings of Lisbon and mortar with a ratio of 1:3:10:6

(cement, hydraulic lime, river sand, yellow sand) with a compressive strength of 1.27 MPa (28 days). The rubble masonry specimens were hand constructed and have 2 m width and 1.6 m high. Walls were built with a thickness of 0.4 m, representative of a 4th floor wall, which directly interferes in the anchor embedment depth (0.35 m) and, consequently, on the response of the anchor to pull-out forces. A pair of parallel anchors were introduced in the masonry specimen in two levels in order to optimize the available resources (see Figure 4.3a). In order to reproduce typical field conditions to make the boreholes, the wall was loaded vertically under compression in order to reproduce the expected compressive stress state caused by permanent loads at a 4th floor. The anchoring system was installed only after the loading of the walls. The 16 mm diameter steel bars were inserted into 50 mm diameter boreholes injected with a Cintec® grout (Presstec™), resulting in a two-anchor system with 280 mm distance between anchors considering a half-timbered wall 120 mm thick plus the constructive distances of the steel angle connecting both walls (see Figure 4.3b). The cement grout provided by Cintec® is part of their standard anchoring solution and presents a tensile strength of 4.5 MPa and a compressive strength of 51.5 MPa, both at 28 days. The steel bars of the anchoring system were made of stainless steel AISI 304 class 70, in order to keep them within the elastic range during the entire test.

Monotonic and cyclic pull-out tests were performed in order to assess the performance of the anchoring system and to characterize its behaviour. The vertical load was applied with actuators designed to apply a constant compressive stress of 0.20 MPa to the masonry wall through the stiff HE200B metallic beams, in order to simulate the effect of quasi-permanent loads in the structure. The pull-out horizontal load, which intends to recreate the seismic action, was applied in the two parallel injected anchors at the same time. Monotonic or cyclic displacements were imposed increasingly until one of these conditions is verified: a 50% decrease in load or the propagation of cracks beyond the expected area of damage. The out-of-plane displacements of the wall are limited by the use of a self-balanced reaction frame. Aiming at accommodating small deformations, a hinge was used between the actuator and the specimen. The test setup is schematically presented in Figure 4.3c. A photograph of the preparation of the test in the laboratory is shown in Figure 4.4.

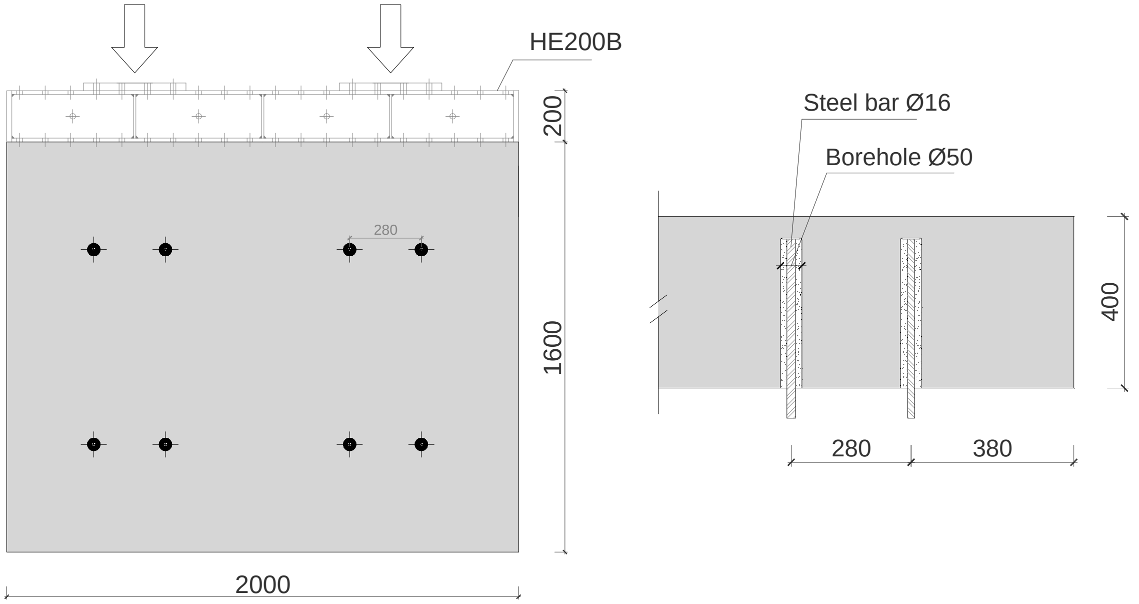

(a) (b)

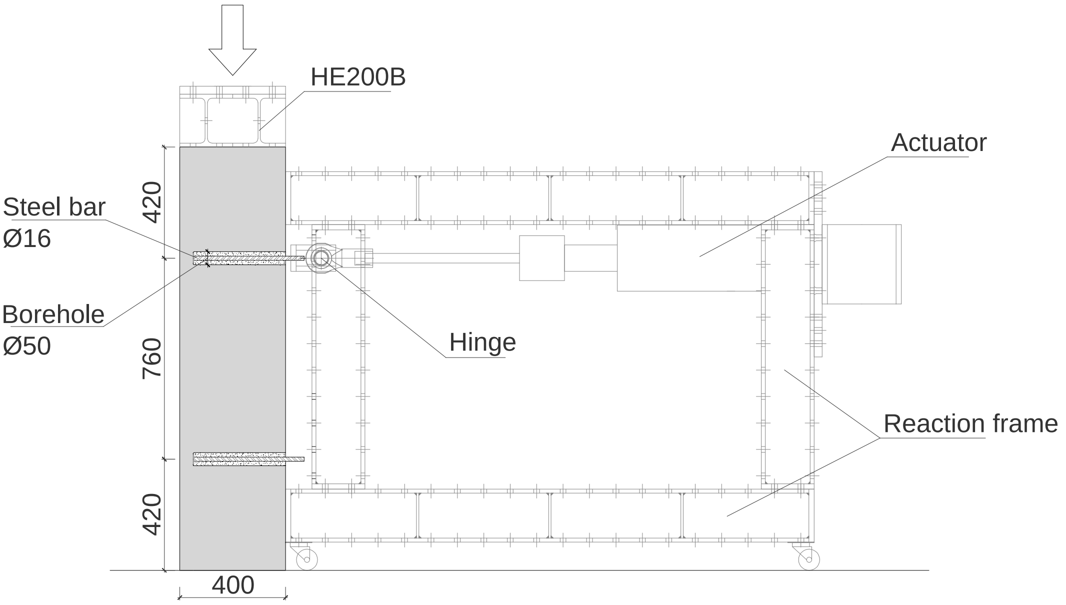

(c)

Figure 4.3 Specimen configuration and test setup (in millimetres): (a) Front view with the location of anchors; (b) Plan view of the anchors; (c) Cross section of wall and test set-up (Moreira et al. 2012).

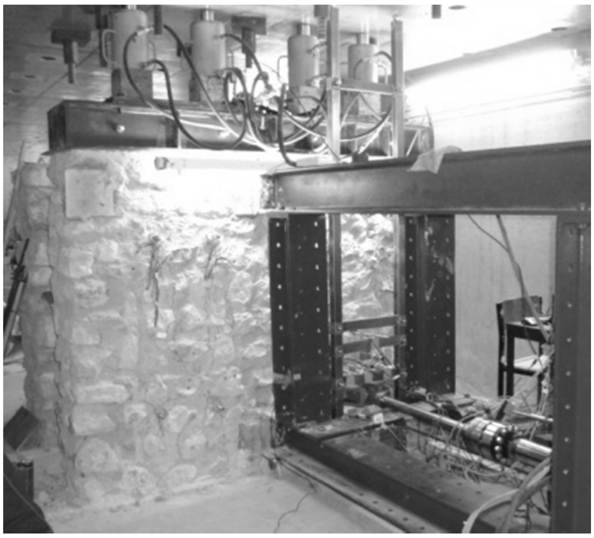

Figure 4.4 Specimen and test setup configuration in the laboratory (Moreira et al. 2012).

Since the material properties assume major influence on the behaviour this system, the experimental campaign also included the mechanical characterization of the base materials. Compression tests were carried out on masonry prisms, mortar cylinders and limestone cores. Diagonal compression tests were also performed on masonry wallets. The average compressive strength resultant from the tests on mortar cylindrical samples was 1.3 MPa. Limestone units' characterization tests indicated an average compressive strength of 107 MPa and an elastic modulus of 51500 MPa. The mechanical characterization of masonry included the construction of five masonry prisms with $0.40\times0.50\times0.80$ m^3, which were subjected to compression tests, and three masonry wallets with 0.8 m^2 per 0.3 m thickness tested by diagonal compression. Masonry mechanical characterization provided by the referred tests is presented in Table 4.1. Further details are given in Moreira et al. (2012).

Table 4.1 Mechanical properties of masonry (Moreira et al. 2012).

		Average	COV [%]
Elastic modulus	E [MPa]	1015	14
Compressive strength	f_c [MPa]	1.7	10
Shear strength	f_v [MPa]	0.29	15
Tensile strength	f_t [MPa]	0.14	15

Although both the upper and lower pairs of anchors applied in the walls were tested, only the upper level tests were considered for the numerical study. The results from one monotonic and two cyclic experimental test are available and will be used for the numerical model validation. After performing the tests, specimens were demolished and carefully surveyed in order to evaluate the cracks development and failure mode (an example is displayed in Figure 4.5). All tests showed that the formation of a shear cone combined with sliding at the grout/masonry interface was the recurrent failure mode. The masonry cone failure is characterised by the formation of a roughly conical fracture surface radiating from the edge of the anchor. During visual inspection it was confirmed that the tests showed an influence of the masonry cone in the failure of the system higher than sliding between the interface materials. This survey showed an overlap between failure cones, which is a direct result of the vicinity between anchors.

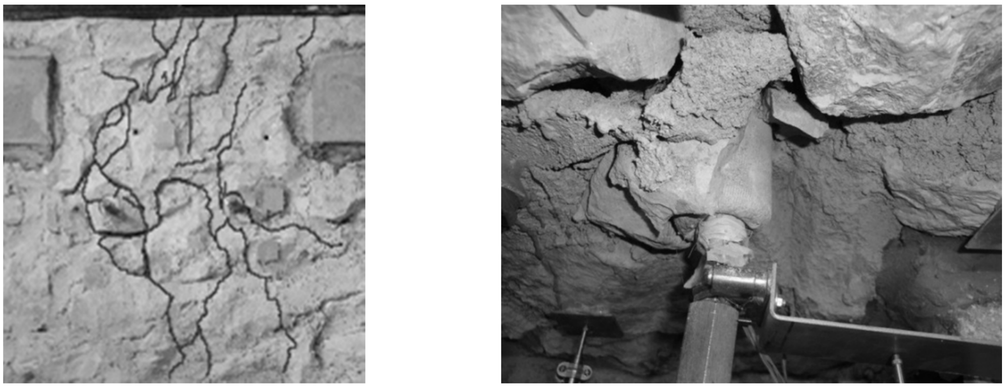
(a) (b)

Figure 4.5 Example of one pair of injected anchors after testing: (a) Crack pattern; (b) Sliding on the grout/masonry interface (Moreira et al. 2012).

The outcome obtained from the LVDT´s installed was used for the definition of the global horizontal force-displacement curves for each test. The displacement chosen to plot the capacity curves was the loaded end of the anchors. Note that the total displacement is a combination of the masonry shear cone formation with the relative displacement of the steel bar-grout (referred as inner interface) and grout-masonry (referred as outer interface) interfaces. Figure 4.6 illustrates the experimental envelope obtained from the combination of the individual force displacement curves of three tests. The average maximum load equals 76.8 kN and the maximum displacement achieved is around 19 millimetres. Force-displacement curves display a long linear branch until 50% to 85% of the peak load and the softening branch tended to an ultimate load interval between 35 kN to 45 kN. For all tests, the post-peak behaviour of the anchors shows a gradual degradation of force and stiffness with the increasing of displacements.

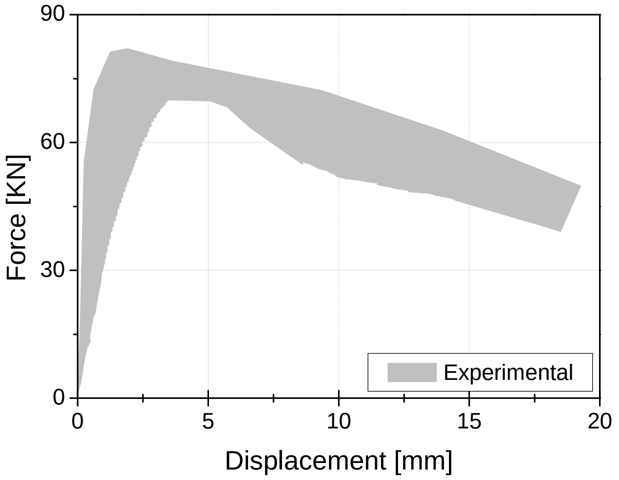

Figure 4.6 Envelope of the force-displacement curves resultant from the experimental tests.

4.3. NUMERICAL STUDY

4.3.1. Introduction

The purpose of the numerical study is to contribute to clarify the behaviour of injected anchors in masonry walls. A number of experimental works are available in literature (as already referred to) but the study cases are limited due to obvious economic, time and resource restrictions. For this reason, numerical modelling is commonly regarded as a complementary approach to further study different conditions and parameters, which is nearly impracticable from the experimental point of view. Still, the confidence in the numerical results implies its validation against experimental data. Considering this, the experimental campaign briefly described in the previous section is the basis of the numerical study. After the validation with experimental data, the numerical model can be used to simulate parametric conditions. For this purpose, the numerical model should be able to simulate not only the experimental test conditions but also the typical behaviour of injected anchors in masonry.

Previous conducted experimental works proved that the failure mechanisms verified for injected anchors in masonry subjected to pull-out load tend to be recurrent. The pulling force is transmitted between the surrounding masonry to the tensile element and includes two interfaces: the outer intersection between masonry and grout, and the inner intersection between grout and the steel element. Depending on the masonry material properties, the embedment depth, the steel strength and also the bond strength between the steel-grout and grout-masonry, injected anchors in masonry loaded in tension exhibit different failure modes. According to several authors (Gigla and Wenzel 2000; Arifpovic and Nielsen 2004; Gigla 2004; Algeri et al. 2010), as described in Chapter 2, injected anchors in masonry when subjected to tensile loading exhibit four main types of failure mechanisms: steel failure; punching shear failure; masonry-grout bond failure and grout-steel bond failure (see Figure 4.2).

Note that, although the main purpose of experimental campaign was to study the connection between masonry and half-timbered walls, the experimental test setup only included the construction of the masonry wall injected with anchors. For this reason, the outcome of this work can provide insight in the context of any strengthening technique involving anchors injected in masonry.

4.3.2. Modelling Strategy

Taking into account the complexity of the system to be modelled, the numerical simulation of the structural behaviour up to failure requires a sophisticated modelling approach, including the use of advanced computational models (Lourenço et al. 1998). Therefore, a detailed 3D finite element model (FEM) was developed in DIANA 9.4 (TNO DIANA 2009) and sophisticated constitute laws were used for masonry, aiming at an accurate simulation of the structural behaviour of the injected anchors in the masonry wall.

The adopted geometry is equal to the one defined for the experimental test setup, i.e., the wall dimensions are 2.0x1.6 m^2 with 0.4 m thickness, the anchor with 16 mm diameter in a 50 mm diameter borehole. The bottom anchors were also included in the model aiming at recreate the real conditions of the experimental setup. The two HE200B steel profiles, used in the experimental tests to uniformly distribute the compression load to the wall, were simulated as an equivalent steel beam in other to simplify the modelling without changing the inertia and weight properties.

Moreover, since this model is intended to simulate the behaviour of injected anchors in masonry, it was required to account separately for bonds between materials in order to reproduce accurately all the failure mechanisms. With this purpose, the approach used to model the anchoring system embraces interface elements between the steel bar and the grout, and between the grout and the masonry, see Figure 4.7. Note that the thickness of the interfaces is merely representative. The outer interface refers to the bond surface between masonry and grout and the inner interface to the bond between the steel bar and grout.

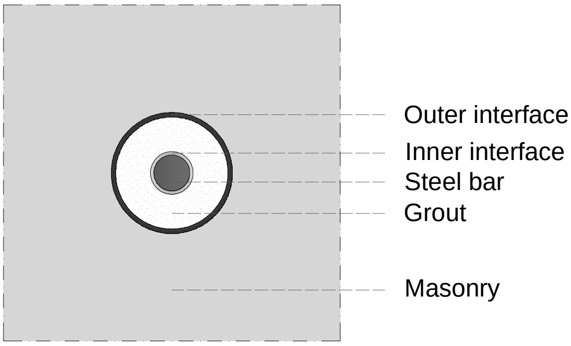

Figure 4.7 Modelling strategy used to model the anchoring system (representative thickness in the interfaces).

The mesh was defined aiming a compromise between accuracy and efficiency. Brick elements of twenty nodes, CHX60 (Figure 4.8a), are predominantly used for the mesh, although some tetrahedral elements of fifteen nodes, CTP45 (Figure 4.8b), were also adopted to accommodate the steel bars geometry. Each node has six degrees of freedom: three translations and three rotations. For the simulation of the bond between different materials, tri-dimensional interface elements of eight nodes in each surface, CQ48I (Figure 4.8c), were used. All the elements include quadratic interpolation, providing a rather good approximation of the displacement field. Detailed information regarding the finite elements used is available in (TNO DIANA 2009).

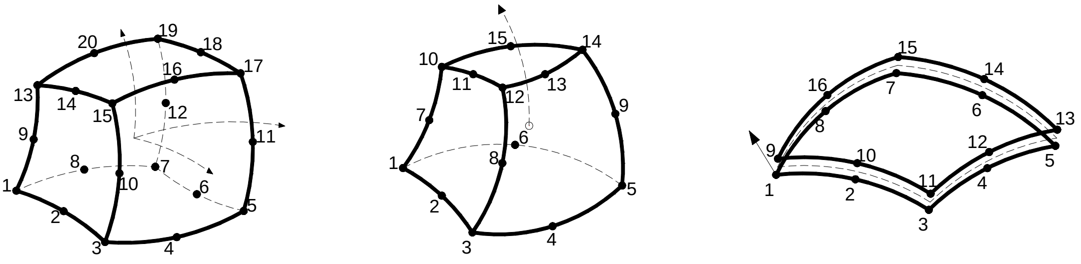

(a) (b) (c)

Figure 4.8 Finite elements used in the model: a) CHX60; b) CTP45 e c) CQ48I (TNO DIANA 2009).

The generated mesh results in 39.555 nodes and 9.441 elements. The mesh discretization was carried out in a compromise between the reliability of the results with controlled computational efforts and time requirements. The huge number of degrees-of-freedom of the model (over 200.000) limited the mesh refinement to the surrounding areas of the anchors since these are the regions where higher stress variations occur. A less refined mesh was adopted in the regions where the stress distribution is smooth. The level of refinement was also optimized through the wall thickness, gradually becoming more refined closer to the anchor's loaded end. The numerical model and meshing discretization is presented in Figure 4.9.

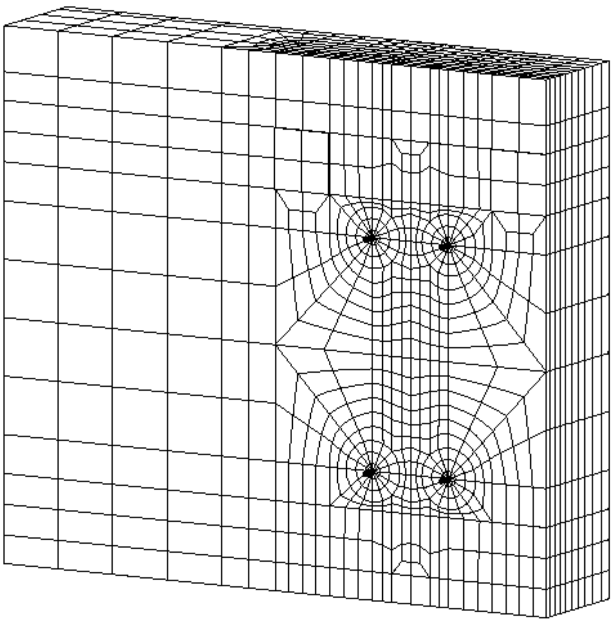

Figure 4.9 Numerical model mesh.

The model is fully restrained at the bottom in order to reproduce the experimental constraints. The areas of the wall in contact with the reaction frame were restrained only for horizontal out-of-plane displacements.

In what concerns the material properties, masonry was assumed as a homogeneous isotropic material with mean-value properties, which is a good compromise between accuracy and efficiency (Lourenço et al. 2007b). The value of the elastic modulus for masonry was based on the compression tests results performed on masonry prisms. The Poisson ratio was set equal to 0.20. Typical values for the elastic modulus and density of steel were used. Regarding the physical and mechanical properties of the grout, information from the technical sheet was used (Cintec 2012). Table 4.2 provides the elastic properties adopted for the materials.

Table 4.2 Material properties adopted.

	E [GPa]	v [-]	γ [Kg/m^3]
Masonry	1.0	0.2	1900
Steel	210	0.3	7850
Grout	30	0.2	2300

Interface elements describe the bond behaviour in terms of a relation between the normal and shear tractions and displacements across the interface (TNO DIANA 2009). Thus, its elastic behaviour is defined by the normal and tangential stiffness of the bond between materials. As the experimental campaign carried out did not include the mechanical characterization of the bond behaviour along the 2 interfaces listed before, the interface stiffness was defined, in an initial phase, according to the available literature. Studies on the bond behaviour of steel-grout are scarce and no suggested values for the bond stiffness were found. For this reason, studies in the field of concrete-steel bond behaviour in reinforced concrete were taken as an initial approximation since the mechanical characteristics of these materials are fairly comparable and no significant differences should be expected. A range of values around 9-400 MPa/mm, depending on the bond conditions, has been indicated for the tangential stiffness of the inner interface according to investigations in this field (Lowes 1999; Zhu and Law 2005; Jeong et al. 2005; Lee et al. 2011).

A number of investigations on the behaviour of grout-masonry interfaces were performed considering different masonry types. Bajer and Barnat (2012) carried out experimental tests and numerical analyses for the study of the glue–concrete interface of bonded anchors under tensile load and a value around 500 MPa/mm was pointed out for the shear stiffness. The bond between grout and surrounding brick masonry was investigated by Gigla (2004), providing values between 55 MPa/mm and 66 MPa/mm for the shear stiffness. Literature studies concerning unit-mortar interface on masonry (which can be also associated to the grout-masonry bond), as well as some expressions for its calculation, were also considered to estimate the interface parameters (Lourenço 1994; Lourenço 1996b; Jarred and Haberfield 1997; Eshghi and Pourazin 2009). Thus, a range of values around 10-500 MPa/mm seems reasonable for the outer tangential stiffness.

The usual elasticity equations relating normal and tangential stiffness indicate that the normal stiffness is approximately twice the tangential one (Oliveira and Lourenço 2004). This range of values will be the starting point for the calibration against the experimental results. The initial values were defined taking into account that the inner interface stiffness is expected to be higher than the outer interface stiffness.

4.3.3. Initial Linear Analysis

A preliminary elastic analysis was carried out in order to guarantee that the experimental wall conditions are accurately simulated by the numerical model. The numerical simplification in the modelling of the HE200B beams (simulated as a rectangular cross section with the same depth as the real, 400 mm, and a height calculated so that the inertia of the element remains unchanged), was evaluated to verify if the vertical load is evenly distributed in the wall. The model simplifications can never compromise the correct simulation of the system behaviour. It should be noted that the density of this material was adapted to the new geometry in order to maintain its actual weight.

The compressive stress (200 kPa) is imposed on the wall through a distributed load in the upper face of the beam. The compressive stress distribution in the wall is presented in Figure 4.10. The analysis of the results showed that the distribution of stresses in the wall is quite homogeneous proving that the modelling simplification adopted for the metallic beams is suitable and simulates with good accuracy the conditions of the experimental tests.

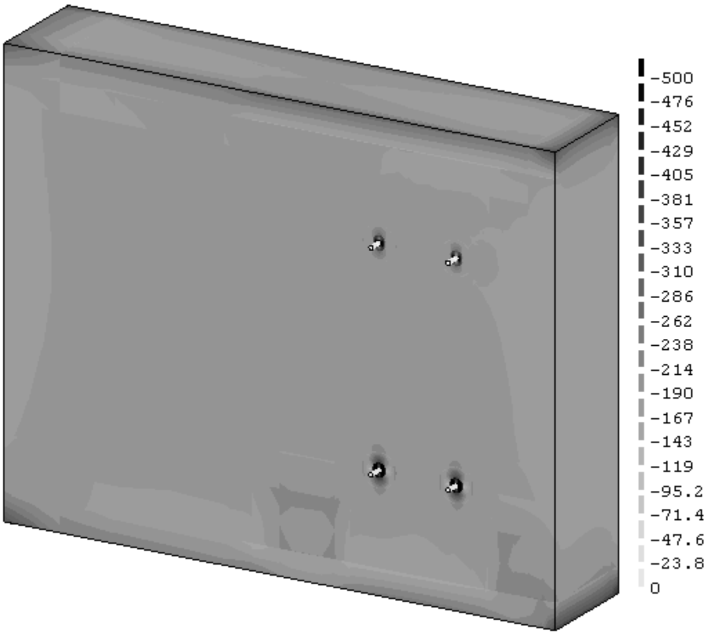

Figure 4.10 Compressive stress distribution on the wall after the application of the vertical load (in kPa).

Afterwards, a quick analysis to assess the ability of the model to simulate the behaviour of injected anchors in masonry was carried out. For that, linear analyses were carried out trying to capture numerically the structural behaviour that identifies each one of the main failure mechanisms defined in Figure 4.2 by varying the interface parameters (within the range defined above). Since the steel failure usually occurs on smaller diameter bolts with longer embedment lengths, which is not the case, only the failure mechanisms associated to the masonry cone formation and sliding along the interfaces were investigated numerically.

The experimental test procedure was followed for the numerical analysis, where the compressive vertical stress was initially applied on the top of the metallic beam and the upper level anchors were put into tension by applying increasing displacements to its outward end.

Predominant relative displacements similar to a sliding failure pattern along the inner interface (steel-grout) were obtained numerically by decreasing its stiffness. This behaviour is perceptible in Figure 4.11 where the maximum principal strains are plotted simultaneously with the deformed shape of the model (the white contour on the bar represents the sliding, relative displacements along the interface). In the same manner, the “sliding failure” along the outer sock-masonry interface was captured by increasing the inner interface stiffness and decreasing the outer one. The “sliding” along the grout-masonry interface is noticeable in the numerical results plotted in Figure 4.12, with the out-of-plane displacement of the whole anchoring system. Finally, the masonry cone failure was numerically simulated by increasing both the interfaces stiffness to assure that concentration of strains develops in the masonry. In Figure 4.13 is perceptible a shear cone formation on the masonry wall near the anchors. As expected, the strain distribution is concentrated around the anchoring system for all the three failure mechanisms simulated. The ability of the numerical model to simulate these three modes proves its adequacy to proceed to the model validation and nonlinear analysis.

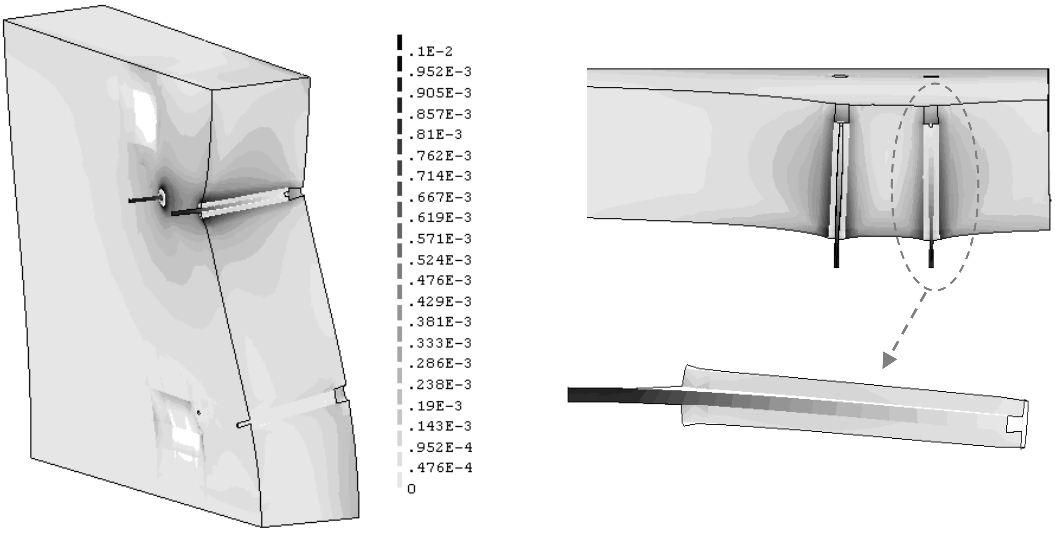
.1E-2
.952E-3
.905E-3
.857E-3
.81E-3
.762E-3
.714E-3
.667E-3
.619E-3
.571E-3
.524E-3
.476E-3
.429E-3
.381E-3
.333E-3
.286E-3
.238E-3
.19E-3
.143E-3
.952E-4
.476E-4
0

Figure 4.11 Sliding failure along the inner interface.

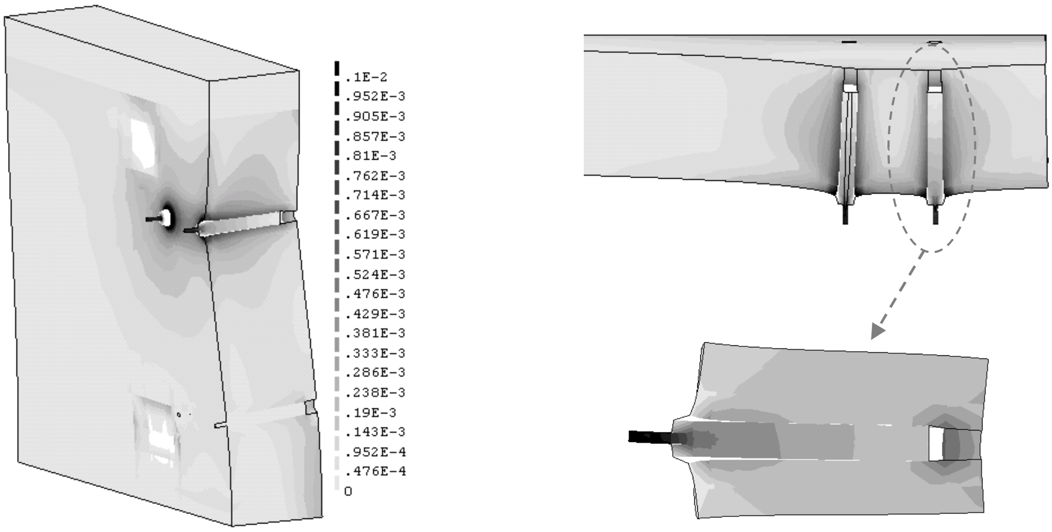
.1E-2
.952E-3
.905E-3
.857E-3
.81E-3
.762E-3
.714E-3
.667E-3
.619E-3
.571E-3
.524E-3
.476E-3
.429E-3
.381E-3
.333E-3
.286E-3
.238E-3
.19E-3
.143E-3
.952E-4
.476E-4
0

Figure 4.12 Sliding failure along the outer interface.

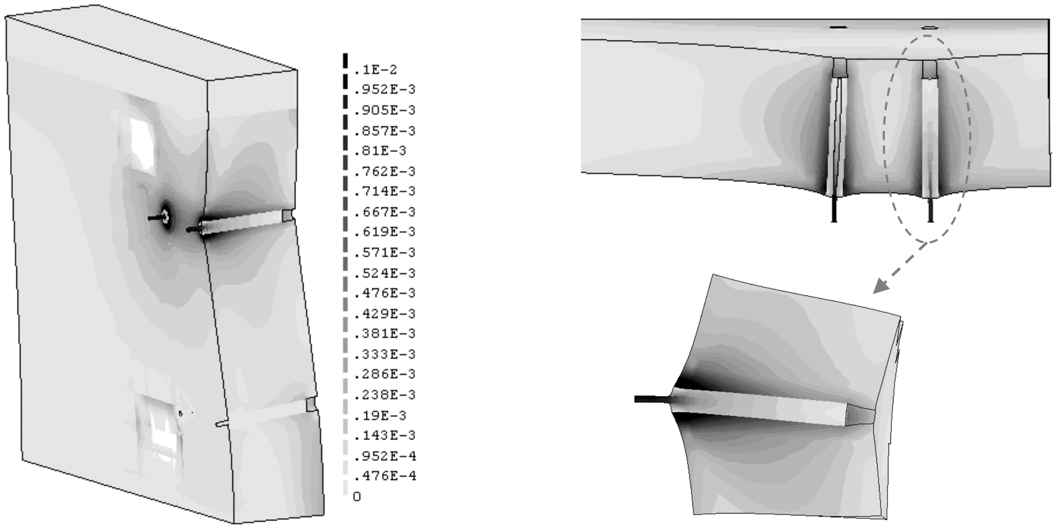
.1E-2
.952E-3
.905E-3
.857E-3
.81E-3
.762E-3
.714E-3
.667E-3
.619E-3
.571E-3
.524E-3
.476E-3
.429E-3
.381E-3
.333E-3
.286E-3
.238E-3
.19E-3
.143E-3
.952E-4
.476E-4
0

Figure 4.13 Masonry cone failure.

4.3.4. Initial Validation

A set of linear elastic analysis was carried out in order to calibrate suitable interface stiffness values that best match the experimental curves in the linear range. Sensitive studies varying the inner and outer interface stiffness were performed. These analyses proved that the values of the normal stiffness do not have a strong influence on the structural behaviour of the system and therefore were considered to be twice of the tangential ones. This inverse fitting process resulted in the values presented in Table 4.3, which are within the range defined in literature. A comparison in terms of force-displacement between the experimental envelope and the linear numerical analysis result is given in Figure 4.14.

Table 4.3 Interface Stiffness.

Inner Interface		**Outer Interface**	
Tangential stiffness	Normal stiffness	Tangential stiffness	Normal stiffness
100	200	50	100

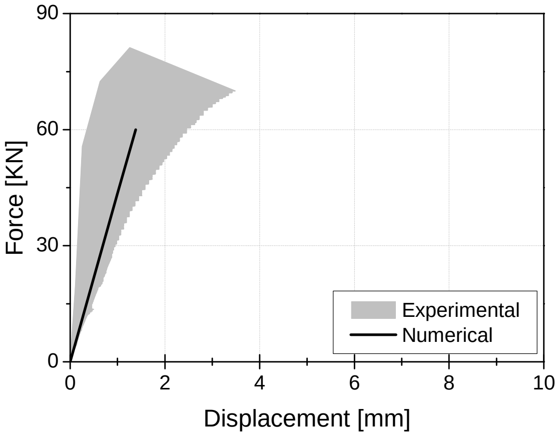

Figure 4.14 Comparison between the experimental envelope and numerical behaviour in the linear range.

4.3.5. Nonlinear Analyses

In this section the procedure followed for the characterization of the nonlinear behaviour of the system is described. Nonlinear analyses were carried out with the purpose to provide additional insight of the behaviour of the system subjected to combined compressive and shear loading and also to the further validation of the numerical model in the non-linear range. Only material nonlinear behaviour is considered, since it is expected that geometric nonlinearities would not provide significant differences in the results.

Nonlinear Formulation

Most of the nonlinearities are expected to concentrate in the masonry, since at the time masonry fails, steel and grout are most probably still in the linear range. After testing, the specimens were demolished and carefully surveyed. The visual inspection revealed that almost no damage was observed in the grout. For this reason the linear behaviour adopted for this material seems to be a reasonable option. Interface elements allow only for linear elastic relative displacement since it is expected that most nonlinear phenomena occur in the masonry. In fact, experimental tests showed an influence of the masonry cone higher than the grout/masonry interface, being the masonry the main contributor to failure.

The non-linear behaviour of the masonry is modelled by adopting two constitutive models based on the total strain crack model: the total strain fixed crack model (FCM) and the total strain rotating crack model (RCM), both available in DIANA 9.4 (2009). These models describe the tensile and compressive behaviour of the masonry with a stress-strain relationship. In both models a crack is initiated when the maximum principal stress equals the tensile strength of the material and the initial orientation of the crack is normal to the maximum principal strain. In the fixed crack model the strain transformation matrix is fixed upon cracking and the crack plane is also fixed during the full analysis process. On the other hand, in the rotating crack model the crack direction rotates with the principal strain axes ensuring that the crack remains normal to the direction of the maximum principal strain. More appealing to the physical nature of cracking is the fixed stress-strain concept in which the stress-strain relationships are evaluated in a coordinate system fixed upon cracking (TNO DIANA 2009). However, the shear stress locking problem can be noted as the main disadvantage (Ghiassi 2013). The rotating crack model is more flexible and allows for a gradual correction of an initially mispredicted crack direction. Both approaches are easily described in the same framework where the crack directions are either fixed or continuously rotating with the principal directions of the strain vector.

In the fixed crack model, a shear retention factor has to be chosen for the definition of the shear behaviour, which leads to some stress built-up and locking. On the contrary, in the rotating crack model a unique shear term is evaluated during the analysis and updated taking into account the current damage state. No shear model is required in this method since it inherently abandons the possibility of incorporating different crack shear models since the crack always occurs in a principal direction (Rots 1988). It is expected that the structural behaviour of the model becomes highly dependent on the shear behaviour of masonry. Fixed and rotating crack formulations were considered, aiming at discussing the most suitable modelling approach.

Masonry is modelled using exponential softening in tension and a parabolic strain-stress relationship in compression, for both fixed and rotating formulations. These sophisticated stress-strain relationships are suitable to describe the behaviour of masonry (Lourenço 1996a). The analysis is physically non-linear. While shear behaviour does not require the user definition within the rotating crack model, in the fixed crack model the post-cracked shear behaviour was modelled using a constant shear retention factor (β). Thus, the behaviour of masonry is expressed by the strain-stress relations described in Figure 4.15a for compression, Figure 4.15b for tension and Figure 4.15c for shear behaviour in the case of FCM.

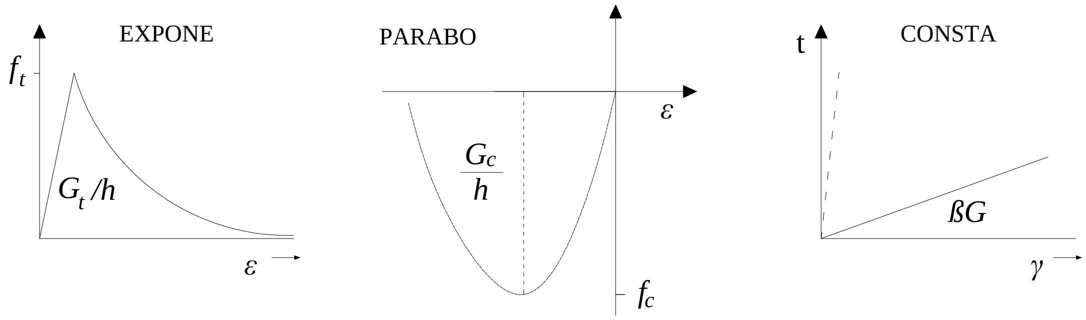

(a) (b) (c)

Figure 4.15 Mechanical behaviour of masonry: (a) Tension; (b) Compression; (c) Shear (applicable for FCM).

The tensile and compressive strength of masonry were defined according to the experimental characterization tests results, given in section 4.2. The tensile and compressive fracture energy values, necessary for the constitutive models definition, were initially estimated based on the relations described in section 3.4 (Equations (3.1) and (3.2)). The shear retention factor (β) was defined for the fixed crack model according to the recommendations found in DIANA 9.4 (2009). Besides the shear behaviour, it is expected that the tensile parameters are the ones with more influence in the nonlinear behaviour. These values are calibrated to fit the experimental nonlinear behaviour, within reasonable limits. The updated values for the definition of the nonlinear constitutive models for masonry are summarized in Table 4.4.

Table 4.4 Non-linear updated parameters for the masonry constitutive laws definition.

Compression		Tensile		Shear
f_c (MPa)	G_c (N/mm)	f_t (MPa)	G_t (N/mm)	β*
1.74	2.8	0.1	0.03	0.01

*Shear factor only for the fixed crack model

The integration scheme for these elements was defined considering the recommendations presented in DIANA 9.4 (2009) and also aiming a reasonable computational time and effort. The 20 nodes brick elements (CHX60) integration scheme, presented in Figure 4.16a, shows a 2×3×3 Gauss integration rule. Three by two Gauss integration points were used for the 15 nodes wedge element (CTP45), as depict in Figure 4.16b. Finally, for the quadrilateral interface element (CQ48I) a numerical 3x3 Lobatto integration scheme was considered (Figure 4.16c). The shape functions obtained according to the integration points, express the approximated displacement field within the element in terms of its nodal variables.

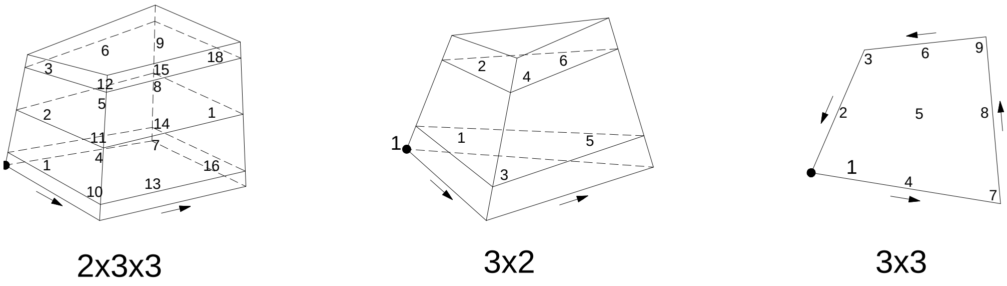

(a) (b) (c)

Figure 4.16 Integration schemes for the numerical elements: (a) CHX60; (b) CTP45; (c) CQ48I (TNO DIANA 2009).

The equilibrium of the system of equations in each step of the non-linear analysis was tested considering distinct iterative solution methods: linear stiffness, the regular and modified Newton-Raphson. The regular Newton-Raphson method, which evaluates the stiffness matrix in every iteration, showed the best results in terms of convergence. For this reason, a regular Newton–Raphson iteration procedure was used in the nonlinear analyses and an energy convergence criterion of 10^{-3}.

Nonlinear Analyses Results

The experimental test procedure was followed for the nonlinear analysis: firstly the self-weight of the system was considered, then the compressive vertical load was applied on the top of the metallic beam and finally the upper pair of anchors was loaded in tension by applying increasing horizontal displacements at its outward end. Nonlinear analyses were carried out considering both FCM and RCM formulations and the material behaviour described in the previous section.

Figure 4.17 presents the force-displacement curves from the FCM and RCM and also the experimental envelope. The comparison of the numerical analyses (FCM and RCM) against the experimental envelope does not show significant differences concerning the linear behaviour and peak force, as expected. Although both numerical curves present a sudden decrease in load capacity just after the peak, the post-peak response exhibits considerable differences. The FCM formulation provides a continuously increase of the force after peak, which is not in agreement with experiments. In fact, the experimental post-peak envelope shows clearly a gradual force decrease with respect to displacement, which is well captured by the RCM formulation. This last approach provides a maximum force of 70 kN (very close to the mean experimental value, 76.8 kN, with an error less than 9%) and an ultimate converged displacement of 15 mm.

The force-displacement response of the RCM and its softening behaviour fits the experimental envelope in a very good manner. Therefore, this model is able to reproduce more accurately the shear strength after cracking. Figure 4.17 also shows clearly that the shear model can have a great influence on the post-peak behaviour of this type of structures, making the difference between a realistic structural modelling of the system and an incorrect overestimation of strength, even if the first peak is independent on the model. The shear stress locking problem in the FCM has resulted in increment of force even after evolution of cracks. Rotating crack models seem more suitable for the study of the strength of anchors injected in masonry problems, in which high shear stresses develop.

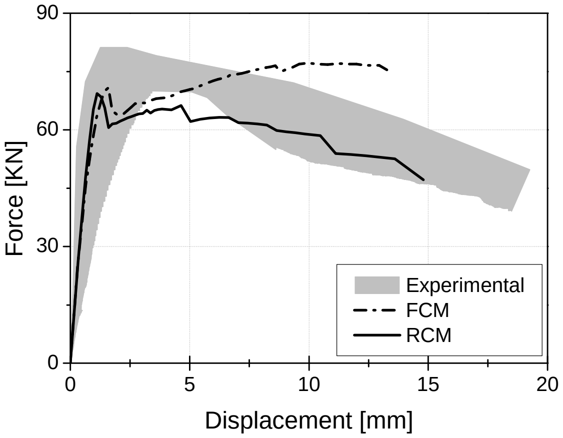

Figure 4.17 Force-displacement curves for the RCM and FCM formulations and experimental envelope.

To further discuss the numerical behaviour provided by the distinct formulations, the maximum (tensile) principal strains are plotted and analysed as an indicator of damage. Aiming at improving the perception of the damage evolution in the internal layers, the model has been divided in some sections as depicted in Figure 4.18.

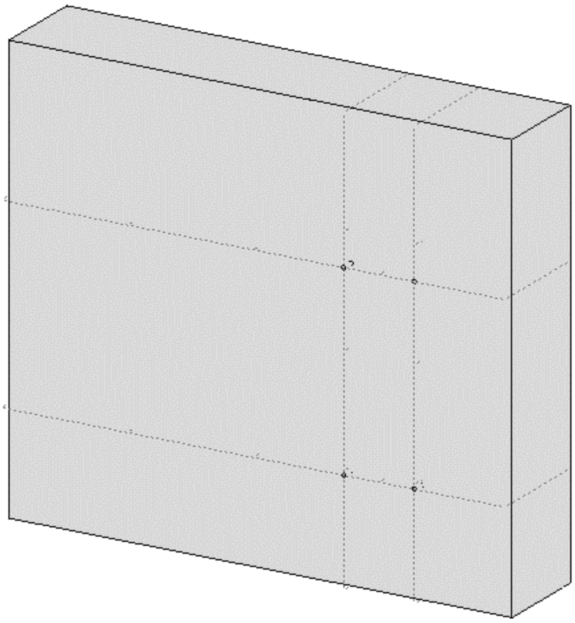

Figure 4.18 Division in sections of the model for the analysis of the results.

Figure 4.19 and Figure 4.20 show the maximum principal strains at peak load, for FCM and RCM respectively. The qualitative distribution of damage is very similar for both models in the surrounding areas of the anchors, although it is more severe in the FCM. The top cross section shows damage along the anchors (near the outer interface) for the FCM while diagonal strain concentrations were found for the RCM. At this stage, in both analyses the crack pattern and deformed shape is characterized by the formation of a shear cone on masonry (more noticeable in RCM) and sliding trough the external interface (more noticeable in FCM). The FCM behaviour is clearly conditioned by the concentration of strains in the interface between grout and masonry, whilst RCM behaviour is characterized by the masonry cone formation. Experimental tests showed an influence of the masonry cone much higher than the interface grout/masonry, as the main contributor for failure. Thus, considering these results, the RCM model seems to accurately describe the development of the failure mechanisms verified experimentally.

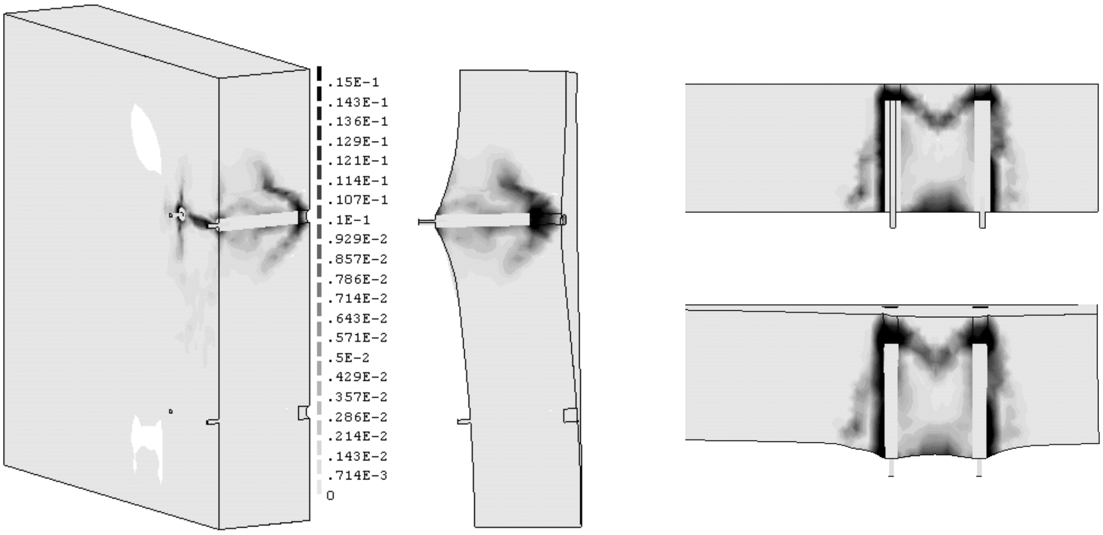
.15E-1
.143E-1
.136E-1
.129E-1
.121E-1
.114E-1
.107E-1
.1E-1
.929E-2
.857E-2
.786E-2
.714E-2
.643E-2
.571E-2
.5E-2
.429E-2
.357E-2
.286E-2
.214E-2
.143E-2
.714E-3
0

(a) (b)

Figure 4.19 Maximum principal strains at peak load for FCM: (a) Lateral view (undeformed and deformed shape); (b) Top view (undeformed and deformed shape).

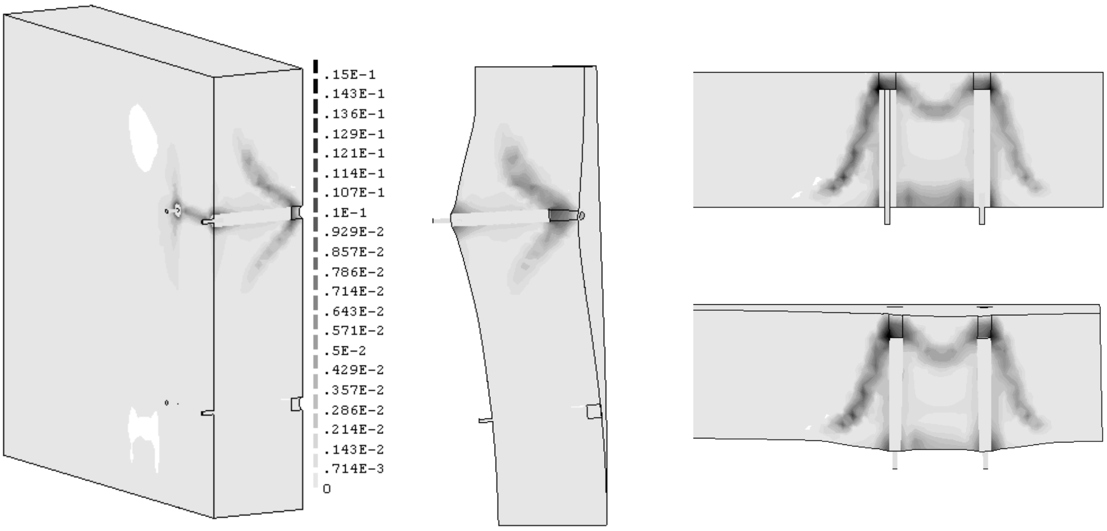
.15E-1
.143E-1
.136E-1
.129E-1
.121E-1
.114E-1
.107E-1
.1E-1
.929E-2
.857E-2
.786E-2
.714E-2
.643E-2
.571E-2
.5E-2
.429E-2
.357E-2
.286E-2
.214E-2
.143E-2
.714E-3
0

(a) (b)

Figure 4.20 Maximum principal strains at peak load for RCM: (a) Lateral view (undeformed and deformed shape); (b) Top view (undeformed and deformed shape).

The damage concentration in the post-peak behaviour for FCM and RCM is presented in Figure 4.21 and Figure 4.22 respectively, by plotting the tensile principal strains. The damage distribution found for FCM analysis results in the post-peak behaviour is similar to the one found for the peak load, presenting higher level of damage (Figure 4.21). The masonry cone formation is more evident at this stage, although the concentration of strains at the grout/masonry interface also predicts a great contribute of the sliding through the outer interface to the failure mode.

The RCM results show a damage distribution which clearly indicates the existence of a masonry shear cone (Figure 4.22). Some differences can be found in the damage distribution in the post-peak behaviour when compared to the peak behaviour. The shear cone formation becomes wider, increasing the wall area that experiences out-of plane displacements. After the peak, the extensive concentration of damage in the areas close to the anchors led to the redistribution of stresses in the intact surrounding areas.

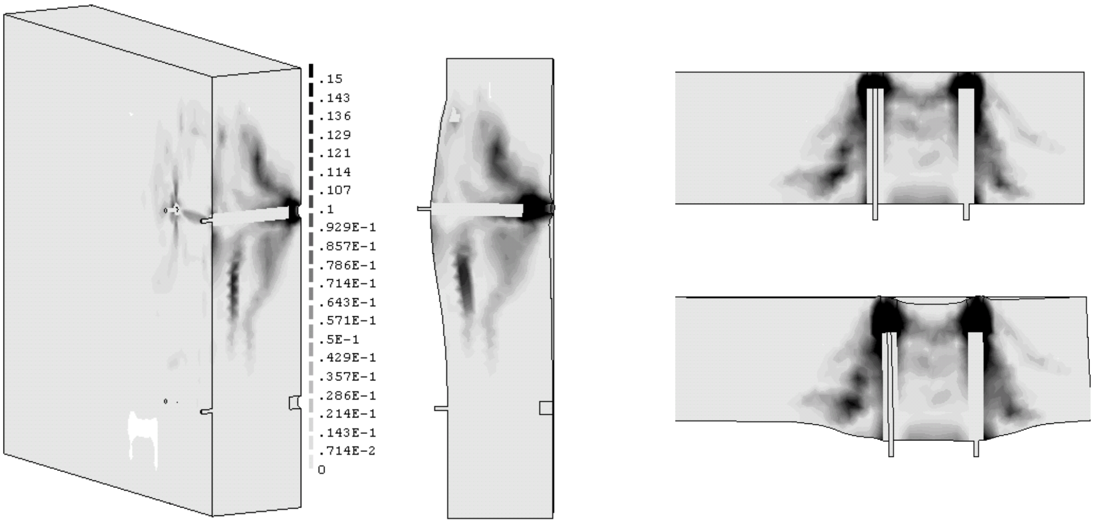
.15
.143
.136
.129
.121
.114
.107
.1
.929E-1
.857E-1
.786E-1
.714E-1
.643E-1
.571E-1
.5E-1
.429E-1
.357E-1
.286E-1
.214E-1
.143E-1
.714E-2
0

(a) (b)

Figure 4.21 Maximum principal strains at final stagefor FCM: (a) Lateral view (undeformed and deformed shape); (b) Top view (undeformed and deformed shape).

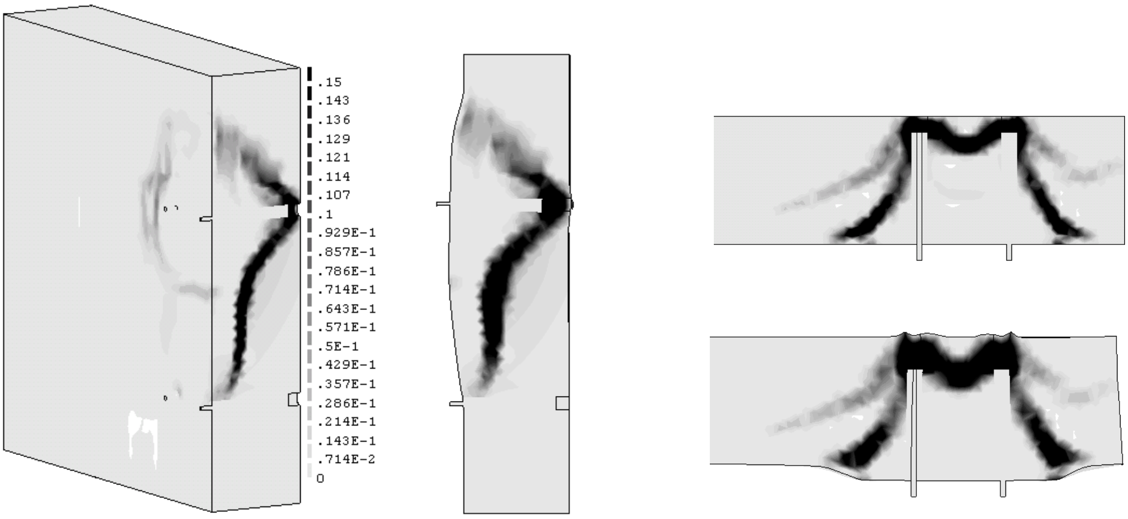
.15
.143
.136
.129
.121
.114
.107
.1
.929E-1
.857E-1
.786E-1
.714E-1
.643E-1
.571E-1
.5E-1
.429E-1
.357E-1
.286E-1
.214E-1
.143E-1
.714E-2
0

(a) (b)

Figure 4.22 Maximum principal strains at final stage for RCM: (a) Lateral view (undeformed and deformed shape); (b) Top view (undeformed and deformed shape).

The analysis of damage concentration in the post-peak behaviour confirm the shear cone in the masonry for both FCM and RCM formulations, although much more evident in the last case. The differences found in the crack patterns of the two analysis (FCM and RCM) are related to the great influence that the distinct shear behaviour provided by these formulations has in the global response of the system. As stressed above, the experimental behaviour observed during the performed pull-out tests showed a combined masonry cone formation with sliding along the outer interface failure, being the masonry cone the major contributor to failure. Comparing the damage distribution resultant from the distinct formulations, it is evident that the RCM failure is characterized by the formation of a cone in masonry, as clearly shown by Figure 4.22, while the FCM shows more influence of the sliding along the outer interface. The masonry cone formation is not very clear in the latter. As verified in the force-displacement curve, the RCM model seems to better simulate the post-peak behaviour of the anchors injected in the wall.

By the analysis of the damage pattern displayed in Figure 4.22, the cone development through the wall thickness and height seems to follow an atypical pattern at certain point. The cracking development may have been conditioned by the mesh discretization, which is more refined near the anchor. Indeed, the numerical model was prepared according to a macro-modelling strategy in which the strain distribution can be dependent on the mesh, as stated by Lourenço (1996a). This means that the masonry cone formation may not have exactly the same shape as the one presented numerically as this depends on the level of mesh refinement. Even though, a good approximation with experiments was found. The strain distribution and obtained failure modes of these analyses further validate the RCM model.

The contour map of the out-of-plane displacements for both analysis is also plotted in order to further discuss the wall nonlinear behaviour (Figure 4.23). As expected for both analysis, the out-of-plane displacements are concentrated near the anchors. The area that suffers out-of-plane displacements is higher in the RCM, which is in accordance with the damage pattern shown above. Note that the contour maps for FCM and RCM were plotted for the same displacement of the anchors, being in this way comparable. The masonry cone formation observed in the experimental tests mobilized a significant area around the anchors, which is reflected by the behaviour found in RCM analysis.

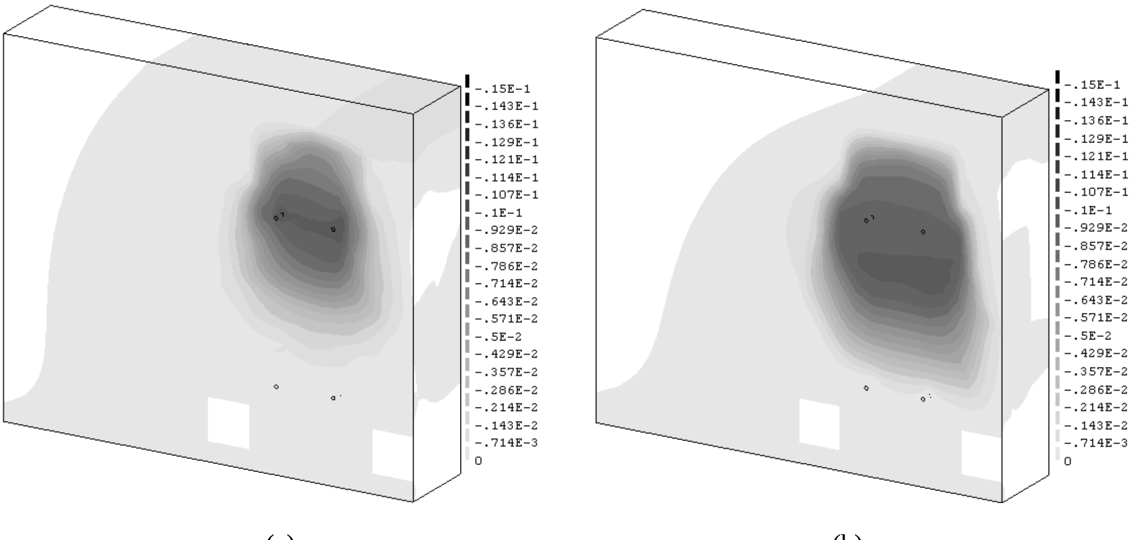

(a) (b)

Figure 4.23 Contour map of the out-of-plane displacements: (a) FCM; (b) RCM.

The comparison between the results provided by the application of FCM and RCM formulations, proved that the RCM simulates the experimental behaviour with a better accuracy. The force-displacement response, damage distribution during the analysis and evaluation of the failure mode allowed the comparison between models behaviour and consequently the definition of a model that describes the experimental behaviour. For this reason the RCM formulation will be used hereinafter for the parametric study.

4.4. PARAMETRICAL STUDY

In this section the validated model is used as a numerical laboratory to perform parametric analyses, aiming at efficiently evaluate the influence of some input parameters.

Experimental campaigns carried out on injected anchors in masonry showed that the primary factors affecting the performance of the anchoring system are the anchor diameter, the anchor embedment depth and the masonry tensile strength (McGinley 2006), although other parameters might influence the behaviour of the system as well. The study of the influence of all these parameters is almost impractical from an experimental point of view and, therefore, numerical investigations based on reliable models appear as an interesting and appealing solution.

This section presents a parametric analysis of the anchoring system, where the influence on the response of the following parameters of masonry were evaluated: (i) elastic modulus; (ii) compressive strength; (iii) compressive fracture energy; (iv) tensile strength; (v) tensile fracture energy. The purpose is to evaluate the variation on the structural response with respect to the reference model, varying each parameter from 50% to 200% of its initial value. Additionally, a few relevant geometric parameters were also varied such as the pre-compression level, anchors dimensions, anchors embedment depth and anchors spacing. The parameters influence is evaluated by comparing the results with reference model (RCM), summarized by Figure 4.17, Figure 4.20 and Figure 4.22.

4.4.1. Masonry Parameters

Elastic Modulus

The influence of the masonry elastic modulus was evaluated by increasing two times and decreasing to half the reference value (1 GPa). Force-displacement responses are compared with the reference model showing, as expected, the decreasing and increasing in the elastic stiffness (see Figure 4.24). The peak load showed an increase of approximately 7% in the analysis considering the upper limit for E and a decrease of 8% regarding the lower limit. The sudden decrease in load capacity after the peak is verified in all the analyses although smoother in the analysis with a higher elastic modulus. The post peak behaviour, for both the upper and lower elastic modulus analysis is very similar to the one found for the reference model. The elastic modulus influences the linear behaviour (elastic stiffness) instead of the nonlinear response, as expected.

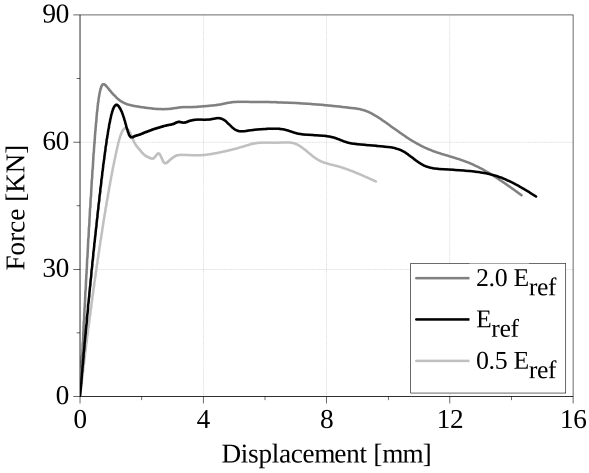

Figure 4.24 Force-displacement curves for the parametric analysis of the masonry elastic modulus.

The tensile principal strains are also plotted in order to evaluate the damage pattern resultant from increasing and decreasing the masonry elastic modulus. The damage distribution for the analysis with 0.5 E_{ref} (Figure 4.25) and 2.0 E_{ref} (Figure 4.26) is very similar to the one verified in the reference model, in which the masonry cone formation is evident. The damage is more severe in the analysis of 2.0 E_{ref} because it was plotted for a higher displacement. Thus, the variation of the masonry elastic modulus does not influence the damage pattern and consequently the failure mode of the system.

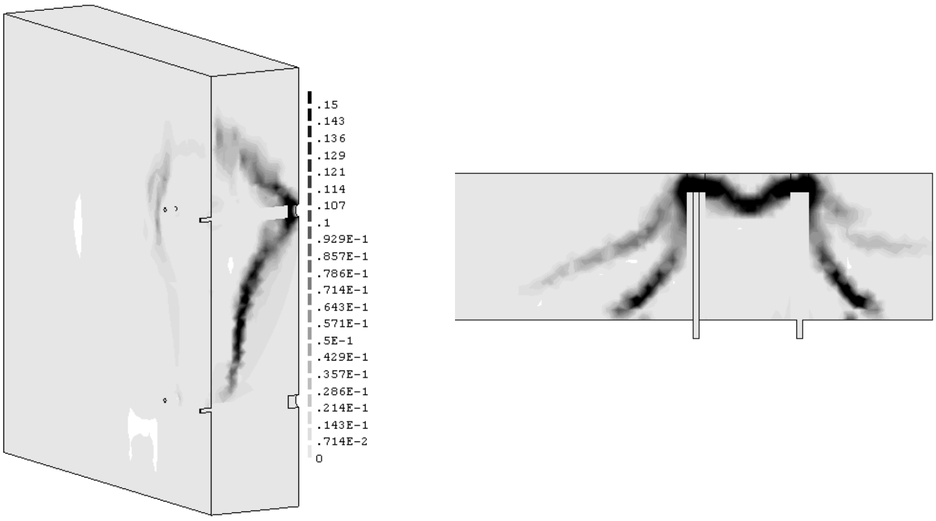
.15
.143
.136
.129
.121
.114
.107
.1
.929E-1
.857E-1
.786E-1
.714E-1
.643E-1
.571E-1
.5E-1
.429E-1
.357E-1
.286E-1
.214E-1
.143E-1
.714E-2
0

(a) (b)

Figure 4.25 Maximum principal strains at final stage for the $0.5 \times E_{ref}$ analysis: (a) Lateral view; (b) Top view.

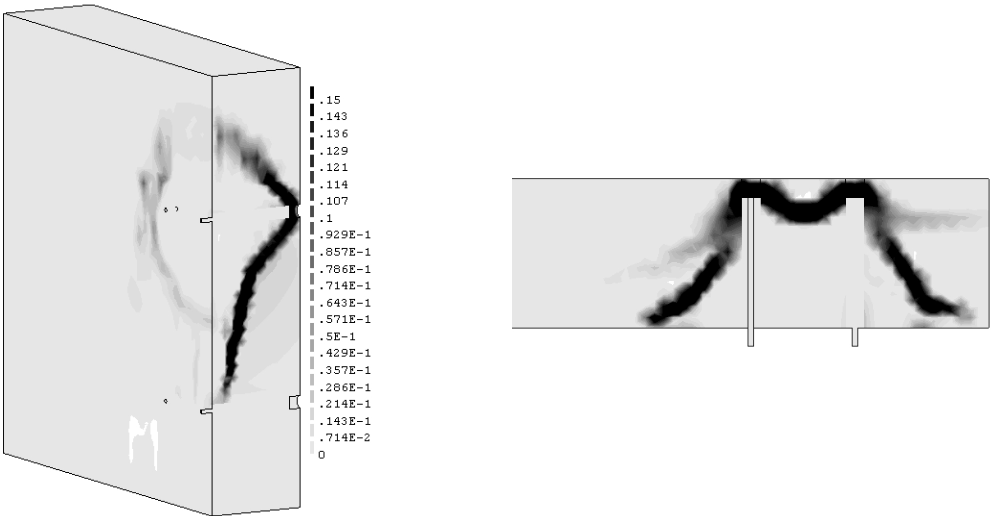

(a) (b)

Figure 4.26 Maximum principal strains at final stage for the $2.0 \times E_{ref}$ analysis: (a) Lateral view; (b) Top view.

Compressive Strength

The compressive strength was studied by decreasing to 0.90 MPa ($0.5 \times f_{c,ref}$) and increasing to 3.50 MPa ($2.0 \times f_{c,ref}$) the reference value (1.74 MPa). The other parameters remained unaffected, including the compressive fracture energy. To get a better insight about the behaviour modifying the compressive strength, Figure 4.27 shows the compressive constitutive laws generated. The curves tend to overlap for a certain level of stain (around 1.25×10^{-2}), being the curve with lower maximum compressive strength the one attaining higher level of stress after that point. This behaviour happened because the fracture energy was kept unchanged.

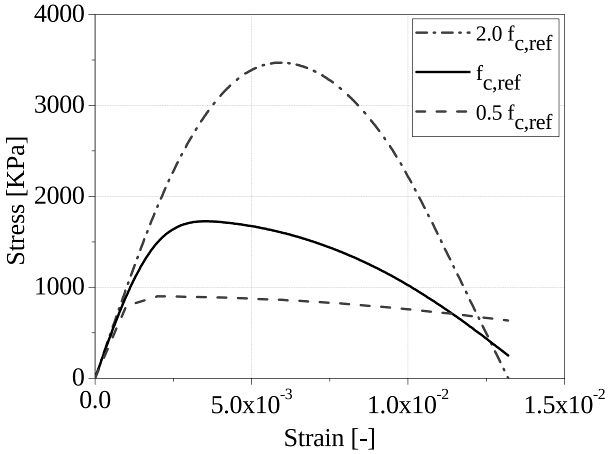

Figure 4.27 Stress-strain compressive behaviour varying the compressive strength.

The results from these variations are presented in Figure 4.28 in terms of force-displacement responses. Although it was expected that the tensile parameters were the ones to have more influence in the system response, the variation of the compressive strength has a relevant impact in the model behaviour. The 50% reduction of the initial compressive strength ($0.5f_{c,ref}$) leads to a reduction on the peak load of around 10% in relation to the reference model, followed by a more pronounced post-peak degradation until failure. In contrast, the doubling of the compressive strength ($2.0f_{c,ref}$) originates an important increase of the applied force, even if this increase occurs after a first peak. The first peak load does not suffer significant variation compared to the reference response. The analysis of these responses proved that the masonry compressive strength can be a relevant parameter in the anchoring system behaviour.

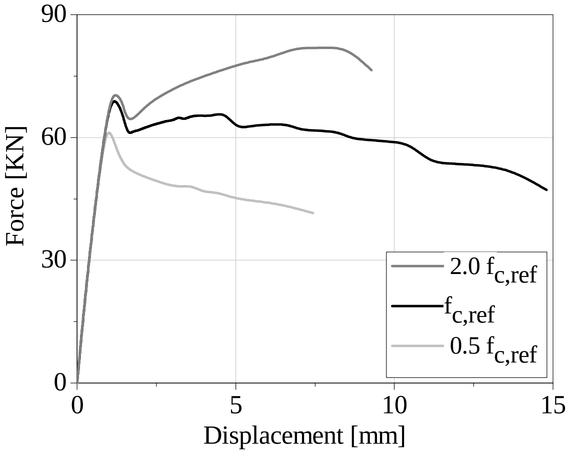

Figure 4.28 Force-displacement curves for the parametric analysis of the masonry compressive strength.

The compressive and tensile strains distribution presented in Figure 4.29 for the $0.5f_{c,ref}$ and Figure 4.30 for $2.0f_{c,ref}$, indicate a typical masonry cone breakout behaviour, as verified in the reference model. Thus, the failure mode is not affected by varying the compressive strength of masonry. The minimum principal strains distribution displayed in Figure 4.29c and Figure 4.29d for the analysis decreasing f_c, shows a concentration of compressive strains near the inward end of the anchors, indicating the crushing of masonry in these areas. In the analysis with increased f_c, the compressive damage distribution is less severe (Figure 4.30c and Figure 4.30d), as expected. The capacity of the anchors is influenced by the masonry compressive strength since the crushing in masonry affects the behaviour of the system.

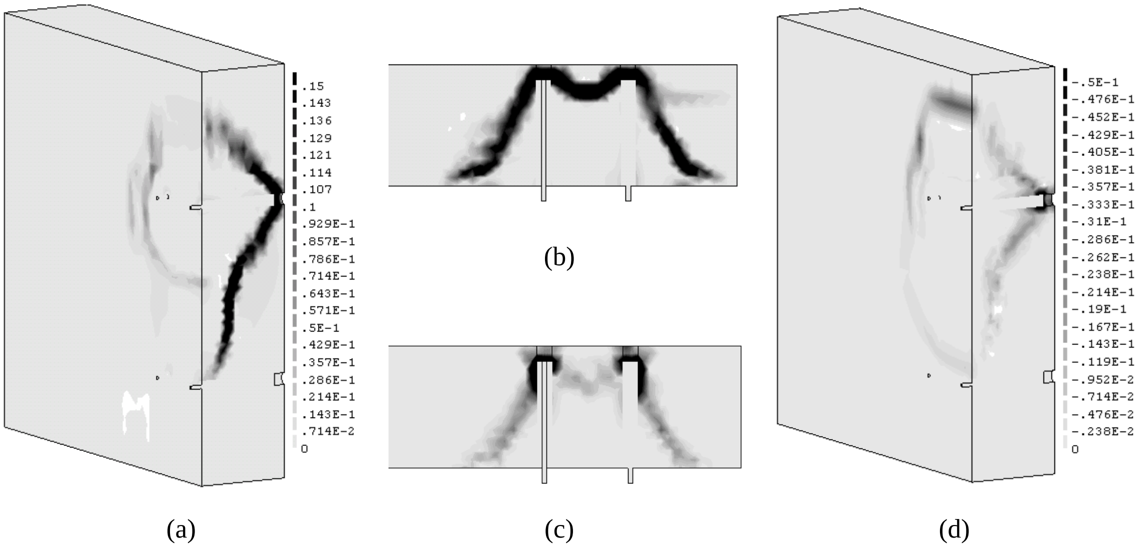
.15
.143
.136
.129
.121
.114
.107
.1
.929E-1
.857E-1
.786E-1
.714E-1
.643E-1
.571E-1
.5E-1
.429E-1
.357E-1
.286E-1
.214E-1
.143E-1
.714E-2
0
(b)
-.5E-1
-.476E-1
-.452E-1
-.429E-1
-.405E-1
-.381E-1
-.357E-1
-.333E-1
-.31E-1
-.286E-1
-.262E-1
-.238E-1
-.214E-1
-.19E-1
-.167E-1
-.143E-1
-.119E-1
-.952E-2
-.714E-2
-.476E-2
-.238E-2
0
(a)
(c)
(d)

Figure 4.29 Strains distribution at final stage for the $0.5 \times f_{c,ref}$ analysis: (a) Tensile -lateral view; (b) Tensile - top view; (c) Compressive -lateral view; (d) Compressive - top view.

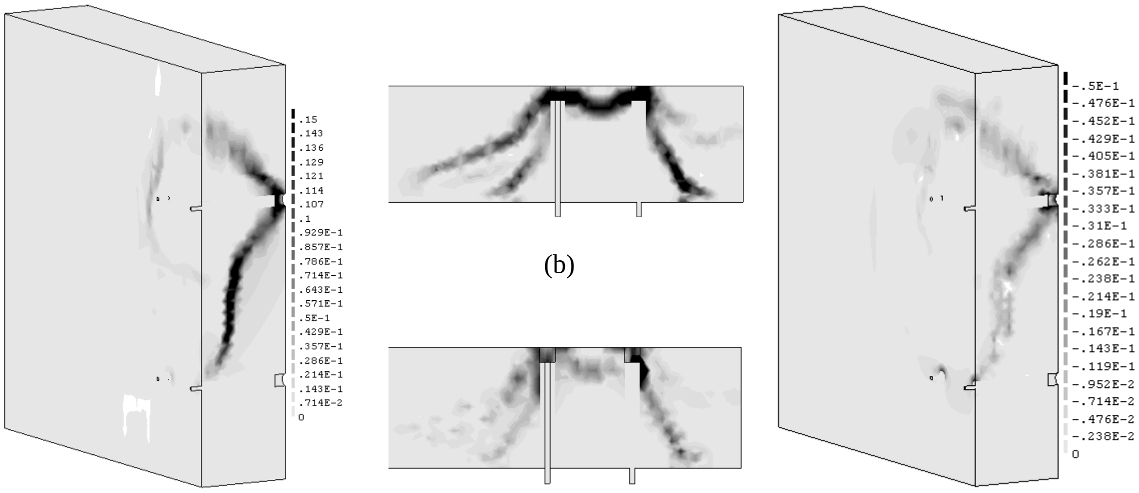
.15
.143
.136
.129
.121
.114
.107
.1
.929E-1
.857E-1
.786E-1
.714E-1
.643E-1
.571E-1
.5E-1
.429E-1
.357E-1
.286E-1
.214E-1
.143E-1
.714E-2
0
-.5E-1
-.476E-1
-.452E-1
-.429E-1
-.405E-1
-.381E-1
-.357E-1
-.333E-1
-.31E-1
-.286E-1
-.262E-1
-.238E-1
-.214E-1
-.19E-1
-.167E-1
-.143E-1
-.119E-1
-.952E-2
-.714E-2
-.476E-2
-.238E-2
0

(b)

(a) (c) (d)

Figure 4.30 Strains distribution at final stage for the $2.0 \times f_{c,ref}$ analysis: (a) Tensile -lateral view; (b) Tensile - top view; (c) Compressive -lateral view; (d) Compressive - top view.

Compressive Fracture Energy

The influence of the masonry compressive facture energy in the response of the system was evaluated by varying to the double (5.56 N/mm) and half (1.39 N/mm) the initial value (2.78 N/mm). Again, the masonry compressive behaviour by varying this parameter is depict in Figure 4.31 for a better insight of the constitutive laws applied to the model. The maximum compressive strength remains unchanged for all the analysis.

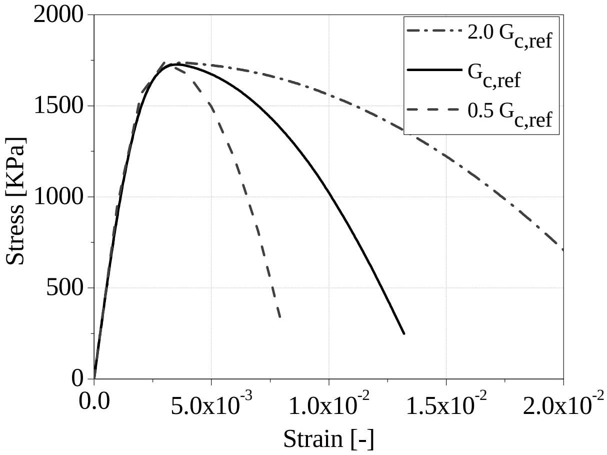

Figure 4.31 Stress-strain compressive behaviour varying the compressive fracture energy.

The analysis applying the constitutive laws defined above, resulted in the response curves exhibited in Figure 4.32. The results prove that this parameter does not influence much the initial behaviour of the system, while some differences in the post-peak behaviour for larger displacements can be found. The main differences are related to the deformation of the system. For the same post-peak load, the anchoring system presents displacements increasing with the compressive fracture energy, i.e. the response becomes more ductile, as expected. The damage pattern resultant from these analyses is presented in Annex B since no significant differences were found in comparison with the reference model. The masonry cone failure mode is recurrent with the clear development of cracks forming the cone shape.

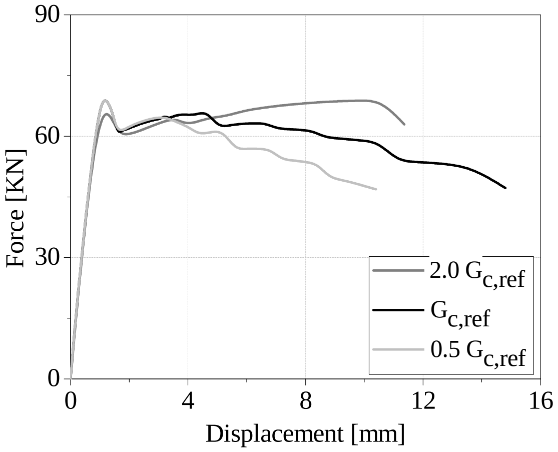

Figure 4.32 Force-displacement curves for the parametric analysis of the masonry compressive fracture energy.

Tensile Strength

Parametric analyses varying the tensile strength from 0.05 MPa (0.5×$f_{t,ref}$) to 0.20 MPa (2.0×$f_{t,ref}$), instead of the value of 0.10 MPa, imply the alteration of the tensile behaviour of masonry. Increasing and decreasing the tensile strength, while the fracture energy remains unchanged, the tensile linear and nonlinear behaviour suffers a significant change, as illustrated by Figure 4.33.

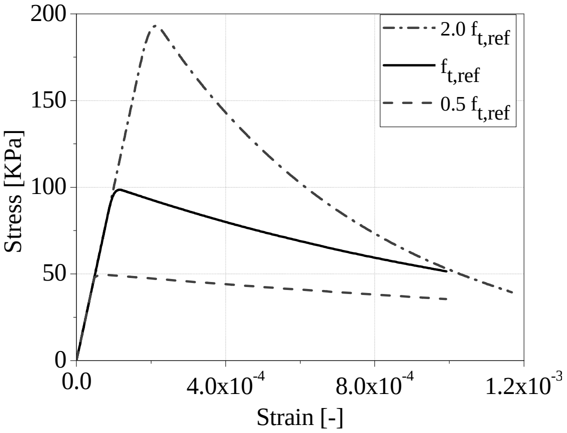

Figure 4.33 Stress-strain tensile behaviour varying the tensile strength.

The nonlinear analyses capacity curves varying the tensile strength are presented in Figure 4.34. With respect to the analysis that adopts a reduction on the tensile strength, the non-linear behaviour is activated for a lower value of force when compared to the reference model, even though it continues to increase up to 80 kN. The fact that the corresponding fracture energy remains unchanged should be highlighted and can justify the high force capacity increase originated by the reduction of the tensile strength.

By increasing the tensile strength, the peak force also reaches a higher value when compared to the corresponding one from the reference model. However, in what concerns the post-peak behaviour, the improvement is not so noteworthy. Indeed, the response of the 2.0$f_{t,ref}$ model exhibits a more fragile behaviour since this model considers a tensile strength increase while keeping the fracture energy value unchanged.

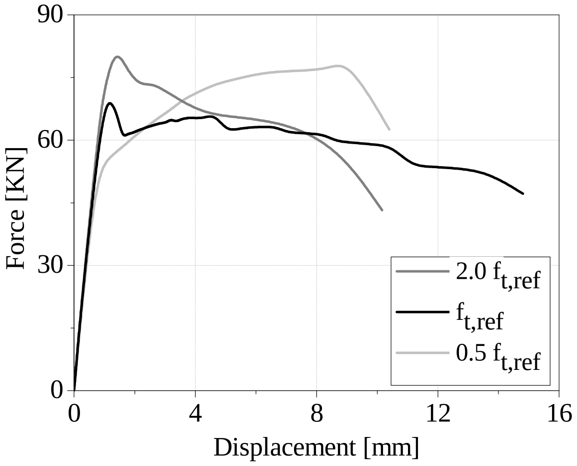

Figure 4.34 Force-displacement curves for the parametric analysis of the masonry tensile strength.

The distribution of tensile strains of both decreasing (Figure 4.35) and increasing (Figure 4.36) of the tensile strength show the masonry cone development through the wall. It can be verified that the masonry cone shape follows different patterns in the analyses. Comparing the two cone shapes, the masonry cone in the 2.0 $f_{t,ref}$ analysis presents a more close configuration with more widespread damage.

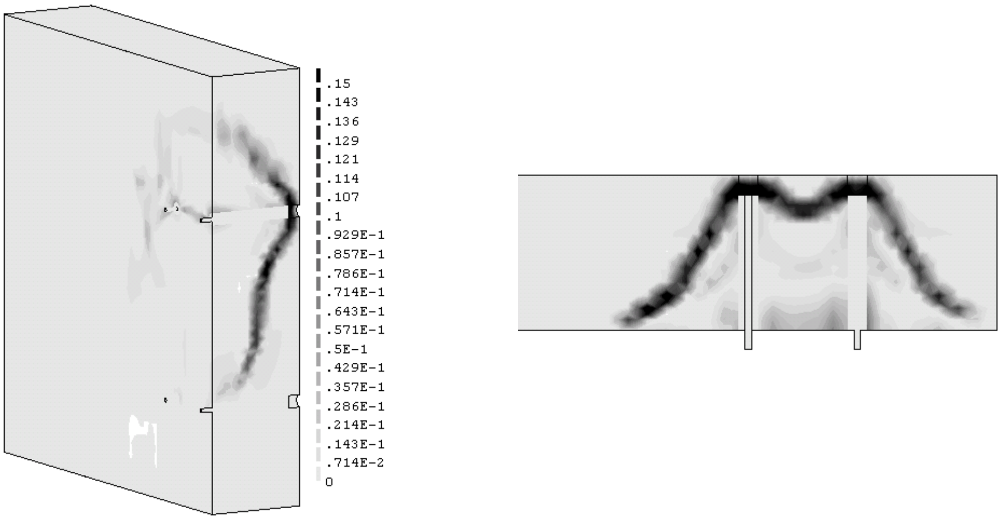
.15
.143
.136
.129
.121
.114
.107
.1
.929E-1
.857E-1
.786E-1
.714E-1
.643E-1
.571E-1
.5E-1
.429E-1
.357E-1
.286E-1
.214E-1
.143E-1
.714E-2
0

(a) (b)

Figure 4.35 Maximum principal strains at final stage for the $0.5 \times f_{t,ref}$ analysis: (a) Lateral view; (b) Top view.

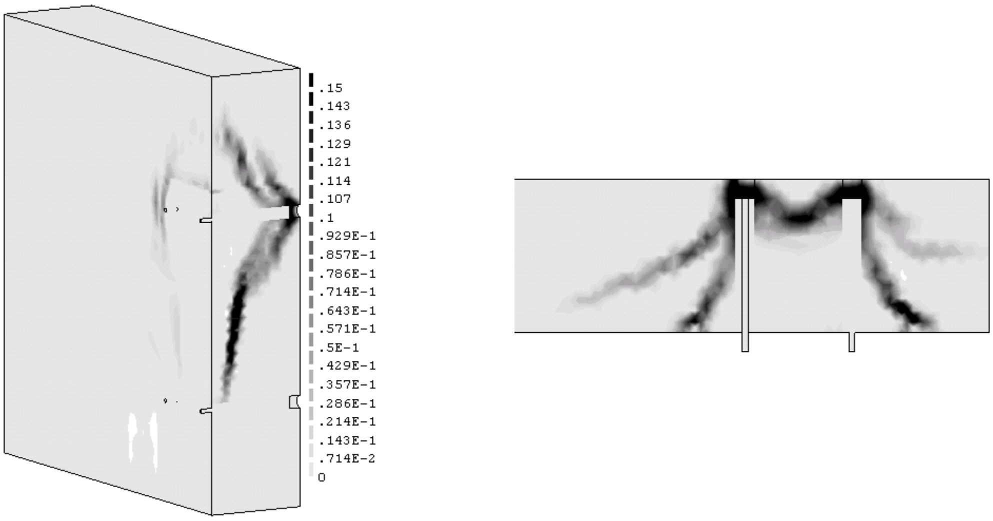

(a) (b)

Figure 4.36 Maximum principal strains at final stage for the $2.0 \times f_{t,ref}$ analysis: (a) Lateral view; (b) Top view.

Tensile Fracture Energy

The nonlinear analyses varying only the tensile fracture energy from 0.015 N/mm ($0.5 \times G_{t,ref}$) to 0.06 N/mm ($2.0 \times G_{t,ref}$), represented by the tensile behaviour described by Figure 4.37, are presented in this section.

The tensile fracture energy sensitivity analysis confirmed the influence of this parameter on the peak load and the significant alteration on the post-peak behaviour of the structure (Figure 4.38). When increasing and decreasing the tensile fracture energy by 50%, while keeping the tensile strength constant, the peak strength is directly affected. Modifying the tensile behaviour by decreasing the fracture energy implies a limitation to the capacity of some elements, which, in consequence, can compromise the capacity of the entire system. The fact that the maximum force value increases after the first peak for the $0.5G_{t,\text{ref}}$ analysis is a consequence of stress redistribution in the elements where the tensile strength was reached throughout adjacent elements, which affects the capacity of the system. The damage distribution indicates a pattern very similar to the reference model, showing the masonry cone development as well (see Annex B).

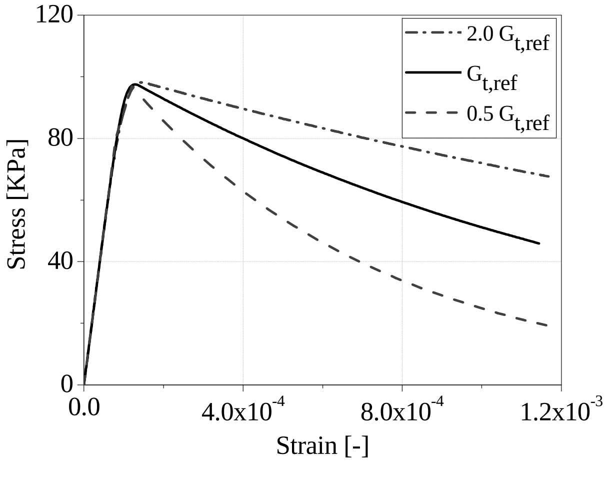

Figure 4.37 Stress-strain tensile behaviour varying the tensile fracture energy.

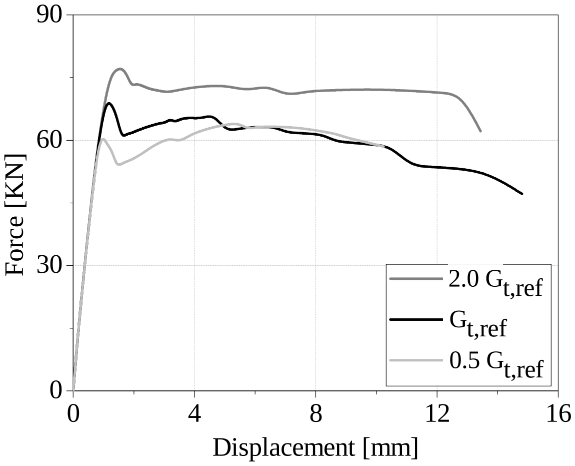

Figure 4.38 Force-displacement curves for the parametric analysis of the masonry tensile fracture energy.

4.4.2. Pre-compression Level

The pre-compression level that the masonry wall is subjected to was decreased to half (100 kPa) and increased two times (400 kPa) with respect to the reference value (200 MPa). The results are depicted in Figure 4.39 in terms of global force-displacement curves. The pre-compression level has a significant influence on the maximum force that the anchoring system can carry. By decreasing the compressive stress on the wall, the peak force suffers a reduction of 14%. Likewise, the increasing of the level of pre-compression on the wall causes a 22% increase in the ultimate capacity of the structure. In both cases, the post-peak configuration is not very much affected. The analysis of the damage patterns shows that the failure mode is kept unchanged (see Annex B).

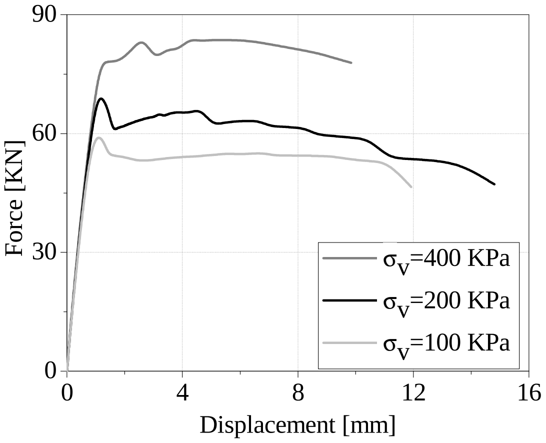

Figure 4.39 Force-displacement curves for the parametric study of the pre-compression level.

4.4.1. Geometric Parameters

Supplementary studies were also carried out in order to evaluate the influence of some of the geometric parameters on the behaviour of the anchoring system, as follows: steel bar diameter and respective borehole, wall width and embedment depth, and the spacing between anchors.

Anchor Dimension

The steel bar diameter and corresponding borehole were studied in order to evaluate how the anchor dimensions can affect the behaviour of the system. A new numerical model was created by modifying the anchor dimensions, the initial 16 mm bar diameter was replaced for a 32 mm diameter and the corresponding borehole of 75 mm, instead of the initial 50 mm (as represented in Figure 4.40). The parametric study showed that an increase of 100% in the anchor diameter (increase of 167% in perimeter) did not provide a significant increase in the ultimate capacity (around 11% regarding the reference model) (Figure 4.41). The post-peak behaviour does not present many changes when compared to the reference model response. The damage distribution is also very similar to the one found for the reference model, again with the masonry cone formation being conditioning (see Annex B). As the dominant failure mode is the masonry cone breakout, the anchoring capacity is not enhanced in a significant way by increasing the anchoring system.

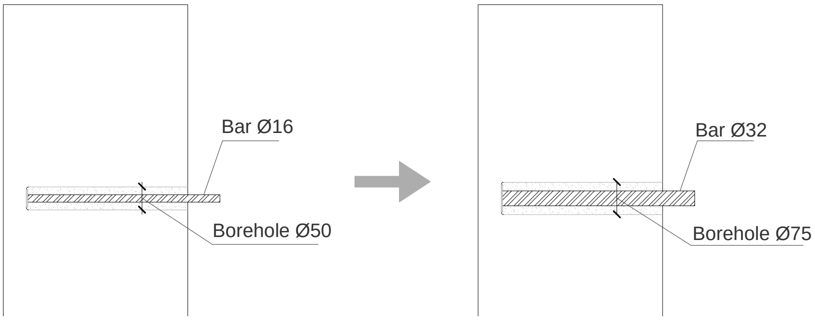

Figure 4.40 Modification of the anchoring system dimension.

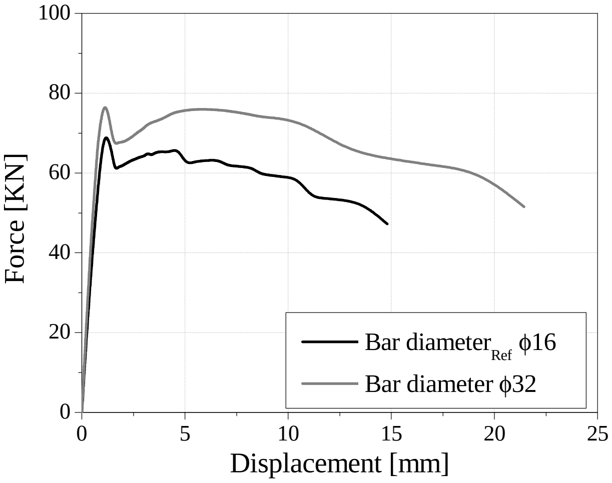

Figure 4.41 Force-displacement curves for the parametric study of the anchor dimensions.

Embedment Depth

According to several authors, the embedment depth of the anchor is a factor with great influence on the behaviour of the anchoring system. For this reason, this aspect was studied by changing the wall thickness from 400 to 600 mm and the embedment depth from 350 mm to 550 mm. In order to accomplish the new geometric features, the numerical model was updated as represented by Figure 4.42.

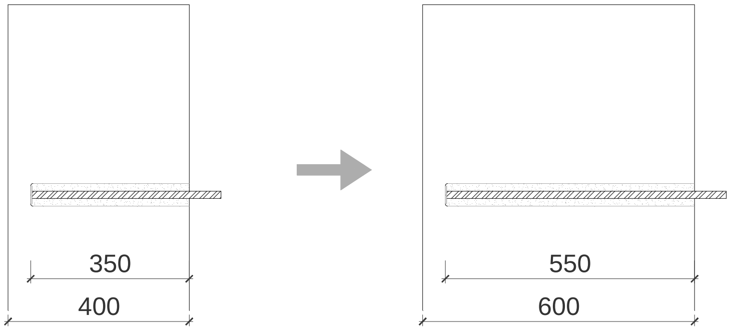

Figure 4.42 Modification of the wall thickness and anchor embedment depth.

The analysis results were compared to the reference model in Figure 4.44, where the differences on the behaviour of the models are apparent. The new model reaches a maximum force of 140 kN opposing to the 70 kN achieved by the reference model. Notwithstanding, the post-peak behaviour of the new model experiments a sharper decrease when compared to the reference model, which shows to be more ductile.

Figure 4.44 illustrates the maximum principal strains in the new model at failure, which can also be seen as an image of the tensile damage. This damage pattern presents significant differences regarding the one from the reference model, see Figure 4.22. The formation of the shear cone on the masonry is not activated for the whole anchor system extension as in the reference model. Instead, sliding along the external interface is perceptible until a certain position followed by the masonry cone development (visible in Figure 4.44b).

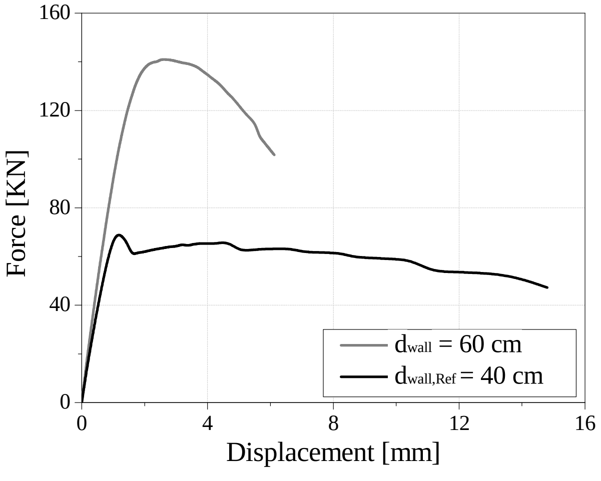

Figure 4.43 Force-displacement curves for the parametric study of the embedment depth.

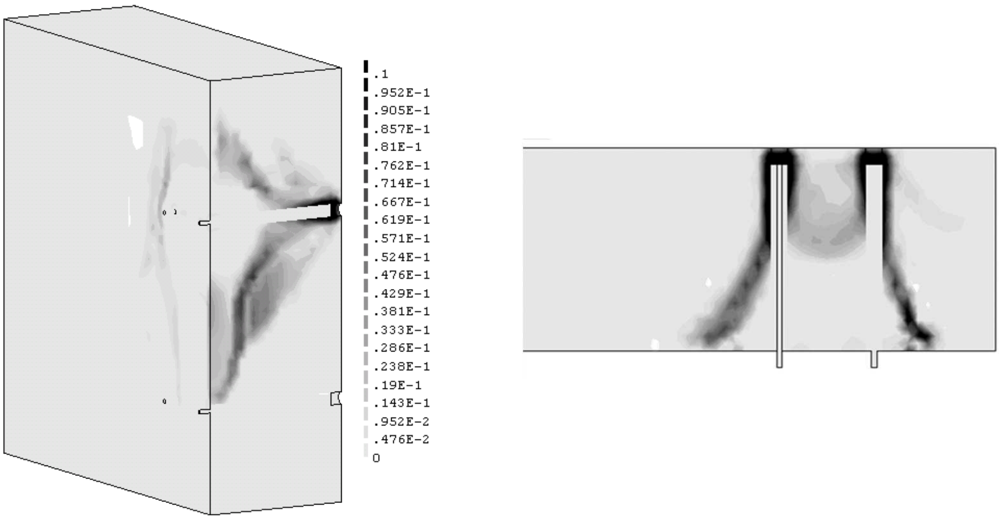

(a) (b)

Figure 4.44 Maximum principal strains at final stage for the embedment depth parametric analysis: (a) Lateral view; (b) Top view.

Anchors Spacing

A study to evaluate the influence of the anchors spacing was also conducted. This parametric study aims at evaluating in which manner the distance between anchors can influence, not only the ultimate capacity of the system, but also the associated failure mode (interaction between the cone formation of each anchor). A numerical model in which the distance between anchors was increased to 420 mm, i.e. a 50% increase of the initial distance, was constructed (see Figure 4.45). By comparing the results of this model with the reference ones, an increase in the ultimate capacity can be confirmed, around 13%, see Figure 4.46. The nonlinear behaviour shown by this parametric analysis is very similar to the reference model response.

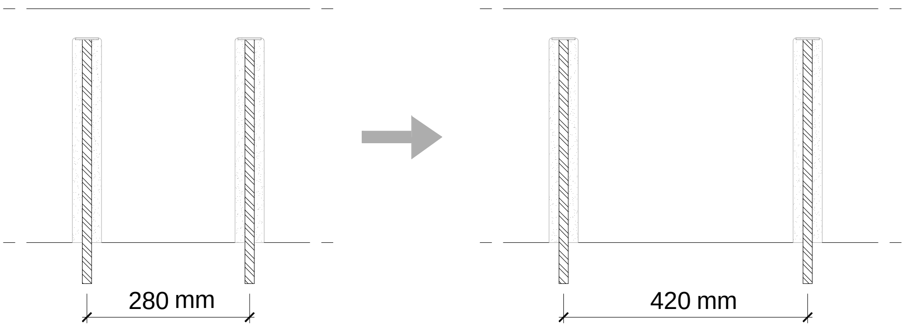

Figure 4.45 Modification of the spacing between anchors.

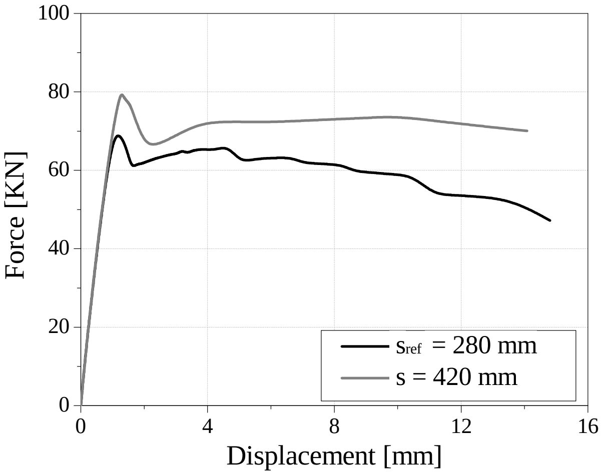

Figure 4.46 Parametrical study of the anchors spacing: (a) Modifications on the model settings; (b) Force-displacement curve.

The principal strains were also analysed as an indicator of damage in order to compare the cone formation evolution of this analysis with the reference results (Figure 4.44). The damage pattern presents a different configuration between the two anchors where the cone formation is more visible. This analysis proved that the tensile capacity of a single anchor is affected by the overlapping of the adjacent anchors. This means that increasing the spacing between anchors, up to an optimized minimum value, allows for the enhancement of the ultimate capacity of the system.

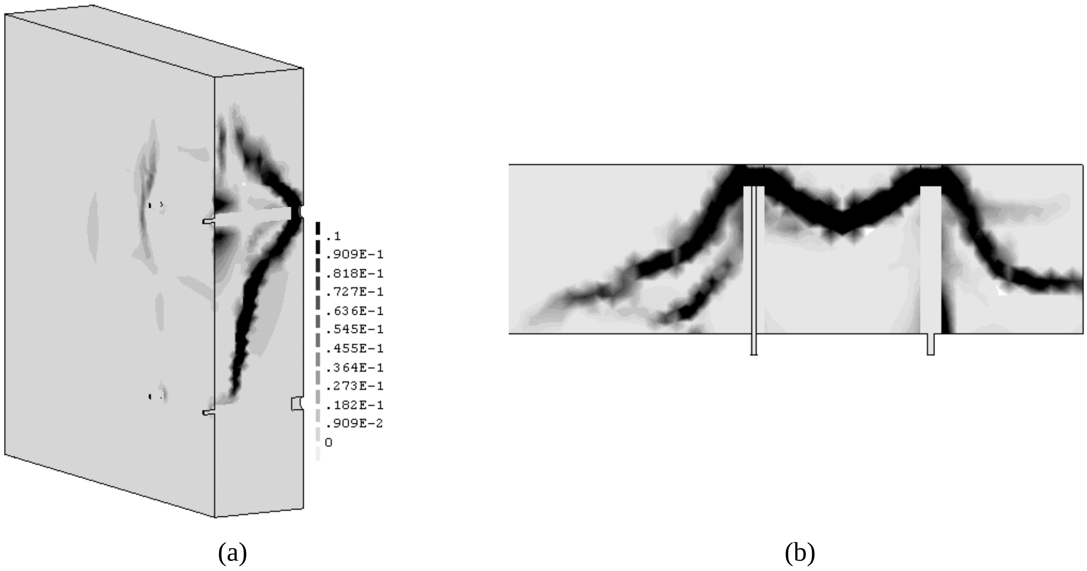

(a) (b)

Figure 4.47 Maximum principal strains at final stage for the anchor spacing parametric analysis: (a) Lateral view; (b) Top view.

4.4.2. Conclusions

The knowledge regarding the load-carrying capacity of anchors in masonry is limited. As such, in order to avoid a physical, comprehensive and time-demanding experimental testing to evaluate the influence of some parameters, a numerical study is carried out instead. The confidence in the results relies on the validation of the numerical model against experimental results.

The assessment of the influence of the mechanical properties of masonry on the behaviour of the anchors in the masonry walls showed that the compressive and tensile strengths are parameters with significant impact on the response of the system.

The parametric studies on wall conditions showed that the anchor embedment depth is the parameter that mostly influences the structural behaviour of the system, increasing significantly the ultimate capacity. Nevertheless, the pre-compression level of the wall, the anchor diameter and the spacing between anchors also influence the behaviour of the structural system, although in a moderate manner. The same failure mode was recurrent in all the analyses, although some differences in the damage pattern were verified in some cases.

4.5. ANALYTICAL EVALUATION

The assessment of the anchoring system capacity by means of complex numerical methods was relevant for a better understanding of the structural behaviour of the system. However, for design purposes, the use of simplified models is required. As mentioned before, despite the fact that injected anchors have been used for many years to strengthen masonry buildings, no generally methodology exists for the design of such anchoring systems.

During the last few decades several analytical models have been proposed to describe the behaviour of anchors in tension (Wenzel and Maus 1992; Gigla and Wenzel 2000; Arifpovic and Nielsen 2004; Gigla 2004; Meyer and Eligehausen 2004; ACI 318 2011; fib Bulletin No. 58 2011; Hilti 2011; MSJC 2013). In general the ultimate tensile load capacity is based on the simplified assumption of separated failure modes (Bajer and Barnat 2012). Moreover, some of the simplified analytical formulations presented in literature are adjusted to achieve a good fit with available test data.

This section reviews the most used analytical methods, associated to distinct failure mechanisms occurring in injected anchors under tensile loading, and applies them to the example under study. Due to the few existing analytical formulations regarding anchors in masonry, formulations regarding anchors in concrete have also been employed. Most of these approaches are similar and the same parameters are recurrently used, such as: the embedment depth (l_{ef}), steel bar diameter (d_s) and area (A_s), borehole diameter (d_B), masonry compressive strength (f_c), anchor yield strength (f_y) and bond strength (τ_u). The symbol T will be used for the anchor capacity loaded in tension.

4.5.1. MSJC Formulation

The analytical expressions provided by the Masonry Standards Joint Committee (MSJC 2013) to predict the anchor behaviour consider two failure mechanisms namely steel yielding and tensile breakout of masonry. This formulation is addressed and discussed by Weigel and Lyvers (2004) and McGinley (2006). Equation (4.1) is used to define the anchor capacity based on the steel yielding f_y:

$$T = A_s \times f_y \tag{4.1}$$

The tensile breakout of masonry is computed using equations (4.2) and (4.3):

$$T = 0.332 \times A_{pt} \times \sqrt{f_m} \tag{4.2}$$

$$A_{pt} = \pi \times {l_{ef}}^2 - \frac{A_0}{2} \tag{4.3}$$

where A_{pt} represents the projected area on the masonry surface of a right circular cone and A_0 is the overlapping area of the anchors. In the experimental tests under consideration f_y is equal to 640 MPa.

4.5.2. Gigla and Wenzel Formulation

Based on the results of 500 pull-out tests performed in laboratory and in-situ, Gigla and Wenzel (2000) proposed simplified expressions for ultimate capacity of anchoring systems. The bond strength between the grout and the surrounding masonry was also evaluated and equation (4.4) was proposed:

$$\tau_u = \emptyset_J \times \left(\frac{{f_{G,c}}^2}{500} + X_{B,W} \right) \tag{4.4}$$

where $\emptyset_J$ is the reduction factor for bed or head joints (assumed equal to 0.6), $f_{G,c}$ is the compressive strength of grout and $X_{B,W}$ is the term to describe the increase of bond strength inside water absorptive stone material (the recommended value is zero if the value is unknown). The bond strength between grout and surrounding masonry is dependent not only on the mechanical properties on the injected grout, but also on the ratio of head and bed joints of masonry, since the support material conditions strongly influence the adherence between materials.

As $f_{G,c}$ is equal to 51.5 MPa, the application of equation (4.4) gives a value for the bond strength around 3 MPa, which seems to be a reasonable value when compared with experimental studies (Gigla 2004; Algeri et al. 2010). This value was also used in the formulations next, since no experimental values are available. The capacity of an injected anchor should be calculated using equation (4.5):

$$T = \tau_u \times \frac{A_B}{A_{g,d}} \times A_{A,d} \tag{4.5}$$

where τ_u is the bond strength , $A_{A,d}$ represents the surface of injected grout surrounding the steel bar, $A_{G,d}$ is the surface of injected grout and A_B is the contact area between grout and units (see Figure 4.48). After the experimental tests carried out on the University of Minho, the walls were carefully demolished in order to assess the distribution of mortar and stone surrounding the grout surface. Considering the three experimental tests, an average value of 37% was found for the area of stone in contact with the grout surface, and a value of 63% for mortar (head and bed joints).

With this information, a more realistic value for the contact area of grout and stone (A_B) was defined.

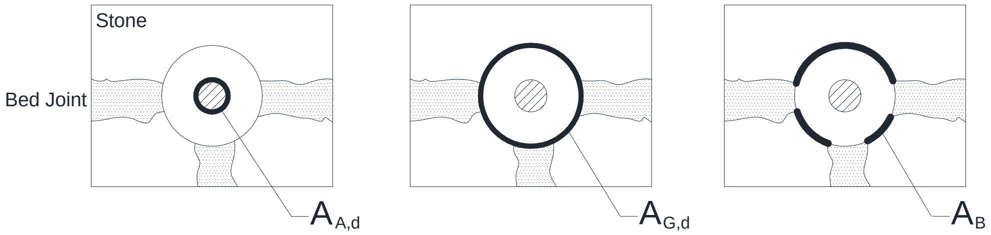

Figure 4.48 Geometrical parameters for equation (4.5) (Gigla 2004).

4.5.3. ACI 318 Formulation

The methodology proposed by ACI 318 Appendix D (ACI 318 2011) for the prediction of the anchor strength in concrete defines three failure modes: steel tensile failure, substrate tensile breakout and bond failure. The design method proposed in Hilti (2011) is based on this code. Weigel and Lyvers (2004) also used these provisions to compared test data of single bolts in masonry.

The strength of an anchor in tension governed by the steel shall be evaluated by calculations based on the properties of the anchor material and the physical dimensions of the anchor, as given by equation (4.6):

$$T = n \times A_s \times f_{uta} \tag{4.6}$$

where n is the number of anchors in the group, and f_{uta} is the specified tensile strength of the anchor steel (equal to 800 MPa for the anchor under study). ACI 318 considers that the tensile strength of anchors is best represented by f_{uta} rather than f_y because the large majority of anchor materials do not exhibit a well-defined yield point (ACI 318 2011).

The base material breakout strength of anchors loaded in tension is defined as follows:

$$T = \frac{A_{Nc}}{A_{Nco}} \times \Psi_{ec,T} \times \Psi_{ed,T} \times \Psi_{c,T} \times \Psi_{cp,T} \times \ n \cdot T_b \tag{4.7}$$

$$A_{Nco} = 9 \times {l_{ef}}^2 \tag{4.8}$$

$$T_b = 4.10 \times \sqrt{f_m} \times {l_{ef}}^{1.5} \ \text{[adapted for use in masonry (Weigel and Lyvers 2004)]} \tag{4.9}$$

$$\Psi_{ed,T} = 0.7 + 0.3 \times \frac{c_a}{1.5\ l_{ef}} \ \ if \ \ c_a < 1.5\ l_{ef} \tag{4.10}$$

where A_{Nc} is the projected failure area of a single anchor or group of anchors limited by the edge distance or spacing, as represented in Figure 4.49, $\Psi_{ec,T}$ is the modification factor for anchor groups loaded eccentrically, which is not the case under study ($\Psi_{ec,T}$ = 1); $\Psi_{ed,N}$ is the modification factor for edge distances less than 1.5 l_{ef}, see equation (4.10), $\Psi_{c,T}$ is equal to 1.0 when the base material indicates cracking at service loads, which is considered to be case for masonry, and $\Psi_{cp,T}$ is the modification factor for splitting, equal to 1 in this case.

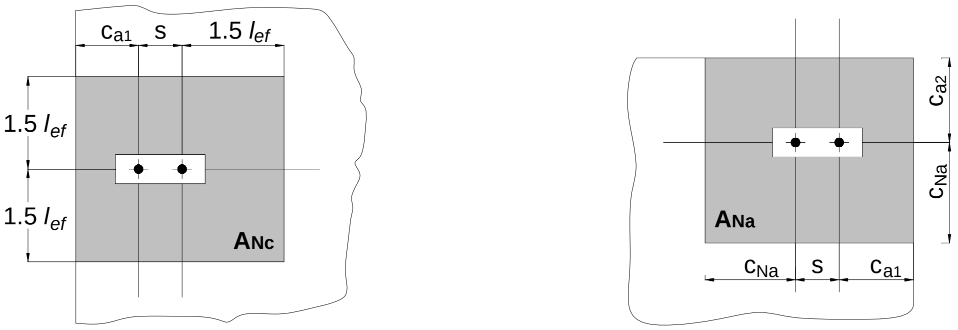

Figure 4.49 Calculation of A_{Nc} and A_{Na} (ACI 318 2011).

According with the same methodology, the bond strength of adhesive anchor in tension is evaluated as follows:

$$T_a = \frac{A_{Na}}{A_{Nao}} \times \Psi_{ec,T_a} \times \Psi_{ed,T_a} \times \Psi_{cp,T_a} \times\ n \cdot T_{ba} \tag{4.11}$$

$$A_{Nao} = (2c_{Na})^2 \tag{4.12}$$

$$c_{Na} = 10 \cdot d_B \sqrt{\frac{\tau_u}{7.58}} \tag{4.13}$$

$$T_{ba} = \tau_u \times \pi \times d_B \times l_{ef} \tag{4.14}$$

where A_{Na} is the projected influence area of a single adhesive anchor or group, represented in Figure 4.49, and A_{Nao} is the projected influence area of a single anchor with an edge distance equal to c_{Na} (obtained by the application of equation (4.13) with the constant 7.58 in N/mm^2), described by equation (4.12) . In this case the parameter Ψ_{ec,T_a} is equal to 1 since the anchor group is not eccentrically loaded. The modification factor for edge effects, Ψ_{ed,T_a}, is equal to 1 when $c_a > c_{Na}$, which is the case, and $\Psi_{cp,T_a}$the modification factor for splitting is also equal to 1.

The analytical formulations recommended by ACI 318 for the substrate tensile failure and bond failure include the interaction between anchor groups. Although the number of anchors n has been considered equal to 1 (in order to easily compare with the other predictions), the strength value obtained by the application of this formulation already takes into account the interaction between anchors.

4.5.4. CEB Formulation

CEB (1994) proposes an approach to the design of anchors in concrete and masonry, where three failure modes are defined. For the definition of the capacity based on the steel failure equation (4.1) is used. As for the assessment capacity based on the base material cone failure the equation (4.15) is proposed by Eligehausen et al. (Eligehausen et al. 1984). Doerr and Klingner (Doerr and Klingner 1989) present the equation (4.16) which attempts to incorporate the combined action of substrate-cone failure and bond failure.

$$T = 0.85 \times {l_{ef}}^{2} \times \sqrt{f_m} \tag{4.15}$$

$$T = \frac{34.7\pi \times \tau_u \times {d_s}^{1.5}}{\lambda^{'}} \times tanh\left[\frac{\lambda^{'} \times \left(l_{ef} - 50\right)}{34.76 \times {d_s}^{0.5}}\right] \tag{4.16}$$

where $\lambda^{'}$ is a parameter that depends on the grout properties (see (Doerr and Klingner 1989)), which equals 0.3 $mm^{-1/2}$ here. In the case of failure at the grout-masonry interface, the bond strength is smaller than the masonry strength. To take this failure mode into account, CEB proposes the following equation, also reported in D'Ayala (2011) and Meyer and Eligehausen (2004):

$$T = \tau_u \times l_{ef} \times \pi \times \, d_B \tag{4.17}$$

4.5.5. Fib Formulation

The design guide for anchors in concrete available in fib Bulletin No. 58 (2011) recommends the prediction of the anchor strength based on three failure modes. In addition, the strength of an anchor is evaluated by taking into consideration the interaction between anchors in a group.

The anchor strength considering the steel failure is given by equation (4.6), as proposed by ACI 318. The combined pullout and substrate cone failure may be obtained as follows:

$$T_p = {T^0}_p \times \frac{A_p}{{A^0}_p} \times \Psi_{s,T_p} \times \Psi_{g,T_p} \times \Psi_{ec,T_p} \times \Psi_{re,T_p} \tag{4.18}$$

$${A^0}_p = \left(s_{cr,N_p}\right)^2 \tag{4.19}$$

$$s_{cr,T_p} = 20 d_s \sqrt{\frac{\tau_u}{7.5}} \tag{4.20}$$

$$c_{cr,T_p} = 0.5 \, s_{cr,T_p} \tag{4.21}$$

where ${T^0}_p$ is computed using the equation (4.14) from ACI; ${A^0}_p$, the bond reference area, and A_p, actual bond influence area limited by overlapping areas of adjacent anchors, is calculated similarly to the method used in ACI 318 (see Figure 4.49). Ψ_{s,T_p} is a factor that takes into account the distribution of stresses due to the edges of the substrate member, equal to 1 in this case because $c > c_{cr,T_p}$ ($c = 380 \, mm$). The factor Ψ_{g,T_p}, which takes into consideration the effect of the failure surface of anchor groups, and the factor Ψ_{ec,T_p}, which refers to non uniform tensile loads, are both equal to 1 in this study (see fib Bulletin No. 58 (2011)). The parameter that reduces the strength of anchors with embedment depth $l_{ef} < 100 \, mm$ (Ψ_{re,T_p}) also takes the value of 1. The strength capacity in the case of the substrate cone failure is obtained from the following procedure:

$$T_c = {T^0}_c \times \frac{A_c}{{A^0}_c} \times \Psi_{s,T_c} \times \Psi_{ec,T_c} \times \Psi_{re,T_c} \tag{4.22}$$

$${A^0}_c = \left(s_{cr,T_c}\right)^2 \tag{4.23}$$

$$s_{cr,T_c} = 3l_{ef} \tag{4.24}$$

where $T^0{}_c$ is given by equation (4.9), the geometric factor $\frac{A_c}{A^0{}_c}$ is equal to the one used in ACI 318 for the same failure mode, see equation (4.7), as well as the Ψ_{s,T_c} factor given by equation (4.10). Ψ_{ec,T_c} and Ψ_{re,T_c} (already defined) are equal to 1.

4.5.6. Arifpovic and Nielsen Formulation

Pull-out tests of single anchors in brick masonry were carried out by Arifpovic and Nielsen (2004) with the purpose of observing the failure modes that govern the behaviour of the system in different conditions. Simplified analytical expressions based on the theory of plasticity were developed from the experimental results in order to predict the load carrying capacity of the anchors. Three failure modes were presented by the authors. The strength capacity of the anchor due to masonry cone failure can be obtained by equation (4.25):

$$T = 0.96(d_s + l_{ef}) \times l_{ef}\sqrt{f'_m} \tag{4.25}$$

For the case of bond failure, Arifpovic and Nielsen defined two expressions for the cases in which the anchor is installed in a mortar joint, equation (4.26), or in a unit, equation (4.27):

$$T = 22.38\sqrt{f_{cj} \times l_{ef}} \times d_s^{\frac{3}{2}} \tag{4.26}$$

$$T = 3.79d_s \times l_{ef}\sqrt{f_{cb}} \tag{4.27}$$

where f_{cj} is the compressive strength of the mortar and f_{cb} represents the compressive strength of the unit. The compressive strength of the mortar and limestone units were experimentally evaluated for the present study and a mean value of 1.3 MPa and 107 MPa, respectively, were obtained. The combined brick-cone failure, which consists in the combination of the masonry cone formation and sliding along both the internal and external interface, can be obtained through equation (4.28):

$$T = [3.93\sqrt{f_{cb}} \times \left(l_{ef} - 5.76 \times d_s\right) \times d_s + 37.44\sqrt{f_{ci}} \times (l_u + d_s) \times d_s]\sqrt{\frac{d_s}{l_{ef}}} \tag{4.28}$$

where f_{ci} is the compressive strength of the interface between mortar and joints and l_u is the unit length. Here, a value around 0.3 MPa was adopted following the recommendations reported in the same report (Arifpovic and Nielsen 2004). An average length (l_u) of 200 mm was considered taking into consideration the stone blocks used.

4.5.7. Results and Discussion

The prediction of the anchor capacity according to the simplified formulations described throughout this section is summarized in Table 4.5. The strength capacity was calculated only for one anchor, although the interaction between anchors, provided by some formulations, was considered whenever possible. The shaded cells in Table 4.5 are associated with the lower value obtained in each formulation.

Table 4.5 Prediction of the anchor strength according to the distinct formulations.

Formulations		Equation	Anchor Capacity [kN]
MSJC (2002)	Steel Failure	(4.1)	129
	Cone Failure	(4.2)	126
Gigla and Wenzel (2000)	General (no failure mode defined)	(4.5)	26
ACI 318 (2005)	Steel Failure	(4.6)	161
	Cone Failure	(4.7)	36
	Bond Failure	(4.11)	238
CEB	Steel Failure	(4.1)	129
	Cone Failure	(4.15)	137
	Combined bond-cone Failure	(4.16)	40
	Bond Failure	(4.17)	165
Fib (2011)	Steel Failure	(4.6)	161
	Combined bond-cone Failure	(4.18)	199
	Cone Failure	(4.22)	37
Arifpovic and Nielsen (2004)	Cone Failure	(4.25)	162
	Bond Failure	(4.26)	30
		(4.27)	219
	Combined bond-cone Failure	(4.28)	51

The prediction of the failure mode through simplified analytical methods appears to agree reasonably well with both the experimental results and numerical analysis. Either the base material cone formation with masonry breakout or the combined bond-cone failure are the recurrent failure modes, achieved in almost all the approaches. MSJC (2013), ACI 318 (2011), CEB (1994) and fib Bulletin No. 58 (2011) predict that the anchor strength is limited by one of these failure modes. Arifpovic and Nielsen (2004) predict the sliding of the anchor installed in a mortar joint as the failure mode limiting the anchor capacity (see Table 4.5). However, the assumptions made in this study for this expression are not valid since the anchor is not completely installed in a mortar joint, therefore the corresponding value found for this failure more is not realistic. Disregarding this value, the failure mode obtained by this formulation is the combined masonry cone formation with sliding along the interface, which is in accordance with experiments. Gigla and Wenzel (2000) do not define a specific failure mode.

In order to provide a better perception on the relation between the experimental and predicted value, Figure 4.50 summarizes the results from the different approaches, considered to predict the anchor capacity, comparing these results to the mean experimental value. In this diagram, a relation near to 1 means that the predicted values are very close to the experimental capacity. According to the experimental results, a mean force of 76.8 kN was reached for the two anchors composing the anchoring solution adopted. As the formulations were used to predict the capacity of one anchor (including the interaction among groups when applicable), the obtained value should be multiplied by two.

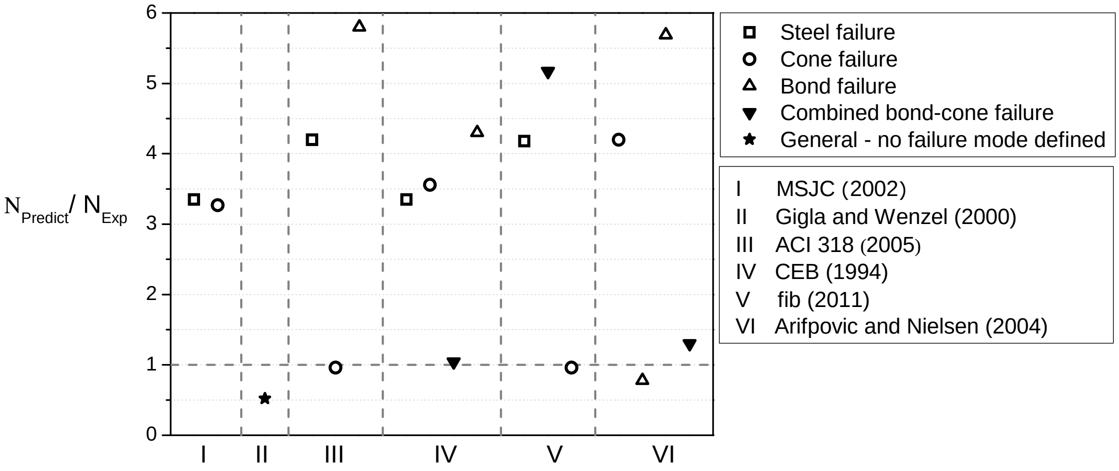

Figure 4.50 Comparison between the experimental mean value and analytical predictions of the anchoring system capacity.

The relations presented in Figure 4.50 show that the predicted strength values by ACI 318 and fib bulletin 58 for the masonry cone failure, and by Doerr and Klingner (1989) in CEB for the combined bond-cone failure, are in very good agreement with the experiments. The good predictions of these two formulations, regarding both the failure mode and the strength value, can be explained by some considerations included in the expressions that are important in the anchoring system under study. Besides MSJC provisions, ACI 318 code and fib are the only that consider the influence of the anchors spacing and possible interaction among them.

The ACI 318 recommendations for concrete, adapted for use in masonry by Weigel and Lyvers (2004), predicted very well the tensile strength of the anchors in masonry. ACI 318 code and fib recommendations consider, beyond the masonry strength and embedment depth, other factors such as the influence of the anchors spacing, edge distance and possibility of splitting. As proved numerically, the anchors spacing influence significantly the cone formation in the masonry and consequently the strength capacity of a single anchor. Simplified analytical expressions that considers the interaction between anchors in a group seem to better describe the behaviour of this anchoring system, as expected.

The formulation provided by Doerr and Klingner (1989) in CEB includes the prediction of a combined failure mode (masonry cone with sliding along the interface), which is the failure mode verified experimentally. This analytical expression provided a very close prediction on the anchoring system strength capacity since it included the contribution of the grout/masonry bond in the formulation, even if factors like the anchor spacing and the edge distance are not considered.

The expression provided by Gigla and Wenzel (2000) predicted very conservative relations that can possibly be explained by conservative assumptions regarding both the reduction factor referent to the contact to mortar joints and the term to describe the increase of the bond strength inside water absorptive stone material, which was considered equal to zero as no information is available.

As previously stated, the provisions recommended by Arifpovic and Nielsen (2004) for the bond failure when the anchor is installed in a mortar, are not applicable to the case under study. The strength capacity for combined bond-cone failure is slightly overestimated but with good approximation to the experimental value. This formulation does not considers the influence of an adjacent anchor.

As expected, the applied analytical formulations based on the steel failure and bond failure achieve considerably high load capacities. The analytical formulation defined by fib bulletin 58 for the combined bond-cone failure also resulted in a high strength value. When compared with other formulations, this analytical expression seems to be more appropriate to define the bond failure.

Finally, the simplified approach recommended by MSJC gives a very high value when compared to experiments and numerical analysis, and even with the other simplified expressions. Weigel and Lyvers (2004) have stated that these provisions may lead to less reliable results. Although the values provided by MSJC and CEB are similar, CEB includes an expression for the combined cone sliding failure, which is the one verified experimentally.

The analytical expressions were also applied considering the walls from the parametric studies: higher anchor dimensions, greater embedment depth and larger spacing between anchors. Here, the analytical predictions are compared with the anchoring system capacity obtained from the numerical results. Figure 4.51 displays the relation between the analytical predictions and the numerical results for the anchors dimensions parametric analysis, Figure 4.52 for the embedment depth parametric analysis and Figure 4.53 for the anchor spacing. The application of the simplified expressions to different anchoring systems by varying some of the key parameters, aim to further discuss the ability of the analytical formulations to estimate the strength capacity of anchoring systems.

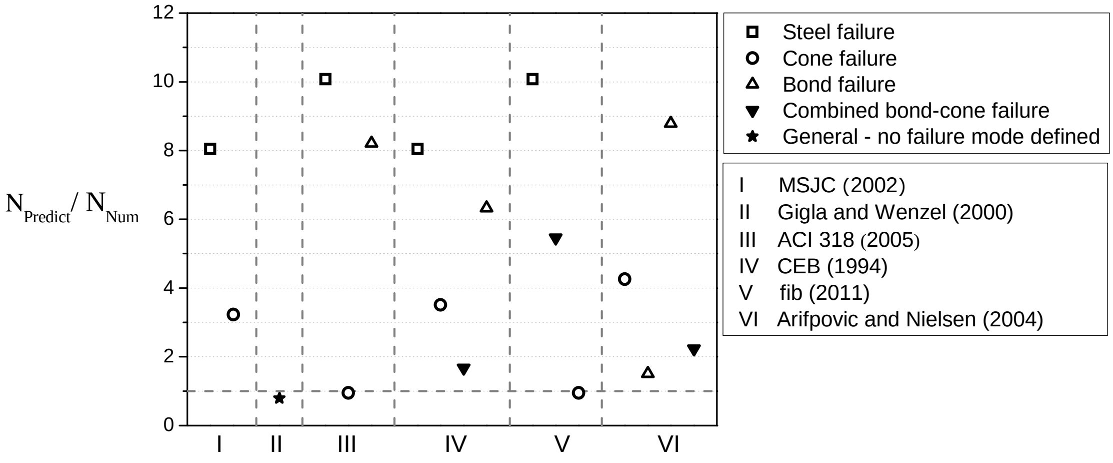

Figure 4.51 Comparison between the analytical expressions and the parametric analysis of the anchor dimension.

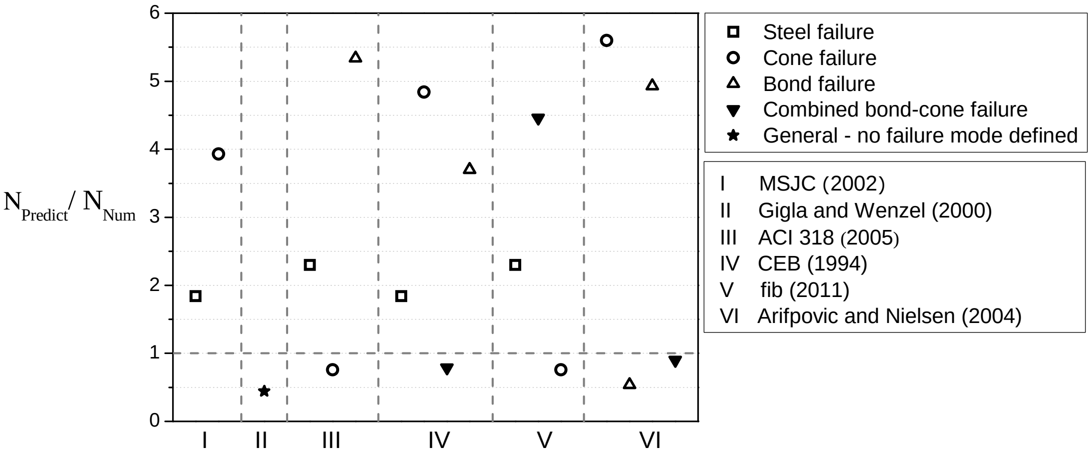

Figure 4.52 Comparison between the analytical expressions and the parametric analysis of the embedment depth.

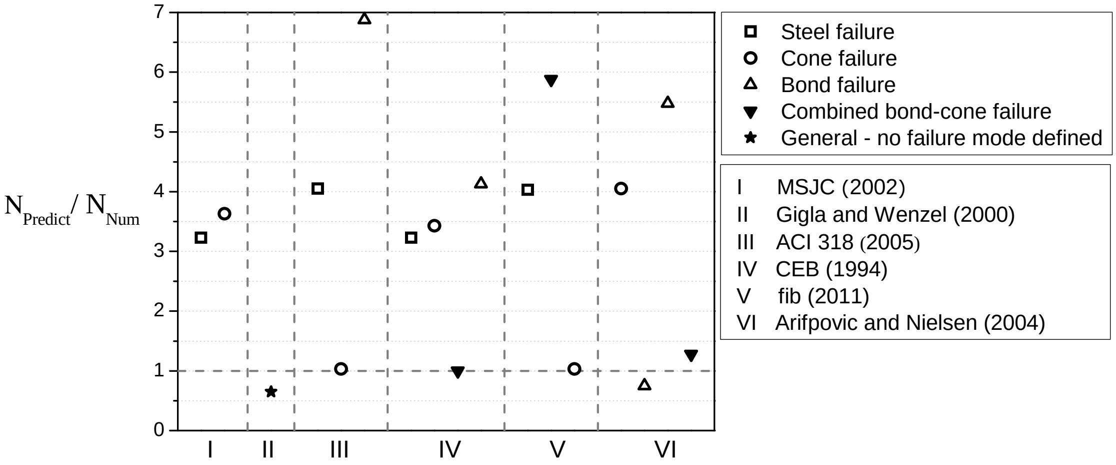

Figure 4.53 Comparison between the analytical expressions and the parametric analysis of the anchors spacing.

The graphical distribution of the analytical and numerical relations of these analysis (see Figure 4.51, Figure 4.52 and Figure 4.53), show similar results in terms of the formulations that can best describe the behaviour of the anchoring system. In what concerns the analytical relations found for the anchor diameter parametric analysis (Figure 4.51), ACI 318 and fib formulations estimated precisely the strength capacity verified numerically. Arifpovic and Nielsen (2004) and Doerr and Klingner (1989) in CEB formulations seem to slightly overestimate the strength capacity since the expressions provided by these formulations for the combined bond-cone failure are very sensitive to the anchor diameter.

For the anchoring system with higher embedment depth (Figure 4.52), the analytical expressions in general tend to underestimate the strength capacity of the system, compared with the numerical results. Even though, ACI 318, CEB, fib and Arifpovic and Nielsen (2004) formulations give an approximate estimation of the strength capacity of the system.

For the system with increased spacing between the anchors (Figure 4.53), the analytical expressions provided relations very similar to the ones obtained for the reference model with a very close approximation from the ACI 318, CEB, fib formulations since in these the spacing between anchors is accurately taking into account. Since Arifpovic and Nielsen (2004) formulation does not considers the interaction between anchors, the analytical prediction by increasing the spacing among the anchors is not affected.

As verified in the analytical study for the reference model, MSJC gives very high strength values and Gigla and Wenzel (2000) provide rather conservative predictions in all the cases.

The application of the formulations considering anchoring systems with distinct characteristics, allowed to verify the formulations that best describe the strength capacity of anchoring systems in different conditions and to assess the sensitivity of the expressions to certain parameters.

4.6. FINAL CONSIDERATIONS

The structural seismic behaviour of masonry buildings depend in the efficiency of its connections. A possible strengthening solution to improve the seismic response of masonry-to-timber connections in masonry buildings was numerically assessed. The present study has proven the potential of numerical analyses when used as a complementary tool to experimental campaigns, allowing for a deeper characterization of the behaviour and for parametric analysis.

The numerical model, prepared in accordance with the experimental setup, was calibrated and validated against the available experimental results. Both the fixed and rotating crack formulations were applied and evaluated by comparing the numerical results with experiments. The rotating crack model (RCM) showed a better agreement regarding the post-peak behaviour, since the shear strength is updated after cracking along the complete analysis. Also the RCM damage pattern observed during the analysis was more compatible with the failure mode observed experimentally. RCM seems to be more suitable to simulate the post-peak response of numerical models when the behaviour is governed by shear. Furthermore, the numerical model described very precisely the force-displacement behaviour found in the experimental tests and also the failure mechanism behaviour.

The parametric analysis carried out on the calibrated model considered mechanical parameters of masonry, wall pre-compression level and geometrical conditions in the anchoring system. In what concerns the masonry mechanical parameters, the analysis showed that the compressive strength and tensile parameters influence the capacity and the non-linear behaviour of the system in a moderate way. The pre-compression level proved to be a parameter that influences the behaviour of the system, as expected. Considering the geometric parameters under study, the behaviour of the anchoring system was greatly influenced by the anchor embedment depth, increasing the capacity to the double although a less ductile behaviour was observed. The study of the influence of the anchor dimensions in the response of the system proved that an increase in the steel diameter (from 16mm to 32mm) did not provide significant enhancement in the system capacity. By increasing the spacing between anchors, to 1.5 times the initial value, a slight increase in the ultimate capacity was verified and the damage distribution showed a more perceptible cone formation between anchors, proving that the tensile capacity of an anchor is affected by the overlapping of adjacent anchors. Parametric analyses revealed the potential of the proposed model, assessing and describing the behaviour of the anchoring system in distinct conditions, giving a valuable contribution in the understanding of injected anchors in masonry behaviour.

The prediction of the anchor capacity injected in masonry walls by means of complex numerical methods became essential for a comprehensive understanding of the system behaviour.

Available analytical formulations for the evaluation of the anchor strength were discussed and applied. A brief review of these simplified expressions is provided in this Chapter and applied in the anchoring system under study. A good agreement between experiments and the failure mode predicted by all the models was attained. In terms of strength capacity, a very good agreement was obtained with the ACI 318 (2011), fib Bulletin No. 58 (2011) and CEB (1994) formulations. On the other hand, the method proposed by MSJC (2013) seems to greatly overestimate the values of the strength capacity. The analytical expressions provided by Arifpovic and Nielsen (2004) estimated with acceptable approximation the strength capacity of the anchors, implying a careful analysis of the failure modes applicable to each case.

Chapter 5

MASONRY BUILDING:
CASE OF STUDY

5.1. INTRODUCTION

In the previous Chapters the study of the behaviour of walls and connections in masonry constructions have proven the potential of numerical analyses when used as a complementary tool for experimental campaigns. The analyses allow deeper characterization of the behaviour and parametrical analysis. The knowledge obtained from these research works are now the basis for the study of a typical masonry building, considering the in-plane behaviour of walls and the effect of the connections.

In this chapter the focus is on the influence of the connections in the global response of the structure. Initially, the description of the building selected for the study is provided. This is a three storey building located in Lisbon, Portugal, constituted by masonry walls and timber floors. Typical masonry constructions generally present poor connections between walls and floors, usually consisting of timber joists supported in the masonry wall. For this reason, the building was studied considering three different structural conditions:

- Assuming that the connections between structural elements are insufficient, the structural response was evaluated by considering only the exterior walls behaviour;
- By strengthening the wall-to-wall connections, making it effective, the building response was studied considering the external and interior walls behaviour;
- By both strengthening wall-to-wall and wall-to-floor connections, the global response of the building is studied.

The design of strengthening solutions for wall-to-wall and wall-to-floor connections is conducted with a simple design tool based on the simplified kinematic approach. The safety verification of the out-of-plane collapse of the façade wall in the case of inefficient connections between elements is also addressed.

The influence of the connections between walls and floors and also the external and interior walls in the global behaviour of the structure is assessed numerically. Finite element models considering the conditions exposed above were constructed. Pushover analysis proportional to the mass were used to assess the seismic response of the building. The usage of numerical simulations to evaluate the behaviour of masonry buildings and assess the efficiency of strengthening solutions is a common procedure. An example is the work described in Cardoso et al. (2005) and Bento et al. (2005) for the study of a Portuguese typical masonry building, evaluating the influence of the connections in the global behaviour and assessing numerically three different strengthening solutions.

The implementation of a simplified procedure to evaluate the building strength in a given direction, based on the individual response of structural components, is also addressed. In this section the analytical expressions discussed in Chapter 3, section 3.7 were the basis to compute the in-plane strength of the walls.

5.2. DESCRIPTION OF THE CASE OF STUDY

Aiming at studying a typical masonry construction, a case study presented by Lamego (2014) of a characteristic building of Lisbon was handpicked. This selection was premised on not only the study of a representative masonry building, but also the possibility of comparing the results from this study with the results provided by simplified approaches carried by Lamego (2014).

The building is located in the Fernando Caldeira Street, Alvalade neighbourhood in Lisbon and is inserted in a set of 302 buildings called as “economical houses”. Almost all of these buildings present similar characteristics, all yellow or pink, with simple and functional architecture (see Figure 5.1). The construction of these buildings started in December of 1946 and ended in September of 1948. Alvalade quarter was planned 70 years ago, establishing harmony between housing and functional facilities.

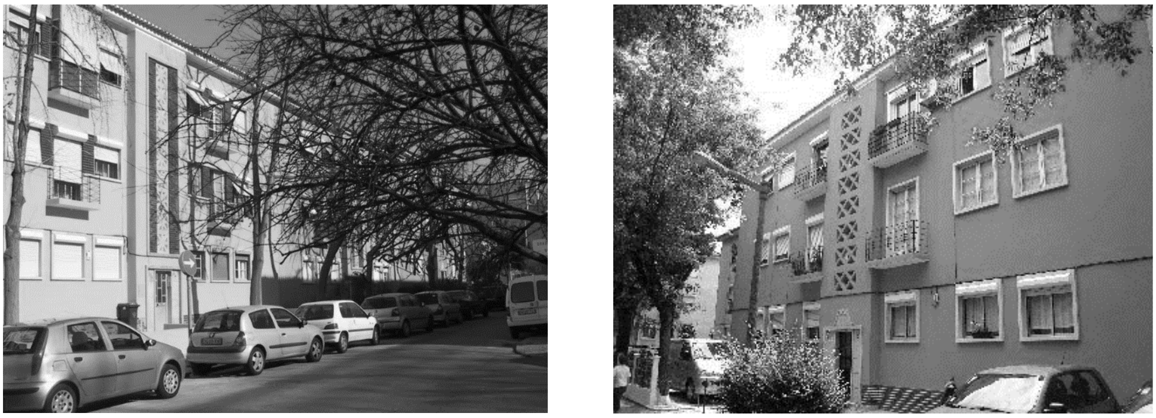
(a) (b)

Figure 5.1 Typical masonry buildings in Alvalade neighbourhood, Lisbon.

The buildings have three floors and two apartments per floor with a total area per floor of 145 m^2. Figure 5.2 shows the main façades of the building with the presence of a few window openings, contrasting with the lateral façades that do not have any openings. Each apartment has an area of 58.7 m^2 distributed by one living room, three bedrooms, a bathroom and a kitchen (see Figure 5.3 and Figure 5.4). The building is very regular with 19.2 m long, 8.2 m wide and 11.5 m of height to the top of the roof and is symmetric in one of the directions.

This building was constructed following the typical organization of most Portuguese traditional buildings composed of load-bearing masonry walls arranged in orthogonal planes, with relatively flexible floor diaphragms. The exterior walls and the walls limiting the stairs in the central part of the building are made of limestone masonry. Solid brick masonry is used for the walls with division purposes in the interior of the building (identified in Figure 5.3 and Figure 5.4). Exterior walls have 0.50 m thick and the interior partition walls have thickness with 0.25 and 0.15 m. The floor diaphragms are flexible, composed by pine wooden joists, typically placed perpendicular to the façade walls and braced by smaller ones that prevent the transverse deformation of the main joists. The roofs are built with timber trusses clad with ceramic tiles type “Lusa”. The floor joists dimension and disposition is unknown, so pine wood joists of 0.18x0.08 m^2 spaced 0.40 m were defined to compose the floor structure. The material properties of the building were defined by

Lamego (2014) according to Table 5.1, where *E* is the elastic modulus, γ is the density and f_c is the compressive strength.

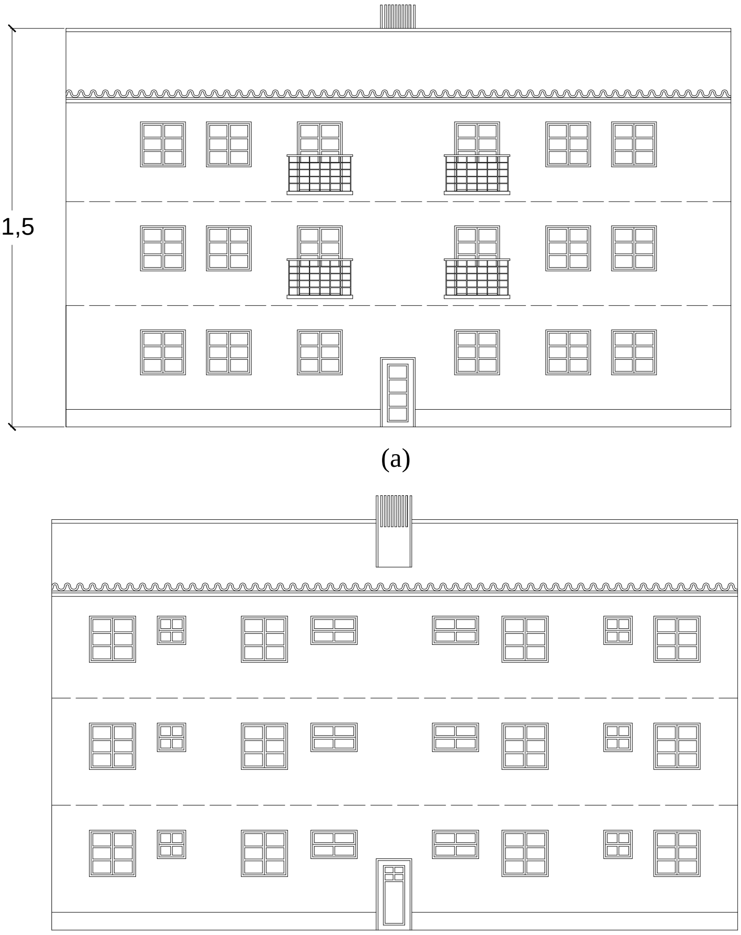

(a)

(b)

Figure 5.2 Elevation of the building: (a) Front elevation; (b) Rear elevation (Lamego 2014).

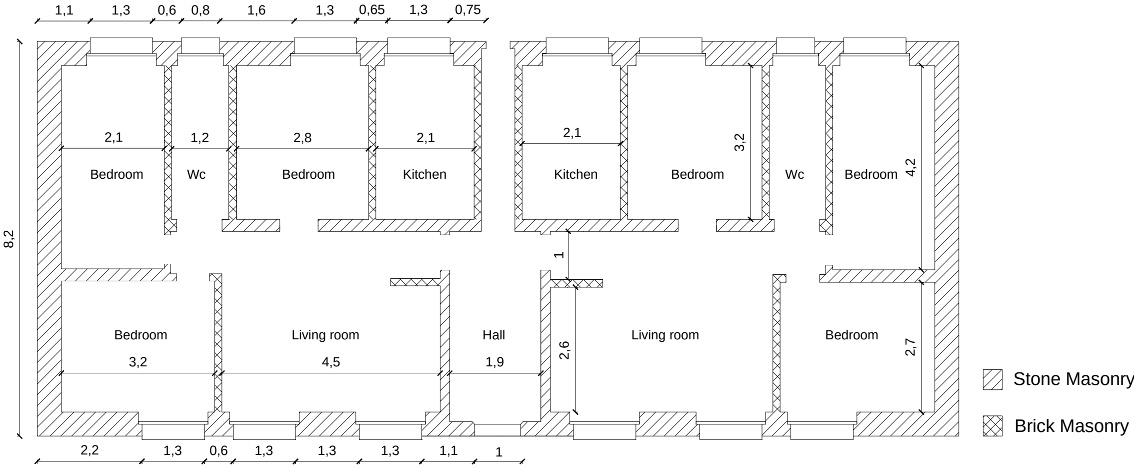
1,1
1,3
0,6
0,8
1,6
1,3
0,65
1,3
0,75
8,2
2,1
Bedroom
1,2
Wc
2,8
Bedroom
2,1
Kitchen
2,1
Kitchen
Bedroom
3,2
Wc
Bedroom
4,2
1
Bedroom
3,2
Living room
4,5
Hall
1,9
2,6
Living room
Bedroom
2,7
2,2
1,3
0,6
1,3
1,3
1,3
1,1
1
Stone Masonry
Brick Masonry

Figure 5.3 Plan of the ground floor (Lamego 2014).

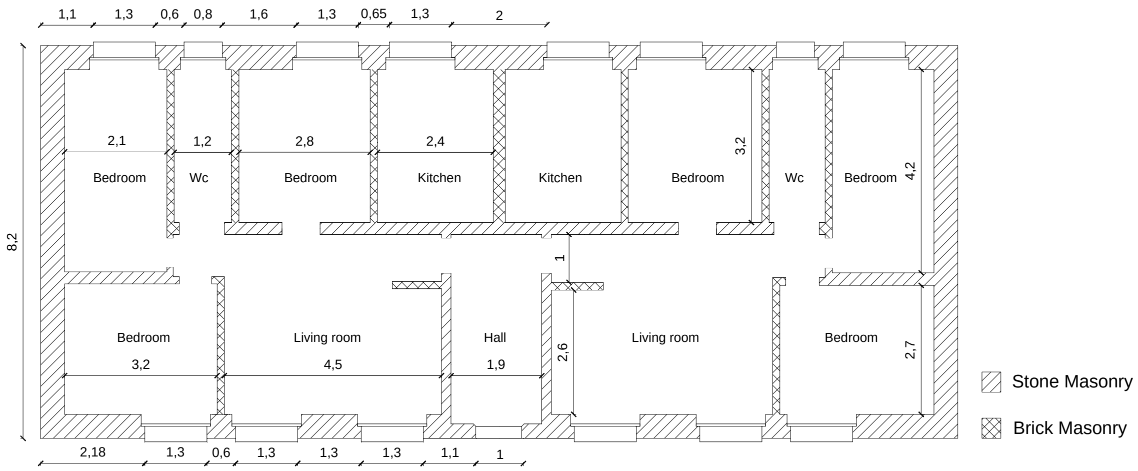

Figure 5.4 Plan of the first and second floors (Lamego 2014).

Table 5.1 Material properties (Lamego 2014).

	E [MPa]	γ [kN/m^3]	f_c [MPa]
Limestone Masonry	1035	19	0.9
Solid brick Masonry	2400	18	2.8
Pine Wood	11500	6	-

5.3. STRENGTHENING SOLUTION/INTERVENTION

As previously addressed, the seismic performance of a typical masonry building is highly dependent on its capability to redistribute the horizontal loads through all the structural elements. Given this, the efficiency of the connections becomes essential to ensure the proper load transmission between elements. Typical masonry buildings are commonly characterized by the lack of effective connections between structural elements.

Wall-to-wall and wall-to-floor connections play a major role in the seismic behaviour of the global structure. For this reason, in this section, assuming that the connections between walls are no longer effective, strengthening solutions to improve the connections above mentioned are presented and designed for the building under study. The selected solutions to strengthen both wall-to-wall and wall-to-floor connections include the introduction of injected anchors in masonry walls and were designed according to the study addressed in Chapter 4.

The design procedure performed is based on the limit equilibrium analysis following the principle of the virtual work. This procedure, with reference to local mechanisms, is developed through the selection of the collapse mechanism and the evaluation of the horizontal forces that activate this kinematic mechanism (OPCM 3431 2005). The safety verification is performed according to OPCM 3431 (2005).

In the absence of effective connections to interior walls and floors, the out-of-plane overturn of the façade walls is the most likely collapse mode. The definition of the kinematic mechanism of the façade wall is represented in Figure 5.5. The wall is supposed infinitely rigid, therefore the horizontal forces are proportional to the masses (inertial forces). The loads considered acting on the rigid bodies composing the kinematic mechanism were the self-weight (W_i), the vertical loads acting at the floor levels (P_i), a system of horizontal loads proportional to the masses (αP_i and αW_i) and distributed horizontal forces which represent the forces to be carried by the strengthening wall-to-wall anchoring system (T_i), not shown in the figure. The horizontal coefficient (α) is the seismic mass multiplier that triggers the mechanism.

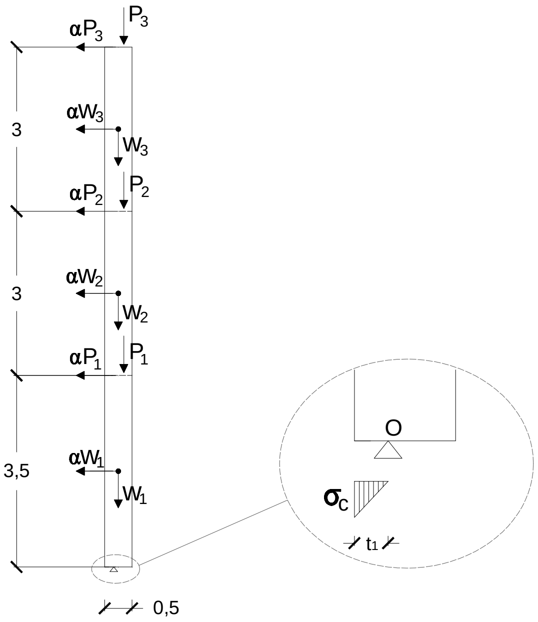

Figure 5.5 Kinematic mechanism concerning the out-of-plane overturn of the façade wall.

With respect to the kinematic mechanism, Table 5.2 displays the loads acting in the rigid bodies. A wall strip 1 m wide is considered. The self-weight of the stone masonry walls is computed for the three floor levels considering the respective openings (W_1, W_2 and W_3). The loads at the floor levels (P_1 and P_2) include the floor structure weight plus the overload according to the seismic combination. The load at the roof level (P_3) comprises the roof weight, timber trusses, ceramic tiles and other coatings (typical values were taken from Brazão Farinha and Correia do Reis (1993) recommendations).

Table 5.2 Loads of the kinematic mechanism in [KN/per 1 meter wall].

W_1	W_2	W_3	P_1	P_2	P_3
28.7	23.4	23.4	3.5	3.5	3.9

5.3.1. Safety Requirements

According to OPCM 3431 (2005) the safety of each mechanism is verified in the linear simplified kinematic approach for ultimate limit state, if the spectral acceleration that activates the failure mechanism ($a^*{}_0$) is greater than the acceleration of the elastic spectrum, adequately amplified to consider the relative height of the portion of the structure involved in the mechanism (equation (5.1).

$$a^{*}{}_{0} \geq \frac{a_g\, S}{q}\left(1 + 1.5\frac{Z}{H}\right) \tag{5.1}$$

where, q is the structure factor assumed equivalent to 2, a_g is the ground acceleration, S is the soil factor, Z is the height of the centre of the masses that generate horizontal forces on the elements of the kinematic mechanism and which are not efficiently transmitted to the other parts of the building and H is the height of the whole structure.

According to the National Annex of EC8 (2003), the ground acceleration for Lisbon is equal to 0.17 g for near-field earthquake (type 1), which is the most demanding. The soil factor (S) for this building was considered type B, in agreement with the geological map of Lisbon, as referred in Lamego (2014). The corrections to this factor proposed by the national annex (EC8-1 2010) were also considered according to equation (5.2), resulting in a value of S equal to 1.27, considering $S_{máx}$ =1.35.

$$S = S_{máx} - \frac{S_{máx} - 1}{3}(a_g - 1) \qquad \text{if} \qquad 1\,m/s^2 < a_g < 4\,m/s^2 \tag{5.2}$$

The height of the centre of the masses (Z) was computed resulting in a height of 4.93 meters, being the total height of the structure (H) 11.5 meters. The spectral acceleration ($a^{*}{}_{0}$) for the activation of the mechanism is computed by the equation (5.3), where F_i is the generic weight force, M* is the participant mass (given by equation (5.4)), g is the gravitational acceleration and e* is the fraction of the mass participant in the kinematism (equation (5.5)).

$$a^{*}{}_{0} = \frac{\alpha\ \sum_{i=1}^{n} F_i}{M^{*}} = \frac{\alpha\ g}{e^{*}} \tag{5.3}$$

$$M^{*} = \frac{\left(\sum_{i=1}^{n} F_i\ \delta_{x,i}\right)^2}{g \sum_{i=1}^{n} F_i\ \delta^2{}_{x,i}} \tag{5.4}$$

$$e^{*} = \frac{g\ M^{*}}{\sum_{i=1}^{n} F_i} \tag{5.5}$$

The participant mass is obtained through the application of equation (5.4), being $\delta_{x,i}$ the virtual horizontal displacement in a control displacement point. Table 5.3 summarizes the calculation procedure for M*. The fraction of the mass participant (e*) in the mechanism is computed using equation (5.5), considering M*=6.82 as previously calculated, and a value of 0.78 was achieved.

Table 5.3 Calculation of the participant mass M*.

	F_i	$\delta_{x,i}$	$\sum_{i=1}^{n} F_i\ \delta_{x,i}$	$\sum_{i=1}^{n} F_i\ \delta^2{}_{x,i}$	
P_1	3.5	0.37	1.3	0.47	
P_2	3.5	0.68	2.4	1.62	
P_3	3.9	1.00	3.9	3.87	
W_1	28.7	0.18	5.3	0.97	
W_2	23.4	0.53	12.3	6.47	
W_3	23.4	0.84	19. 7	16.57	**M***
		$\sum$	44.8	29.97	**6.82**

In this manner, the wall safety is verified if the relation given by equation (5.6) is satisfied, being α the horizontal coefficient that activates the mechanism. Computing this inequality, the load coefficient α that activates the mechanism has to be higher than 0.138 to meet the safety requirements (equation (5.7)).

$$\frac{\alpha}{0.78} \geq \frac{0.17 \cdot 1.27}{2}\left(1 + 1.5\frac{4.93}{11.5}\right) \qquad [g] \tag{5.6}$$

$$\alpha \geq 0.138 \text{ g} \tag{5.7}$$

5.3.2. Evaluation of the Wall Safety

In order to assess the need of the strengthening solution, the safety of the mechanism was evaluated. The load multiplier α was calculated through the principle of virtual work by the simple rotation equilibrium of the horizontal and vertical forces around to the hinge O (Figure 5.5). The position of the hinge (distance t_1) is given by limiting the maximum stress on the most compressed edge to 1 MPa, considering the limestone masonry compressive properties (calculated through equation (5.8)).

$$\frac{\sigma_c \times t_1}{2} = W_1 + W_2 + W_3 + P_1 + P_2 + P_3 \quad \Leftrightarrow \; t_1 = \frac{2(W_1 + W_2 + W_3 + P_1 + P_2 + P_3)}{\sigma_c} \tag{5.8}$$

Thus, the rigid body stability is assured by the equilibrium of vertical and horizontal forces around O with a distance (t_1) of 0.17 meters, as given by equation (5.9). A load coefficient (α) of 0.018 was attained. Thus, the inequality granted by equation (5.7), related to the safety requirements, is not verified for the wall without the strengthening system. The capacity parameter is below the demand parameter: 0.018g ≤ 0.138g. This proves the need to design strengthening solutions to avoid the out-of-plane collapse of the wall.

$$\begin{gathered} W_1(0.25 - t_1) + W_2(0.25 - t_1) + W_3(0.25 - t_1) + P_1(0.35 - t_1) + P_2(0.35 - t_1) + P_3(0.35 - t_1) \\ - \alpha(W_1 \cdot 1.75 + W_2 \cdot 5 + W_3 \cdot 8 + P_1 \cdot 3.5 + P_2 \cdot 6.5 + P_3 \cdot 9.5) = 0 \end{gathered} \tag{5.9}$$

5.3.3. Wall-to-wall Connections

A possible strengthening solution to improve the performance of wall-to-wall connections is presented in Chapter 2, section 2.4 (lustrated in Figure 2.13) and studied in Chapter 4. It consists on parallel anchors introduced in the bearing wall and connected to the perpendicular wall by means of steel plates. A scheme of the considered strengthening solution is provided in Figure 5.6. As referred, the stone masonry bearing wall is 0.50 m thick and the anchor embedment depth was considered with 0.35 m. The anchors embedment depth was chosen according to the wall thickness and also taking into consideration the testing conditions studied in the previous Chapter. The perpendicular interior walls of the building, most of them made of brick masonry, present a thickness varying from 0.15 to 0.25 m. Since the spacing between anchors is dependent on the wall thickness (as clearly demonstrated in Figure 5.6), the design procedure will be carried out in function of the worst case scenario, associated with the smallest spacing between anchors (according to the parametric analysis performed in the previous Chapter).

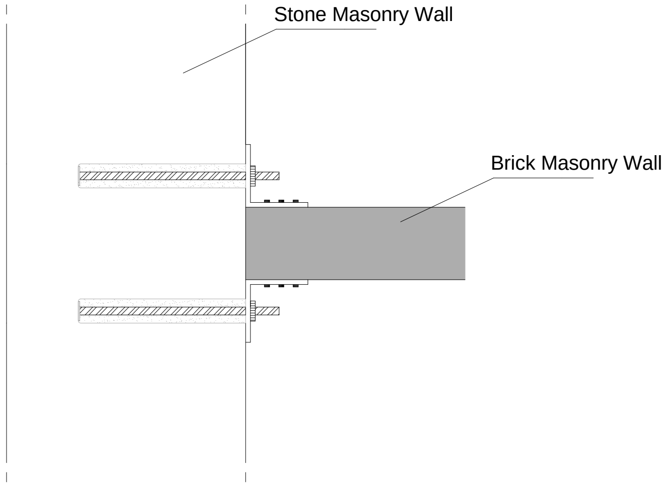

Figure 5.6 Wall-to-wall strengthening solution (plan view).

To design the wall-to-wall strengthening solution, the simplified kinematic approach proposed by OPCM 3431 (2005) is followed. The hypothesized kinematic mechanism of the wall façade, including the forces to be carried by the strengthening solution, is represented in Figure 5.7. The forces acting in the wall were defined in Table 5.2. The distributed horizontal load at each floor level (T_1, T_2 and T_3), with respect to the strengthening system to be designed, is calculated through the principle of the virtual work assuring the equilibrium of the wall.

In order to meet the safety requirements, the load coefficient α that triggers the mechanism has to be greater than 0.138 (as defined in section 5.3.1). For this reason, this value is on the basis of the design of the anchoring system.

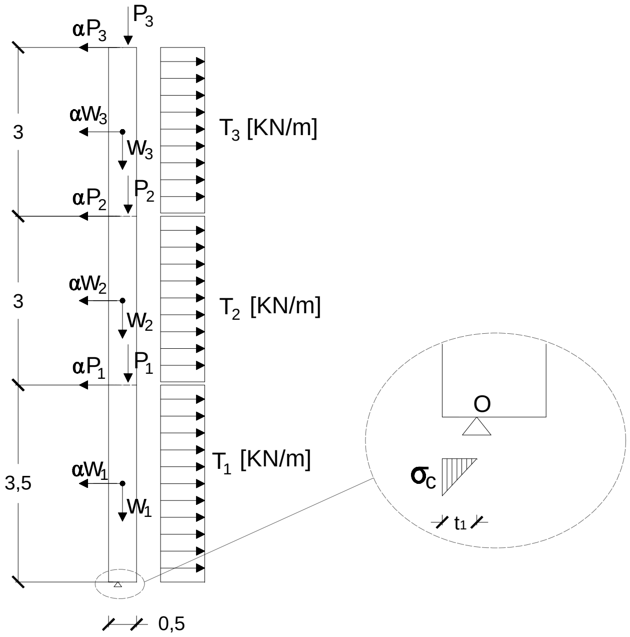

Figure 5.7 Kinematic mechanism concerning the out-of-plane overturn of the façade wall with the consideration of the wall-to-wall strengthening system.

The calculation of the tensile stresses to be carried by the strengthening system of the second floor (T_3), is carried out considering the equilibrium of the upper part of the wall, as displayed in Figure

5.8. The position of hinge A is determined, once again, by limiting the maximum stress at the compressive edge to 1 MPa, computed by equation (5.10) resulting in a distance of 0.054 m.

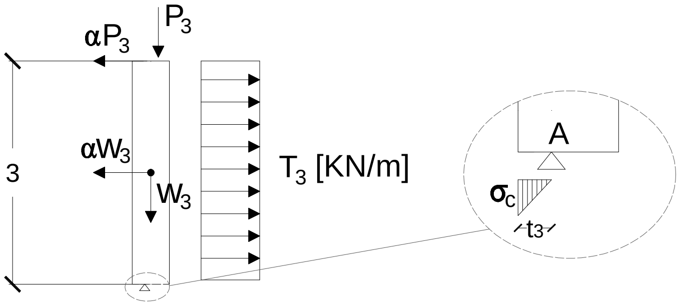

Figure 5.8 Equilibrium of the upper part of the wall used for the calculation of T_3.

$$t_3 = \frac{2(W_3+P_3)}{\sigma_c} \tag{5.10}$$

The equilibrium of the rigid body is given by equation (5.11):

$$W_3(0.25 - t_3) + P_3(0.35 - t_3) + T_3 \times 3 \times 1.5 - \alpha(W_3 \times 1.5 + P_3 \times 3) = 0 \tag{5.11}$$

Considering α equal to 0.138 (in order to satisfy the safety requirements), the distributed force T_3 is determined through this equation, resulting in 0.16 kN/m for 1 meter wide. A wall band 6 meters wide is considered taking into account the worst case scenario of the interior walls distribution in the building, reaching a total of 3 kN for each wall-to-wall connection.

The wall-to-wall strengthening solution includes the introduction of an anchoring system in the masonry wall. According to the parametrical analysis carried out on the previous Chapter and considering the stone masonry mechanical properties, the strength capacity of the anchoring system can be set in 65 kN (T). This capacity is reduced to around 22 kN, by the application of a safety factor of γ=3.0 (T / γ). Comparing the strength capacity of the anchoring system (22 kN) with the horizontal force required to fulfil the safety requirements (3 kN), it is obvious that one anchoring system in each wall-to-wall connection is enough to assure the safety of the building. The following calculations will be carried out according to the design of the strengthening solution at this level, this means with a force of 22kN in each wall-to wall connection (1.2 kN/m per 1 meter wide).

The determination of T_2 force is carried out following a similar procedure, considering the equilibrium of the rigid body presented in Figure 5.9. Firstly, the distance t_2 is calculated by limiting the compressive stress (t_2 = 0.11 m). Then, the principle of virtual works is used to determine the force T_2. Since the parameter α is known (0.138) and the force T_3 was already defined (0.95 kN/m per 1 meter wide), the equilibrium around the hinge B gives the force T_2 (equation (5.12)):

$$\begin{aligned} &W_2(0.25 - t_2) + W_3(0.25 - t_2) + P_2(0.35 - t_2) + P_3(0.35 - t_2) + T_2 \times 3 \times 1.5 + T_3 \times 3 \\ &\times 4.5 - \alpha(W_2 \times 1.5 + W_3 \times 4.5 + P_2 \times 3 + P_3 \times 6) = 0 \end{aligned} \tag{5.12}$$

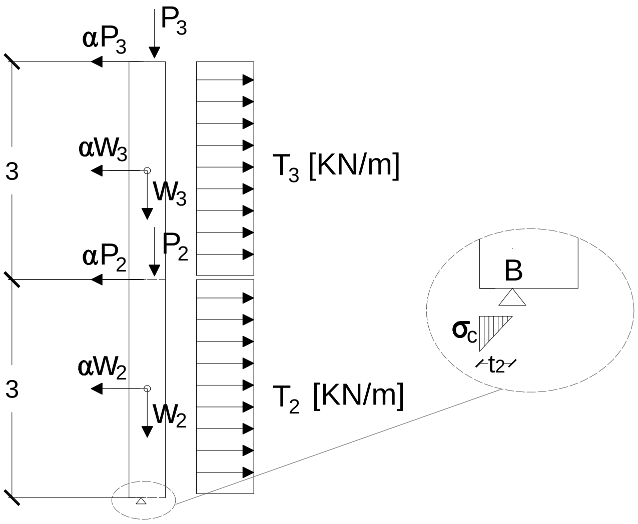

Figure 5.9 Equilibrium of the upper part of the wall used for the calculation of T_2.

By computing the equilibrium equation (5.12), it was verified that the force T_2 is not necessary to guarantee the stability of the system. This means that the anchoring system introduced in the upper wall-to-wall connections is sufficient to assure the safety verifications. Nonetheless, in order to guarantee that the seismic forces are transmitted through all the elements, the installation of an anchoring system for the wall-to-wall connections at this level (first floor) is also proposed. In the same manner, the equilibrium of the whole wall was assessed resorting to the kinematic mechanism presented in Figure 5.7. At ground level the wall safety is assured by the strength capacity of one anchoring system (22 kN), since the equilibrium of the three floor resulted in T_1 equal to 0.88 kN/m, around 16 kN for a wall band of 6 meters.

Thus, the design of the strengthening solution for wall-to-wall connections through the kinematic approach proved that one anchoring system placed in each connection between perpendicular walls is enough to guarantee the safety verifications (as represented in Figure 5.10). The anchoring system is placed at half height of the wall.

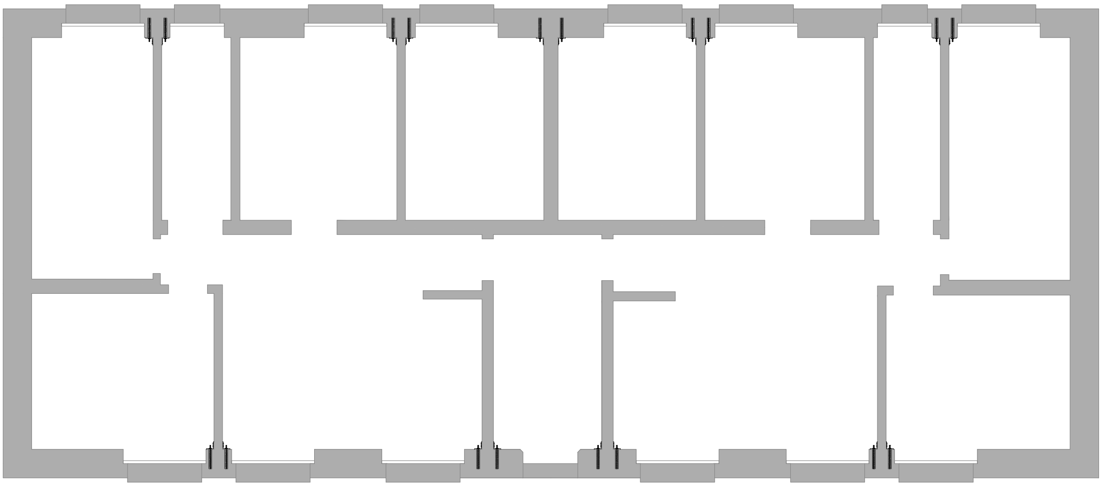

Figure 5.10 Schematic representation of the wall-to-wall strengthening solution in each floor level.

5.3.4. Wall-to-floor Connections

The wall-to-floor connections efficiency is assured by the strengthening solution presented in Figure 5.11, which includes the introduction of two parallel anchors in the masonry wall, as in the previous solution. The anchors inserted in the masonry wall are connected to the timber floor through steel angles. The numerical study performed in injected anchors in masonry (Chapter 4) is once again used as basis for the design of this strengthening solution. The adopted spacing between anchors was 28 cm, as the system experimentally/numerically studied.

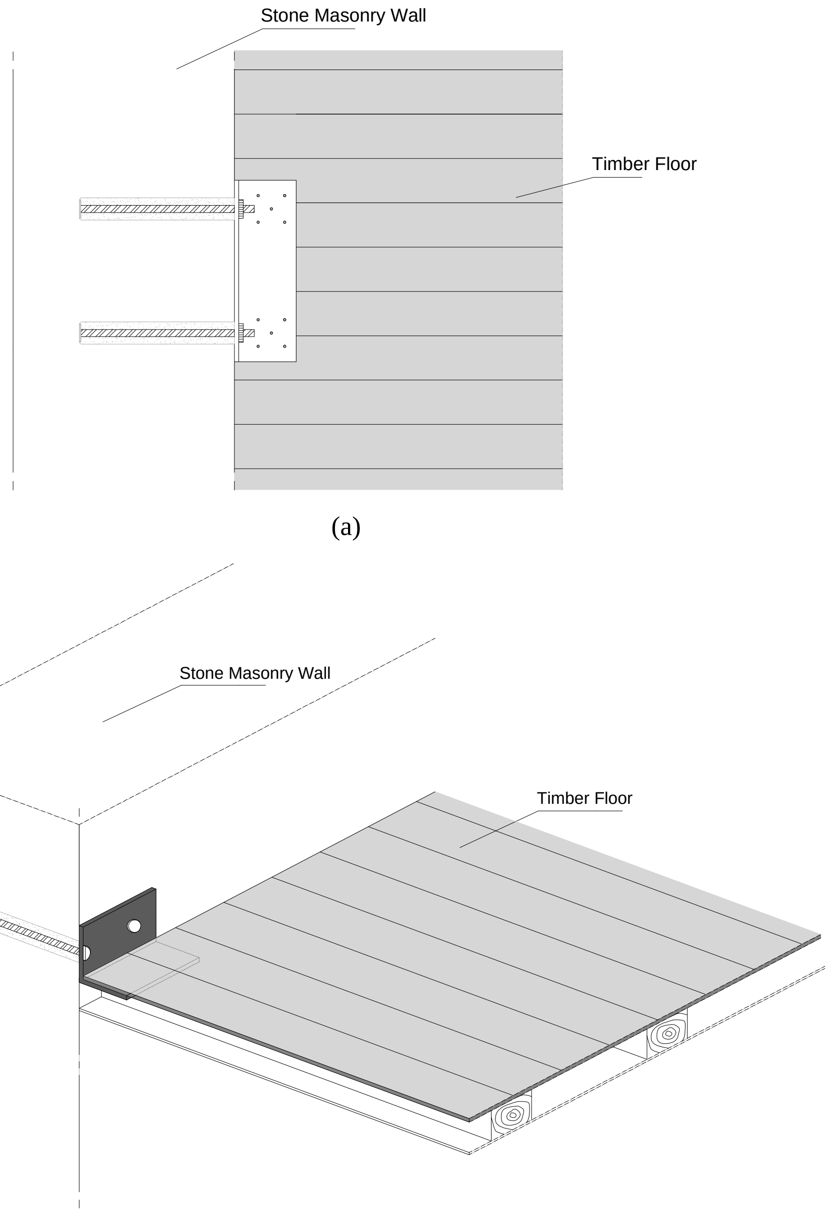

(a)

(b)

Figure 5.11 Wall-to-floor strengthening solution: (a) Plan view; (b) Perspective.

The procedure previously described for the design of the strengthening solution of wall-to-wall connections is followed here and for this reason a brief explanation is given. The kinematic mechanism, with the inclusion of the forces to be carried by the anchoring system at the floors levels (T_i), is defined in Figure 5.12. A wall band 1 meter wide is considered. The safety of the wall is verified if the load coefficient α is higher than 0.138, as demonstrated in section 5.3.1.

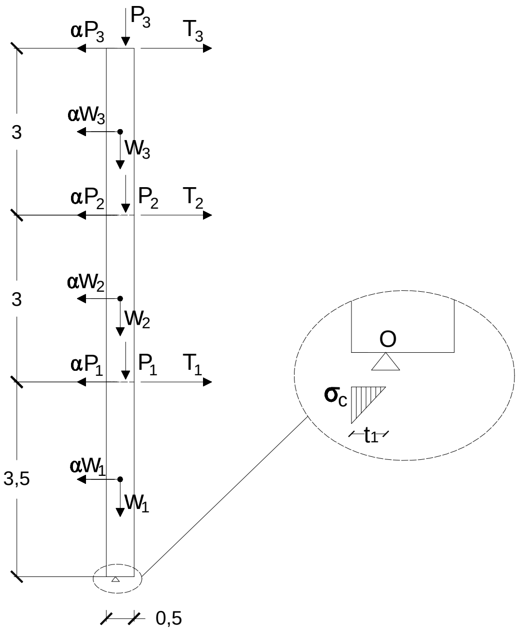

Figure 5.12 Kinematic mechanism concerning the out-of-plane overturn of the façade wall with the consideration of the wall-to-floor strengthening system.

To estimate the force to be carried by the strengthening system (T_1, T_2 and T_3), the equilibrium of the wall in the three levels is assured. Firstly, the tension in T_3 is determined by the rotation equilibrium around the hinge A of the upper level of the wall (see Figure 5.13a). The hinge position is calculated by limiting the compressive stress, computed by equation (5.10), and the forces acting in the wall were already defined (see Table 5.2). Accordingly, the force T_3 calculated for 1 meter of wall is 0.25 kN. Considering the total width of the wall, a force of around 5 kN, is required for the top wall equilibrium. The capacity of the anchoring system to be used in this building, already reduced by the safety factor (γ=3.0), is 22 kN. Since the capacity of the strengthening system is significantly higher than the demand force, one anchoring system is proposed for this level.

Similarly, the tension in T_2 is determined by computing the rotation equilibrium of the two top floors around hinge B with t_2= 0.11 m (see Figure 5.13b). The tension T_2 resulted in 2.9 kN per 1 meter of wall, which means 56 kN for the total wall width. To meet the safety requirements, the installation of three anchoring systems in wall-to-floor connections along the wall width are recommended. Finally, the tension T_1 applied at the first floor level is calculated considering the designed solutions of the top floors connections (T_2 and T_3). The equilibrium around hinge O, positioned at 0.18 m from the edge, gives a tension for T_1 of 112 kN. This means that six anchoring systems are necessary at this level to guarantee the safety requirements.

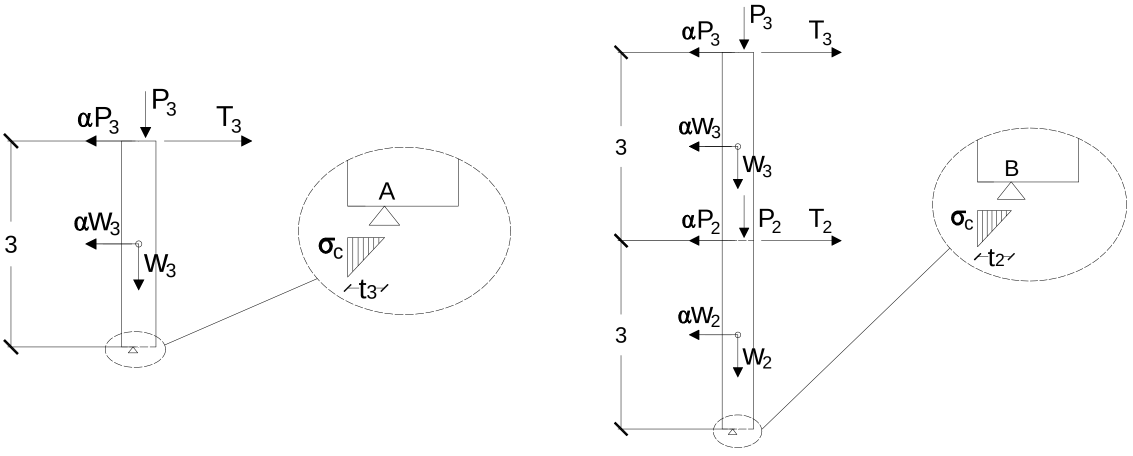

(a) (b)

Figure 5.13 Equilibrium mechanisms: (a) Upper part of the wall for the calculation of T_3; (b) Two upper floors of the wall for the calculation of T_2.

Summarizing, the design of the strengthening solution to wall-to-floor connections revealed that one anchoring system is required at the top floor diaphragm, three at the second floor level and five at the first floor level. However, for practical and aesthetics purposes, three anchoring systems at each level have been adopted (spaced 4.8 m from each other), see Figure 5.14. The equilibrium of each level was recalculated based on this new arrangement proving the wall safety.

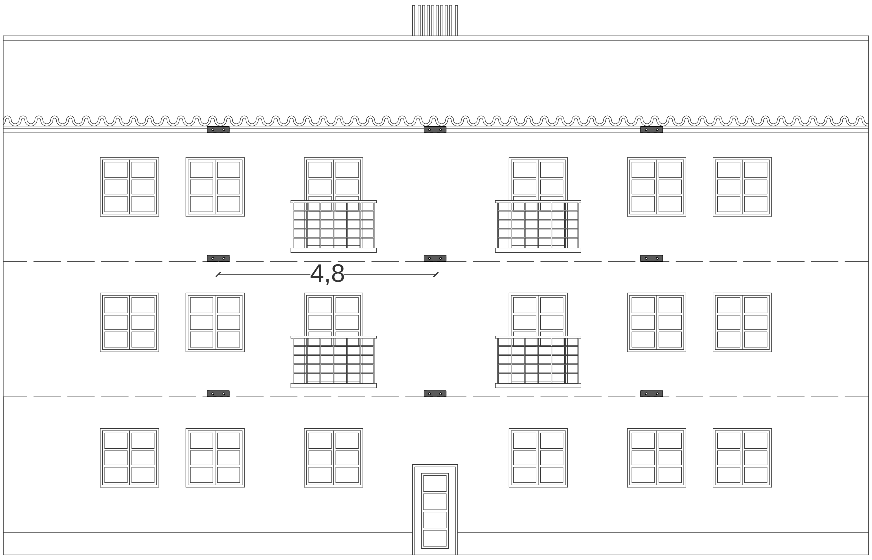

Figure 5.14 Schematic representation of the wall-to-floor strengthening solution.

5.4. NUMERICAL STUDY

The numerical characterization of the seismic behaviour of the building comprises the study of the structure using three numerical models. Firstly, only the contribution of the external walls is considered (assuming that the connections between structural elements are inefficient), named Model 1; then the contribution of the external and interior walls is studied (assuming the efficient application of the strengthening solution for wall-to-wall connections, designed in the previous Chapter), named Model 2; and at last the global behaviour of the structure is considered (considering also wall-to-floor efficient connections), named Model 3. Thus, three numerical models were prepared in order to fulfil these conditions. The configuration of the model attempts to reproduce the structural behaviour of the building, while adopting the necessary simplifications. The numerical model was prepared using the TNO DIANA (2009) software using the geometrical information gathered from Lamego (2014). Three-dimensional finite element models were constructed using shell elements to simulate the masonry walls. Eight-node quadrilateral isoparametric curved shell elements (CQ40S) were used to discretize the mesh (see Figure 5.15). These elements have quadratic interpolation and Gauss integration.

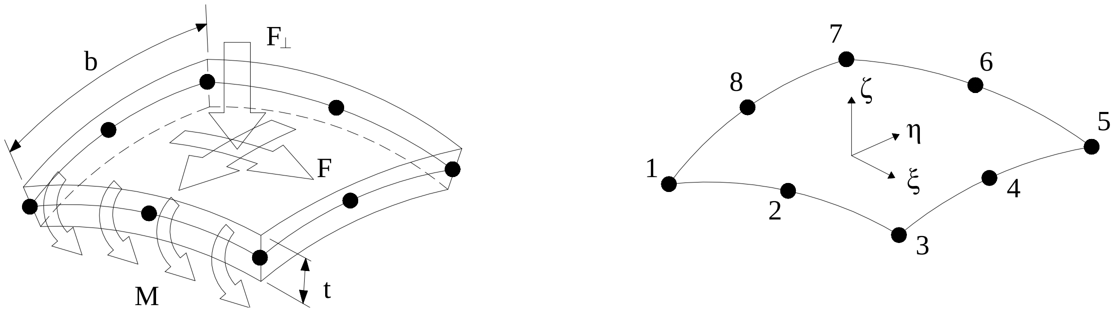

Figure 5.15 Curved shell element (CQ40S) (adapted from TNO DIANA (2009)).

Taking into account the conclusions provided by the study carried out in Chapter 4 related to the application of the FCM and RCM formulations, the total strain rotating crack model with rotating crack model with exponential stress-strain relationship in tension and parabolic in compression (as represented in Figure 3.7). The nonlinear material properties were defined according to Table 5.1, following the recommendations used in the previous Chapters. The stone and brick masonry were simulated considering a unique homogeneous isotropic material, as previously discussed. Stone and brick masonry behaviour were defined according to Table 5.4, in which f_c and G_c are the compressive strength and fracture energy, f_t and G_t are the tensile strength and fracture energy.

Table 5.4 Non-linear properties.

	γ [kN/m^3]	E [MPa]	f_c [MPa]	G_c [N/mm]	f_t [MPa]	G_t [MPa]
Stone Masonry	19	1035	0.9	1.44	0.1	0.02
Brick Masonry	18	2400	2.8	4.48	0.28	0.03

The seismic assessment of the building considering the conditions previously described is carried out considering this formulation. In the last decade, research community has recognized non-linear static procedures as effective tools for the prediction of seismic performance, avoiding complex, even if rigorous, non-linear time-history analyses (Parisi 2010). Pushover analysis is a non-linear static structural analysis method, commonly used for the seismic assessment of existing masonry buildings and has been introduced in many seismic codes, such as (EC8 2003) and (OPCM 3274 2003). Pushover analysis, which includes material nonlinear behaviour and consists on applying an incremental monotonic loading on the structure in order to determine its ability to resist to seismic actions, has been gaining significance over recent years as a tool for the assessment of masonry structures, e.g. (Modena et al. 2010) and (Antoniou and Pinho 2004).

As recommended in (Lourenço et al. 2011), a mass proportional pushover approach is carried out in the direction perpendicular to the façade walls (as represented in Figure 5.16). The solution procedures used the regular Newton-Raphson method and an energy convergence criterion, with a tolerance of 0.001.

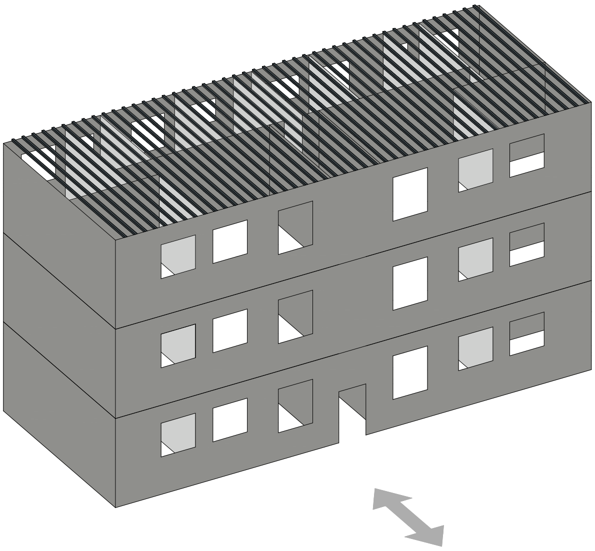

Figure 5.16 Global view of the building with the representation of the loading direction.

The connections between structural elements were not explicitly modelled, in the case of model 2 and 3, since it is considered that the lateral loads are efficiently transmitted through the elements. Instead, the elements were modelled perfectly connected among each other.

5.4.1. Model 1

As referred above, model 1 aims to study the seismic performance of the building in the case of ineffective connections between structural elements. For this reason, only exterior stone masonry walls were modelled. The mesh was automatically generated by DIANA and then manipulated and controlled in order to obtain a good quality mesh, resulting in 11.204 nodes and 3466 elements (Figure 5.17).

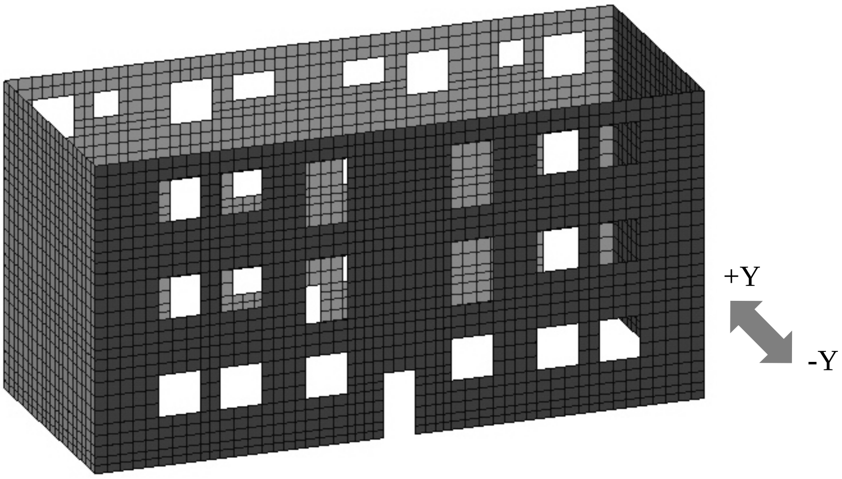

Figure 5.17 Mesh of the numerical Model 1.

Pushover analysis proportional to the mass were carried out for the positive and negative orientations of lateral forces, perpendicular to the façade walls (represented in Figure 5.17). The capacity curve for both directions, computed by the relation of the load factor (α) and the displacement at the top of the wall, is presented in Figure 5.18. The behaviour of the building until the first peak is independent on the load direction since +Y and –Y capacity curves present exactly the same response. After this point, the building response in –Y direction indicates an increase in the seismic coefficient until 0.056g, before exhibiting an abrupt loss of capacity. On the contrary, the response in +Y direction reveals a more ductile behaviour with high displacement capacity. Pushover analyses demonstrated that the maximum seismic capacity attained in –Y direction is 0.056g and 0.049g in +Y direction. The seismic factor attained numerically is greater than the value determined through the limit equilibrium of the out-of-plane collapse of the façade wall in section 5.3.2 (α=0.018g). The differences are related to the global response of the building due to the flange contributions of the in-plane lateral walls, considered in the numerical model, and also to the excessive reduction in the rotation line by using a triangular stress distribution in the base. The pushover analyses proved that the seismic capacity of the building does not fulfil the safety requirements expressed in section 5.3.1, further proving that strengthening measures should be implemented.

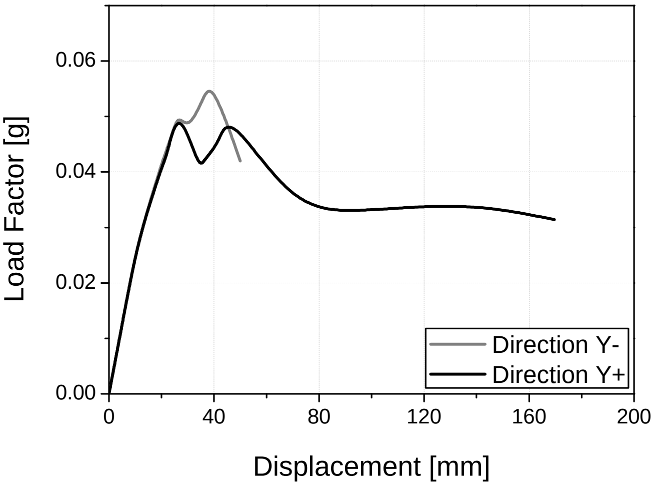

Figure 5.18 Capacity curves for Model 1.

Complementary to the analysis of the capacity curve of the structure, the evaluation of damage and collapse mechanisms are essential for the assessment of the seismic performance of this building. The maximum principal strains distribution is plotted as an indicator of damage, which, in addiction with the deformed shape, conveys the perception of the collapse mechanism. The evolution of damage resultant from the pushover analysis in +Y direction is presented in Figure 5.19. The damage distribution in the façade walls is widespread until the load capacity reaches the second peak, showing, however, more severe concentration of strains in the corners of some windows (Figure 5.19a). After the drop capacity, corresponding to 80mm of displacement, the damage distribution is more severe and the cracks are clearly defined (Figure 5.19b). Two symmetric diagonal cracks develop in the façade wall, starting from the top of the structure (following the window corner) and propagate towards the base corner. Severe vertical cracks are also visible between openings. At the final stage, the damage follows the same pattern and the collapse is associated to the diagonal cracks, causing the out-of-plane collapse of the central part of the wall (easily perceptible from the deformed shape shown in Figure 5.19c).

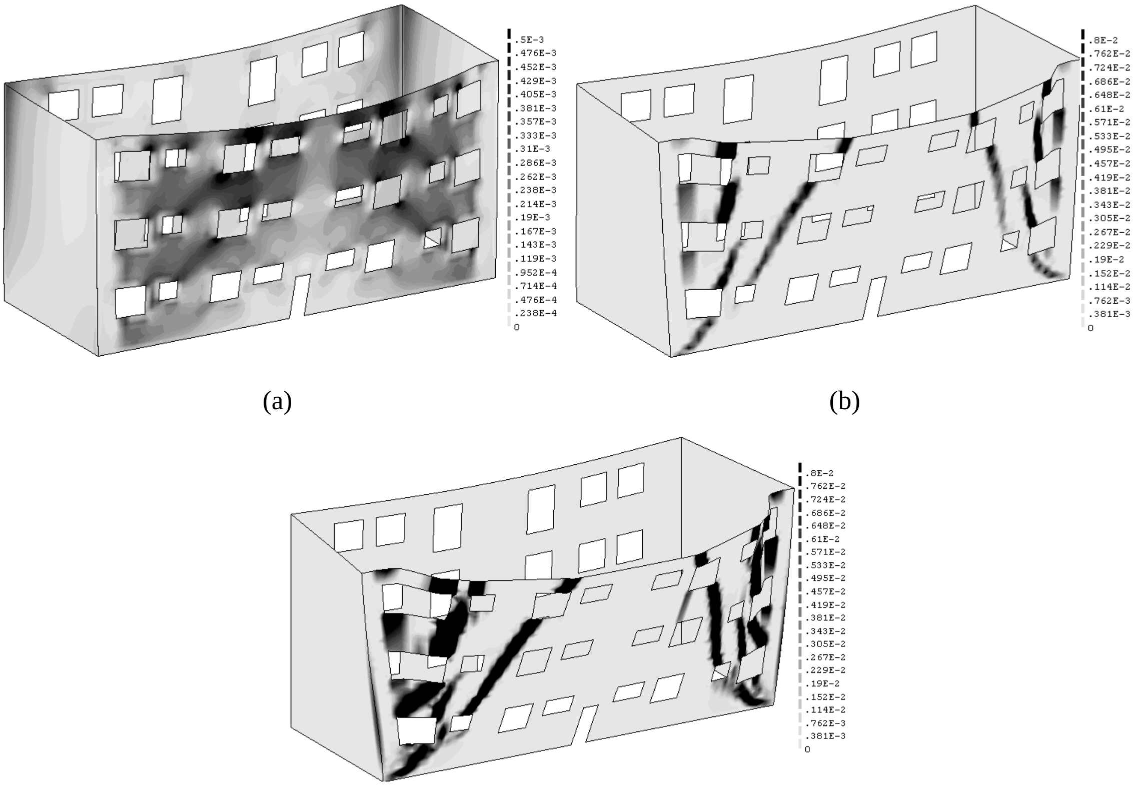
.5E-3
.476E-3
.452E-3
.429E-3
.405E-3
.381E-3
.357E-3
.333E-3
.31E-3
.286E-3
.262E-3
.238E-3
.214E-3
.19E-3
.167E-3
.143E-3
.119E-3
.952E-4
.714E-4
.476E-4
.238E-4
0
.8E-2
.762E-2
.724E-2
.686E-2
.648E-2
.61E-2
.571E-2
.533E-2
.495E-2
.457E-2
.419E-2
.381E-2
.343E-2
.305E-2
.267E-2
.229E-2
.19E-2
.152E-2
.114E-2
.762E-3
.381E-3
0

(a) (b)

(c)

Figure 5.19 Maximum principal strains distribution showing the damage evolution in +Y direction: (a) Second peak load; (b) Drop after the peak (80 mm); (c) Final stage.

The damage evolution resultant from the pushover analysis in –Y direction is depicted in Figure 5.20. The principal strains distribution presented in Figure 5.20a, referent to the first inflection point of the curve, show that the damage is concentrated in the central spandrels in the top floors and at the corners of the rear façade wall. Similar damage distribution was found for the peak load, although more severe (Figure 5.20b). The sudden decreased in the capacity verified in the pushover curve response is related to the loss of the horizontal stability of the building. The vertical cracks that form in the wall intersections, as represented in Figure 5.20c, indicates the out-of-plane collapse of the whole façade wall.

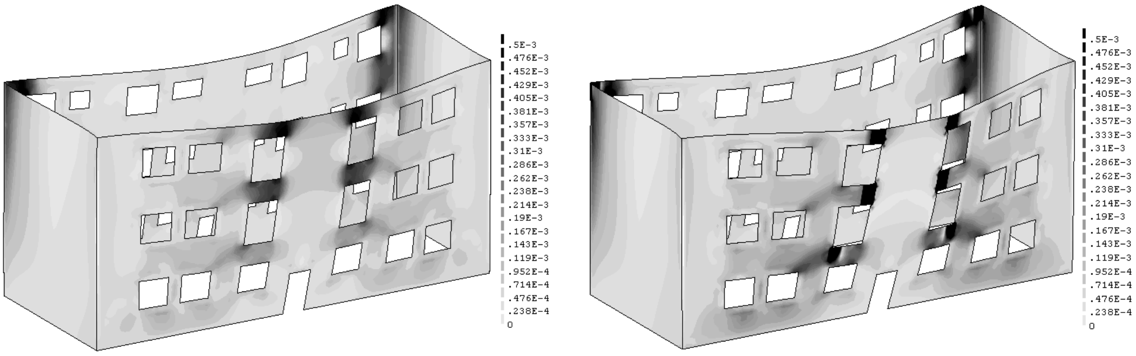
.5E-3
.476E-3
.452E-3
.429E-3
.405E-3
.381E-3
.357E-3
.333E-3
.31E-3
.286E-3
.262E-3
.238E-3
.214E-3
.19E-3
.167E-3
.143E-3
.119E-3
.952E-4
.714E-4
.476E-4
.238E-4
0

(a) (b)

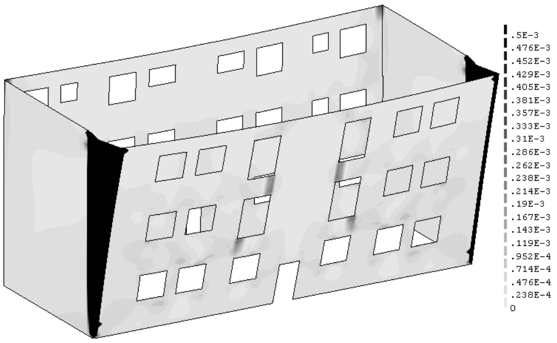

(c)

Figure 5.20 Maximum principal strains distribution showing the damage evolution in –Y direction: (a) Inflection point; (b) Peak load; (c) Final stage.

As proved by the numerical analyses, the collapse mechanisms expected for a building with deficient connections between elements are local with the collapse of parts of the façade or even the collapse of the whole façade.

5.4.2. Model 2

Model 2 aims at studying the seismic performance of the building considering effective connections among walls. The proposed strengthening solution is installed to improve the behaviour of the connections, allowing the lateral forces to be transmitted through these elements. A numerical model that includes the modelling of the internal walls was constructed using shell elements, resulting in a mesh of 26406 nodes and 8614 elements.

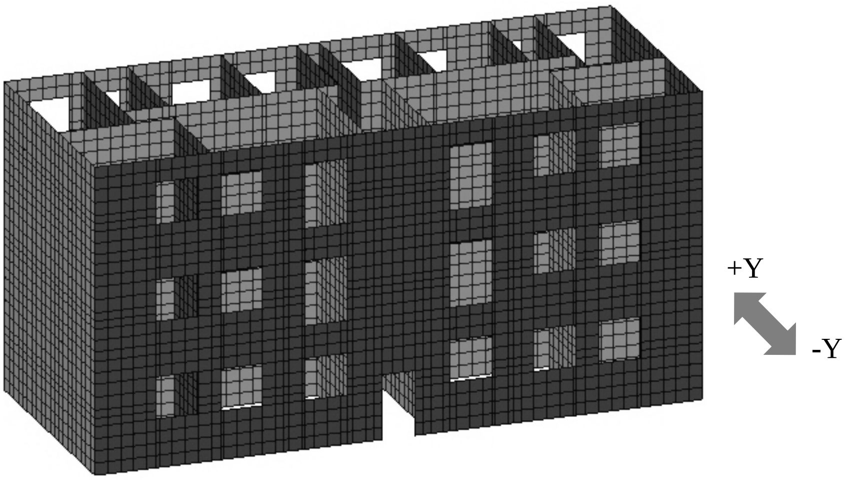

Figure 5.21 Mesh of the numerical Model 2.

Proportional to the mass pushover analyses considering both +Y and –Y directions were carried out and the capacity curves plotted in Figure 5.22. The capacity curves of both directions overlap in the linear range and the nonlinear branch shows a more ductile response in the direction –Y, contrarily to the results found for model 1. The capacity in the direction +Y is slightly higher, reaching 0.36g, but after the peak the structure suffered a decrease in the load coefficient, exhibiting a brittle behaviour. On the other direction the building presents a ductile behaviour after the peak load (0.34g), attaining great displacement capacity. Comparing this model, which considers the inclusion of the strengthening solution for wall-to-wall connections, with Model 1, the previous model only had about 15% load capacity of the new solution. This proves the influence of wall-to-wall connections in the global behaviour of a typical masonry building.

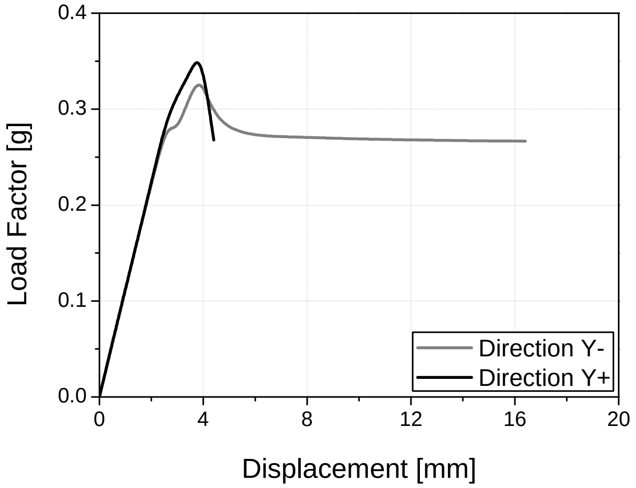

Figure 5.22 Capacity curves for Model 2.

In order to further evaluate the behaviour of the building, the principal strains distribution is plotted for direction +Y in Figure 5.23 and for direction –Y in Figure 5.24. The damage distribution resultant from the pushover analysis in +Y direction at the peak load shows widespread concentration of strains in all the building (see Figure 5.23a). At the final stage, Figure 5.23b shows severe concentration of damage in the interior walls. A diagonal crack is developed in the interior wall, located in the central part of the building, and the connection between this wall and the perpendicular one is compromised by the formation of a vertical crack along the height. Since the building is symmetric along this axis the same happens in the other part. This damage pattern can be explained by the large spacing between interior walls in this direction, so most of the lateral forces are transmitted through these central in-plane walls. Besides, these walls are thicker when compared to the other in-plane walls. Thus, the capacity of the building in this direction is limited by these walls.

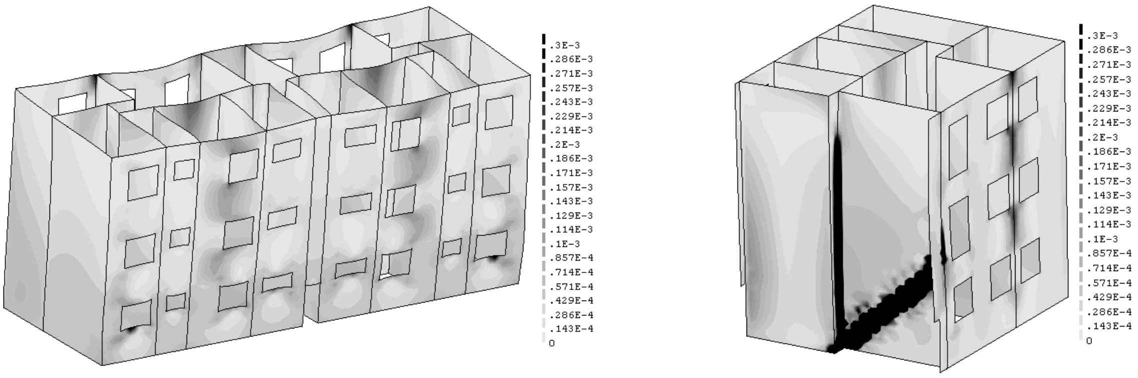

(a) (b)

Figure 5.23 Maximum principal strains distribution showing the damage evolution in +Y direction: (a) Peak load; (b) Final stage.

The damaged pattern obtained for the peak load for –Y direction shows the presence of vertical cracks following the opening edges at the centre of the building (Figure 5.24a). At the final stage, the damage propagates to the in-plane interior walls, where significant cracks due to in-plane loading are perceptible (see Figure 5.24b). The damage in some of the spandrels is severe and can originate the out-of-plane detachment of smaller parts of the building. In-plane damage in the interior walls also control the global performance of the building.

By considering efficient connections between the walls a global response of the structure was attained in both directions.

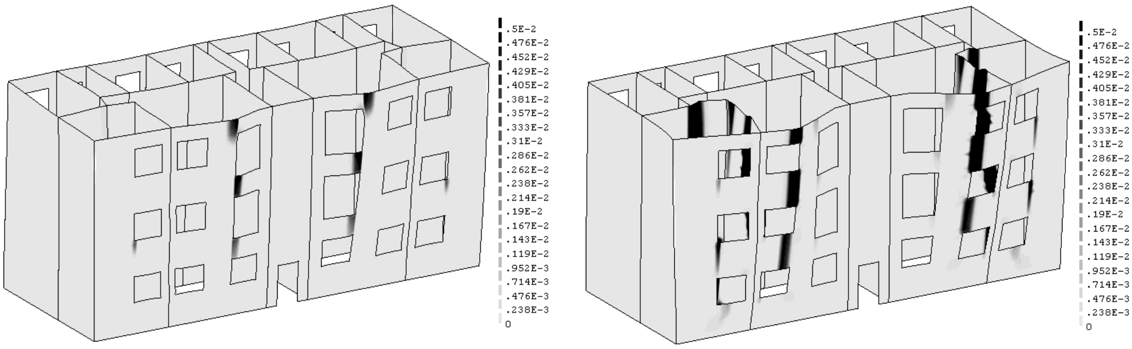

(a) (b)

Figure 5.24 Maximum principal strains distribution showing the damage evolution in –Y direction: (a) First inflection point; (b) Peak load; (c) Final stage.

5.4.3. Model 3

The global behaviour of the building is assessed by the consideration of effective connections among all the structural elements. Model 3 was constructed assuming that the strengthening solution previously proposed for wall-to-floor connections is applied to the building. Rigid connections between walls and the floor structure are assumed. The timber joists were simulated by bars that transmit only axial forces, rotations are free at the connections points and there is no shear deformation. The two-node truss elements, L6TRU, used to simulate the timber joists are represented in Figure 5.25.

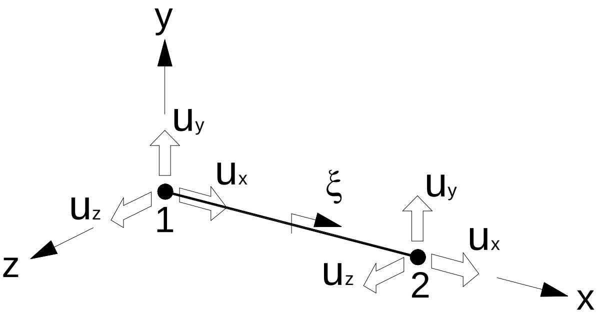

Figure 5.25 Truss element (L6TRU) (adapted from TNO DIANA (2009)).

In relation to Model 2, this model additionally includes the simulation of the floor structure. The timber joists distribution in each floor is illustrated by Figure 5.26, including the representation of the building materials. Since most of the nonlinearities are expected to concentrate in masonry, linear behaviour was assumed for timber. The generated mesh for the numerical model is presented in Figure 5.27 and has 25.400 elements and 8.662 nodes.

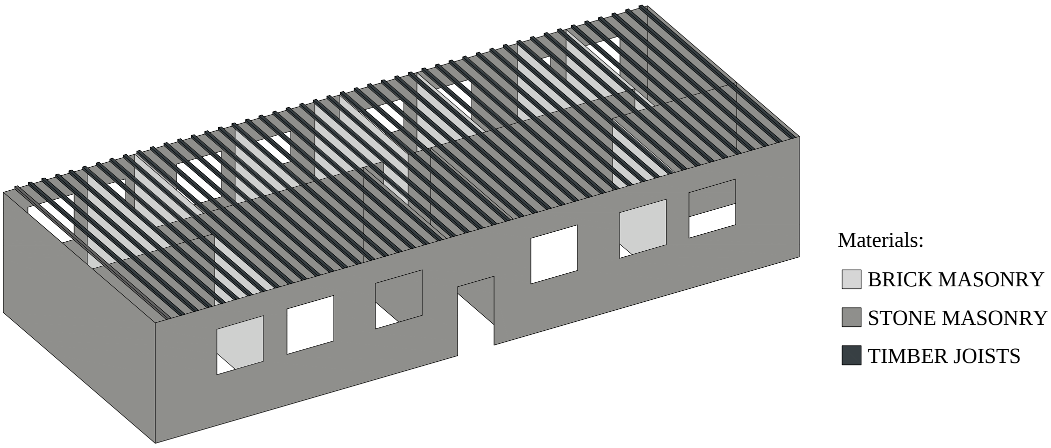

Figure 5.26 Schematic representation of one floor of the building, including the description of the materials.

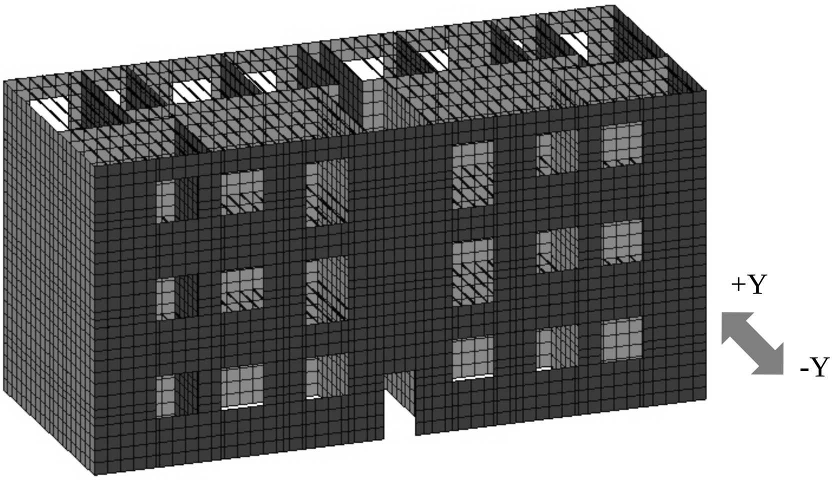

Figure 5.27 Mesh of the numerical Model 3.

Proportional to the mass pushover analyses were carried out considering the modifications implemented in Model 3. The global response of the building in Y direction is given by the capacity curves plotted in Figure 5.28. According to the pushover analyses, the building capacity in –Y direction (0.45g of load factor) is higher than the obtained in the other direction (0.39g), presenting, as verified in the previous analysis model, a more ductile behaviour. Comparing with the results obtained for Model 2, an increase in the building capacity of around 25% for direction –Y is verified and only 8% of growth in direction +Y.

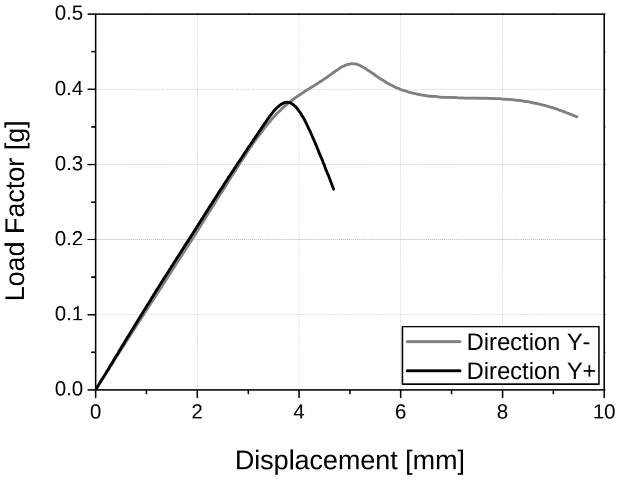

Figure 5.28 Capacity curves for Model 3.

Analysing the damage distribution for direction +Y (Figure 5.29) and –Y (Figure 5.30), similar crack pattern is found compared the previous model analyses. The global behaviour of the structure is noticeable by the damage distribution resultant from the pushover analysis. The building in the direction that presents the lower capacity exhibits damage in the interior in-plane walls (Figure 5.29b). The ductile response of the building in –Y direction is confirmed by the damage distribution throughout the structure.

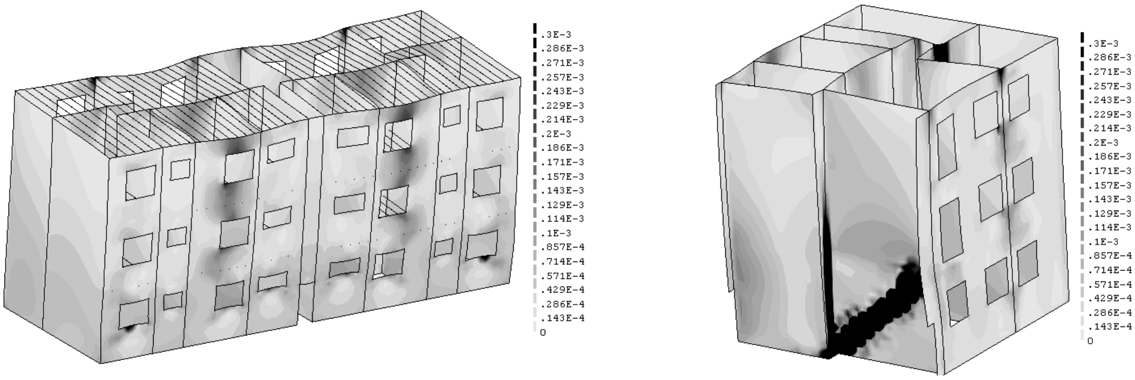
.3E-3
.286E-3
.271E-3
.257E-3
.243E-3
.229E-3
.214E-3
.2E-3
.186E-3
.171E-3
.157E-3
.143E-3
.129E-3
.114E-3
.1E-3
.857E-4
.714E-4
.571E-4
.429E-4
.286E-4
.143E-4
0

(a) (b)

Figure 5.29 Maximum principal strains distribution showing the damage evolution in +Y direction: (a) First inflection point; (b) Peak load; (c) Final stage.

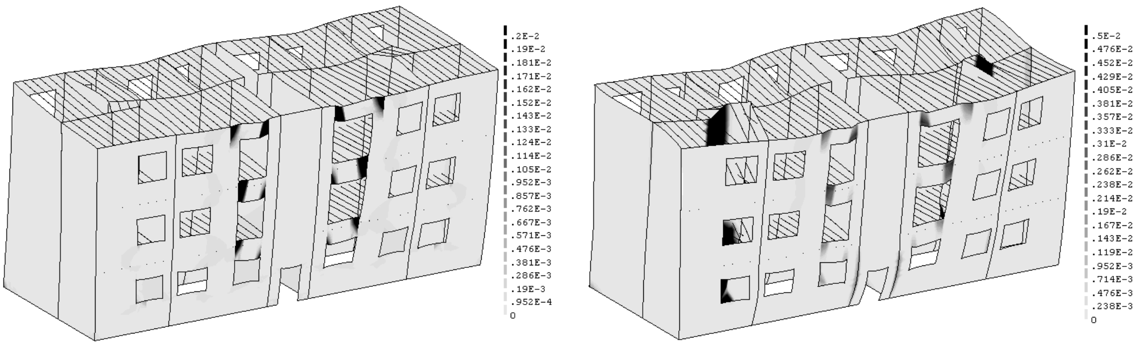
.2E-2
.19E-2
.181E-2
.171E-2
.162E-2
.152E-2
.143E-2
.133E-2
.124E-2
.114E-2
.105E-2
.952E-3
.857E-3
.762E-3
.667E-3
.571E-3
.476E-3
.381E-3
.286E-3
.19E-3
.952E-4
0
.5E-2
.476E-2
.452E-2
.429E-2
.405E-2
.381E-2
.357E-2
.333E-2
.31E-2
.286E-2
.262E-2
.238E-2
.214E-2
.19E-2
.167E-2
.143E-2
.119E-2
.952E-3
.714E-3
.476E-3
.238E-3
0

(a) (b)

Figure 5.30 Maximum principal strains distribution showing the damage evolution in –Y direction: (a) First inflection point; (b) Peak load; (c) Final stage.

5.4.4. Comparison between the models

The comparison between the model responses, as a manner to assess the influence of the connections in the behaviour of the building, is given in Figure 5.31. It is clear the difference between the first model (considering the connections inefficient) and the other two (Model 2 and 3), both in terms of stiffness and seismic capacity. By comparing the Model 2 with the Model 3, it could be concluded that the introduction of the floor structure (modelled by the timber joists) do not provide more stiffness to the structure response. Instead, the seismic capacity is enhanced, mainly in –Y direction with an increase of 25% in the load factor.

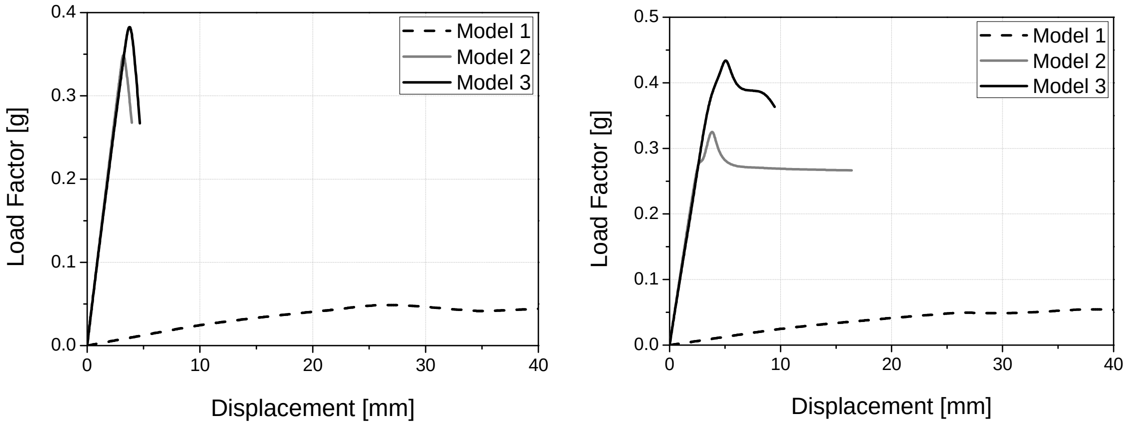

(a) (b)

Figure 5.31 Comparison between the model responses: (a) +Y direction; (b) –Y direction.

5.5. VALIDATION OF THE BUILDING CAPACITY BY SIMPLIFIED METHODS

5.5.1. Bilinear Pushover Curves

Bilinear approximation approach, in which the nonlinear behaviour is idealized with a bilinear curve, represents a useful and common approach followed by code provisions currently available worldwide (FEMA 356 2000; EC8 2003; OPCM 3431 2005). The bilinear approximation of the capacity curves obtained by the analyses results of Model 3 were defined according to Figure 5.32, resulting in the bilinear curves presented in Figure 5.33 for both +Y and –Y directions.

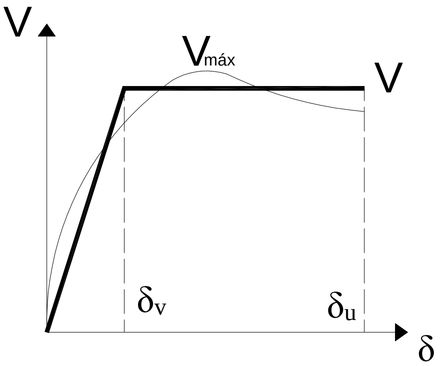

Figure 5.32 Bilinear approximation.

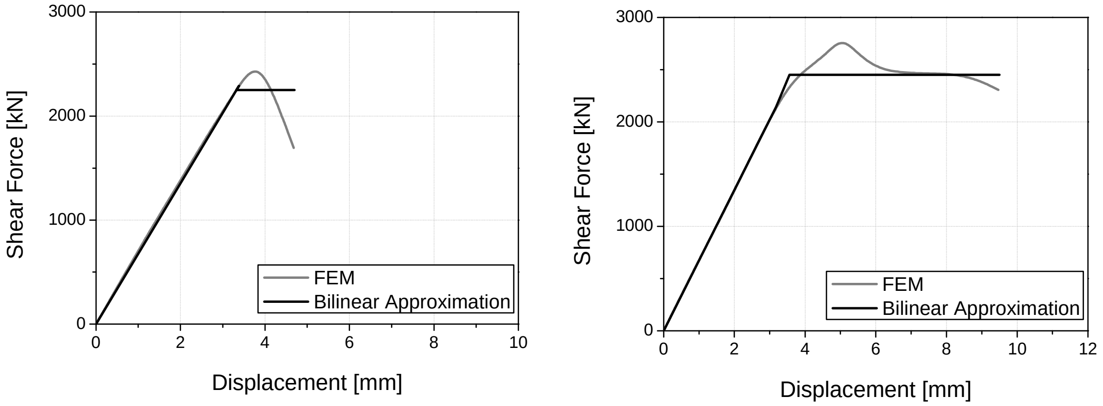

(a) (b)

Figure 5.33 Bilinear approximation of FEM results: (a) +Y direction; (b) -Y direction.

5.5.2. Macro-block approach

The work carried out by Lamego (2014) included the study of this building using macro-elements (see Figure 5.34). The software used to carry pushover analysis proportional to the 1st vibration mode was the 3Muri. Although different approaches can lead to different results and considering that in the present study pushover proportional to the mass was chosen instead proportional to the 1st vibration mode, the results will be compared. The analyses results of the global model (Model 3) are compared to the results provided by Lamego (2014).

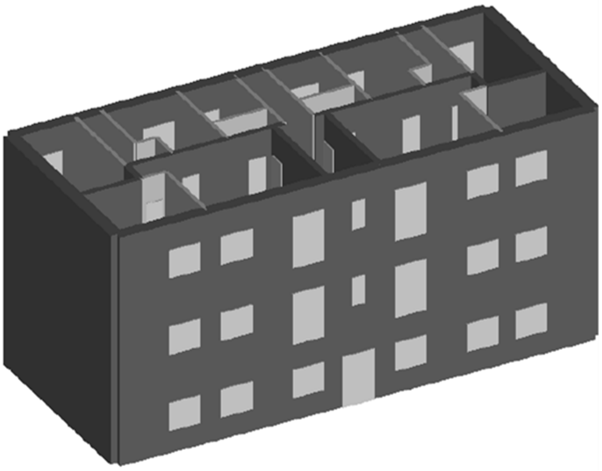

Figure 5.34 Model using macro-elements (taken from (Lamego 2014)).

Comparison between the FEM results with the results obtained by using the macro-modelling approach are presented in Figure 5.35. Both the stiffness and the seismic capacity present important differences. The results provided by the macro-modelling approach are more conservative than the ones obtained by the FEM, even if FEM considers out-of-plane effects and the macro-modelling approaches ignores them. Most probably these differences are related to the pushover load pattern adopted to carry the analysis, proportional to the mass or proportional to the first vibration mode. In addition, the constitutive laws adopted in this model are more sophisticated than the ones used in the macro-model, which may lead to slight difference results.

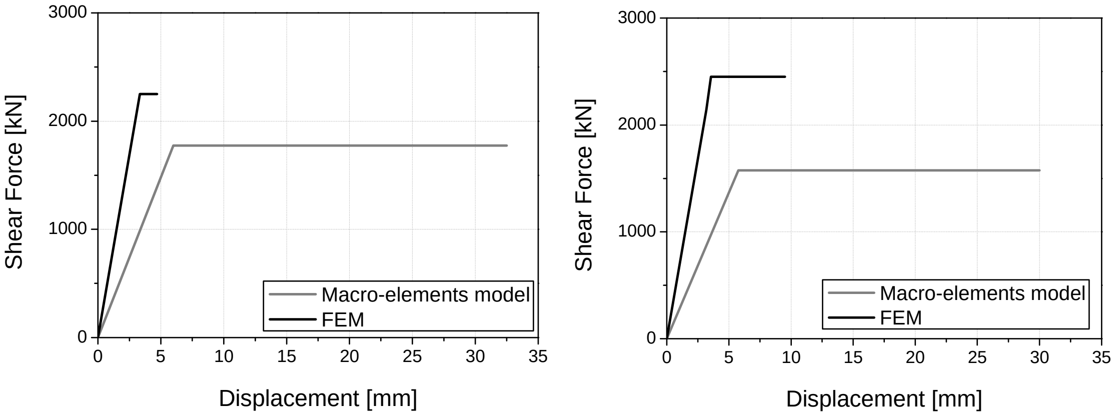

(a) (b)

Figure 5.35 Comparison between the FEM results with the results obtained by using the macro-modelling approach: (a) +Y direction; (b) -Y direction.

5.6. FEMA

In alternative to finite element analyses, which are very time consuming and require high computational efforts, expeditious methods have been proposed for estimating the seismic capacity of structures based on the behaviour of individual walls components. An example is the simplified linear static procedure included in FEMA 356 (2000) guidelines. Aiming at compare the FEM results with the building lateral capacity estimated through simplified approaches, the simplified model provided by FEMA 356 (2000) is applied. This method focused primarily on the response of individual in-plane piers taking into account the typical failure mechanisms reported in the literature (discussed in section 2.3.3 and studied in Chapter 3) (Abrams 2001). The global response of the entire building in terms of shear strength is then determined by combining the individual responses of each wall (Moon 2004). This simplified procedure relies in two basic assumptions: the parallel walls deform together, assuming that forces are transmitted through all the structural elements; and the lateral strength of the building in a given direction is calculated as the sum of the strength capacity of all walls parallel to this direction. The efficiency of the connections between the structural elements activates the monolithic behaviour of the building, making the role of walls paramount with regards to the lateral seismic resistance of the structure. Indeed, post-earthquake investigations have shown that, once the out-of-plane mechanisms are prevented, the seismic performance of a masonry building depends on the strength capacity of its piers (Vasconcelos and Lourenço 2009).

In the building under study the efficiency of the connections between structural elements is assured by the strengthening solutions designed in the previous section. Thus, the regular shape of the building and its box-like behaviour under lateral actions, suggests that the simplified approach is applicable and can give an approximate estimation of the lateral strength of the building.

The lateral capacity of the building was evaluated considering the direction perpendicular to the wall façades. The components of the building that resist to lateral loads in this direction are the in-plane lateral walls. Both of the lateral walls have the same characteristics, not presenting any opening, as verified by the plants of Figure 5.3 and Figure 5.4. The lateral wall with the definition of the structural components is presented in Figure 5.36, in which three piers are distinguished according to the floor levels. The forces acting at the floor levels (p_1, p_2 and p_3) are calculated following the same considerations taken in the section 5.3. Since the timber joists are placed parallel to these walls, only a small part of the forces from the floors are transferred to the lateral walls. Thus, p_1 and p_2 were taken equal to 4.6 kN/m and p_3 2.0 kN/m.

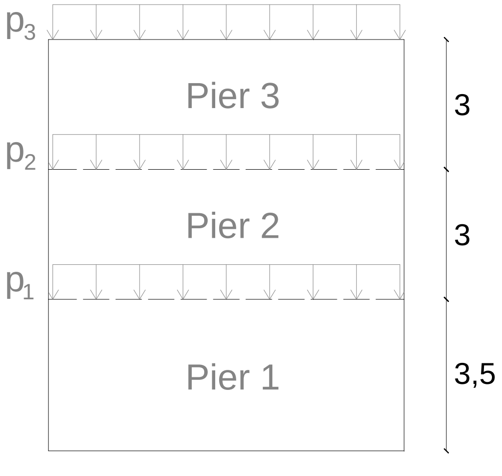

Figure 5.36 Schematic illustrating the definition of structural components in lateral walls.

The strength capacity of the piers is evaluated through the analytical expressions provided in FEMA 356 (2000) based on one of four possible behavioural states: bed joint sliding, rocking, diagonal tension or toe compression (discussed and applied in Chapter 3, section 3.7). The failure mode and corresponding lateral strength of a pier is controlled by the failure mode with lowest strength. Equations (3.4), (3.7), (3.9) and (3.12) described in section 3.7 were used to compute the strength capacity of the piers described above according to the failure mode. The material properties and the parameters used to compute the strength of each pier according to the failure mode are summarized in Table 5.5, where l is the length, h is the height of the pier and t the thickness, W is the weight of each pier and N the axial compressive force acting in each level. The parameter α_2 is related to the boundary conditions of each pier. Fixed-fixed conditions were defined for pier 1 and 2 (α_2=1.0) because the wall develops for the next floors, granting the support for these piers at the top. Since the timber trusses are disposed perpendicular to the façade walls, it was considered that the roof structure would not grant enough support to the top pier. For this reason cantilever conditions were conservatively assumed for pier 3 (α_2=0.5).

Table 5.5 Parameters used to compute the strength capacity of each pier.

	l [m]	h [m]	t [m]	W [kN]	N [KN]	c [MPa]	f_c [MPa]	f_t [MPa]	α_2	μ
Pier 3	8.2	3	0.5	233.7	250.1	0.1	0.9	0.1	0.5	0.75
Pier 2	8.2	3	0.5	233.7	521.5	0.1	0.9	0.1	1.0	0.75
Pier 1	8.2	3.5	0.5	272.7	831.9	0.1	0.9	0.1	1.0	0.75

The calculated strength and controlling failure mode for each pier are shown in Table 5.6. For pier 1 and 2 the shear sliding governs, whilst flexural behaviour by toe crushing governs the failure of the top pier. The strength capacity of the lateral wall is computed by the sum of the contribution given by the component at the base level since it include the weight of all the piers, i.e. 931.4 kN (pier 1). As a result, the global strength of the building to lateral loads in the direction perpendicular to the façade walls is estimated by the sum of the strength of the two in-plane walls, totalizing around 1863 kN.

Table 5.6 Strength of the piers.

	Toe Crushing [kN]	**Rocking [kN]**	**Sliding [kN]**	**Diagonal Tension [kN]**
Pier 3	308.7	307.6	495.1	1218.8
Pier 2	1137.7	1282.9	698.6	1689.2
Pier 1	1321.3	1754.1	931.4	1671.8

The lateral strength capacity obtained by this simplified procedure was compared to the results from FEM analyses. Since the in-plane capacity of these walls can only be fully exploited if the building behaves as a monolithic structure, as assumed by the FEMA simplified procedure, the comparison with the numerical results is performed considering the Model 3 in which the global response governs. The maximum lateral capacity obtained by FEM in the bilinear approximation was 2300 kN (see Figure 5.33). The prediction given by the simplified procedure proposed in FEMA 356 (2000) underestimates the strength of the building when compared with the pushover analyses results, but still provides very approximate values. Similar results were found by Yi

(2004), which concluded that the strength predicted by FEMA 356 is conservative when compared to the actual strength of the building experimentally tested. The underestimation of the strength capacity can be related to the fact that the current FEMA methods do not take into account some global characteristics of the test structure such as the flange effects. This method primarily relies on individual components to describe the behaviour of the in-plane walls possibly neglecting important global characteristics of the structure, but still it can estimates with reasonable approximation of the building capacity.

5.7. FINAL REMARKS

The capabilities and application of the studies carried out on the previous Chapters are revealed through its application in the study of the seismic behaviour of a typical masonry building. Since the global structural performance of masonry buildings, under earthquake loading, is affected by the efficiency of wall-to-wall and wall-to-floor connections, strengthening solutions were designed based on the knowledge provided in the study carried out in Chapter 4. The kinematic limit analysis approach which considers the seismic individual response of selected mechanisms was applied to assess the safety of the wall without connections to the structural element and then for the design of the strengthening solutions.

Finite element models were developed with the purpose of evaluating the influence of the connections between structural elements. Pushover analyses results proved that the seismic capacity of the building considering inefficient connections is very low and that proper strengthening measures would provide a great enhance on the capacity of the building. Considering effective connections among walls the seismic capacity is highly improved and when combined to efficient strengthen of wall-to-floor connections the seismic response of the building is even more improved.

Chapter 6

CONCLUSIONS AND FUTURE WORK

6.1. CONCLUSIONS

A numerical approach to study the structural behaviour of walls and strengthened connections in traditional masonry buildings was presented, providing valuable contributions on this topic. These works demonstrated that the use of sophisticated numerical analysis for the characterization of experimentally tested specimens, not only provides reliable results, including the accurate characterization of the nonlinear behaviour, ultimate capacity and failure mechanisms, but also appears as a powerful tool for the development of parametric analyses.

During this thesis, special attention was given to the numerical model validation procedure against experimental data, assuring in this manner the confidence in the sequent parametric numerical results. The results provided by the parametric analyses contributed to extend the available database on the characterization of the behaviour of masonry walls and injected anchors in masonry.

This thesis can be divided into three main parts: the study of wall components; the study of strengthened connections using injected anchors in masonry and the application of the results provided by these studies in the seismic assessment of a typical masonry building. In the following the main conclusions of each of these studies are addressed.

6.1.1. Masonry Walls Study

The study of the in-plane behaviour of masonry walls was carried out resorting to finite element models to simulate the numerically the walls response. The evaluation of the walls experimental response compared with the preliminary linear analyses results, allowed to conclude that the elastic stiffness is dependent on the pre-compression level of the wall and on the construction procedure. For this reason, the numerical model should incorporate this aspect so the masonry elastic modulus was adjusted according to the experimental response. A good correspondence between numerical and experimental responses has been found for all the walls proving the potential of the presented numerical strategy to simulate the in-plane behaviour of masonry walls with good accuracy. The non-linear response, strength capacity and failure mechanism predicted by the numerical analyses present good correlation with the experimental results for all the walls.

The validated numerical models were used as a numerical laboratory to assess the response of walls with different geometric relations and pre-compression levels. A total of five more walls were numerically estimated regarding the, nonlinear response, stress distribution, strength capacity and failure mode. The comparison between the walls responses, demonstrated that flexure failure modes are predominant in slender walls with low levels of pre-compression. The in-plane capacity of the walls is improved by the increase on the pre-compression level and lower slenderness ratios (squat walls), but leading to a decrease in the lateral displacement capacity of the walls.

The drift capacity of the walls was evaluated according to EC8 recommendations. The comparison between the drift capacities estimated by numerical analyses and the limit proposed by the codes showed that a number of walls did not fulfilled the requirements. Different and more realistic boundary conditions were then considered, which allowed to fulfil the drift limit for 94% of the walls.

Finally, analytical simplified formulations available in literature, which are associated to distinct failure modes, were presented and discussed. The application of the simplified expressions to the numerically studied walls, showed good agreement between the numerical lateral resistance and the predicted values based on by simplified models.

6.1.2. Injected Anchors Study

The study of injected anchors in masonry as a tool to strengthen the connection between elements, included the construction of a detailed three-dimensional finite element model. Aiming at investigating the formulation that best describes the behaviour of the system, fixed and rotating crack models were used. Rotating crack model simulates the behaviour of the anchoring system with a better accuracy since the force-displacement response, damage distribution and failure mode are in better agreement with the experimental results.

The validated numerical model was used to study the influence of some input parameters and model conditions. The response of other configurations was successfully evaluated through parametric analysis proving, in this manner, the potential of the numerical model. Parametric analysis revealed that the embedment depth is the aspect that most influences the capacity of injected anchors in masonry, in comparison with the other studied parameters.

Finally, a good agreement between experiments and the failure modes predicted by available analytical formulations was achieved. In terms of strength capacity, a very good agreement was obtained with the ACI 318 (2011), fib Bulletin No. 58 (2011) and CEB (1994) formulations. On the other hand, the method proposed by MSJC (2013) seems to greatly overestimate the values of the strength capacity. Gigla and Wenzel (2000) expressions provide rather conservative predictions in all the cases.

6.1.3. Typical Masonry Building

A traditional masonry building located in Lisbon was used to evaluate the role of connections in its seismic performance. Strengthening solutions using injected anchors in masonry walls were designed for wall-to-wall and wall-to-floor connections. The strength capacity values were estimated in accordance with the results provided in Chapter 4.

Finite element models confirm the great influence that the connections have in the seismic capacity of a structure. Pushover analysis proportional to the mass were used to assess the seismic behaviour of the regular building. Considering ineffective connections among the structural elements, pushover analysis showed low seismic capacity limited by local collapse mechanisms. With the improvement of the connections among exterior and interior walls (obtained by the installation of the designed strengthening solution) the building capacity increases around 85% with regard to the previous model. The analysis considering that the structure behaves as a global system (by improving the wall-to-floor connections) lead to an increase of around 20% in the building capacity. These two last numerical models presented a damage pattern that indicates a global behaviour of the structure. The influence of the connections between structural elements was clearly demonstrated by the numerical analysis results found.

The numerical results were also compared to a simplified macro-modelling approach available in Lamego (2014) and differences were found, which can be related to the modelling approach used.

6.2. FUTURE WORKS

The research presented and discussed in this thesis can be used as a basis for future developments in theoretical, numerical, and even experimental fields. Further research is proposed as follows:

- The study reported in Chapter 3 focused on the behaviour of stone masonry walls. This numerical approach can be used for the study of other masonry types, geometric aspect ratios, and other structural aspects (boundary conditions, levels of compression, etc.).
- In Chapter 4 a numerical approach was followed to describe the behaviour of injected anchors in masonry. The conditions studied through parametrical analysis can be further explored, including additional parameters that can influence the behaviour of the anchoring system.
- The approach followed in Chapter 4 could also be expanded for the study of other types of strengthening solutions.
- The application of dynamic analysis and incremental dynamic analysis in the assessment of the seismic performance of traditional masonry buildings is suggested to validate the use of simple approaches, more suitable for professionals.

BIBLIOGRAPHY

Abrams D (2001) Performance-based engineering concepts for unreinforced masonry building structures. Progress in Structural Engineering and Materials 3:48–56. doi: 10.1002/pse.70

Abrams D, Shah N (1992) Cyclic Load Testing of Unreinforced Masonry Walls. Department of Civil Engineering University of Illinois at Urbana-Champaing 98:1–46.

Abruzzese D, Miccoli L, Vari A, et al. (2009) Dynamic investigations on medieval masonry towers : Vibration measurement and structural identification. Protection of Historical Buildings 807–813.

ACI 318 (2011) Building Code Requirements for Structural Concrete (ACI 318-11) and Commentary.

Alcaino P, Santa-Maria H (2008) Experimental Response of Externally Retrofitted Masonry Walls Subjected to Shear Loading. Journal of Composites for Construction 12:489–498. doi: 10.1061/(ASCE)1090-0268(2008)12:5(489)

Algeri C, Poverello E, Plizzari G, Giuriani E (2010) Experimental Study On The Injected Anchors Behaviour On Historical Masonry. Advanced Materials Research 133-134:423–428.

Andreini M, De Falco A, Giresini L, Sassu M (2013) Mechanical Characterization of Masonry Walls with Chaotic Texture: Procedures and Results of In-situ tests. International Journal of Architectural Heritage

Angelini L, Beconcini ML, Sassu M (2007) Prove di compressione e taglio in sito su pannelli in muratura : la tecnica dei maschi murari contrapposti. Proc. XII ANIDIS

(Italian National Association of Earthquake Engineering) Conference on “L’Ingegneria Sismica in Italia.”p Paper 135

Annecchiarico M, Portioli F, Landolfo R (2009) FE simulation of masonry wall samples of Mustafa Pasha mosque by homogeneous continuum models : Analysis and calibration. Protection of Historical Buildings - PROHITECH 09 95–100.

Anthoine A, Magonette G, Magenes G (1995) Shear-compression testing and analysis of brick masonry walls. 10th European Conference on Earthquake Engineering. Rotterdam, pp 1657–1662

Antoniou S, Pinho R (2010) Development and Verification of a Displacement-Based Adaptative Pushover Procedure. Journal of Earthquake Engineering 8:643–661. doi: 10.1080/13632460409350504

Antoniou S, Pinho R (2004) Advantages and limitations of adaptive and non-adaptive force-based pushover procedures. Journal of Earthquake Engineering 8:497–522. doi: 10.1080/13632460409350498

Araújo AS, Lourenço PB, Oliveira D V, Leite JC (2012) Seismic assessment of St. James Church by means of pushover analysis: before and after the New Zealand earthquake. The Open Civil Engineering Journal 6:160–172.

Arifpovic F, Nielsen MP (2004) Strength of anchors in masonry. Department of Civil Engineering, Technical University of Denmark

Ashour AF, Alqedra MA (2005) Concrete breakout strength of single anchors in tension using neural networks. Advances in Engineering Software 36:87–97. doi: 10.1016/j.advengsoft.2004.08.001

Augenti N, Parisi F (2009) Non-linear static analysis of masonry structures. 13th Italian National Conference on Earthquake Engineering

Bajer M, Barnat J (2012) The glue–concrete interface of bonded anchors. Construction and Building Materials 34:267–274. doi: 10.1016/j.conbuildmat.2012.02.030

Baldessari C, Piazza M, Tomasi R (2009) The refurbishment of existing timber floors : Characterization of the in-plane behaviour. Protection of Historical Buildings - PROHITECH 09

Bento R, Lopes M, Cardoso R (2005) Seismic evaluation of old masonry buildings . Part II : Analysis of strengthening solutions for a case study. Engineering Structures 27:2014–2023. doi: 10.1016/j.engstruct.2005.06.011

Beolchini GC, Cifani G, Pucci GG, et al. (2002) Repertorio dei meccanismi di danno, delle tecniche di intervento e dei relativi costi negli edifici in muratura.

Berto L, Saetta A, Scotta R, Vitaliani R (2004) Shear behaviour of masonry panel: parametric FE analyses. International Journal of Solids and Structures 41:4383–4405. doi: 10.1016/j.ijsolstr.2004.02.046

Betti M, Vignoli A (2008a) Assessment of seismic resistance of a basilica-type church under earthquake loading: Modelling and analysis. Advances in Engineering Software 39:258–283. doi: 10.1016/j.advengsoft.2007.01.004

Betti M, Vignoli A (2008b) Modelling and analysis of a Romanesque church under earthquake loading: Assessment of seismic resistance. Engineering Structures 30:352–367. doi: 10.1016/j.engstruct.2007.03.027

Betti M, Vignoli A (2011) Numerical assessment of the static and seismic behaviour of the basilica of Santa Maria all’Impruneta (Italy). Construction and Building Materials. doi: 10.1016/j.conbuildmat.2010.12.028

Beyer K (2012) Peak and residual strengths of brick masonry spandrels. Engineering Structures 41:533–547. doi: 10.1016/j.engstruct.2012.03.015

Binda L, Cardani G, Gentile C, Zanzi L (2009) Investigation , diagnosis and conservation design of the church of St . Lorenzo in Cremona , Italy. In: Mazzolani (ed) Protection of Historical Buildings - PROHITECH 09. Taylor & Francis Group, London,, Rome, Italy, pp 115–124

Binda L, Cardani G, Saisi A, Valluzzi MR (2006) Vulnerability analysis of the historical buildings in seismic area by a multilevel approach. 7:343–357.

Binda L, Saisi A (2005) Research on historic structures in seismic areas in Italy. Progress in Structural Engineering and Materials 7:71–85. doi: 10.1002/pse.194

Branco JM (2009) Portuguese traditional timber structures : Survey , analysis and strengthening. Protection of Historical Buildings - PROHITECH 09 261–266.

Brazão Farinha J, Correia do Reis A (1993) Tabelas Técnicas, P.O.B. 1–633.

Brencich A, Gambarotta L, Ghia A (2001) Structural models for the assessment of the masonry dome of the Basilica of S . Maria of Carignano in Genoa. In: Lourenço PB, Roca P (eds) Historical Constructions. Guimarães, Portugal, pp 675–684

Brignola A, Podestà S (2009) The role of the in-plane stiffness of timber floors in the seismic response of un-reinforced masonry buildings.

Calderini C, Cattari S, Lagomarsino S (2008) In-plane strength of unreinforced masonry piers. Earthquake Engineering & Structural Dynamics. doi: 10.1002/eqe

Calvi GM, Kingsley G, Magenes G (1996) Testing of Unreinforced Masonry Structures for Seismic Assessment. Earthquake Spectra 12:145–162. doi: 10.1193/1.1585872

Capozucca R (2011) Shear Behaviour of Historic Masonry Made of Clay Bricks. The Open Construction and Building Technology Journal 5:89–96. doi: 10.2174/1874836801105010089

Cardoso R, Lopes M, Bento R (2005) Seismic evaluation of old masonry buildings . Part I : Method description and application to a case-study. Engineering Structures 27:2024–2035. doi: 10.1016/j.engstruct.2005.06.012

Casarin F (2006) Structural Assessment and Seismic Vulnerability Analysis of a Complex Historical Building. University of Trento

CEB (1994) Fastenings to Concrete and Masonry Structures. Comite Euro-International du Beton

Chopra AK, Goel RK (2001) A Modal Pushover Analysis Procedure to Estimate Seismic Demands for Buildings : Theory and Preliminary Evaluation. Pacific Earthquake Engineering Research Center

Churilov S, Dumova-Jovanoska E (2010) In-plane shear behaviour of unreinforced masonry walls. 14th European Conference in Earthquake Engineering

Churilov S, Dumova-Jovanoska E (2013) In-plane shear behaviour of unreinforced and jacketed brick masonry walls. Soil Dynamics and Earthquake Engineering 50:85–105. doi: 10.1016/j.soildyn.2013.03.006

Cintec (2012) Cintec International - Anchoring and Reinforcement. http://www.cintec.com. Accessed 11 Apr 2013

Cóias V (2007) Reabilitação Estrutural de Edifícios Antigos. 1–4.

Corradi M, Borri a, Vignoli a (2002) Strengthening techniques tested on masonry structures struck by the Umbria–Marche earthquake of 1997–1998. Construction and Building Materials 16:229–239. doi: 10.1016/S0950-0618(02)00014-4

Corradi M, Tedeschi C, Binda L, Borri A (2008) Experimental evaluation of shear and compression strength of masonry wall before and after reinforcement: Deep repointing. Construction and Building Materials 22:463–472. doi: 10.1016/j.conbuildmat.2006.11.021

Costa A (2007) Experimental testing of lateral capacity of masonry piers . An application to seismic assessment of AAC masonry buildings. Rose School

D'Ayala D (2011) The role of connections in the seismic resilience of historic masonry structures. XIV Convegno ANIDIS "L'Ingegneria Sismica in Italia"

D'Ayala D, Paganoni S (2014) Testing and design protocol of dissipative devices for out-of-plane damage. Proceedings of the ICE - Structures and Buildings 167:26–40. doi: 10.1680/stbu.12.00087

D'Ayala D, Speranza E (2002) An Integrated Procedure for the Assessment of Seismic Vulnerability of Historic Buildings. 12th European Conference on Earthquake Engineering. p Paper 561

D'Ayala DF, Paganoni S (2010) Assessment and analysis of damage in L'Aquila historic city centre after 6th April 2009. Bulletin of Earthquake Engineering 9:81–104. doi: 10.1007/s10518-010-9224-4

Di A, La C, Battista SG, et al. (2002) Linee guida per gli interventi di riparazione del danno e miglioramento sismico per gli edifici di culto e monumentali - Allegato A.3.1. Unità Operativa Ingegneristico Geologico

Doerr GT, Klingner RE (1989) Adhesive Anchors: Behavior and Spacing Requirements. Austin, Texas

Dogangun A, Sezen H, Livaoglu R, Do A (2009) Performance evaluation of historical masonry monumental structures during the 1999 Turkey earthquakes. Protection of Historical Buildings - PROHITECH 09 1465–1470.

Dyavanal SS, Annigeri SA (2009) Performance based seismic evaluation of multistory buildings with openings in infill walls. Protection of Historical Buildings - PROHITECH 09 1471–1475.

EC6-3 (2005) Eurocode 6 - Design of masonry structures - Part 3: Simplified calculation methods for unreinforced masonry structures Eurocode. Eurocode 6 - Design of masonry structures

EC8 (2003) Eurocode 8 - Design of structures for earthquake resistance.

EC8-1 (2010) Eurocódigo 8 - Projecto de estruturas para a resistência aos sismos Parte 1: Regras gerais, acções sísmicas e regras para edifícios. European Standard

EC8-3 (2004) Eurocode 8 - Design of structures for earthquake resistance Part 3: Assessment and retrofitting of buildings. European Standard

Eligehausen R, Mallée R, Rehm G (1984) Befestigungen mit Verbundankern (Fastenings with bonded anchors). Betonwrk + Fertigteil-Technik

Elmenshawi A, Sorour M, Mufti AA, et al. (2010) In-plane seismic behaviour of historic stone masonry. Canadian Journal of Civil Engineering 37:465–476. doi: 10.1139/L09-166

Eshghi S, Pourazin K (2009) In-plane Behaviour of Confined Masonry Walls - With and Without Opening. International Journal of Civil Engineering 7:49–60.

Fajfar P, Eeri M (2000) A Nonlinear Analysis Method for Performance Based Seismic Design. Earthquake Spectra 16:573–592.

FEMA 306 (1998) Evaluation of Earthquake Damaged Concrete and Masonry Wall Buildings. Federal Emergency Management Agency

FEMA 356 (2000) Prestandard and commentary for the seismic rehabilitation of buildings. FEMA 356

Ferracuti B, Pinho R, Savoia M, Francia R (2009) Verification of displacement-based adaptive pushover through multi-ground motion incremental dynamic analyses. Engineering Structures 31:1789–1799. doi: 10.1016/j.engstruct.2009.02.035

fib Bulletin No. 58 (2011) Design of anchorages in concrete: Guide to Good Practice.

Franchetti P (2009) Damage and collapsing mechanisms in existing (particularly historical) structures – 1 / 2. SAHC

Freeda C, Tensing D, Mercy S (2012) In-plane shear behaviour of Brick Masonry – A Literature Review on experimental study. International Journal of Civil and Structural Engineering 2:1144–1152.

Freeman SA (1998) The Capacity Spectrum Method as a Tool for Seismic Design. 11th European on Earthquake Engineering

Furukawa A, Kiyono J (2009) Casualty estimation in the collapse of masonry structures due to earthquakes. Protection of Historical Buildings - PROHITECH 09 423–429.

Galasco A, Lagomarsino S, Penna A (2006) On the use of pushover analysis for existing masonry buildings. First European Conference on Earthquake Engineering and Seismology. Geneva, Switzerland, pp 1–10

Galasco A, Magenes G, Paré M Da, Penna A (2009) Risposta ciclica sperimentale di pannelli in muratura di pietra. ANIDIS

Galasco A, Magenes G, Penna A, Da Paré M (2010) In-plane cyclic shear tests of undressed double leaf stone masonry panels. 14th European Conference in Earthquake Engineering

Gattesco N (2009) Novel engineering techniques to improve the in-plane stiffness of wooden floors. 307–312.

Gavrilovic P, Jekic G (2009) Structural consolidation and seismic strengthening of Fatih (Prishtina) and Sinan Pasha (Prizren) Mosques – Kosovo. Protection of Historical Buildings - PROHITECH 09 1281–1286.

Ghiassi B (2013) Durability analysis of bond between composite materials and masonry substrates. University of Minho

Gigla B (2004) Bond Strength of Injection Anchors as Supplementary Reinforcement Inside Historic Masonry. In: Martens D, Vermeltfoort A (eds) 13th International Brick and Block Conference. Amestedam, pp 119–128

Gigla B, Wenzel F (2000) Design Recommendations For Injection Anchors As Supplementary Reinforcement Of Historic Masonry. 12th International Brick/Block Masonry Conference. Madrid, Spain, pp 691–706

Haman A, Jaeger W (2011) Experimental Investigation of Grouted Anchors in Natural Stone Masonry Walls under Static and Cyclic Loading. 9th Australasian Masonry Conference. Queenstown, New Zealand, pp 41–50

Hilti (2011) North American Product Technical Guide - Volume 2: Anchor Fastening Technical Guide.

Ingham JM (2011) Commentary to Assessment and Improvement of Unreinforced Masonry Buildings for Earthquake Resistance.

Jarred D, Haberfield C (1997) Tendon/Grout Interface Performance in Grouted Anchors. In: Littlejohn GS (ed) Ground anchorages and anchored structures. Tomas Telford, London, U.K., pp 3–12

Jeong YJ, Kim HY, Koo HB, Kim ST (2005) Steel-concrete interface behavior and analysis for push-out. KSCE Journal of Civil Engineering 9:119–124. doi: 10.1007/BF02829065

Kalkan E, Asce SM, Kunnath SK, Asce M (2006) Adaptive Modal Combination Procedure for Nonlinear Static Analysis of Building Structures. Journal of Structural Engineering 1721–1731.

Lagomarsino S (2006) On the vulnerability assessment of monumental buildings. Bulletin of Earthquake Engineering 4:445–463. doi: 10.1007/s10518-006-9025-y

Lagomarsino S (1998a) A new methodology for the post-earthquake investigation of ancient churches. 11th European on Earthquake Engineering. pp 1–12

Lagomarsino S (1998b) Seismic Damage Survey of the Churches in Umbria. Proc. of the Workshop on Seismic Performance of Monuments. pp 167–176

Lamego PRP da C (2014) Reforço sísmico de edifícios de habitação. Viabilidade da mitigação do risco. University of Minho

Lee Y-H, Joo YT, Lee T, Ha D-H (2011) Mechanical properties of constitutive parameters in steel–concrete interface. Engineering Structures 33:1277–1290. doi: 10.1016/j.engstruct.2011.01.005

Lemos J V (2007) Discrete Element Modeling of Masonry Structures. International Journal of Architectural Heritage 1:190–213. doi: 10.1080/15583050601176868

Lourenço PB (2002) Computations on historic masonry structures. Progress in Structural Engineering and Materials 4:301–319. doi: 10.1002/pse.120

Lourenço PB (2000) Anisotropic softening model for masonry plates and shells. Structural Engineering 126(9):1008–1016.

Lourenço PB (1996a) Computational strategies for masonry structures. Delft University of Technology

Lourenço PB (2001) Analysis of historical constructions: From thrust-lines to advanced simulations. In: Lourenço PB, Roca P (eds) Historical constructions. Citeseer, Guimarães, pp 91–116

Lourenço PB (2009a) Recent advances in masonry structures: Micromodelling and homogenisation, in: Multiscale Modeling in Solid Mechanics: Computational Approaches. In: Galvanetto U, Aliabadi MH (eds)Imperial College Press, pp 251–294

Lourenço PB (2009b) Recent Advances in Masonry Modelling: Micromodelling and Homogenisation. In: Galvanetto U, Aliabadi MH (eds) Multiscale Modeling In Solid Mechanics Computational Approaches, Imperial C. Imperial College Press, pp 251–294

Lourenço PB (2009c) Material Data to Use. Slides of the Advanced Master in Structural Analysis of Monuments and Historical Constructions- SAHC

Lourenço PB (1994) Analysis of Masonry Structures with Interface Elements Theory and Applications. Delft University of Techonology 1–25.

Lourenço PB (1996b) A user / programmer guide for the micro-modeling of masonry structures. 1–46.

Lourenço PB, Krakowiak KJ, Fernandes FM, Ramos LF (2007a) Failure analysis of Monastery of Jerónimos, Lisbon: How to learn from sophisticated numerical models. Engineering Failure Analysis 14:280–300. doi: 10.1016/j.engfailanal.2006.02.002

Lourenço PB, Mendes N, Marques R (2009) Earthquake Design and Assessment of Masonry Structures : Review and Applications. 20th International conference on Civil, Structural and Environmental Engineering Computing 1–24.

Lourenço PB, Mendes N, Ramos LF, Oliveira D V (2011) Analysis of Masonry Structures Without Box Behavior. International Journal of Architectural Heritage 5:369–382. doi: 10.1080/15583058.2010.528824

Lourenço PB, Milani G, Tralli A, Zucchini A (2007b) Analysis of masonry structures: review of and recent trends in homogenization techniques. Canadian Journal of Civil Engineering 34:1443–1457. doi: 10.1139/L07-097

Lourenço PB, Mourão S (2001) Safety assessment of Monastery of Jerónimos , Lisbon. Historical Constructions 697–706.

Lourenço PB, Roque JCA (2006) Simplified indexes for the seismic vulnerability of ancient masonry buildings. Construction and Building Materials 20 (4):200–208.

Lourenço PB, Rots JG (1997) Multisurface interface model for analysis of masonry structures. Journal of engineering mechanics 123:606–668. doi: 10.1061/(ASCE)0733-9399(1997)123:7(660)

Lourenço PB, Rots JG, Blaauwendraad J (1998) Continuum Model for Masonry: Parameter Estimation and Validation. Structural Engineering

Lowes LN (1999) Finite Element Modeling of Reinforced Concrete Beam-Column Bridge Connections. PhD Thesis 4–6.

Lu DG, Song PY, Cui SS, Chen ZH (2010) Vertical Incremental Dynamics for Assessing Progressive Collapse Resistance and Failure Modes are Structures. Proceedings of the 4th International Workshop on Reliable Engineering Computing Robust Design – Coping with Hazards, Risk and Uncertainty – REC 2010 31:159–172. doi: 10.3850/978-981-08-5118-7_064

Magenes G (2006) Masonry Building Design in Seismic Areas: Recent Experiences and Prospects from a European Standpoint. 1st European Conference on Earthquake Engineering and Seismology. Geneva, Switzerland, pp 1–22

Magenes G (2000) A method for pushover analysis in seismic assessment of masonry buildings. Proceedings of the Twelfth World Conference on Earthquake Engineering, Auckland, New Zealand 1–8.

Magenes G, Calvi GM (1997) In-plane seismic response of brick masonry walls. Earthquake Engineering & Structural Dynamics 26:1091–1112. doi: 10.1002/(SICI)1096-9845(199711)26:11<1091::AID-EQE693>3.0.CO;2-6

Magenes G, Calvi GM (1992) Cyclic behaviour of brick masonry walls. 10th World Conference in Earthquake Engineering. Rotterdam, pp 3517–3522

Magenes G, Griffith M (2009a) Example of Assessment with rigid-body Mechanism Analysis.

Magenes G, Griffith M (2009b) Unreinforced Masonry in Shear.

Magenes G, Morandi P, Penna A (2008a) In-plane cyclic tests of calcium silicate masonry walls. 14th International Brick & Block Masonry Conference

Magenes G, Morandi P, Penna A (2008b) Experimental in-plane cyclic response of masonry walls with clay units. 14 th World Conference on Earthquake Engineering

Magenes G, Penna A (2011) Seismic Design and Assessment of Masonry Buildings in Europe: Recent Research and Code Development Issues. 9 th Australasian Masonry Conference. Queenstown, New Zealand, pp 583–603

Magenes G, Penna A, Galasco A (2010a) A full-scale shaking table test on a two-storey stone masonry building. 14th European Conference in Earthquake Engineering

Magenes G, Penna A, Galasco A, Da Paré M (2010b) In-plane cyclic shear tests of undressed double-leaf stone masonry panels. 8th International Masonry Conference

Magenes G, Penna A, Galasco A, Rota M (2010c) Experimental characterisation of stone masonry mechanical properties. 8th International Masonry Conference. Dresden, pp 1–10

Mallardo V, Malvezzi R, Milani E, Milani G (2008) Seismic vulnerability of historical masonry buildings: A case study in Ferrara. Engineering Structures 30:2223–2241. doi: 10.1016/j.engstruct.2007.11.006

Mandara A, Ramundo F, Spina G (2009) Performance levels under seismic actions of masonry structures retrofitted with steel elements. Protection of Historical Buildings - PROHITECH 09 1045–1050.

Mander JB, Dhakal RP, Mashiko N, Lecturer S (2006) Incremental dynamic analysis applied to seismic risk assessment of bridges. 8th US National Conference on Earthquake Engineering (8NCEE) 29:1–10. doi: 10.1016/j.engstruct.2006.12.015

Mann W, Muller H (1982) Failure of shear-stressed masonry. An enlarged theory, tests and application to shear walls. Proc. of the British Ceramic Society. pp 223–235

Marcari G, Abrams D (2009) Seismic Behaviour and Structural Dynamics. SAHC

Marcari G, Manfredi G, Prota A, Pecce M (2007) In-plane shear performance of masonry panels strengthened with FRP. Composites Part B: Engineering 38:887–901. doi: 10.1016/j.compositesb.2006.11.004

Mazzolani FM, Faggiano B, Marzo A, Grippa MR (2009) The diplomatic hall of the Royal Palace of Naples : Diagnosis , analysis and retrofitting of the timber structures. Protecion of Historical Buildings - PROHITECH 09 367–373.

McGinley WM (2006) Design of anchor bolts in masonry. Progress in Structural Engineering and Materials 8:155–164. doi: 10.1002/pse

Mele E, Luca A De, Giordano A (2003) Modelling and analysis of a basilica under earthquake loading. Journal of Cultural Heritage 4:355–367. doi: 10.1016/j.culher.2003.03.002

Mendes N, Lourenço PB (2010) Seismic Assessment of Masonry “Gaioleiro” Buildings in Lisbon, Portugal. Earthquake Engineering 14:80–101. doi: 10.1080/13632460902977474

Meyer A, Eligehausen R (2004) Injection Anchors for use in Masonry Structures. In: Martens D, Vermeltfoort A (eds) 13th International Brick and Block Conference. Amestedam, pp 109–117

Milani G, Lourenço PB, Tralli A (2007) 3D Homogenized limit analysis of masonry buildings under horizontal loads. European Conference on Computational Mechanics Solids, Structures and Coupled Problems in Engineering 29(11):3134–3148.

Modena C, Porto F Da, Casarin F, et al. (2010) Cultural Heritage Buildings and the Abruzzo Earthquake: Performance and Post- Earthquake Actions. Advanced Materials Research 133-134:623–628.

Moon FL (2004) Seismic strengthening of low-rise unreinforced masonry structures with flexible diaphragms. Georgia Institute of Technology

Moreira S, Ramos LF, Oliveira D V, et al. (2012) Experimental seismic behaviour of wall-to-half-timbered wall connections. 8th International Conference on Structural Analysis of Historical Constructions

MSJC (2013) Building Code Requirements for Masonry Structures (TMS 402-13/ ACI 530-13/ ASCE 5-13).

Nardone F, Prota A, Manfredi G (2009) Considerazioni sulla valutazione della resistenza a taglio di pannelli murari rinforzati con FRP. 3th Mechanics of masonry structures strengthened with composite materials. Venezia, Italy, pp 367–374

NTC 08 (2009) Istruzioni per l'applicazione delle "Nuove norme tecniche per le costruzioni" C8. costruzioni esistenti. Nuove norme tecniche per le costruzioni. pp 279–303

NTC 08 (2008) Norme Tecniche per le Costruzioni.

NZSEE (2006) Assesment and Improvement of the Structural Performance of Buildings in Earthquakes.

Oliveira D V (2003) Experimental and numerical analysis of blocky masonry structures under cyclic loading. University of Minho

Oliveira D V, Lourenço PB (2004) Implementation and validation of a constitutive model for the cyclic behaviour of interface elements. Computers & Structures 82:1451–1461.

OPCM 3274 (2003) OPCM 3274 - Norme Tecniche per ol Progetto, la Valutazione e e L'Adeguamento Sismico degli Edifici. OPCM 3274

OPCM 3274/2003 (2003) Primi elementi in materia di criteri generali per la classificazione sismica del territorio nazionale e di normative tecniche per le costruzioni in zona sismica (in Italian). Rome, Italy

OPCM 3431 (2005) Ulteriori modifiche ed integrazioni all'O.P.C.M. 20 marzo 2003 n. 3274. (In Italian)

Orduña A (2003) Seismic Assessment of Ancient Masonry Structures by Rigid Blocks Limit Analysis. Universidade do Minho

Pan P, Ohsaki M (2006) Nonlinear multimodal pushover analysis method for spatial structures. International Symposium on New Olympics New Shell and Spatial structures 1–8.

Parisi F (2010) Non-Linear Seismic Analysis of Masonry Buildings. PhD Thesis 1–313.

Park J, Towashiraporn P, Craig J, Goodno B (2008) Seismic fragility analysis of low-rise unreinforced masonry structures. Engineering Structures 31:125–137. doi: 10.1016/j.engstruct.2008.07.021

Paulay T, Priestley M (1992) Seismic Design of Reinforced Concrete and Masonry Buildings. 621–625.

Penna A, Cattari S, Galasco A, et al. (2004) Seismic assessment of masonry structures by non-linear macro-element analysis. IV International Seminar on Structural Analysis of Historical Construction-Possibilities of Numerical and Experimental Techniques. pp 1157–1164

Penna A, Lagomarsino S, Galasco A (2013) A nonlinear macroelement model for the seismic analysis of masonry buildings. Earthquake Engineering & Structural Dynamics. doi: 10.1002/eqe

Petry S, Beyer K (2014) Influence of boundary conditions and size effect on the drift capacity of URM walls. Engineering Structures 65:76–88. doi: 10.1016/j.engstruct.2014.01.048

Priestley M (2000) Performance based seismic design. 12th World Conference on Earthquake Engineering. pp 1–22

Romano A (2005) Modelling, Analysis and Testing of Masonry Structures. Università degli Studi di Napoli Federico II

Roque JCA (2002) Reabilitação Estrutural de Paredes Antigas de Alvenaria. University of Minho

Rots JG (1988) Computational Modeling of Concrete Fracture. PhD Thesis

Russell AP (2010) Characterisation and Seismic Assessment of Unreinforced Masonry Buildings. The University of Auckland, New Zealand

Salonikios T (2003) Comparative inelastic pushover analysis of masonry frames. Engineering Structures 25:1515–1523. doi: 10.1016/S0141-0296(03)00118-4

Schnept S, Stempniewski L, Lungu D (2007) Application of the Capacity Spectrum Method for Seismic Evaluation of Structures. International Symposium on Strong Vrancea Earthquakes and Risk Mitigation. pp 378–382

Seki M, Vacareanu R, Saito T, Cotofana D (2008) Cyclic Shear Tests on Plain and FRP Retrofitted Masonry Walls. 14 th World Conference on Earthquake Engineering

Senaldi I, Magenes G, Ingham JM (2012) The seismic performance of unreinforced stone masonry buildings during the 2010-2011 Canterbury earthquake sequence. 15th World Conference on Earthquake Engineering

Senaldi I, Magenes G, Penna A, et al. (2013) The Effect of Stiffened Floor and Roof Diaphragms on the Experimental Seismic Response of a Full Scale Unreinforced Stone Masonry Building. Journal of Earthquake Engineering 131231091850007. doi: 10.1080/13632469.2013.876946

Sendova VI, Gavrilovic P, Stojanoski B, Jekic G (2009) Reconstruction and seismic strengthening of St . Athanasius church damaged by explosion. Protection of Historical Buildings - PROHITECH 09 1423–1428.

Silva BL (2012) Diagnosis and Strengthening of Historical Masonry Structures: Numerical and Experimental Analysis. University of Brescia

Simões A, Bento R (2013) Seismic Pushover Analysis of “Gaioleiro ” Buildings in Lisbon. International Conference on Earthquake Engineering

Simões A, Bento R, Gago A, Lopes M (2012) Seismic Vulnerability of Old Masonry “ Gaioleiro ” Buildings in Lisbon. 15th World Conference on Earthquake Engineering

Sturm T, Astroza M, Saragoni GR (2009) Vulnerability analysis of two centennial buildings that survived undamaged the two large Valparaiso earthquakes of 1906 and 1985. 1647:1547–1552.

TNO DIANA (2009) DIANA, DIsplacement method ANAlyser, release 9.4, User’s Manual.

Tomaževič M (1999) Earthquake-Resistant Design of Masonry Buildings, Series on. Imperial College Press

Tomaževič M (1978) The computer program POR.

Turnsek V, Cacovic F (1971) Some experimental results on the strength of brick masonry walls. 2º International Brick Masonry Conference

Turnsek V, Sheppard P (1980) The shear and flexural resistance of masonry walls. Research Conference on Earthquake Engineering. Skopje, pp 517–573

Valluzzi MR (2002) Shear behavior of masonry panels strengthened by FRP laminates. Construction and Building Materials 16:409–416. doi: 10.1016/S0950-0618(02)00043-0

Vamvatsikos D, Cornell CA (2002) Incremental dynamic analysis. Earthquake Engineering & Structural Dynamics 31:491–514. doi: 10.1002/eqe.141

Vasconcelos G (2005) Experimental investigations on the mechanics of stone masonry: Characterization of granites and behavior of ancient masonry shear walls. University of Minho

Vasconcelos G, Lourenço PB (2009) In-Plane Experimental Behavior of Stone Masonry Walls under Cyclic Loading. Journal of Structural Engineering 135:1269–1278.

Vélez LFR (2003) A Simplified Mechanics – Based Procedure for the Seismic Risk Assessment of Unreinforced Masonry Buildings. Rose School - European School of Advanced Studies in Reduction of Seismic Risk

Weigel TA, Lyvers G (2004) Statistical Analysis of Masonry Fastners. 13th International Brick and Block Conference. Amestedam, pp 89–98

Wenzel F, Maus H (1992) Repair of Masonry Structures. Meccanica 27:223–232.

Yi T (2004) Experimental investigation and numerical simulation of an Unreinforced Masonry Structure with Flexible Diaphragms. PhD Thesis. doi: 10.1016/j.jmr.2010.02.023

Zhu XQ, Law SS (2005) Damage detection of reinforced concrete structures based on concrete-steel interface element. IMAC-XXIII: Conference & Exposition on Structural Dynamics - Structural Health Monitoring

Zhuge Y (2008) FRP Retrofitted URM Walls under In-Plane Shear - A Review of Avaiable Design Models. 14th International Brick & Block Masonry Conference

ANNEX A

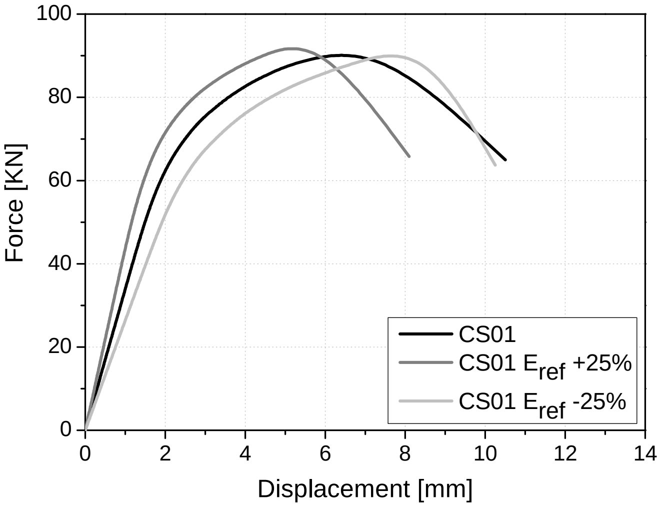

Figure A. 1 Force-displacement curves for the parametric analysis of the masonry elastic modulus (CS01 wall).

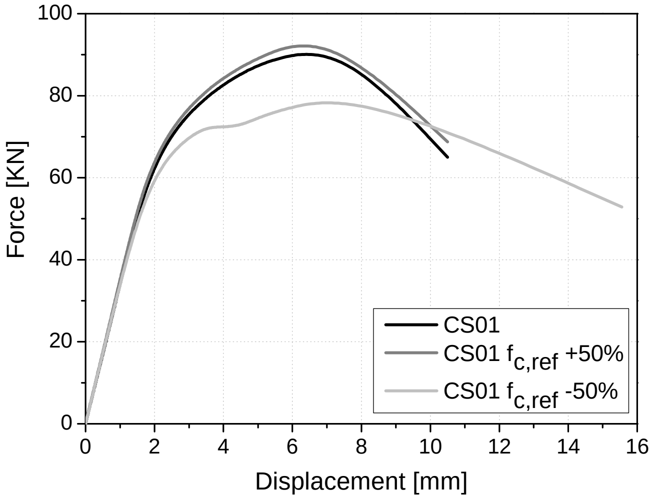

Figure A. 2 Force-displacement curves for the parametric analysis of the masonry compressive strength (CS01 wall).

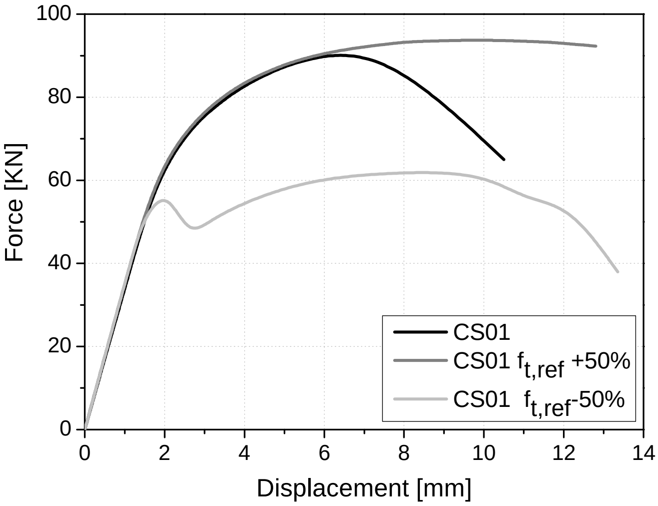

Figure A. 3 Force-displacement curves for the parametric analysis of the masonry tensile strength (CS01 wall).

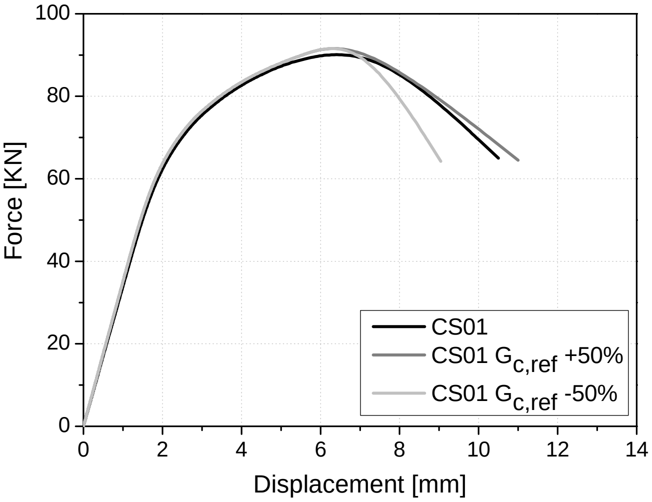

Figure A. 4 Force-displacement curves for the parametric analysis of the masonry compressive fracture energy (CS01 wall).

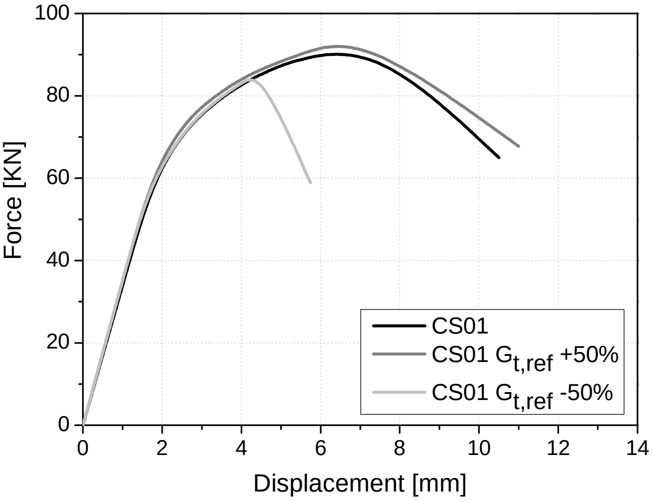

Figure A. 5 Force-displacement curves for the parametric analysis of the masonry tensile fracture energy (CS01 wall).

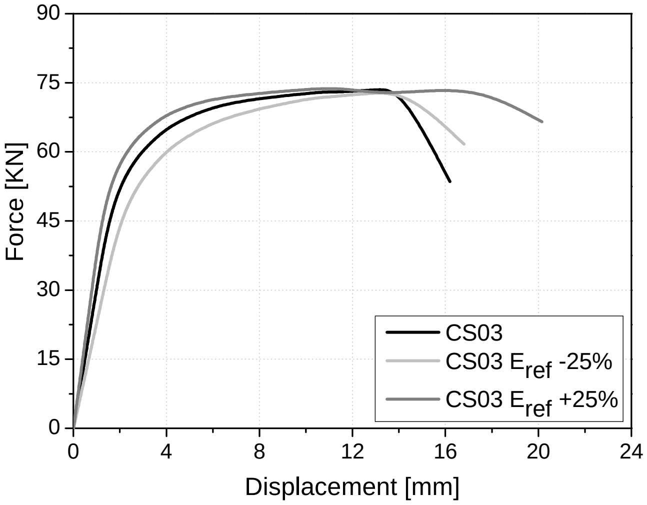

Figure A. 6 Force-displacement curves for the parametric analysis of the masonry elastic modulus energy (CS03 wall).

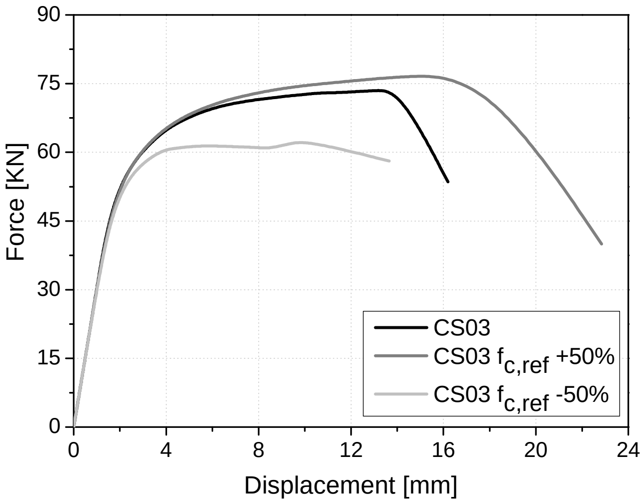

Figure A. 7 Force-displacement curves for the parametric analysis of the masonry compressive strength (CS03 wall).

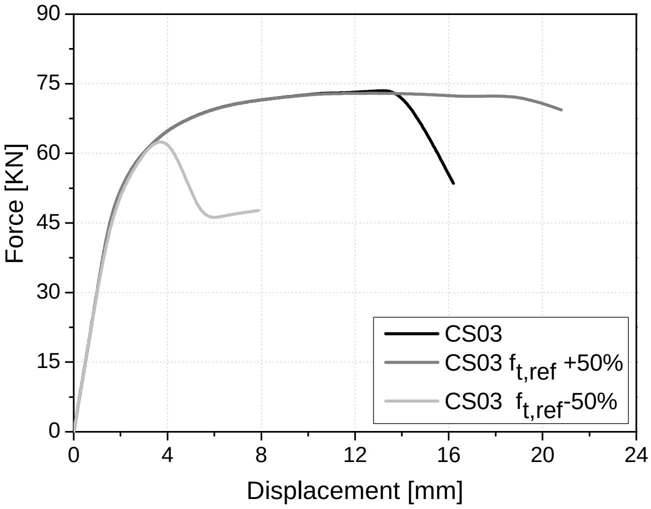

Figure A. 8 Force-displacement curves for the parametric analysis of the masonry tensile strength (CS03 wall).

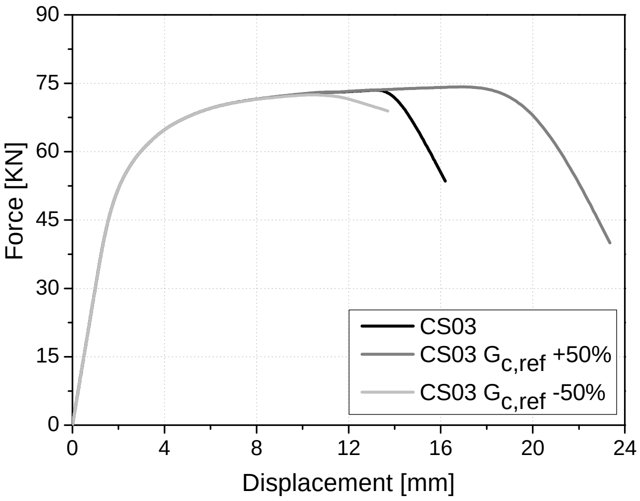

Figure A. 9 Force-displacement curves for the parametric analysis of the masonry compressive fracture energy (CS03 wall).

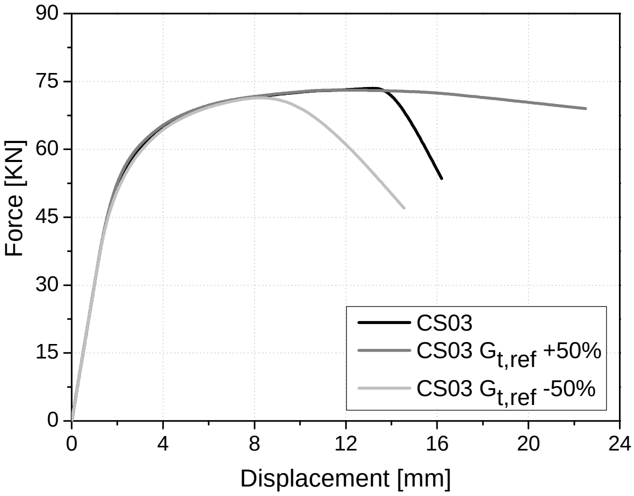

Figure A. 10 Force-displacement curves for the parametric analysis of the masonry tensile fracture energy (CS03 wall).

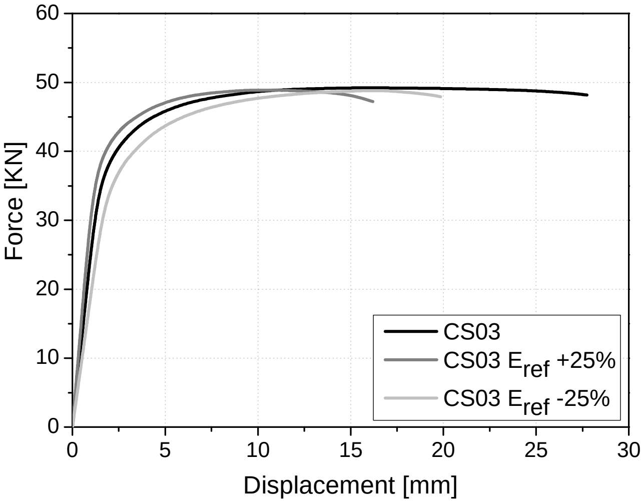

Figure A. 11 Force-displacement curves for the parametric analysis of the masonry elastic modulus energy (CS02 wall).

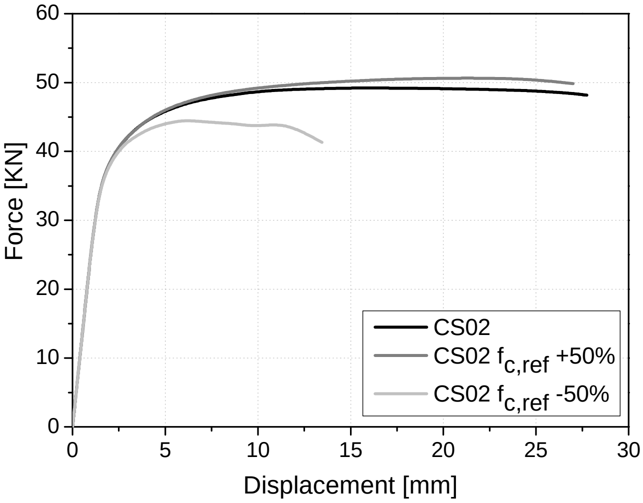

Figure A. 12 Force-displacement curves for the parametric analysis of the masonry compressive strength (CS02 wall).7

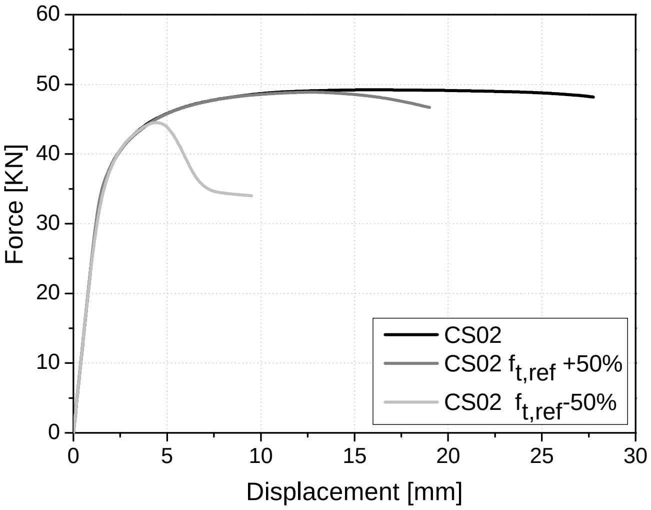

Figure A. 13 Force-displacement curves for the parametric analysis of the masonry tensile strength (CS02 wall).

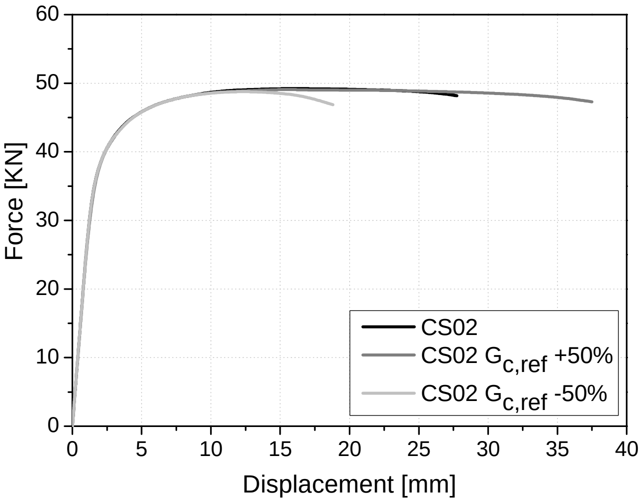

Figure A. 14 Force-displacement curves for the parametric analysis of the masonry compressive fracture energy (CS02 wall).

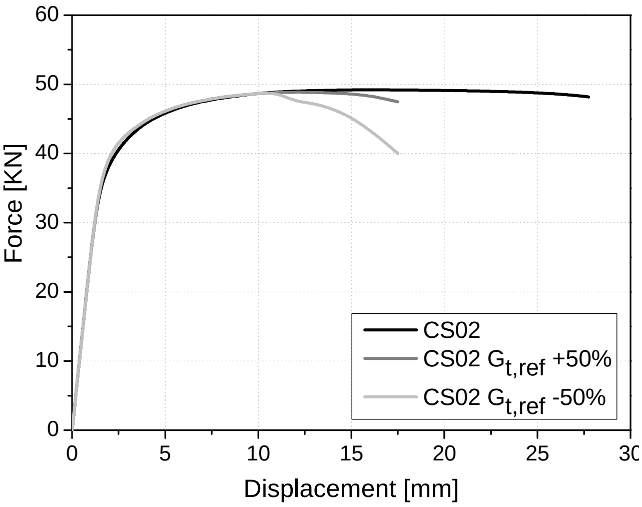

Figure A. 15 Force-displacement curves for the parametric analysis of the masonry tensile fracture energy (CS02 wall).

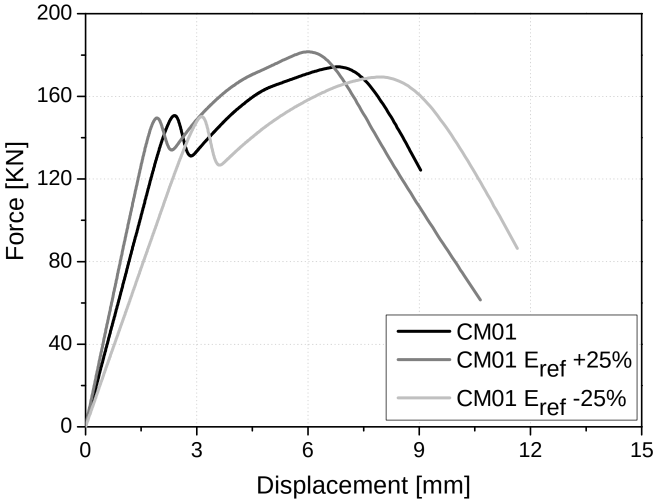

Figure A. 16 Force-displacement curves for the parametric analysis of the masonry elastic modulus energy (CM01 wall).

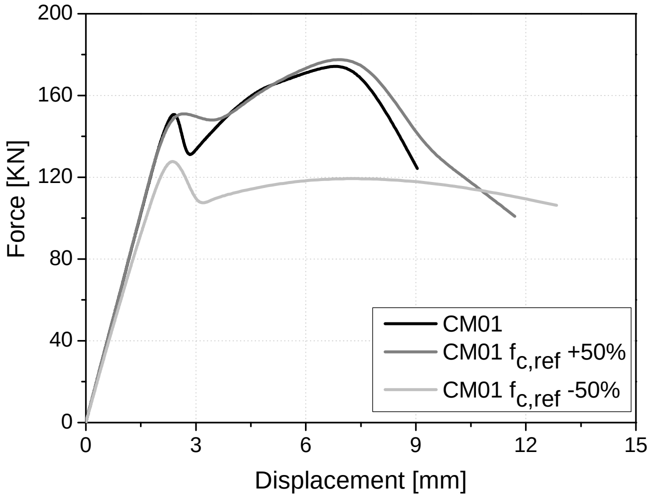

Figure A. 17 Force-displacement curves for the parametric analysis of the masonry compressive strength (CM01 wall).

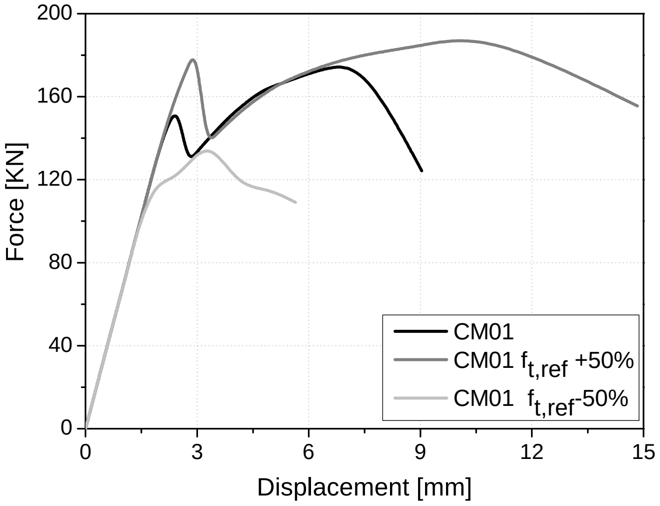

Figure A. 18 Force-displacement curves for the parametric analysis of the masonry tensile strength (CM01 wall).

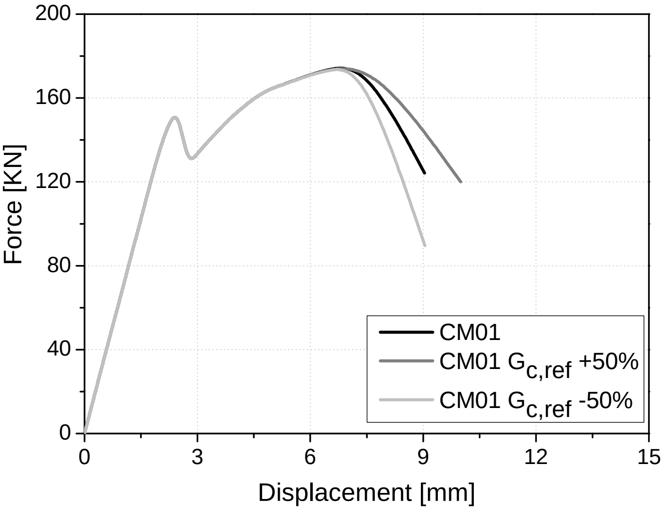

Figure A. 19 Force-displacement curves for the parametric analysis of the masonry compressive fracture energy (CM01 wall).

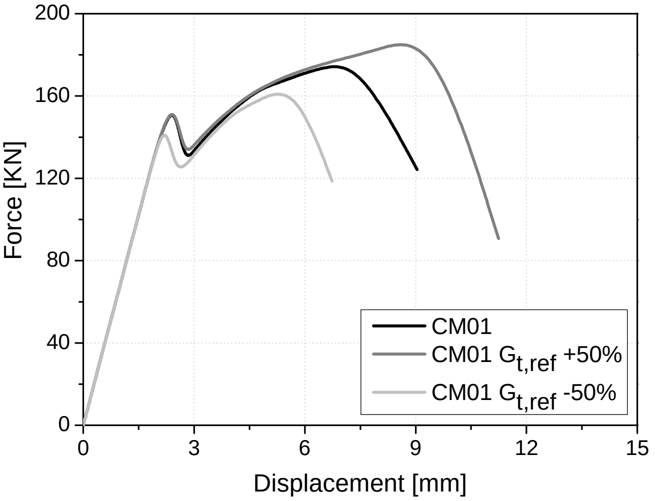

Figure A. 20 Force-displacement curves for the parametric analysis of the masonry tensile fracture energy (CM01 wall).

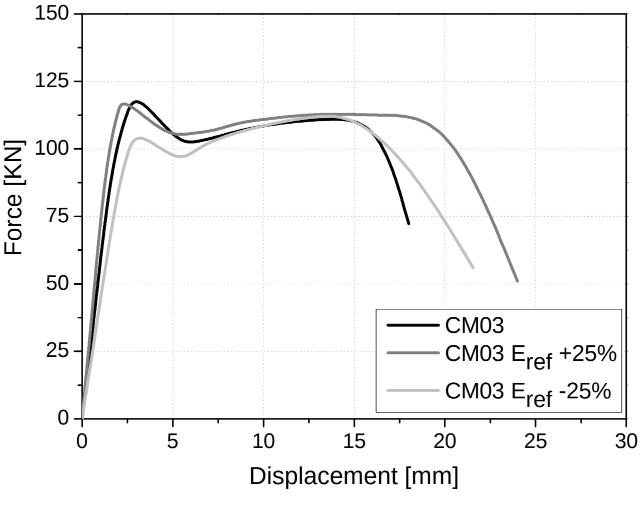

Figure A. 21 Force-displacement curves for the parametric analysis of the masonry elastic modulus energy (CM03 wall).

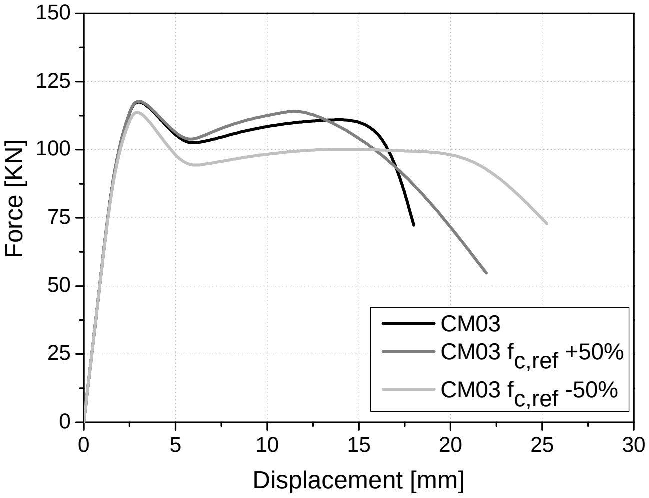

Figure A. 22 Force-displacement curves for the parametric analysis of the masonry compressive strength (CM03 wall).

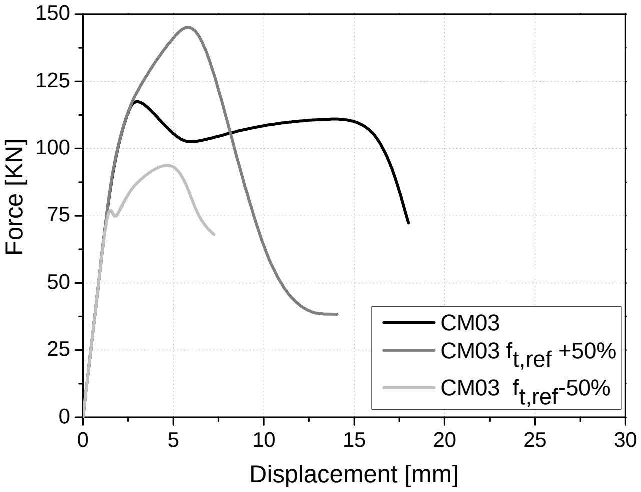

Figure A. 23 Force-displacement curves for the parametric analysis of the masonry tensile strength (CM03 wall).

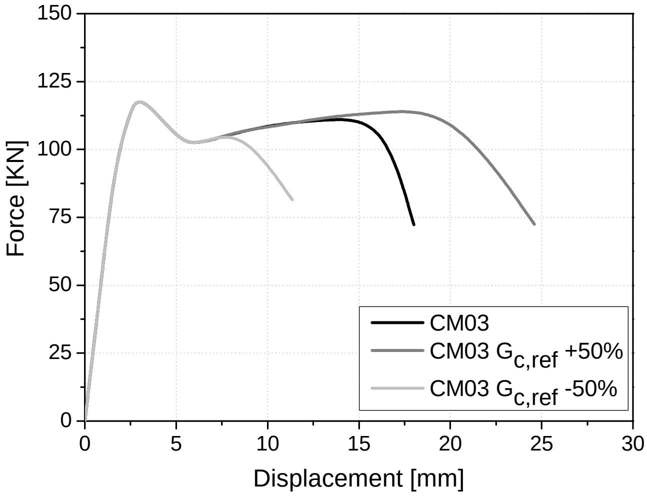

Figure A. 24 Force-displacement curves for the parametric analysis of the masonry compressive fracture energy (CM03 wall).

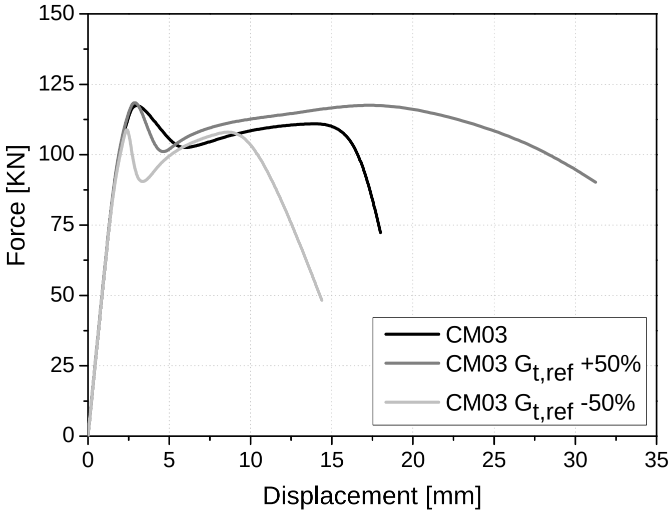

Figure A. 25 Force-displacement curves for the parametric analysis of the masonry tensile fracture energy (CM03 wall).

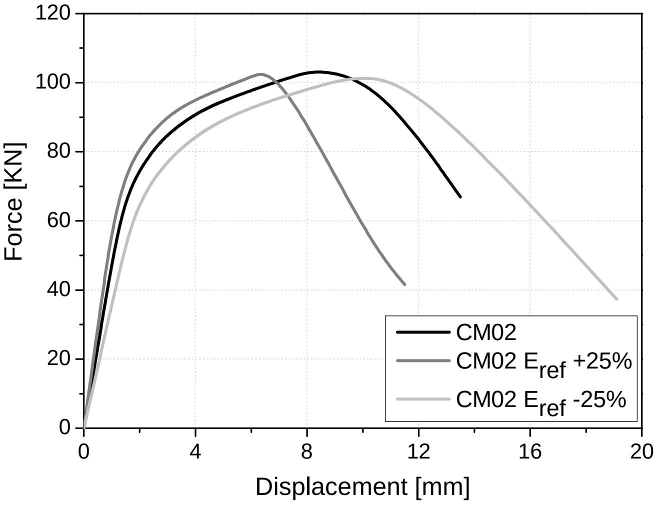

Figure A. 26 Force-displacement curves for the parametric analysis of the masonry elastic modulus energy (CM02 wall).

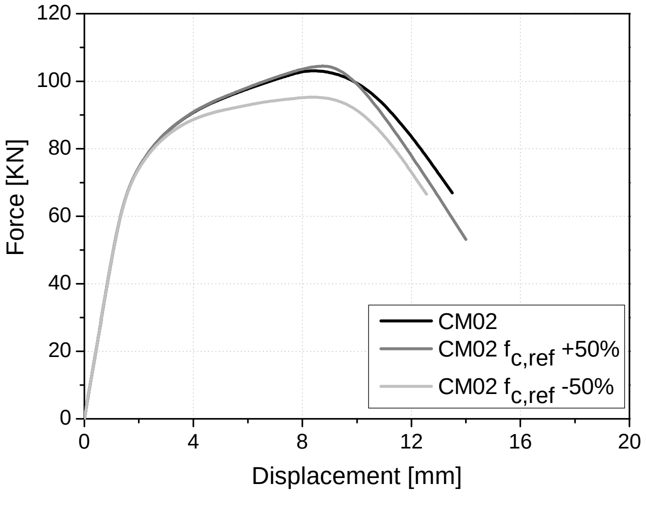

Figure A. 27 Force-displacement curves for the parametric analysis of the masonry compressive strength (CM02 wall).

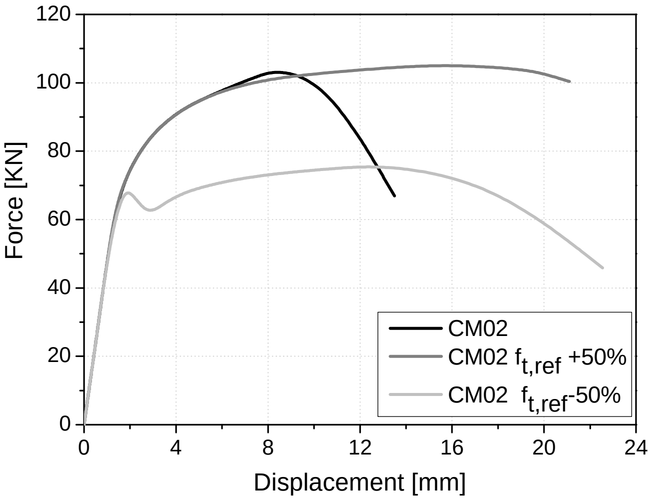

Figure A. 28 Force-displacement curves for the parametric analysis of the masonry tensile strength (CM02 wall).

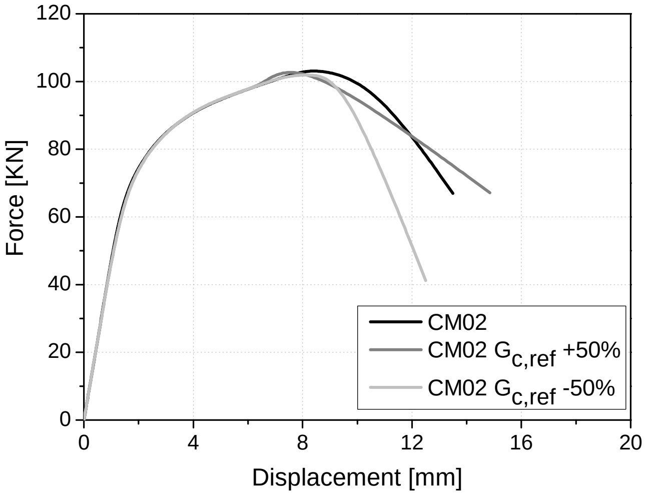

Figure A. 29 Force-displacement curves for the parametric analysis of the masonry compressive fracture energy (CM02 wall).

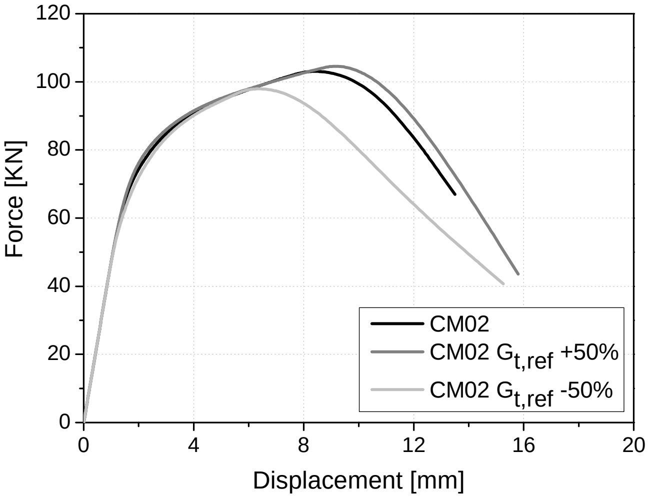

Figure A. 30 Force-displacement curves for the parametric analysis of the masonry tensile fracture energy (CM02 wall).

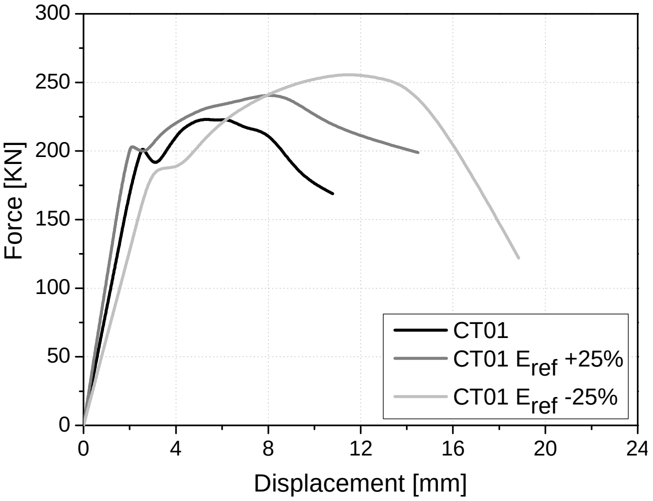

Figure A. 31 Force-displacement curves for the parametric analysis of the masonry elastic modulus energy (CT01 wall).

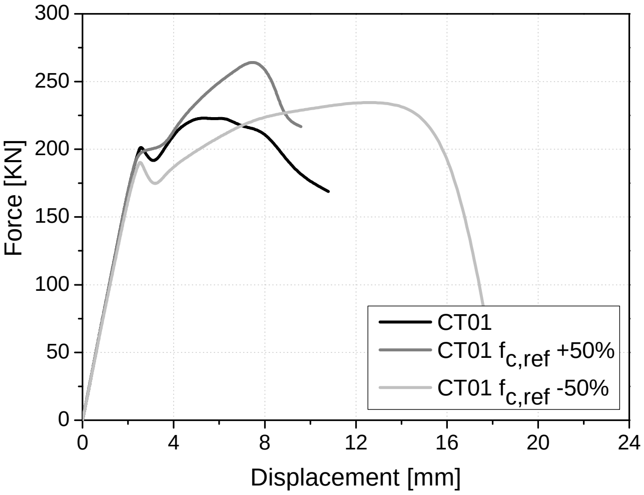

Figure A. 32 Force-displacement curves for the parametric analysis of the masonry compressive strength (CT01 wall).

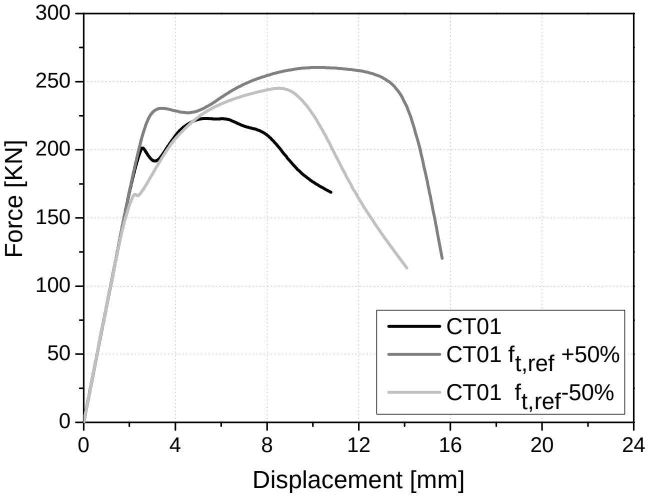

Figure A. 33 Force-displacement curves for the parametric analysis of the masonry tensile strength (CT01 wall).

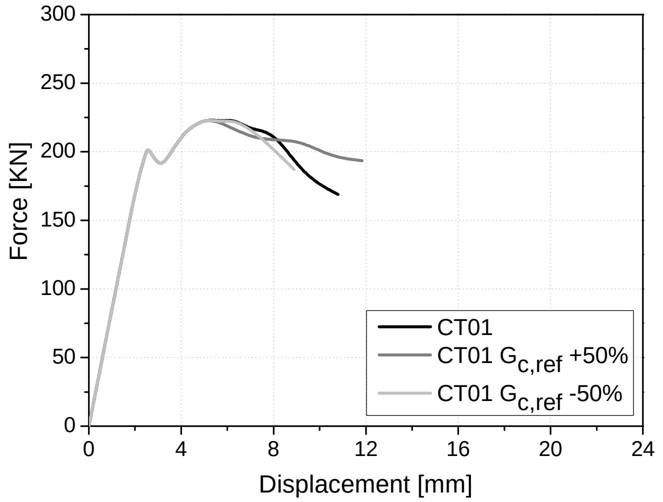

Figure A. 34 Force-displacement curves for the parametric analysis of the masonry compressive fracture energy (CT01 wall).

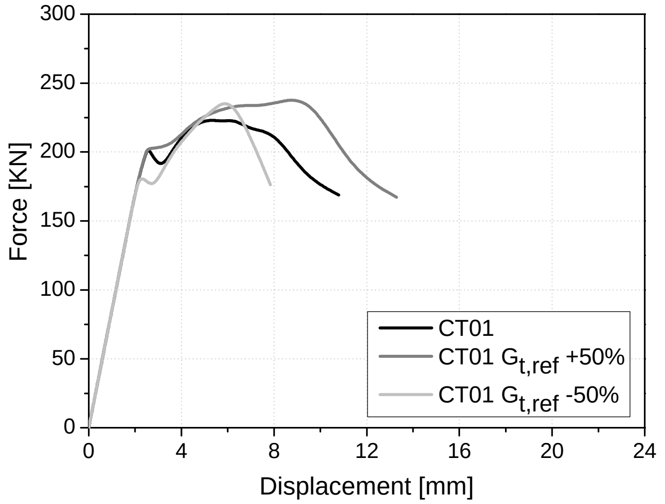

Figure A. 35 Force-displacement curves for the parametric analysis of the masonry tensile fracture energy (CT01 wall).

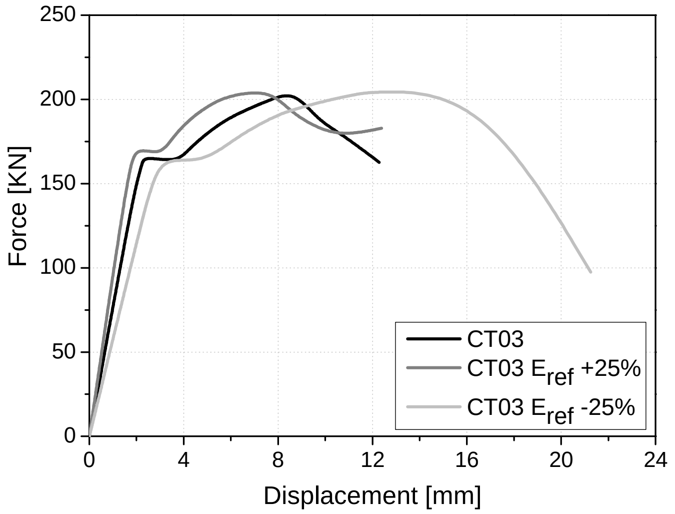

Figure A. 36 Force-displacement curves for the parametric analysis of the masonry elastic modulus energy (CT03 wall).

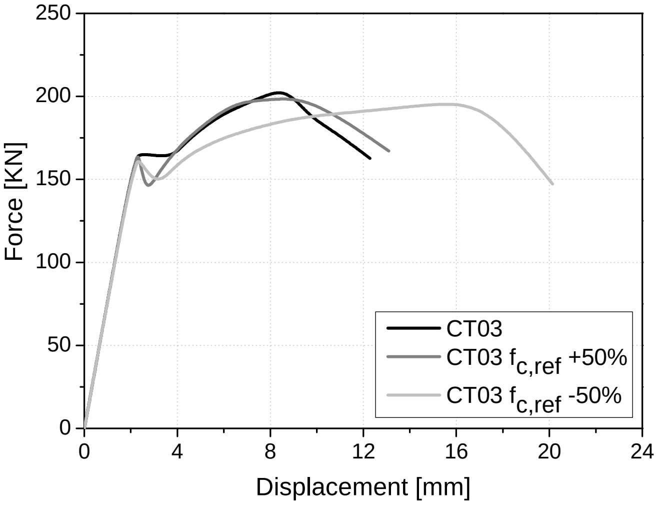

Figure A. 37 Force-displacement curves for the parametric analysis of the masonry compressive strength (CT03 wall).

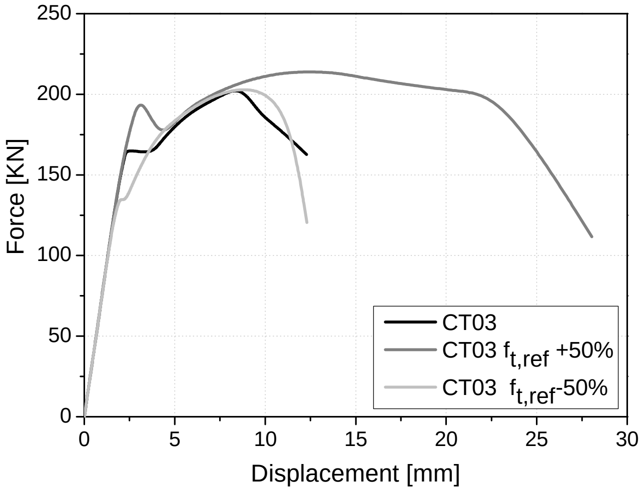

Figure A. 38 Force-displacement curves for the parametric analysis of the masonry tensile strength (CT03 wall).

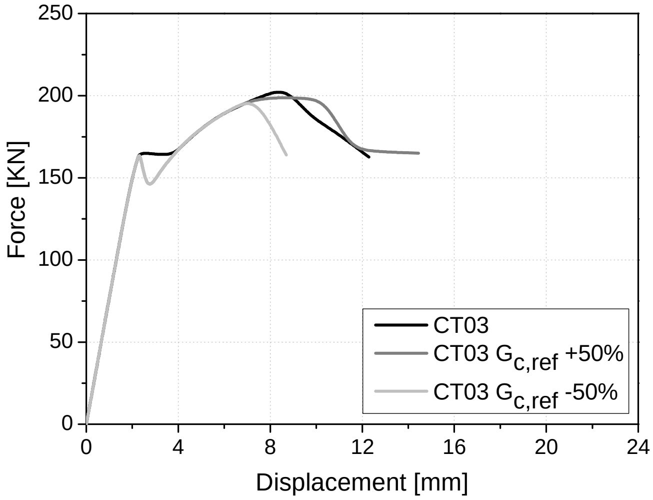

Figure A. 39 Force-displacement curves for the parametric analysis of the masonry compressive fracture energy (CT03 wall).

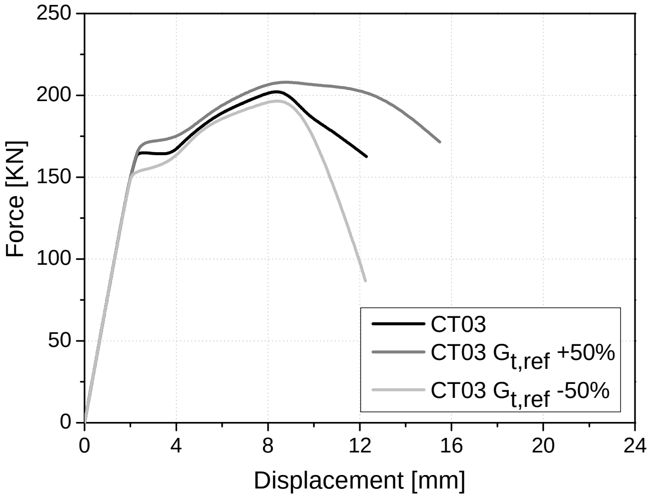

Figure A. 40 Force-displacement curves for the parametric analysis of the masonry tensile fracture energy (CT03 wall).

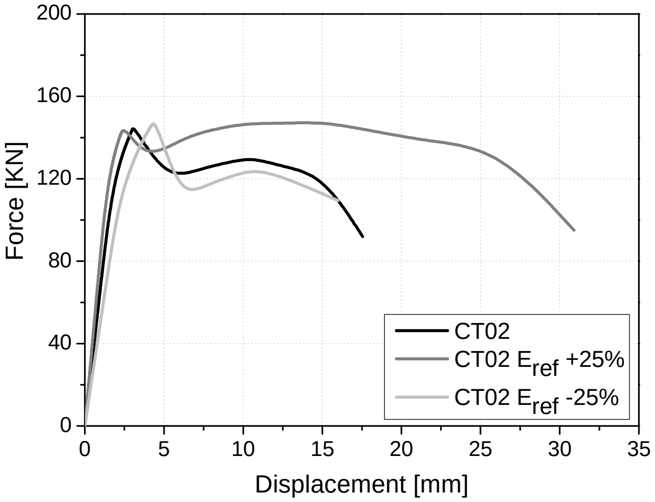

Figure A. 41 Force-displacement curves for the parametric analysis of the masonry elastic modulus energy (CT02 wall).

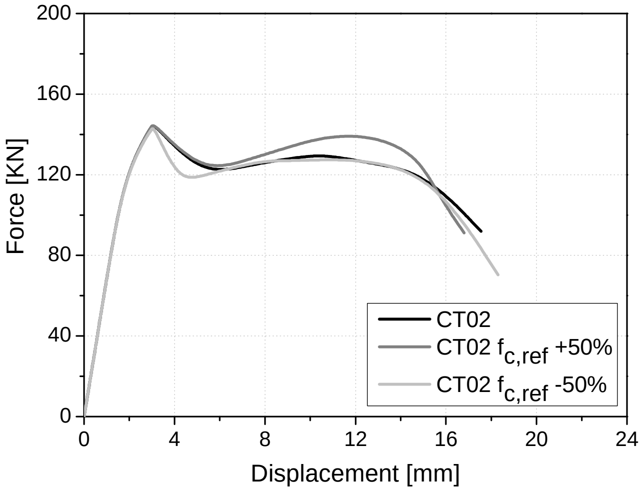

Figure A. 42 Force-displacement curves for the parametric analysis of the masonry compressive strength (CT02 wall).

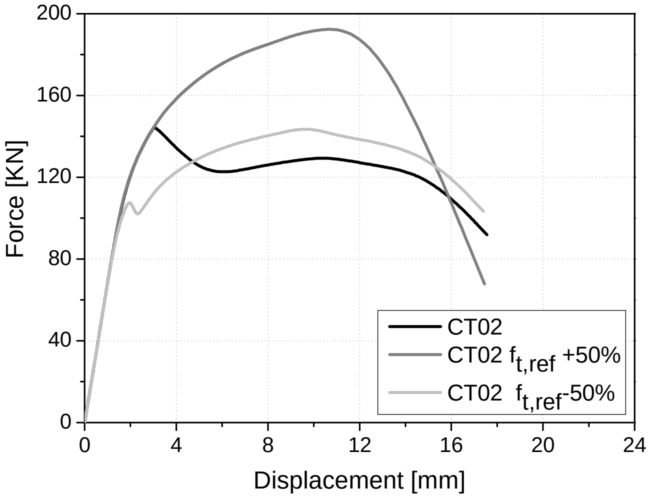

Figure A. 43 Force-displacement curves for the parametric analysis of the masonry tensile strength (CT02 wall).

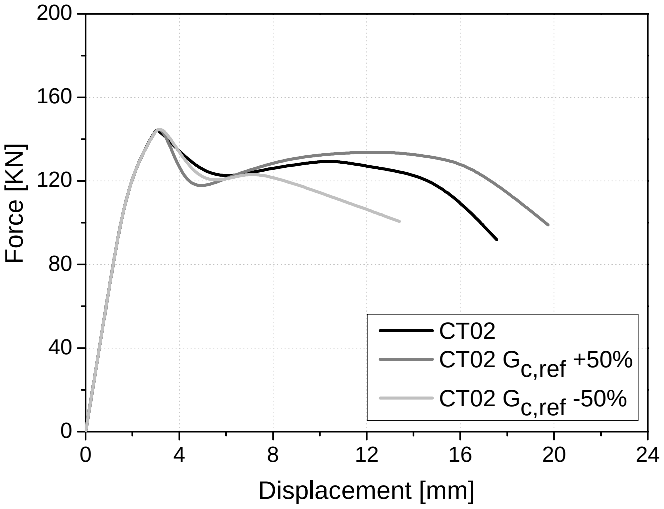

Figure A. 44 Force-displacement curves for the parametric analysis of the masonry compressive fracture energy (CT02wall).

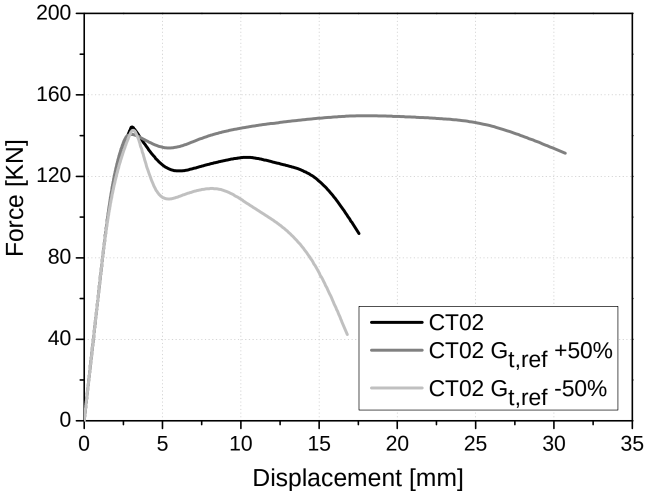

Figure A. 45 Force-displacement curves for the parametric analysis of the masonry tensile fracture energy (CT02 wall).

ANNEX B

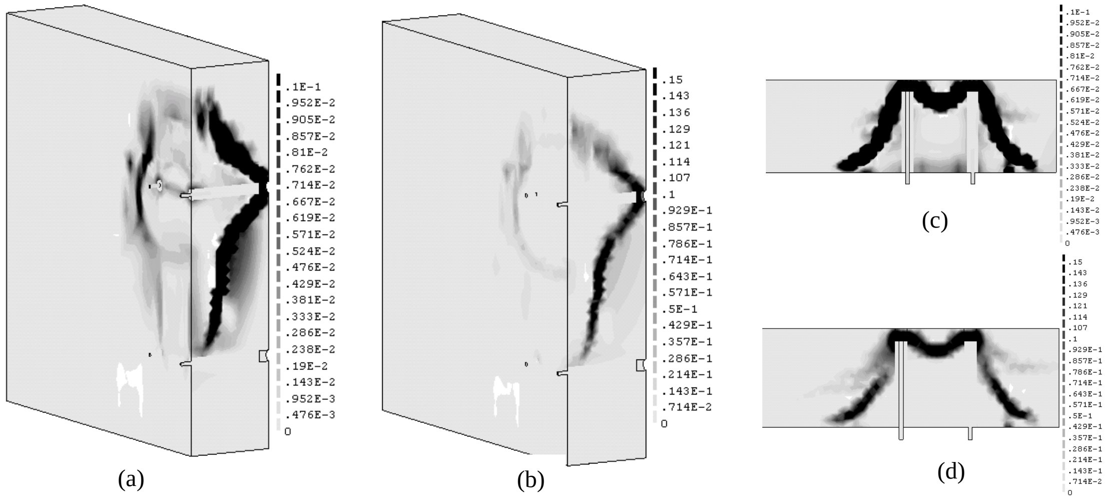

(a) (b) (c) (d)

Figure B.1 Maximum principal strain for the 0.5 × $G_{c,ref}$ analysis: (a) Peak load – lateral section; (b) Final stage – lateral section; (c) Peak load – top section; (d) Final stage – top section.

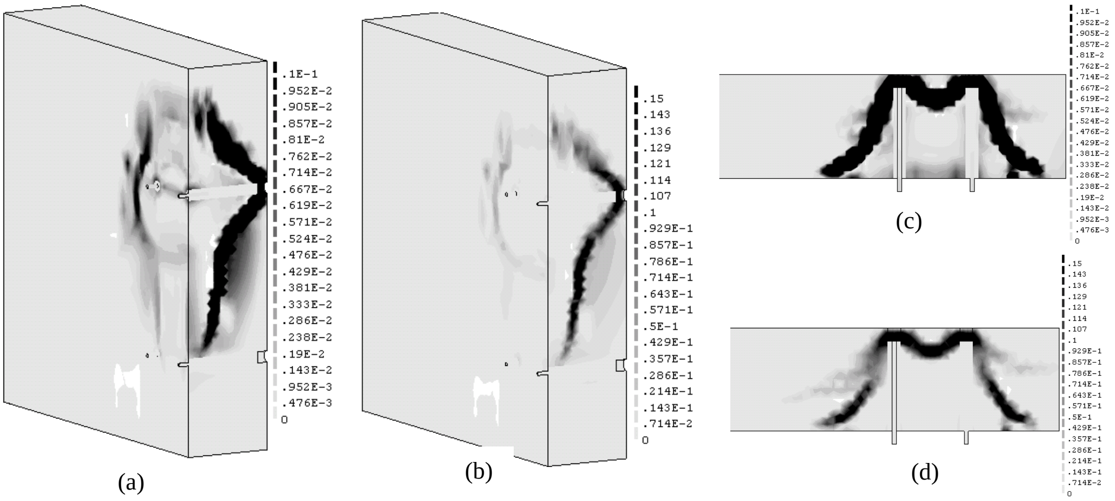

(a) (b) (c) (d)

Figure B.2 Maximum principal strain for the 2.0 × $G_{c,ref}$ analysis: (a) Peak load – lateral section; (b) Final stage – lateral section; (c) Peak load – top section; (d) Final stage – top section.

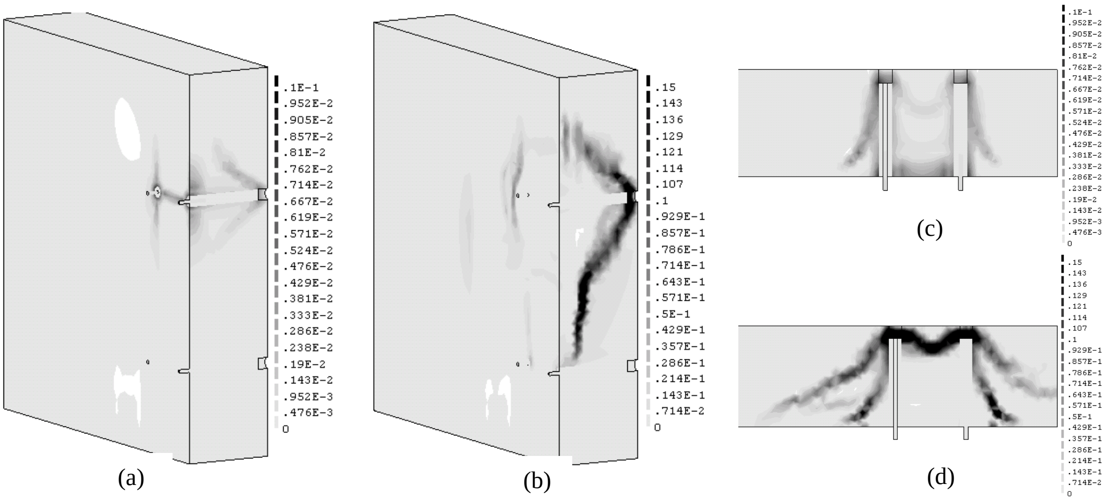

(a) (b) (c) (d)

Figure B.3 Maximum principal strain for the 0.5 × $G_{t,ref}$ analysis: (a) Peak load – lateral section; (b) Final stage – lateral section; (c) Peak load – top section; (d) Final stage – top section.

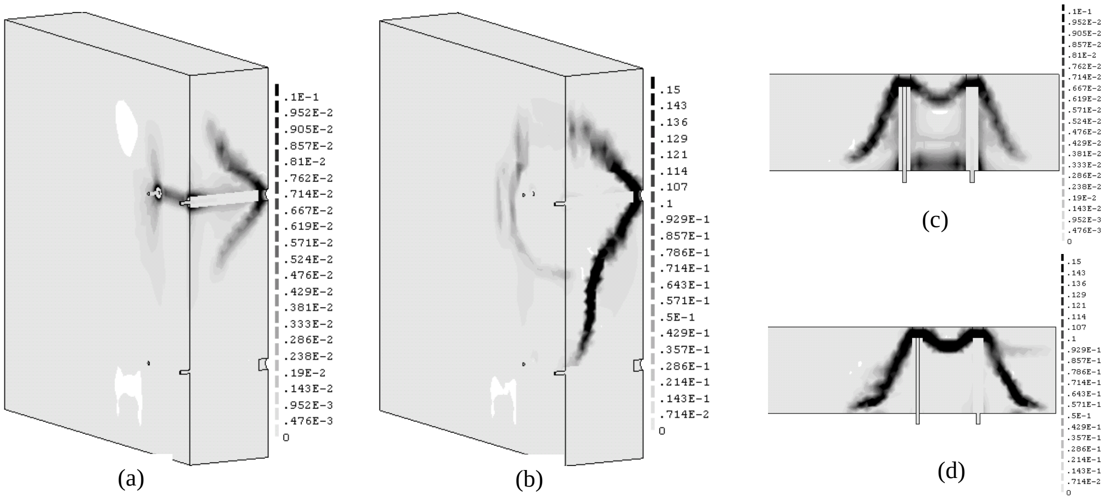
.1E-1
.952E-2
.905E-2
.857E-2
.81E-2
.762E-2
.714E-2
.667E-2
.619E-2
.571E-2
.524E-2
.476E-2
.429E-2
.381E-2
.333E-2
.286E-2
.238E-2
.19E-2
.143E-2
.952E-3
.476E-3
0
.15
.143
.136
.129
.121
.114
.107
.1
.929E-1
.857E-1
.786E-1
.714E-1
.643E-1
.571E-1
.5E-1
.429E-1
.357E-1
.286E-1
.214E-1
.143E-1
.714E-2
0
(a)
(b)
(c)
(d)

Figure B.4 Maximum principal strain for the 2.0 × $G_{t,ref}$ analysis: (a) Peak load – lateral section; (b) Final stage – lateral section; (c) Peak load – top section; (d) Final stage – top section.

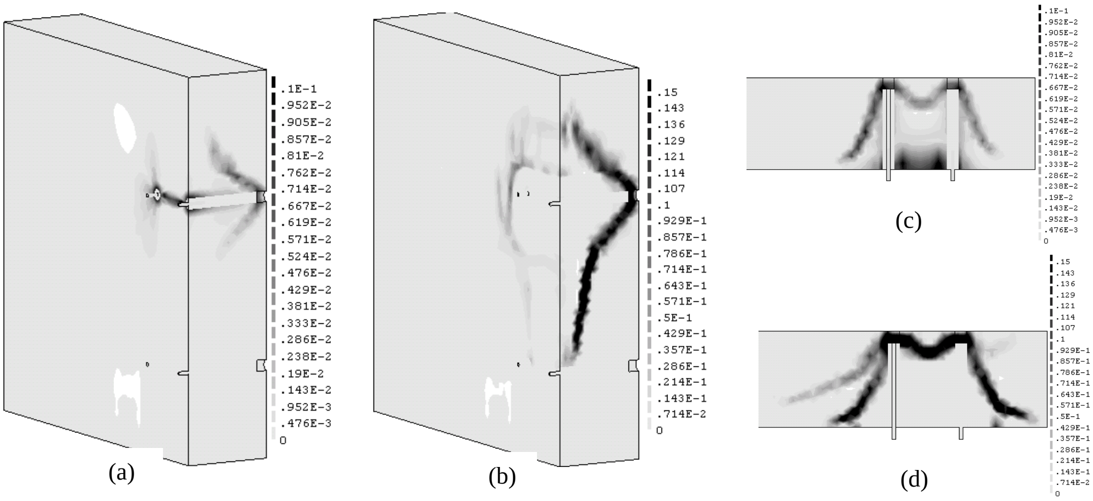
.1E-1
.952E-2
.905E-2
.857E-2
.81E-2
.762E-2
.714E-2
.667E-2
.619E-2
.571E-2
.524E-2
.476E-2
.429E-2
.381E-2
.333E-2
.286E-2
.238E-2
.19E-2
.143E-2
.952E-3
.476E-3
0
.15
.143
.136
.129
.121
.114
.107
.1
.929E-1
.857E-1
.786E-1
.714E-1
.643E-1
.571E-1
.5E-1
.429E-1
.357E-1
.286E-1
.214E-1
.143E-1
.714E-2
0
(a)
(b)
(c)
(d)

Figure B.5 Maximum principal strain for the 0.5 × $\sigma_{v,ref}$ analysis: (a) Peak load – lateral section; (b) Final stage lateral section; (c) Peak load – top section; (d) Final stage – top section.

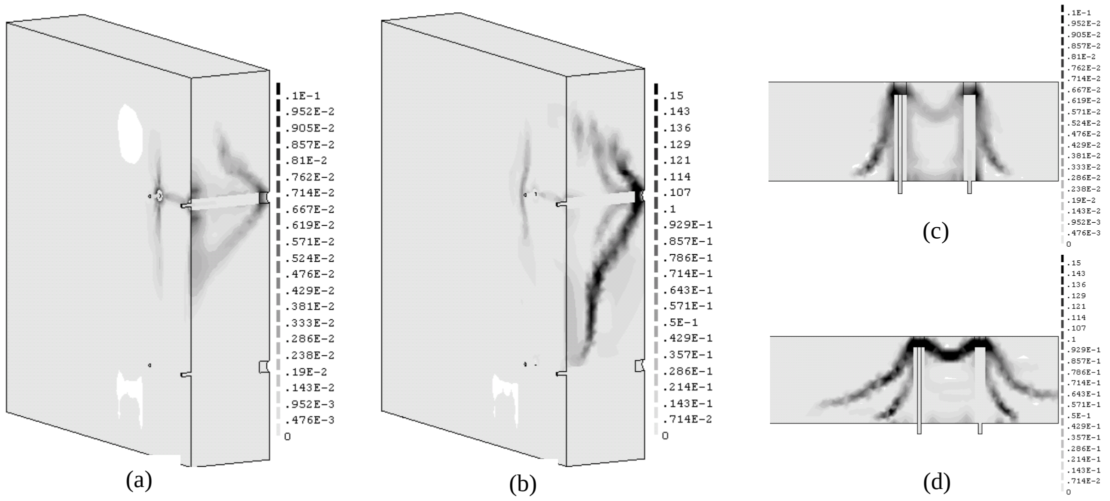
.1E-1
.952E-2
.905E-2
.857E-2
.81E-2
.762E-2
.714E-2
.667E-2
.619E-2
.571E-2
.524E-2
.476E-2
.429E-2
.381E-2
.333E-2
.286E-2
.238E-2
.19E-2
.143E-2
.952E-3
.476E-3
0
.15
.143
.136
.129
.121
.114
.107
.1
.929E-1
.857E-1
.786E-1
.714E-1
.643E-1
.571E-1
.5E-1
.429E-1
.357E-1
.286E-1
.214E-1
.143E-1
.714E-2
0
(a)
(b)
(c)
(d)

Figure B.6 Maximum principal strain for the 2.0 × $\sigma_{v,ref}$ analysis: (a) Peak load – lateral section; (b) Final stage – lateral section; (c) Peak load – top section; (d) Final stage – top section.

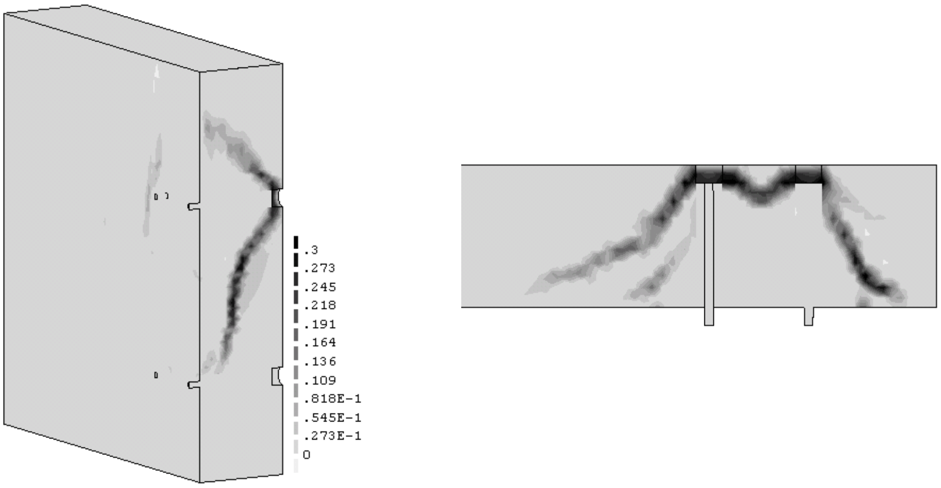
.3
.273
.245
.218
.191
.164
.136
.109
.818E-1
.545E-1
.273E-1
0

(a) (b)

Figure B.7 Maximum principal strains at final stage for the anchor diameter parametric analysis: (a) Lateral view; (b) Top view.